2014 Annual Technical Report
COVER PAGE

Federal Agency to which Report is submitted: DOE EERE – Wind & Water Power Program
Recipient: Electric Power Research Institute, DUNS: 062511126
Award Number: DE-EE0006382
Project Title: Assessment of Potential Impact of Electromagnetic Fields from Undersea Cable on Migratory Fish Behavior
Project Period: January 1, 2014 to December 31, 2015
Principle Investigator: Rob Kavet, Project Manager and Senior Technical Executive
Email: RKAVET@epri.com, Phone: 650-855-1061
Report Submitted by: Rob Kavet
Date of Report: March 6, 2014
Covering Period: January 1, 2014 to December 31, 2014
Report Frequency: Annual

Working Partners:

Electric Power Research Institute:

Rob Kavet, Project Manager and Senior Technical Executive at EPRI
Phone: 650-855-1061 Address: PO Box 10412
Email: RKAVET@epri.com 3420 Hillview Avenue
Palo Alto, CA 94303

University of California-Davis:

A. Peter Klimley, Adjunct Professor, University of California-Davis
Phone: 530-752-5830 Address: 1334 Academic Surge Building
Email: One Shields Ave.
Davis, CA 95616

Megan Wyman, Postdoctoral Researcher, University of California-Davis
Phone: 530-752-5372 Address: 1331 Academic Surge Building
Email: One Shields Ave.
Davis, CA 95616

Cost-Sharing Partners:

- Electric Power Research Institute
- Biotelemetry Laboratory, Department of Wildlife, Fish, and Conservation Biology, University of California-Davis

DOE Project Team: DOE HQ Technology office Director - Jose Zayas
DOE HQ Program Manager – Hoyt Battey
DOE Field Contracting Officer – Pamela Brodie
DOE Field Grants Management Specialist – Kristen Cadigan
DOE Field Project Officer – Tim Ramsey
DOE/CNJV Project Monitor – Erik Mauer
DOE/WWPTO - Samantha Bickel
DOE/WWPTO - Jocelyn Brown-Saracino

Signature of Submitting Official: Robert Kavet (electronic signature is acceptable)

ACCOMPLISHMENTS

Project Objective:

The objective of this study is to assess the overall effect of the magnetic field on migratory fish movements. The study addresses the following specific questions based on fish detections and measurements and projections of the magnetic field produced by an existing high voltage DC power line submerged beneath the San Francisco Bay between Pittsburg, CA and the Potrero substation in San Francisco, CA.

Project Goals:

(1) Does the presence of a magnetic field from an operating power cable alter the behavior and path of bony fishes and sharks along a migratory corridor?

(2) Does the magnetic field from an operating power cable guide migratory movements or pose an obstacle to movement?

Goal Status:

i. Major activities

A. Magnetometer survey (Q2-Q3)

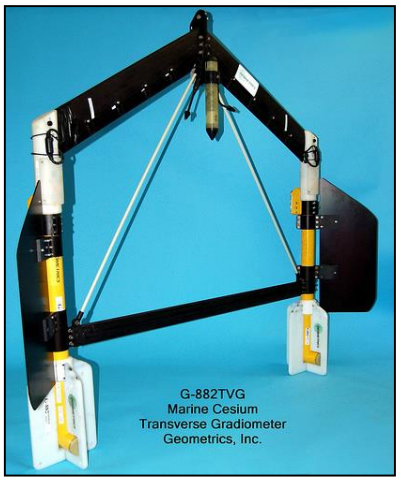

Figure 1. G-882 TVG Marine Cesium Transverse Gradiometer, Geometrics.

Magnetic field surveys were conducted in select locations of the San Francisco Bay between July 10th and August 8th, 2014. Surveys were performed with a G-882 TVG cesium magnetometer and transverse gradiometer rented from Geometrics, Inc. (San Jose, CA). The G-882 TVG (Figure 1) is equipped with two cesium vapor magnetometer 'fish' with stabilizer weights and fins. The dual cesium sensors are synchronized to 1 ms sampling with sensitivities up to 0.004 nT/√Hz RMS or approximately 0.01 nT peak to peak at 10 Hz. A depth sensor (depth under the water surface, 0.5% accuracy) and an echo-sounder altimeter (height above the sea floor, 1% resolution) attached to the frame provide positional information to the operators. Data was transmitted through the reinforced tow line to our onboard Panasonic toughbook computer for display and analysis in real time, using Geometric's MagLog software and our own Trimble GeoXT GPS (submeter accuracy).

In preparation for the survey, Megan Wyman consulted with experienced Geometrics staff, downloaded the operational manual and associated software for the G-882 TVG, and traveled to Geometrics' San Jose office on May 30, 2014 for an in-person training session on the technical aspects of the survey operation (e.g., software, hardware, methodologies). This meeting included hands-on experience with the magnetometers and private instruction by Mikhail Tchernychev and Naiema Jackson of Geometrics on how to use their custom software, including MagLog (for planning survey lines and collecting data), MagPick (for analyzing survey data), and MagMap (for mapping the survey data).

Additionally, a wooden platform and A-frame (Figure 2) was constructed on top of the University of California-Davis (UCD) Biotelemetry Laboratory's Research Vessel Tracker to deploy, tow, and retrieve the twin magnetometers. This structure, consisting of a moveable A-frame, winch, pulleys, and a capstan, was designed and constructed by Megan Wyman, Eric Chapman, Michael Thomas, Ryan Battleson, and Tommy Agosta of the UCD Biotelemetry Lab.

Figure 2. Platform, A-frame, and magnetometers on the UC Davis Research Vessel Tracker.

The locations and tracts of the survey lines were planned by Rob Kavet, Bernard Clairmont, and Justin Bell of the Electric Power Research Institute (EPRI) and Peter Klimley and Megan Wyman of UCD. The survey was conducted by Megan Wyman, Ryan Battleson, Tommy Agosta, Eric Chapman, Jamilynn Poletto, and Matthew Pagel of UCD. Three types of survey lines were conducted:

1. Survey tracts parallel to the fish detecting arrays along a) the Bay, Richmond, and Benicia Bridges, and b) a non-bridge location in San Pablo Bay. These lines extended along the entire span of the bridges (as far towards the banks as possible) and at least 1 km outwards from the fish detection array in San Pablo Bay. Transect lines started as close to the bridge/array as possible on each side and were repeated every 100 m away from the bridge/array up to 1 km.
   -The purpose of these survey tracts was to verify the model of the magnetic fields produced by the cable and to provide data needed to create a total magnetic field map and a magnetic field anomaly map of the area within the detection range of the fish detecting monitors.

2. Survey tracts perpendicular to the bridges (out to 1 km on both sides of the bridge). Two or three of these transects were conducted per bridge site, at least 1 km away from the cable.
   -The purpose of these transects was to measure the magnetic field distortion created by the bridges.

3. Survey tracts parallel to the cable at varying distances from the cable, including directly over the cable and at varying distances (e.g., 10 m, 20 m, 100 m) to the sides of the cable.
   -The purpose of these survey tracts was to help verify the model of the magnetic fields produced by the cable.

These survey tracts were conducted close to the surface (0 - 3 m below the water surface) and at greater depth in deeper locations (maximum of 12 m off the channel bottom). We were conducting tows at these two depths in order to ensure that we were sampling both the upper and lower magnetic field profiles of the water channel.

B. Post-processing and mapping of survey data (Q3-Q4)

After the survey was completed, Megan Wyman traveled to Geometrics on September 28, 2014 to receive additional training from Mikhail Tchernychev on the post-processing and mapping of the survey lines using the MagPick and MagMap software. Post-processing includes 1) correcting the Global Positioning System (GPS) points to get sub-meter accuracy on survey locations, 2) correcting for tidal stage (based on tidal stage data downloaded from the nearest NOAA port stations), 3) correcting for fluctuations in the Earth's magnetic field (by subtracting the base station data from Jasper Ridge from our field measures), and 4) removing DC offset between the two magnetometers on the transverse gradiometer.

After post-processing was complete, two types of maps were constructed: total field maps of the local magnetic anomalies and quasi-analytic signal maps (i.e., map of the rate of change in the local magnetic anomalies in nT/m). These maps were created for the surface and deep tows at each survey location (see section 'ii B' below and Appendix A).

C. Fish detection data summary (Q3-Q4)

This project utilizes fish movement behavior data from previous biotelemetry studies carried out both before and after the Trans Bay Cable was installed through the San Francisco Bay. In these studies, fish were tagged with uniquely coded ultrasonic transmitters and detected throughout the San Francisco Bay by receivers attached to bridges or anchored on the channel bottom. These previous biotelemetry studies were conducted between 2005 and 2014 by a range of agencies and organizations, such as UCD, the National Marines Fisheries Service, California Department of Fish and Wildlife, etc.

In Quarter 3, Megan Wyman and Matt Pagel of UCD downloaded fish detections from locations of interest from the SQL database maintained by the Biotelemetry Lab at UCD. Over 3.5 million detections were downloaded from acoustic monitor arrays located at Benicia, Richmond, Bay, and Golden Gate Bridges as well as the San Pablo Bay. The following fish species were included in these detections: Chinook salmon *Oncorhynchus tshawytscha*, steelhead *Oncorhynchus mykiss*, green sturgeon *Acipenser medirostris*, white sturgeon *Acipenser transmontanus*, sevengill sharks *Notorynchus cepedianus*, and striped bass *Morone saxatilis*. In Quarter 4, Megan Wyman and Eric Chapman contacted the owners of these fish detections and obtained permission to use them for the purpose of this study. These fish detections were summarized for each location per year per species between 2005 and 2014 (see section 'ii C' below).

D. Modeling of cable magnetic fields and comparison of empirical and modeled data (Q3-Q4)

In Q4, Rob Kavet and Justin Bell compared the modeled and measured cable-specific anomalies to help assess the predictability of anomalies based on documented load current, cable depth, and several parameters relating to the height of the measurement (or modeling) point above the bay floor, line geometry, cable direction, and the local geomagnetic field. The results of the analysis are presented in section 'ii D' and Appendix I, II.

ii. Significant results, including major findings, developments or conclusions (positive or negative)

A. Magnetometer survey

In total, 475 survey lines were completed with data logging covering 582.4 linear km (Figure 3). Locations included (from approximately north to south: Benicia Bridge, San Pablo Bay, Richmond Bridge, and Bay Bridge).

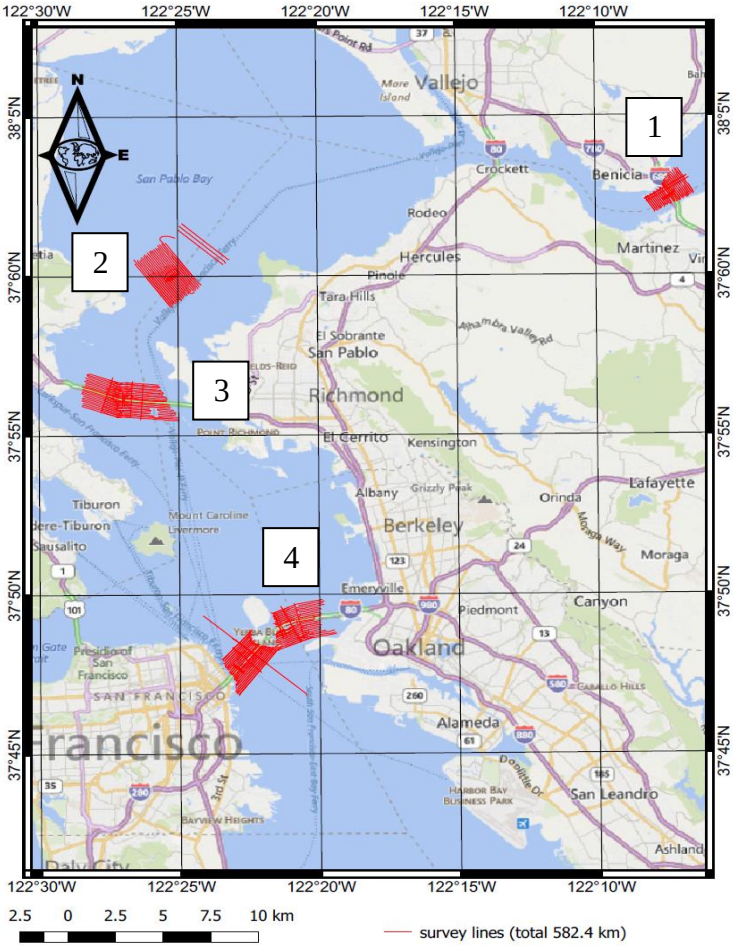

Figure 3. Survey lines (in red) completed in the San Francisco Bay: 1) Benicia Bridge, 2) San Pablo Bay, 3) Richmond Bridge, and 4) Bay Bridge.

B. Post-processing and mapping of survey data

After post-processing the data, we found that the cable is detectable by the magnetometers both at the surface tows and the deep tows. As expected, the cable is more clearly visible in the magnetic field maps of the deep tows than the surface tows. We also found that the bridges significantly distorted the local magnetic field lines. These observations are visible in the total magnetic field maps and quasi-analytic signal maps (e.g., Figures 4-5, see Appendix A for all maps) that were constructed at survey locations from the survey lines running perpendicular to the cable and separated by 100 m. Maps were constructed for both the surface and deep tows. The track of the cable is indicated by the thin red line running across the survey line paths. The measured anomalies associated with the cable can be seen as small peaks in the survey line data from the magnetometers. The bridge distortions are visible as the large purple/blue sections in the middle of the bridge location maps.

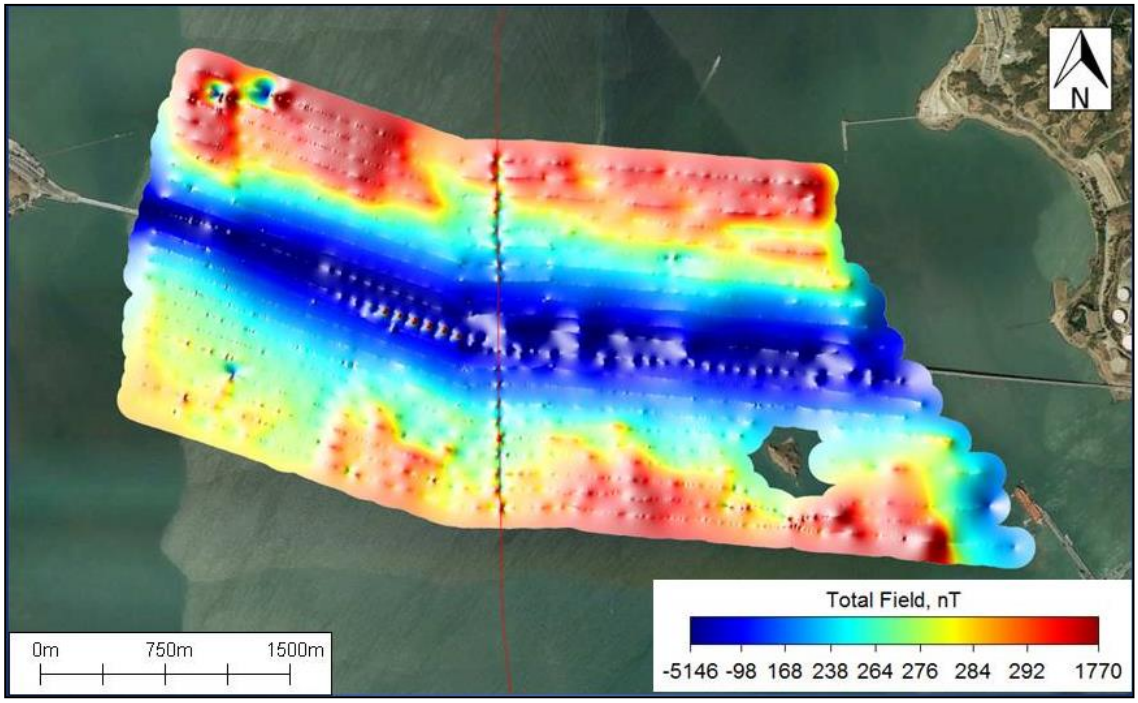

Figure 4. Total magnetic field map of local magnetic anomalies generated by surface tows in Richmond Bridge survey location.

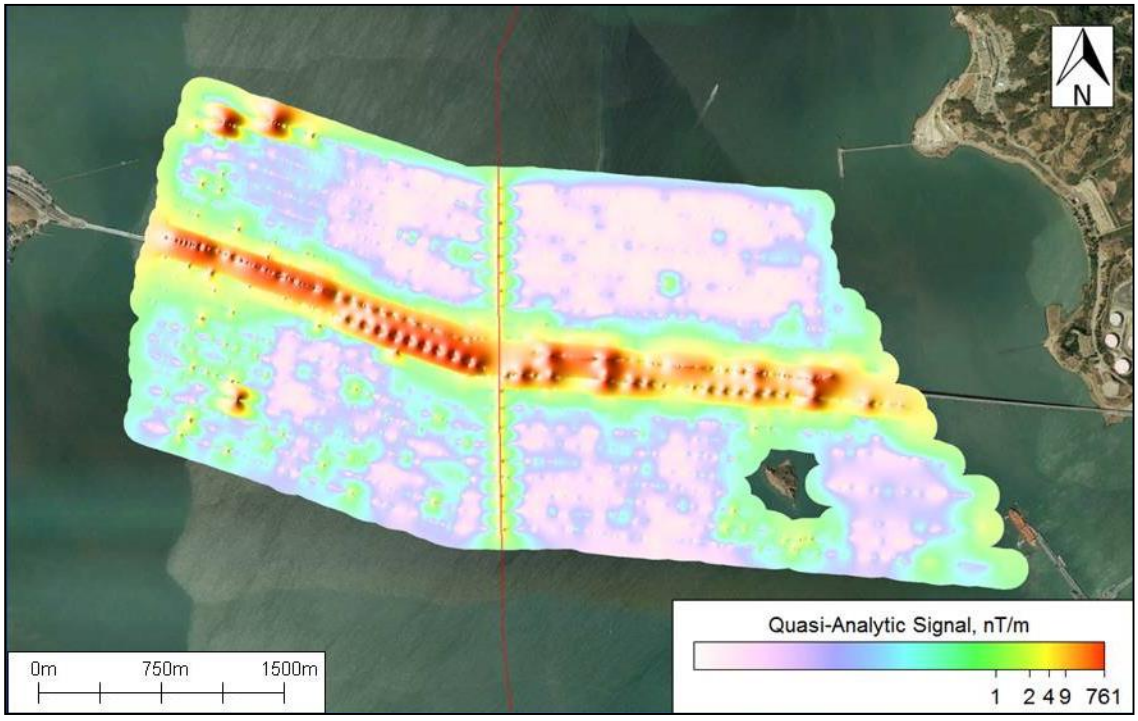

Figure 5. Quasi-magnetic field map of the rate of change in local magnetic anomalies generated by surface tows in Richmond Bridge survey location.

A major aim of this study is to quantify the magnetic field anomalies attributable to the power cable. We define an anomaly as the difference between the maximum and minimum field amplitudes when a measured field profile is clearly associated with the cable (see small arrows in upper panel of Figure 6). In the figure, distance along the survey route is plotted on the X axis (m) and the magnetic field (in nanoTesla or nT) is plotted on the Y axis with the geomagnetic field subtracted). Magnetometer #1 data is in red and magnetometer #2 data is in blue.

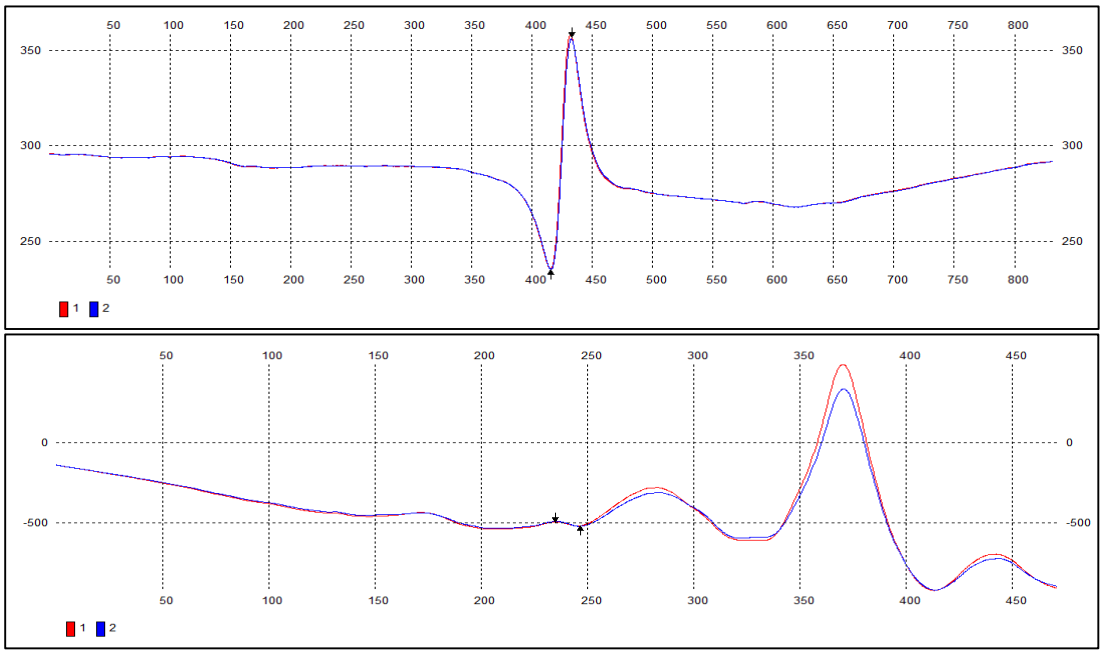

Figure 6. Survey profile line examples from the Richmond Bridge location at approximately 1 km from the bridge (upper) and in close proximity to the bridge (lower).

The anomalies are summarized in Table 1 along with the depth (distance below the surface) and altitude (distance above the channel bottom) of the magnetometers. Amplitudes were only measured in profiles where the anomaly associated with the cable was clearly visible. This was not always possible in the lines closer to the bridges due to the high level of bridge-based distortions. The average amplitude measured during surface tows at the locations ranged from 86.5 nT at Richmond Bridge to 129.83 nT at Benicia Bridge.

Table 1. Summary of magnetic field anomalies associated with TVG cable path. Data includes the amplitude of the anomaly ('MF' in nT) as well as the depth ('Depth' in m) and altitude ('Alt.' m) from magnetometer #2.

	Benicia Bridge			San Pablo Bay			Richmond Bridge			Bay Bridge		
	MF	Depth	Alt.	MF	Depth	Alt.	MF	Depth	Alt.	MF	Depth	Alt.
# Lines	21			21			18			6		
Mean	129.83	0.96	11.68	106.49	0.81	13.88	86.58	1.58	13.7	100.17	1.11	19.82
Median	117.03	0.94	11.67	111.87	0.62	13.93	89.96	1.77	13.78	105.66	1.16	20.21
Min	2.83	0.11	8.1	28.06	-0.08	11.39	22.47	-0.81	9.77	71.03	-0.07	17.66
Max	402.65	2.08	16.42	162.26	2.56	15.52	121.05	3.72	16.91	111.23	2.04	21.67

C. Fish detection summary

Tagged fish species detected at Benicia, Richmond, Bay, and Golden Gate Bridges and San Pablo Bay include: Chinook salmon, steelhead, green sturgeon, white sturgeon, sevengill sharks, and striped bass. Detections were available from 2005 through 2014, depending on the location and species of interest. The acoustic tags in these species are owned by a wide range of agencies/organizations, including the Biotelemetry Lab at UC Davis, National Oceanic and Atmospheric Administration, National Marine Fisheries Service, US Bureau of Reclamation, California Department of Water Resources, California Department of Fish and Wildlife, Oregon Department of Fish and Wildlife, Washington Department of Fish and Wildlife, US Fish and Wildlife, East Bay Municipal Utility District, US Army Corps of Engineers, and H.T. Harvey and Associates.

We have contacted the Principal Investigators or data owners of these groups and obtained permission to use the fish detections summarized in Tables 2-7. The unbracketed number in each cell represents the number of fish detections per location and per year. The bracketed number indicates the number of unique fish present at each location in each year. The dashed lines ('--') present in cells indicate years where monitors were not operational at particular locations. Zeros indicate that no tagged fish were detected at that location in that year. Persistent zeros across locations within the same year suggest that no tagged fish of that species were present in the system in that year. Although we have permission to use all listed detections, we may not ultimately include all in the final analysis as it is important to compare similar groups (e.g., fish size, release location, etc.) both before and after the cable was activated. If comparative data is not available, data may not be included.

Table 2. Fish detection data summary for Chinook salmon.

Year	Benicia Bridge	San Pablo Bay	Richmond Bridge	Bay Bridge	Golden Gate Bridge	SubTotal
2005	--	--	--	--	0	0
2006	--	--	14 [2]	--	52 [6]	66
2007	6014 [80]	--	1047 [43]	1 [1]	1771 [48]	8833
2008	13522 [165]	372 [17]	1170 [76]	333 [14]	2040 [65]	17437
2009	16397 [403]	3556 [174]	4005 [212]	1041 [77]	3385 [165]	28384
2010	159963 [361]	6469 [161]	69425 [214]	2951 [77]	7672 [172]	246480
2011	24105 [53]	2028 [28]	4081 [32]	11989 [16]	692 [24]	42895
2012	13961 [54]	5141 [10]	4839 [35]	1081 [12]	1840 [32]	26862
2013	2326 [7]	--	1183 [6]	353 [2]	134 [3]	3996
2014	1 [1]	--	1 [1]	0	0	2
					Total detections	374955

Table 3. Fish detection data summary for steelhead.

Year	Benicia Bridge	San Pablo Bay	Richmond Bridge	Bay Bridge	Golden Gate Bridge	SubTotal
2005	--	--	--	--	0	0
2006	--	--	0	--	0	0
2007	8320 [53]	--	1298 [38]	149 [5]	1803 [31]	11570
2008	38795 [119]	0	2705 [80]	291 [7]	5526 [72]	47317
2009	6316 [236]	939 [96]	1714 [127]	1727 [67]	988 [103]	11684
2010	4866 [114]	1797 [53]	2223 [99]	695 [32]	2077 [74]	11658
2011	12607 [39]	466 [20]	407 [34]	483 [16]	345 [23]	14308
2012	0	0	0	0	0	0
2013	0	--	0	0	0	0
2014	0	--	0	0	0	0
					Total detections	96537

Table 4. Fish detection data summary for green sturgeon.

Year	Benicia Bridge	San Pablo Bay	Richmond Bridge	Bay Bridge	Golden Gate Bridge	SubTotal
2005	--	--	--	--	10414 [46]	10414
2006	--	--	0	--	1965 [16]	1965
2007	3094 [8]	--	404 [9]	9 [1]	8296 [20]	11803
2008	2525 [11]	0	409 [9]	69 [2]	511 [13]	3514
2009	10601 [22]	3684 [20]	5573 [27]	385 [7]	2941 [26]	23184
2010	13183 [37]	11142 [31]	7687 [38]	1525 [6]	3537 [39]	37074
2011	34932 [37]	7064 [27]	11232 [33]	2363 [9]	3626 [32]	59217
2012	49127 [79]	12353 [45]	285176 [83]	10318 [29]	14364 [83]	371338
2013	38398 [58]	--	78293 [64]	12743 [37]	18649 [60]	148083
2014	5341 [30]	--	88518 [38]	2665 [14]	1580 [24]	98104
					Total detections	764696

Table 5. Fish detection data summary for white sturgeon.

Year	Benicia Bridge	San Pablo Bay	Richmond Bridge	Bay Bridge	Golden Gate Bridge	SubTotal
2005	--	--	--	--	0	0
2006	--	--	0	--	0	0
2007	0	--	0	0	0	0
2008	0	0	0	0	0	0
2009	0	0	0	0	0	0
2010	61686 [56]	10423 [20]	1606 [7]	4638 [4]	2800 [1]	81153
2011	163412 [132]	44135 [49]	183096 [30]	12439 [15]	3534 [9]	223520
2012	163945 [151]	17406 [36]	86296 [30]	6832 [29]	2077 [11]	276556
2013	132623 [102]	--	80148 [20]	6148 [12]	1679 [3]	220598
2014	403690 [88]	--	87323 [21]	10450 [13]	99 [4]	501562
					Total detections	1303389

Table 6. Fish detection data summary for sevengill sharks.

Year	Benicia Bridge	San Pablo Bay	Richmond Bridge	Bay Bridge	Golden Gate Bridge	SubTotal
2005	--	--	--	--	0	0
2006	--	--	0	--	0	0
2007	0	--	0	0	0	0
2008	0	0	0	346 [8]	248330 [21]	248676
2009	0	1298 [2]	1864 [7]	6669 [14]	302555 [18]	312386
2010	0	1 [1]	0	2396 [6]	121393 [6]	123790
2011	0	0	0	2386 [3]	42985 [3]	45371
2012	0	0	0	529 [2]	9187 [3]	9716
2013	0	--	0	11 [1]	77 [1]	88
2014	0	--	0	1 [1]	6 [1]	7
					Total detections	740034

Table 7. Fish detection data summary for striped bass.

Year	Benicia Bridge	San Pablo Bay	Richmond Bridge	Bay Bridge	Golden Gate Bridge	SubTotal
2005	--	--	--	--	0	0
2006	--	--	0	--	0	0
2007	0	--	0	0	0	0
2008	0	0	0	0	0	0
2009	0	0	0	0	0	0
2010	18615 [72]	10892 [48]	20064 [46]	9669 [15]	45 [2]	59285
2011	18264 [55]	7845 [41]	23242 [47]	4463 [21]	280 [3]	54094
2012	12350 [27]	1306 [15]	6630 [25]	762 [10]	20 [2]	21068
2013	10401 [17]	--	10804 [10]	29 [3]	0	21234
2014	3432 [10]	--	15789 [7]	3391 [3]	69 [1]	22681
					Total detections	178362

D. Modeling of cable magnetic fields and comparison of empirical and modeled data (Q3-Q4)

Magnetic Field Basics

Fundamentals

The flow of electrical current through a conductor produces a magnetic field that manifests as invisible lines of force in concentric circles around the conductor. The magnetic field is a vector quantity, meaning that it has magnitude and direction. For this simple example of a single conductor, the field's magnitude (or strength) increases directly proportionally to current decreases as the inverse distance from the conductor; in other words, doubling the distance from the conductor halves the field strength; the equation in Figure 7 describes this relationship (all figures in section D are presented at the end of the section). The magnetic field vector's direction follows the "right-hand rule" whereby when pointing one's thumb in the direction of the current, the fingers will curl approximating the direction of the magnetic vector field attributable to that current flow (Figure 8). The quantity for the magnetic field used in this report is technically referred to as the *magnetic flux density*, symbolized by *B*. The international unit of magnetic flux density is the tesla (T). In this study, the most commonly used unit will be microtesla (μT, one millionth of a tesla, 10^{-6} T) or nanotesla (nT, one billionth of a tesla, 10^{-9} T). In the US, the English unit of milligauss (mG) is often used (1 μT=10 mG). The term magnetic

field will be synonymous with magnetic flux density. There is another quantity referred to as magnetic field intensity, expressed as *H* in units of amperes/meter (A/m). B and H are related to each other by a constant value in air and water, and only B will be used in this report.

Magnetic field vectors from different sources produce an additive field if they point in the same direction, and likewise exhibit at least partial cancellation when pointing in opposite directions with a resulting vector equal to the difference between the two, pointing in the direction of the vector with the greater magnitude. If two opposing vectors are of equal magnitude at a particular point in space, they totally cancel one another, as if no field were present at all at that point (Figure 9). A magnetic field in space can be deconstructed into vectors along the x-, y- and z-axes, with the total, or *resultant*, calculated as follows:

$$B_{Resultant} = \sqrt{B_x^2 + B_y^2 + B_z^2} \quad (1)$$

The term, *frequency*, refers to the number of times line voltage and/or its current (load) reverses polarity each second. For example, the AC (alternating current) electrical system in the US operates at 60 Hertz (Hz), with Hz signifying cycles per second. The Trans Bay Cable is DC (direct current) or 0 Hz (like a flashlight battery), with one of its two conductors (or poles) energized at +200,000 volts or 200 kilovolts (kV) and the other at -200 kV, for a total voltage of 400 kV. The line is rated at 400 megawatts (MW). Since power, P=voltage x current, one would calculate that the line is designed to carry $4x10^6/400x10^3$=1,000 amperes (A). The current, however, fluctuates with load demand, and is not constant over time (like the line voltage), but in practical terms, it can also be considered DC.

Fields from a Direct Current Cable

With these principles in mind, power cables such as the Trans Bay DC line produce fields that can be modeled with fundamental vector computations. Figure 10 is a sketch of the Trans Bay Cable cross-section based on the current information available. Figure 11 illustrates an example of a computation of the magnetic fields from the Trans Bay cable with one line marked by the **x** 0.05715 m (2-¼ inches) to the right of the vertical axis representing 1,000 amperes going into the plane of the figure, and the second line 0.05715 m to the left of the vertical axis (●) representing 1,000 amperes coming out of the plane of the figure; this example assumes a horizontal configuration of the two conductors. Alternatively, one could consider a vertical configuration of the conductors, and examples for each follow.

Suppose one is interested in characterizing the magnetic field vector 0.25 m to the right of the vertical axis and 0.35 m above the horizontal axis due to the currents in the two conductors. Intuitively, because this point in space is closer to the conductor on the right, the field magnitude at that point due to current in the right conductor will exceed the field from the left conductor further away. To calculate the resultant vector, straightforward trigonometry allows one to dissect each contributing vector into their respective horizontal and vertical components, sum the pairs in each direction, and derive the resultant. For both horizontal (left) and vertical (right) configuration examples, the resultant vector (red) has a magnitude lower than either of the two fields from the separate conductors as a result of partial cancellation. Also, for the horizontal configuration, the resultant points in such a manner (up and to the right) reflecting that the horizontal contribution to the field from the right conductor exceeded that from the left conductor, and the vertical contribution from the conductor on the left exceeded that from the right. For the vertical configuration, the resultant points down and to the right, reflecting a

greater influence from the upper conductor. The individual vector values due to each conductor in both cases are similar, but the direction of the resultant is very different.

Another way to display a field map is with an isopleth (or isocontour) map that traces a contour along which the field maintains the same magnitude. For a line such as the Trans Bay (at least as we currently understand its configuration) the isopleths may be approximated very closely by elliptical contours, and with distance, circular patterns may be assumed. When the distance from the line to the measurement point, *r*, is large (~>x10) compared to the separation between the conductors (*s*), the magnetic field, *B*, may be approximated as,

$$B = (I/5) \times (s/r^2) \text{ microTesla } (\mu T), \quad (2)$$

where *I* is the current in each conductor in amperes (A).

For both horizontal (left) and vertical (right) configurations, Figure 12 shows the contours for fields from 0.1 μT to 10 μT (top) and 10 μT to 1,000 μT (bottom). Because the conductors of the Trans Bay Cable are closely spaced there is not much that differentiates the two sets of curves, with the approximation above applicable in most cases (Eq. 2).

Additional field maps, shown in Figure 13, display the contours of a specific magnitude (20 μT in this case), together with the vector headings along that contour for both horizontal and vertical configurations. The vectors point in the direction leading from the contours. The overall contours for both configurations are virtually identical, but the line configuration determines the vector headings around the contour, as exemplified in Figure 11.

The Cable Field Combined with the Geomagnetic Field

The magnetic field from the Trans Bay Cable does not exist in isolation, as it coexists with the DC magnetic field produced by the Earth or the geomagnetic field (Figure 14). This field originates mainly from the Earth's core but also has sources from magnetic materials in the Earth's crust. In the San Francisco Bay, the field has a total magnitude of about 48.8 μT, with a vertical component (i.e., perpendicular to the Earth's plane) of about 42.8 μT, pointing into the Earth (down); a component pointing east with a magnitude of about 5.6 μT; and a component pointing north with a magnitude of about 22.7 μT. Beyond a few meters from the Trans Bay Cable, the Earth's field is clearly dominant (compare to values in Figure 12), and the cable's presence manifests as a perturbation or "anomaly" in the ambient field. The manner in which the two fields combine is represented in Figure 15. In this hypothetical case, the cables field adds to the Earth's field in the east direction and partially cancels in the north and vertical directions.

Quantifying the Anomaly Attributable to the Trans Bay Cable

In July and August of 2014, the UC Davis team conducted magnetic field surveys across various locations in the San Francisco estuary, including areas around the Bay Bridge, the Richmond-San Rafael Bridge, San Pablo Bay, and the Benicia Bridge. The survey vessel dropped a pair of magnetometers (described elsewhere) into the water, with the system recording the latitude-longitude position of each measurement and the height of the magnetometers above the bottom of the bay.

The formulas that follow determine the total field at any point, assuming that the only influences to the total field are the cable and the earth. The parameters for the fields from the cable are defined as follows in Table 8:

Table 8. Parameters for computing field from DC cable

Parameter	Symbol	Units
Current	I	Amps (A)
Conductor separation	s	meters (m)
Height of magnetometer above bottom (Figure 16)	h	m
Buried depth of cable (Figure 16)	a	m
Lateral distance of magnetometer from cable (Figure 16)	x	m
Cable twist (Figure 17)	Θ	radians
Profile angle relative to East-West (Figure 17)	Φ	radians
North component of cable field	$B_{LineNorth}$	μT
East component of cable field	$B_{LineEast}$	μT
Vertical component of cable field	$B_{LineVertical}$	μT

Thus,

$$B_{LineNorth}=(I/5)*SIN(\Phi)*\{((h+a)-(s/2)*SIN(\Theta))/[(x-(s/2)*COS(\Theta))^2+((h+a)-(s/2)*SIN(\Theta))^2]-((h+a)+(s/2)*SIN(\Theta))/[(x+(s/2)*COS(\Theta))^2+((h+a)+(s/2)*SIN(\Theta))^2]\} \quad (3)$$

$$B_{LineEast}=(I/5)*COS(\Phi)*\{((h+a)-(s/2)*SIN(\Theta))/[(x-(s/2)*COS(\Theta))^2+((h+a)-(s/2)*SIN(\Theta))^2]-((h+a)+(s/2)*SIN(\Theta))/[(x+(s/2)*COS(\Theta))^2+((h+a)+(s/2)*SIN(\Theta))^2]\} \quad (4)$$

$$B_{LineVertical} =(I/5)*\{(x-(s/2)*COS(\Theta))/[(x-(s/2)*COS(\Theta))^2+((h+a)-(s/2)*SIN(\Theta))^2]-(x+(s/2)*COS(\Theta))/[(x+(s/2)*COS(\Theta))^2+((h+a)+(s/2)*SIN(\Theta)]^2)\} \quad (5)$$

Then, with the north, east and vertical components of the geomagnetic field defined as $B_{GeoNorth}$, $B_{GeoEast}$, and $B_{GeoVertical}$, respectively, the magnitude of the total field, B_{Total}, is:

$$B_{Total} = [(B_{LineNorth}+B_{GeoNorth})^2+(B_{LineEast}+B_{GeoEast})^2+(B_{LineVertical}+B_{GeoVertical})^2]^{0.5} \quad (6)$$

The geomagnetic field, $B_{GeoTotal}$ is calculated as:

$$B_{GeoTotal} = (B_{GeoNorth}^2+B_{GeoEast}^2+B_{GeoVertical}^2)^{0.5} \quad (7)$$

Finally, the ***anomaly*** itself is expressed as B_{Net}, which is $B_{GeoTotal}$ subtracted from B_{Total}:

$$B_{Net} = B_{Total}-B_{GeoTotal} \quad (8)$$

The expressions provide a characterization of either B_{Total} or B_{Net} versus lateral distance, x. Appendix I provides an example of how B_{total} versus x varies with Θ and Φ. B_{Net} is easily derived by subtracting the ambient geomagnetic field. In addition to Θ and Φ having an effect on the shape of the anomaly, a final chart in the appendix indicates how, the magnitude of the anomaly (maximum field minus minimum field) is a function of Θ and Φ. The examples in the appendix assume a value of 5 m for h and 0 m for a (i.e., unburied cable), and the anomaly decreases with the inverse square of h.

Magnetic Field Surveys

Methods

To illustrate the modeling methodology, the following discussion focuses on measurements in 2014 taken with the two magnetometers deployed from the survey vessel on July 28 (Day 1) and July 29 (Day 2) in San Pablo Bay (SP), and on August 1 (Day 3) and August 4 (Day 4) north and

south of the Richmond-San Rafael Bridge (RSR). For each magnetometer (1 and 2), the raw data for each measurement point included:

- Profile number
- Latitude and longitude (degrees)
- z1 and z2, the magnetometers' depth beneath the surface (m)
- ALT1 and ALT2, the magnetometers' heights above bottom (m)
- T1 and T2, the magnetic field (nanoTesla, nT; 1,000 nT= 1 μT)
- A single date and time stamp for each pair of data points

A total of 21 profiles were collected in SP Bay, 13 on Day 1 and 8 on Day 2, and 20 were collected at the RSR Bridge, 11 on Day 3 and 9 on Day 4. The objective of the exercise was to conduct regressions of the observed field profiles (field versus distance) using the theoretical relationships in Equations 3 through 8 to derive estimates of current (I), twist angle (Θ), and line depth (a). The angle of the profile relative to East-West was observed empirically and was nominally 0° for RSR and -53° for SP. Distance along the profile was determined by transforming the difference between the latitude and longitude of successive measurement points into an interval (meters) using the haversine formula, and transforming each latitude longitude pair into a cumulative distance across the profile. Thus, the distance, d, between two points located at LAT1/LONG1 and LAT2/LONG2 is:

$$d=\{2*6371*ASIN[SQRT\{(1-COS(2\pi*LAT2/360-2\pi*LAT1/360))/2+COS(2\pi*LAT1/360)*COS(2\pi*LAT2/360)*(1-COS(2\pi*LONG2/360-2\pi*LONG1/360))/2\}]\}*1000 \text{ meters} \quad (9)$$

where 6,371 is an estimate of the Earth's radius in kilometers.

For those profiles with a clear anomaly above the cable crossing, a nominal estimate of the point designated x=0 m (an estimate of the center of the line, see Figure 16) was assigned as the value of d corresponding to the average of the distances of the maximum and the minimum fields within the anomaly. A nominal reference (approximate zero) value of the magnetic field was obtained by subtracting the crude average field across the profile from each measurement point. Then, to perform the regression the profile was truncated to extend from between x = -100 to -75 m TO +75 to +100 m. This excluded irregular field patterns beyond these distances to allow a "cleaner" regression of the anomaly.

The curve fittings were performed on the non-linear regression platform of JMP, Version 5.0.1. The cable separation used was 0.1143 m (~4-½ in) and the distance from the magnetometer to the bottom, h, was regressed with every measurement point to derive a, line depth. The components of the Earth's field for the measurement locales were obtained from the NOAA website, http://www.ngdc.noaa.gov/geomag-web/#igrfwmm. In addition to the I, Θ and a, the regression used two fitting parameters (not shown) to transpose the fitted curve horizontally (x, distance from center of line) and vertically (B, the magnetic field) to match the observed anomaly as closely as possible.

Results

By convention, the profiles shown left to right on the charts were drawn with the left representing the eastern (or southeastern) end of each profile. This may be a bit confusing, but the results are not affected, and having a convention means the currents will not change polarity

(and the angles will not flip) as one "switchbacks" between successive profiles. The numbers of measured and regressed profiles are listed in Table 9. Profiles that were regressed are shown in Appendix II, displaying both the measured and modeled B_{Net} values for each profile. Profiles that were not regressed were irregular without a clear signature of a cable-specific anomaly, and are shown in Appendix III. Examples of the curve-fitting results for SP and RSR are shown in Figure 18. Profiles RSR09 through RSR13 straddle the bridge, and display transitional profiles RSR09 and RSR13 that display an indication of a cable fingerprint; RSR 10 through 12 closer to the bridge give no such indication. In addition, this appendix has a profile labeled "Path 22" taken in another set of measurements near the RSR Bridge that ostensibly shows a pattern of anomalies resulting from evenly-spaced bridge components.

Table 9. Number of Profiles Measured and Regressed

Location	Day	Profiles Regressed	Not Regressed
San Pablo Bay	1 (7/28/14)	11	2
	2 (7/29/14)	5	5
Richmond-San Rafael Bridge	3 (8/1/14)	6	5
	4 (8/4/14)	8	1

As shown in Appendix II, the regressed anomalies were qualitatively superimposed on the measured anomalies. The absolute values of the modeled anomalies were virtually identical to those derived from the regression model, as shown in Figure 19. The distances separating the maxima from the minima were moderately underestimated in the model, with the regression reporting 97.7% (5.6% std dev) of the observed value for SP, and 95.0% (5.6% sd) for RSR; these values were not significantly different from each other (p>0.2). The trend for underestimation by the model is shown in Figure 20 with more points falling below the line of identity than above, especially for RSR.

The descriptive statistics for the values I, Θ, and a derived from the regressions are shown in Figures 21, 22 and 23, respectively. At SP, the computed load current, I, was significantly greater (p<0.01) on Day 1 (1,098 A) than Day 2 (827 A) (standard deviations shown in figure); at RSR, the currents on Days 3 and 4 were statistically indistinguishable (average of 849 A) (Figure 21).

The twist angle, Θ, remained relatively constant within each of the two sites, but were significantly different between the two sites (p<0.0001). The angles suggest an approximate vertical orientation that changed between the two sites from 117° at SP to 83° at RSR (Figure 22).

The calculated cable depths, a, were not statistically significantly different from each other between sites or between measurement days. The pooled average was 1.39 m (0.90 m sd) or about 4 feet, 7 inches (Figure 23). The variability in the computed value of this parameter was notable with two of the 30 depths having modest negative values of -0.9 m and -0.4 m, which would physically translate to the cable being above the bottom. This is not surprising as most of the magnetometers' height above the cable ($h_{Total}=h+a$) is accounted for by h (the average of ALT1 and ALT2), with the derived value of a an average of about 10% of h for SP and about an 18% average for RSR. This difference is due to the fact that h had an average value of 13.9 m for SP and 7.7 m for RSR.

The spread in *h*'s values across the two sites allowed a regression of measured and modeled magnetic field to assess how $B_{Anomaly}$ (equal to maximum-minimum difference of the field at the anomaly) attenuated with h_{Total}.

The following model was used for this exercise:

$$B_{Anomaly} = \alpha \times I * h_{Total}^{\beta} * (1 + Dummy_{SP} * 0.048) \quad (9)$$

In other word, $B_{Anomaly}$ is expected to scale with current and attenuate exponentially. Note that an anomaly's magnitude is also determined by Θ and Φ (see Appendix I, last chart). With all else equal (current, height), the anomaly with computed average Θ and assigned Φ for SP would be expected to produce about a 4.8% greater anomaly compared to RSR. Therefore, a dummy variable of 1.0 for the SP profiles was incorporated into the regression.

The regression results are shown in Table 10, and the predicted values for the SP and RSR anomalies based on the regression are plotted against h_{Total} in Figure 24. The key results of this exercise are that (1) the solution for the exponential term, β, is consistent with an inverse square relationship of field with distance from the cable (as one would expect on a theoretical basis), and (2) the values produced by the regression map well to the observed data on a qualitative basis, as indicated in Figure 24. This exercise also lends confidence to the derived estimates of average cable depth, *a*, computed from the individual profiles.

Table 10. Results of Regressing $B_{Anomaly}$ against h_{Total}

Parameter	Estimate	ApproxStdErr	Lower CL	Upper CL
α	0.0239	0.0037	0.0176	0.0328
β	-1.961	0.067	-2.100	-1.827

Discussion

This section of the report described the key basics about DC magnetic fields, how DC power lines (such as the Trans Bay Cable) produce magnetic fields, and how these sum with the geomagnetic field. The analyses presented a methodology for first transforming the raw magnetometry data taken in two areas of the San Francisco estuary into magnetic field into profiles with distance on the horizontal axis, and then regressing (curve-fitting) those profiles with fundamentally-based formulas that characterize the net magnetic field, B_{Net}, in these scenarios. B_{Net} equals the resultant of the vector sums of the cable's fields with the geomagnetic field minus the resultant of the background geomagnetic field (i.e., were the line not present).

The curve fitting resulted in estimates of the load current on the cable, *I*, angle of line twist, Θ, and cable depth, *a*. The regression's solutions produced a good match with the profiles acquired from the magnetometry surveys. The field anomaly attributable to the cable equals the maximum minus the minimum field as the magnetometers pass across the cable's path; these varied between about 0.1 to 0.4 μT (100 to 400 nT). The anomalies resulting from the curve fitting were essentially identical to the measured values (Figure 19).

The model modestly underestimated the distance between the maximum and minimum field locations, with the discrepancy slight greater at RSR (5.0%) than at SP (2.3%) (Figure 20). The modeling formulas (Equations 3 through 8) predict that max-min distance varies linearly with

h_{Total} (not shown), given constant I, Θ and Φ. Consequently, one would expect greater max-min differences at SP than at RSR, as was observed, with a 19.4 m average for SP and a 11.7 m average for RSR; the modeled averages were 18.9 m and 11.1 m, respectively. Any practical implications of this discrepancy are not apparent.

In conclusion, the magnetometry methodology employed in this study detected the magnitudes and spatial patterns of the magnetic field anomalies attributable to the Trans Bay Cable. Furthermore, the anomalies reported by the surveys were consistent with the magnitudes and patterns one would predict from first principles based on the study team's a priori understanding of the line characteristics (nominal loading, conductor separation, and approximate cable depth). The smallest anomalies reported (~0.1 μT or ~100 nT) here were about one-fifth of a percent of the background geomagnetic field (~48 μT or ~48,000 nT), with a clear indication that the magnetometers would resolve smaller line-specific anomalies were the load currents lower than those flowing at the time of the surveys and/or if the magnetometers were deployed at a greater height above the cable. Large metallic structures, such as the Richmond-San Rafael Bridge, perturbed the geomagnetic field in a manner that, in many cases, obliterated any evidence that the cable was present. Such perturbations, which could be many times the cable-specific anomalies, are reported empirically in this study, as modeling them (if practical) is a separate undertaking unto itself.

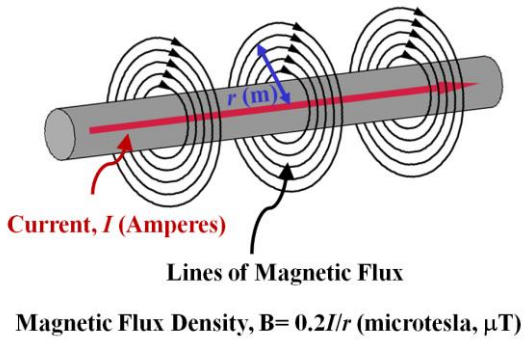

Figure 7. Magnetic field from a single conductor.

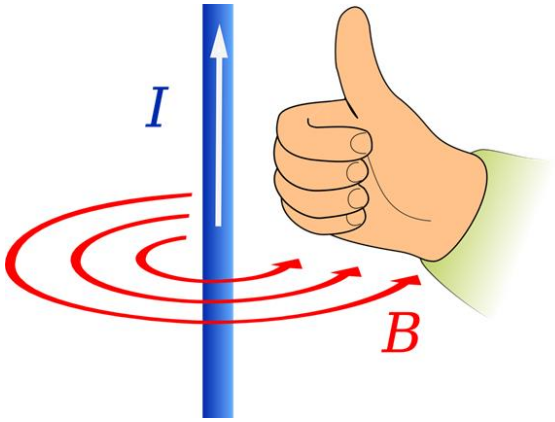

Figure 8. The right-hand rule.

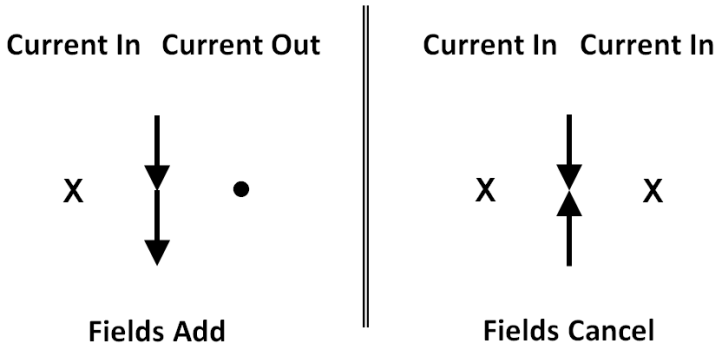

Figure 9. Magnetic fields from conductor pairs with equal amounts current may add (currents opposing directions) or cancel (currents in the same direction). Currents are pictured either going into (X) or out of (●) the figure.

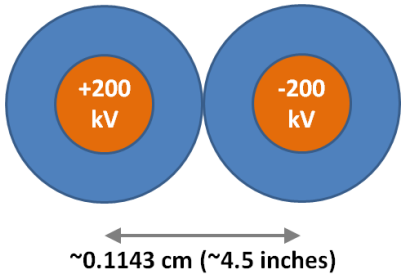

Figure 10. Sketch of presumed cross-section of Trans Bay Cable. One conductor (or pole) is energized to +200 kilovolts (kV) and the other to -200 kV. Operating at 400 megawatts (MW) means that the cable can supply a load of nominally 1,000 Amperes (A).

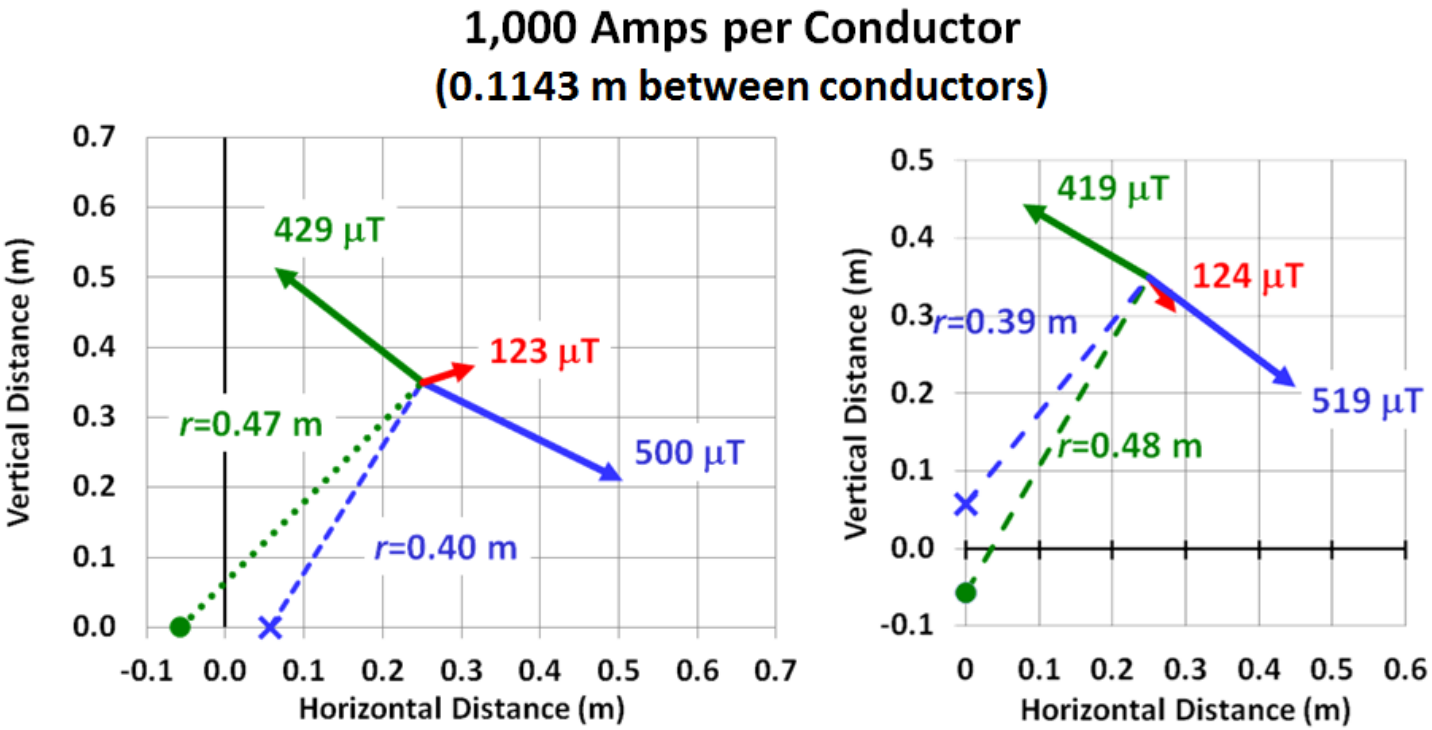

Figure 11. Magnetic field vectors (green and blue arrows) from two conductors each with 1,000 amperes separated by 0.1143 m (~4-½ inches) and their resultant (red arrow). Left: Horizontal configuration. Right: Vertical configuration.

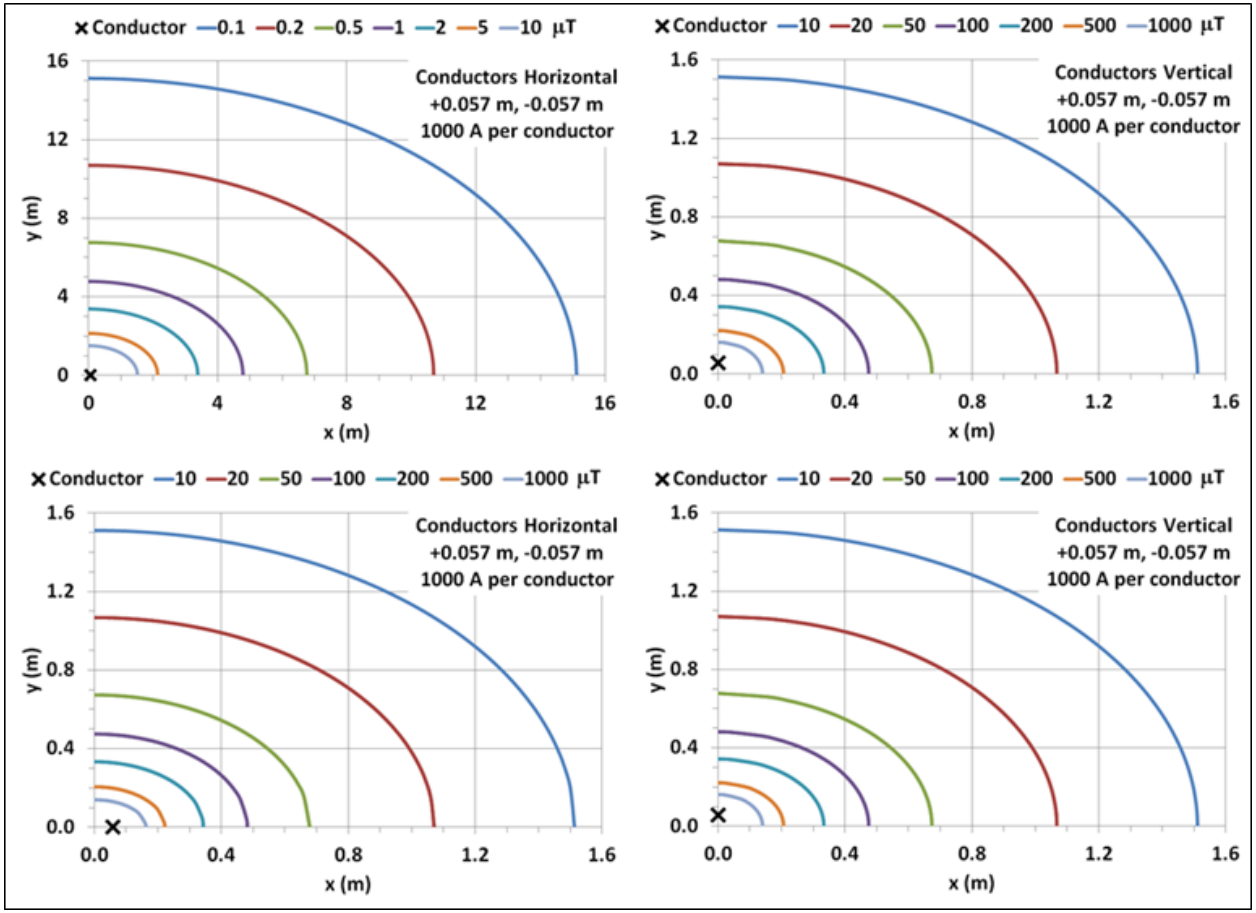

Figure 12. Iso-contours of the field attributable to a DC line. Field magnitudes are constant along each contour. Left: Horizontal configuration. Right: Vertical configuration.

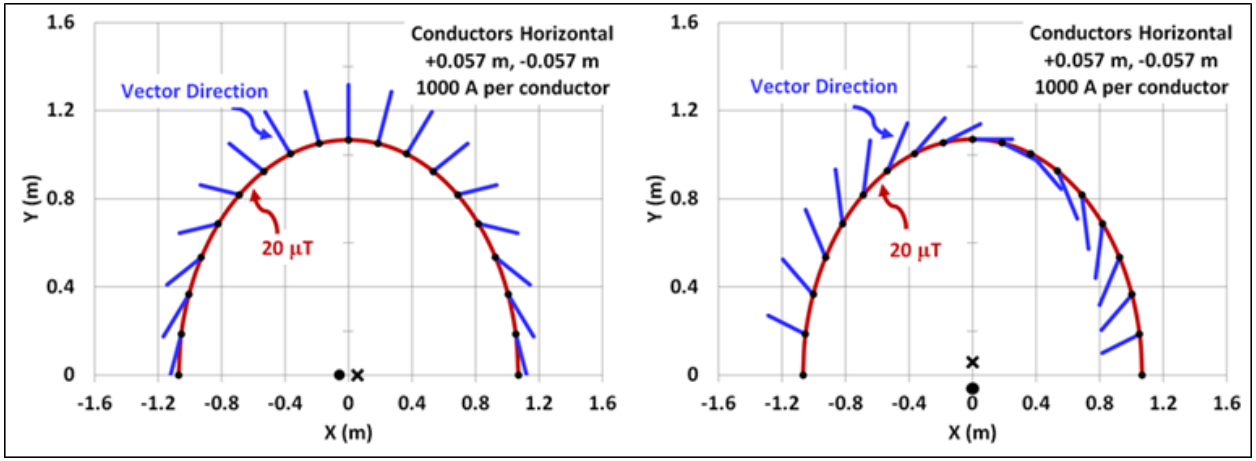

Figure 13. The vector directions around a 20 μT iso-contour produced by the DC cable. The vectors point in the direction away from the contour.

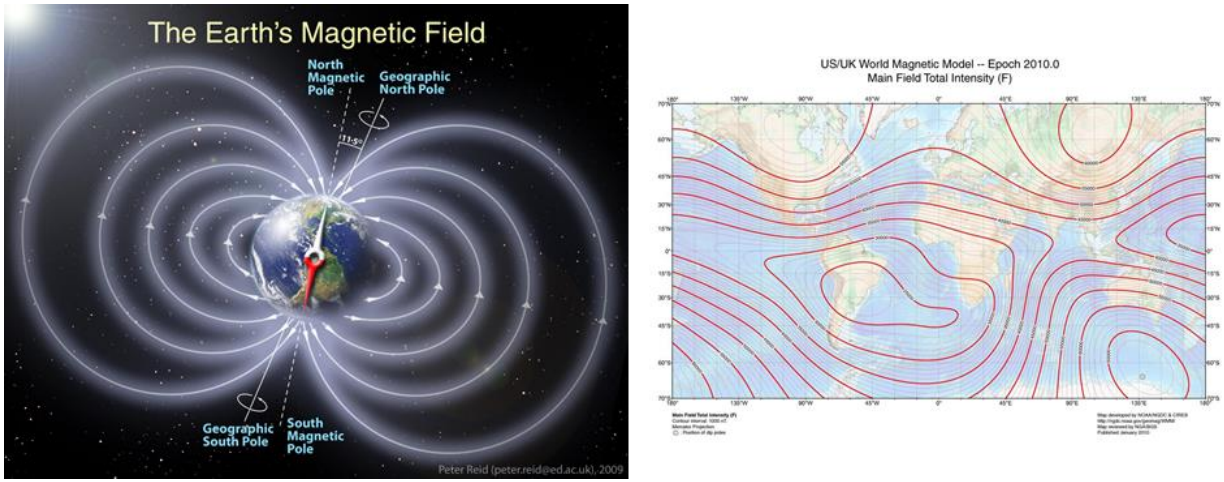

Figure 14. The geomagnetic field. Left: conceptual view from a high elevation above the Earth. Right: Iso-contours of the geomagnetic field at the Earth's surface.

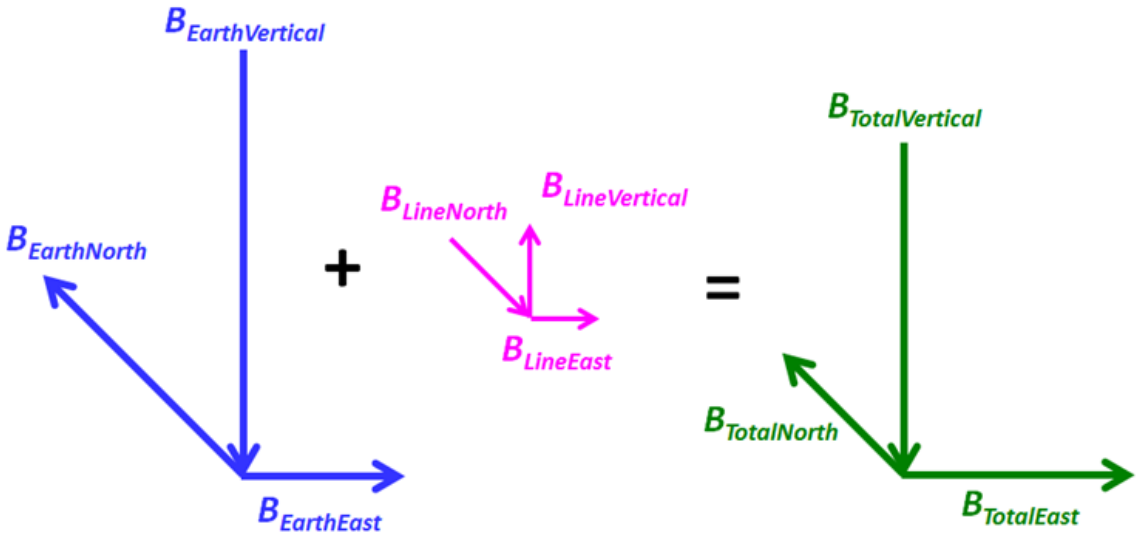

Figure 15. The vector addition of magnetic fields produced by the DC cable with the geomagnetic field.

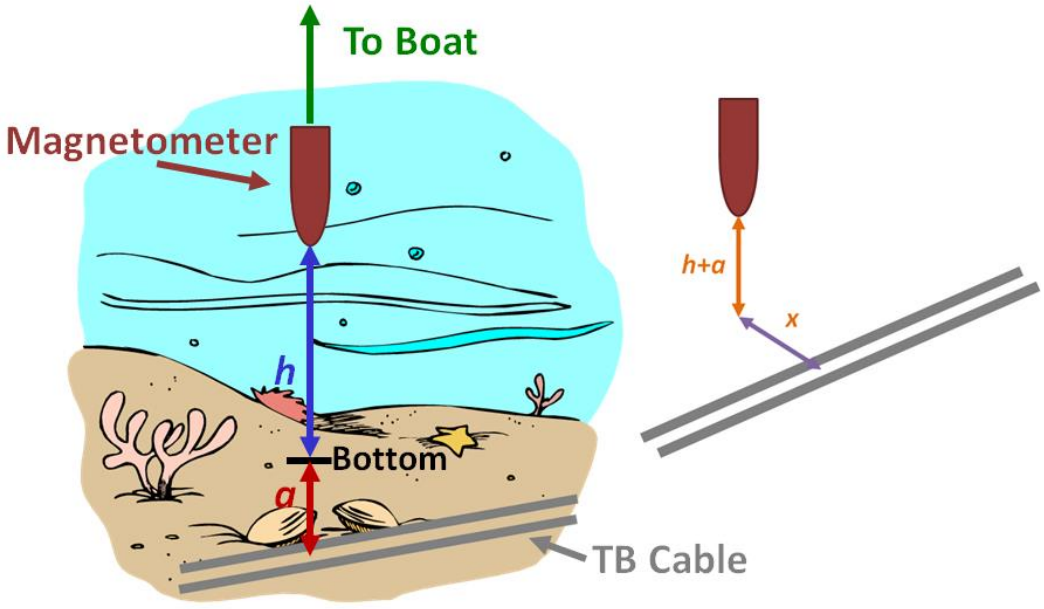

Figure 16. Height of the magnetometer above the bottom of the bay (*h*), cable depth (*a*), and lateral distance (*x*) along a field profile.

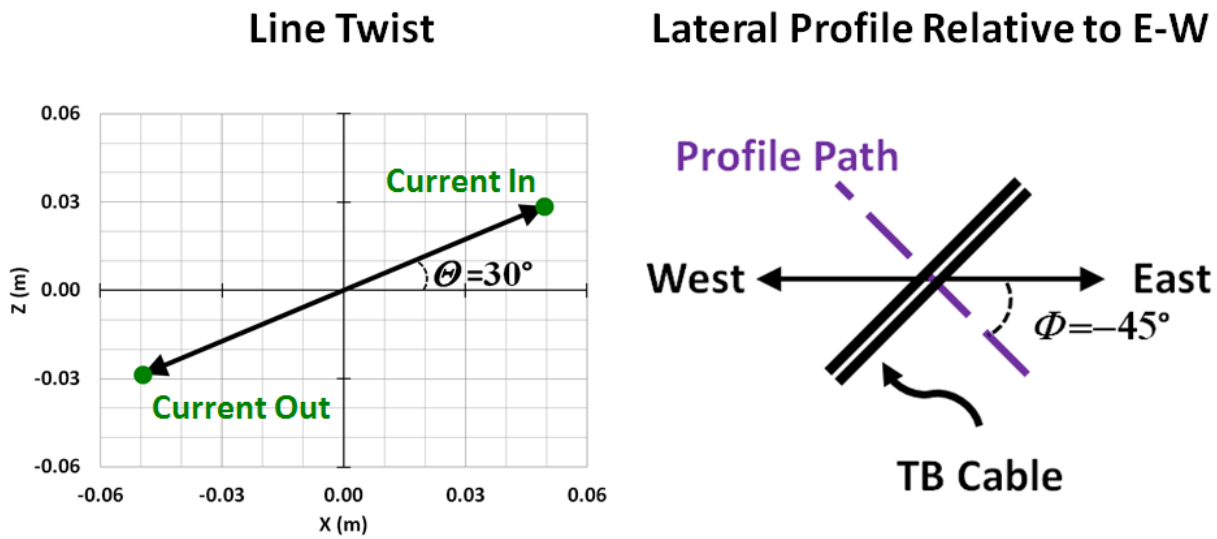

Figure 17. Definition of the angle of line twist (Θ), and the angle of the lateral profile relative to geographic East-West (Φ).

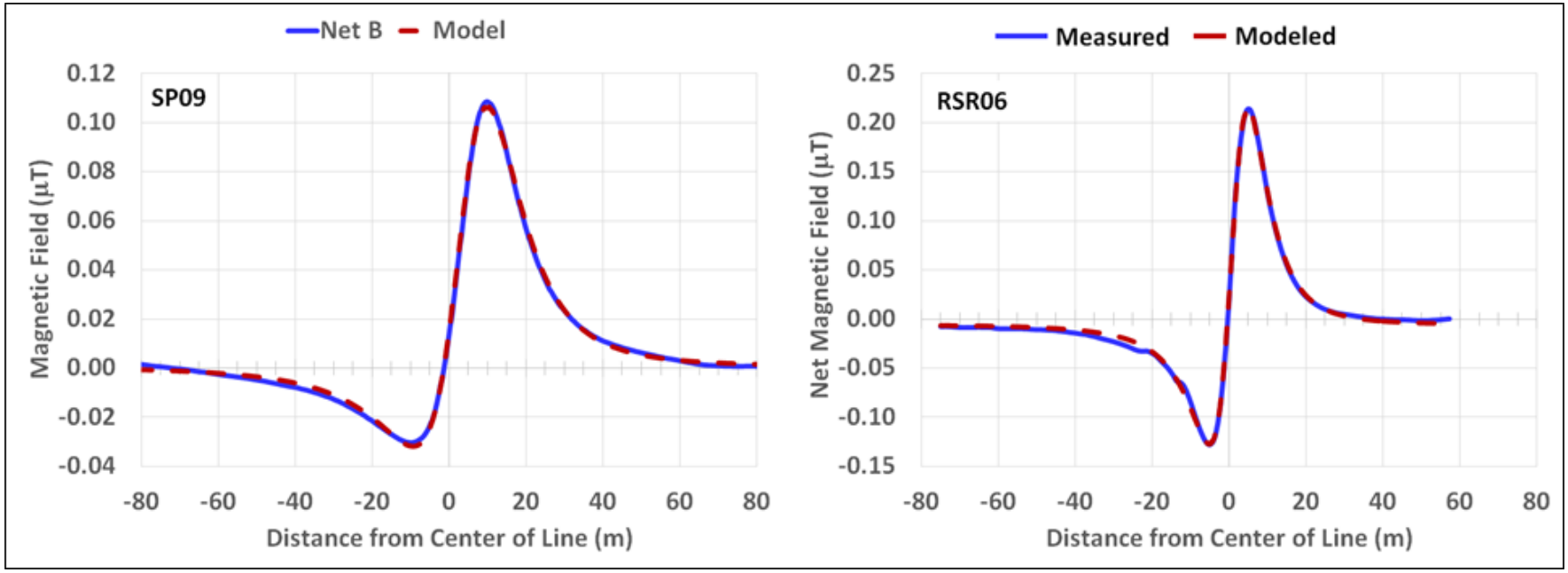

Figure 18. Examples of measured and modeled profiles for SP (left) and RSR (right).

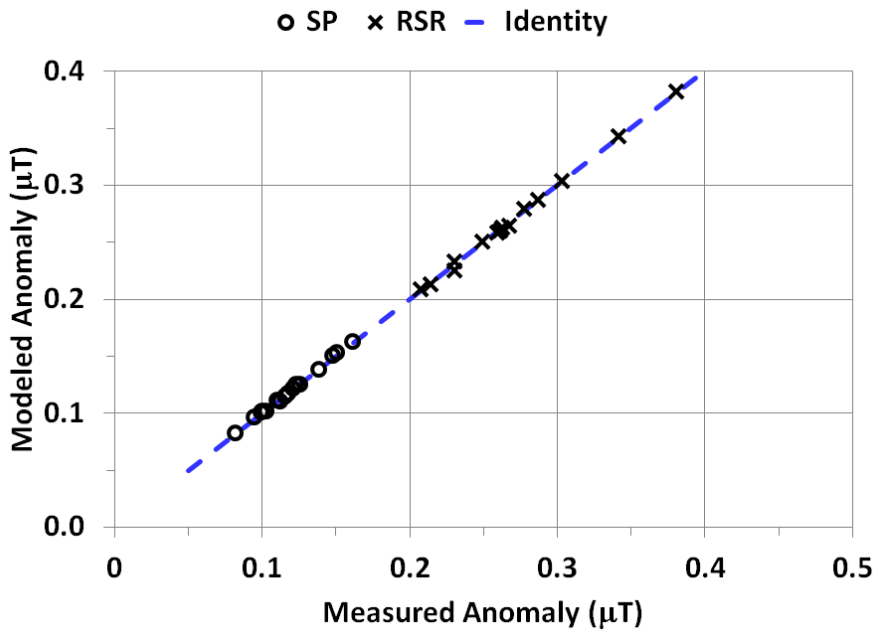

Figure 19. Modeled versus measured anomaly for each profile, defined as the difference between the field's maximum and minimum values.

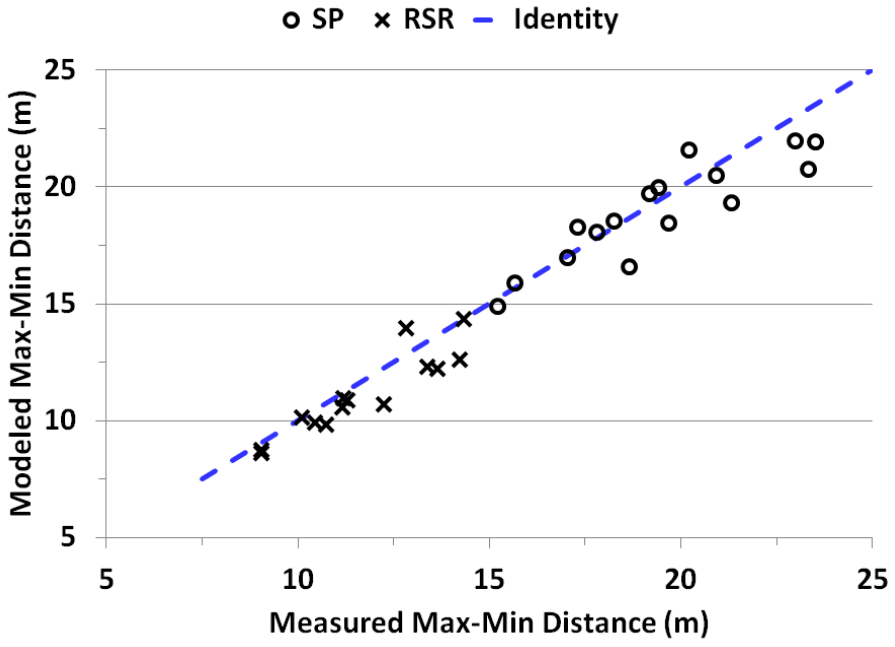

Figure 20. Measured and modeled distances between maxima and minima.

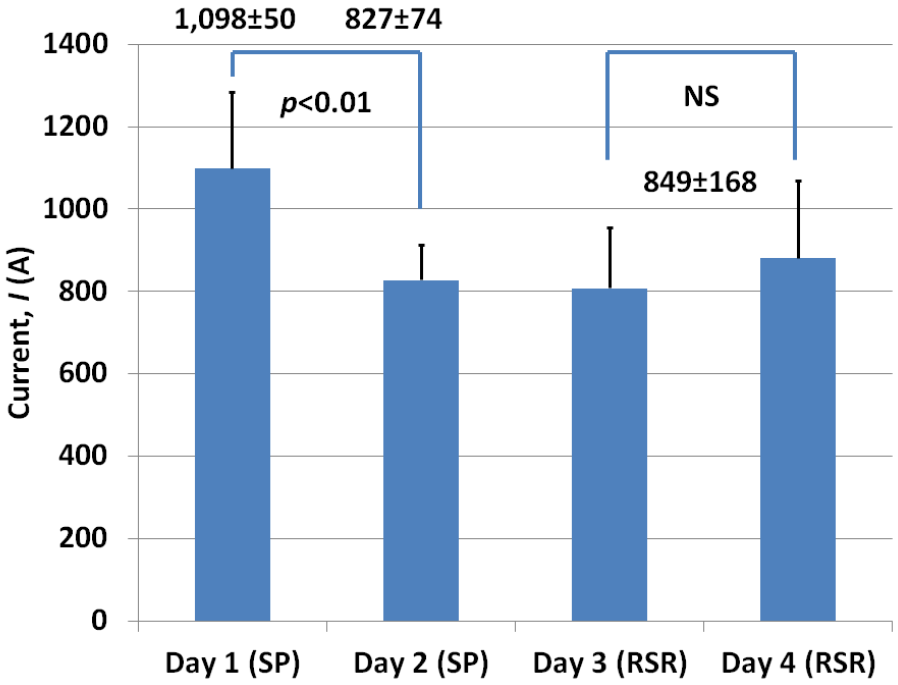

Figure 21. Currents derived from the regression using Eq. 2 through 7.

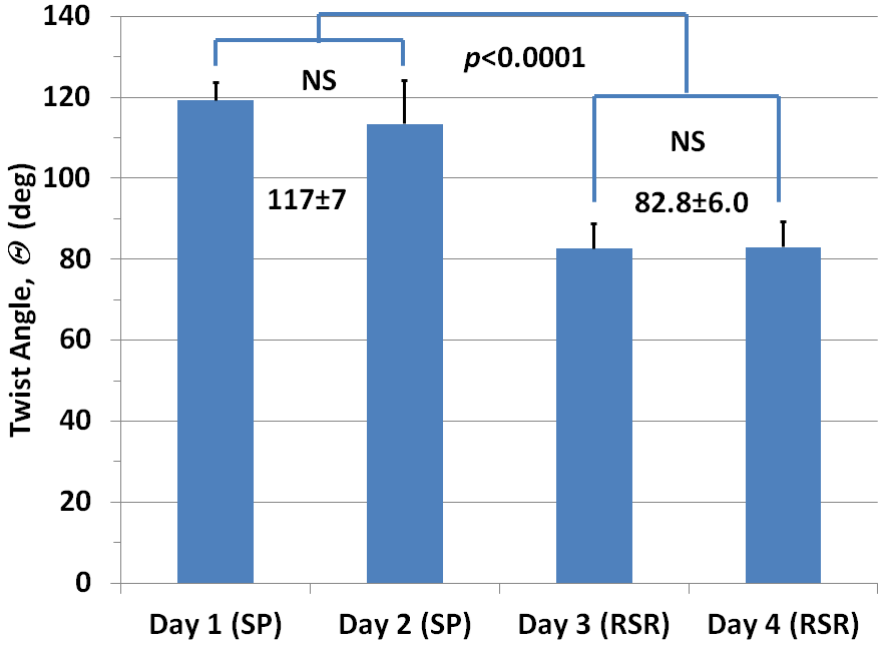

Figure 22. Twist angles derived from the regression using Eq. 2 through 7.

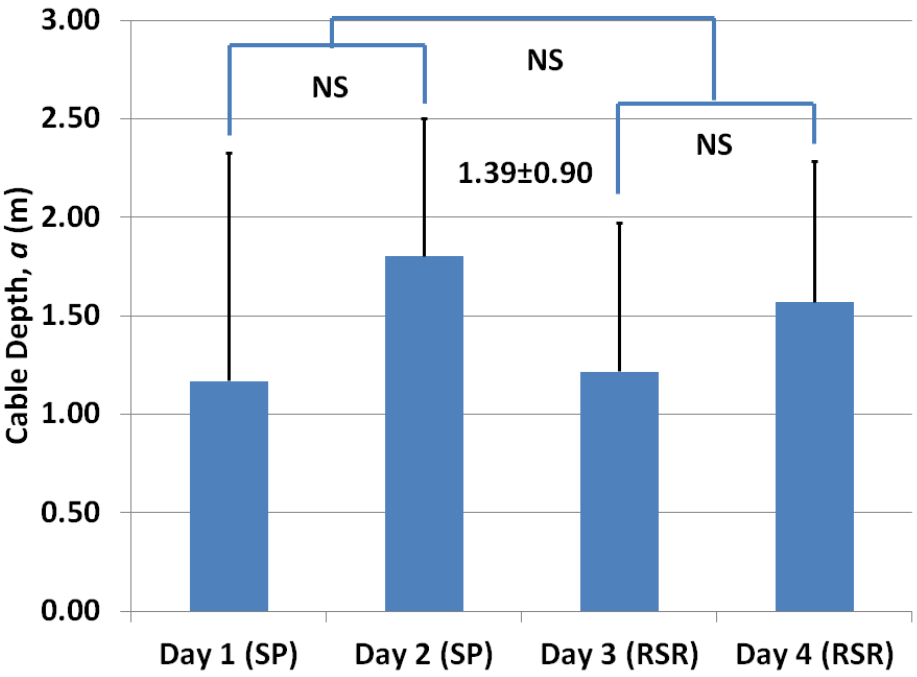

Figure 23. Cable depths derived from the regression using Eq. 2 through 7.

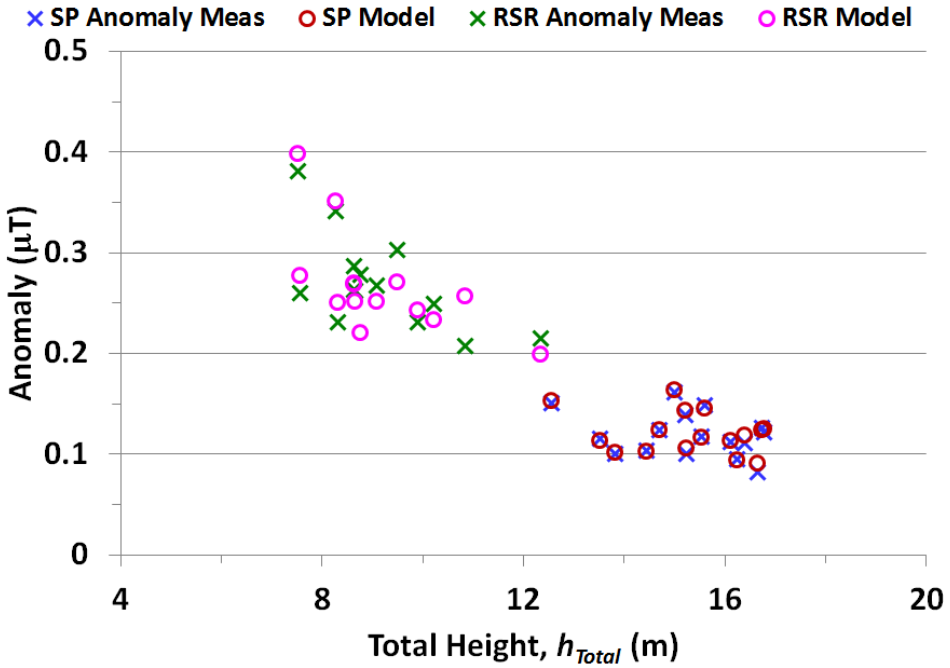

Figure 24. Measured anomaly versus height of magnetometer above the cable ($h_{Total}=h+a$), and anomaly as predicted by the regressed parameters from Eq. 9.

Plans for Year 2

1. Q5, Quantifying environmental factors during fish detection events

Environmental conditions found along the path of fish migration through the San Francisco Bay may vary both spatially and temporally. In order to assess the influence of these factors on fish migration behavior, it is necessary to quantify these variables for the time and location at which fish detection events occurred. These values will be averaged across the detection range of the monitors. Detection ranges vary depending on the size of the tag. As an example, a previous study in the San Francisco Bay area determined that the detection range of large tags (V16, Vemco, Inc., used in adult sturgeon) per monitor was approximately 70-75 m (defined by a detection efficiency of 75%, see Chapman et al. 2009: 2008-2009 Annual Report, University of California Davis and US Army Corp of Engineers).

During this task, we will work to quantify the following environmental factors present at each monitor at the time of fish detection events: magnetic field intensity (e.g., total field, cable field above ambient, distance from cable, and gradient measures), depth, discharge, water speed, water direction, and salinity. Magnetic field data will be based on the theoretical models, empirical field surveys, and load data from the cable at the time of each fish detection. Depth data will likely be based on the published San Francisco Bay, CA (P090) Bathymetric Digital Elevation Model (30 meter resolution) derived from Source Hydrographic Survey Soundings collected by NOAA.

We acknowledge that accurate historic data on discharge, water speed, water direction, and salinity will be difficult to obtain for the locations and times of all past detections. Therefore, we will widen our data collection efforts to include historic and modern data from monitoring sources as close to our sites of interest as possible. While quality historic data is preferable, modern data or survey measurements will at least allow us to, respectively, assess general relationships between tidal stage, currents, and salinity and determine relative current profiles at key tidal stages along the array (i.e., which monitors are likely to experience the highest currents during peak flood period).

Regarding tidal current data, NOAA provides daily tidal current predictions for previous years in their "Tidal Current Tables". These tables list the estimated times, directions, and maximum currents present at the slack and flood tidal stages, as well as guides for calculating the currents at any time of day, for stations at Yerba Buena Island (Bay Bridge), Richmond, Carquinez Straight (West End Bridge), and Benicia Bridge. In addition to using these tables, we will also contact NOAA in an effort to obtain actual values, not just predicted, for the times and locations of interest. In addition, actual tidal and current data are available for numerous sites in the San Francisco Bay since 2012 from Physical Oceanographic Real-Time Systems (PORTS) operated by the National Ocean Service (NOS). Additionally, the California Data Exchange Center provides historic hourly salinity data from a monitoring station at Martinez, west of the Benicia Bridge array, operated by the CA Dept. of Water Resources. We will continue to search out additional environmental data sources over the course of this task.

Overall, since not all environmental factors may be available for the time and location of each fish detection event, we will accordingly adjust the data analysis procedures to accommodate this fact (i.e., salinity may not be included in the analysis models of some arrays if sufficient estimates of this variable cannot be obtained at nearby locations). Ultimately, the estimates of these environmental factors (magnetic field, depth, flow, salinity, etc.) will serve as the independent variable data input for the multivariate models in the subsequent data analysis.

2. Q6-7, Data analysis and synthesis

Data analysis for this project will progress from general tests of distributions to more sophisticated tests assessing which environmental variables predict fish movement behaviors. The final development of these statistical models will be completed in consultation with a statistician at UCD. All statistical tests will be run in the R software package. In complement to the statistical analysis, an ArcGIS-based map (e.g., geo-referenced shapefile) will be produced which includes data on coastline, bathymetry, cable trace, receivers, measured and/or modeled magnetic fields, and fish detections.

For each bridge array, plots of the frequency of detection of tagged fish species at the different monitors will be superimposed on profiles of depth and cable-based magnetic field calculations. The plots will help visualize where individuals of the species are most frequently detected in relation to these environmental factors.

The default condition—that there are no differences in frequency of detection between monitors—will be tested using Chi-Square goodness of fit tests. These tests will be separately conducted per species on both before-cable distributions and after-cable distributions. If there are differences (as highly anticipated in this case), the distributions of detection frequencies across each bridge array will be compared before and after the cable was deployed using non-parametric statistical tests (e.g., Mann-Whitney tests, two-sample Kolmogorov Smirnov tests).

Subsequently, a more detailed generalized linear model (general linear or additive model) will be constructed to determine the relative importance of the different environmental factors in predicting fish movement behavior. Contingent upon available data, the predictor (or independent) variables will include total magnetic field, magnetic field produced by the cable above ambient levels, depth, discharge, water speed, water direction, salinity, and distance from the cable. The response (or dependent) variables, tested within different models, will include residency (or exposure) time at each monitor and the number of detections (or individuals) recorded at each monitor.

To assess if the cable could serve as an obstacle or an aid to navigation during migration movements, we will conduct a transit time analysis. This analysis will compare the amount of time and rates of movement between arrays throughout the San Francisco Bay to determine if the fish moved quicker through the system before vs. after the cable was activated.

3. Q8, Communication of primary results

We will prepare a manuscript for submission to the peer-reviewed literature. The paper will provide the appropriate background; detail the methods used; present the results with descriptive figures and tables, supported by appropriate statistical analysis; and discuss the authors' interpretation and perspectives of their observations.

The topics of the paper will include, but not necessarily be limited to:

- a description of the methods for characterizing the magnetic field, and mapping the fish locations on the field maps; and

- a presentation of the data describing effects of the underwater magnetic field environment on migration and fish behavior.

PRODUCTS / DELIVERABLES

Products / Deliverables: [List any products and/or deliverables resulting from the project during the reporting period.]

Examples of products / deliverables include:

- Publications, conference papers, and presentations [Identify and attach all publications and presentations made for industry or government groups resulting from the award during this quarter. Briefly identify travel accomplished as part of the project, showing number of people, dates of travel and destination];
- Website(s) or other Internet site(s);
- Technologies or techniques;
- Inventions, patent applications, and/or licenses; and
- Other products, such as data or databases, physical collections, audio or video products, software or NetWare, models, educational aids or curricula, instruments, or equipment
- Any other public release of information related to the project.

Products and Deliverables:

1. Magnetic field maps from surface and deep tows of the areas surveyed in the San Francisco Bay, including Benicia Bridge, San Pablo Bay, Richmond Bridge, and Bay Bridge (see Appendix A).

2. Summary of the amplitude of magnetic field anomalies associated with locations where the survey line crossed the cable (see Table 1 and Figure 6 above).

3. Summary of fish detection data by location, year, and species (see Tables 2 - 7 above).

4. Comparison of the measured and modeled magnetic field generated by the TransBay Cable (see Appendix I, II).

Patents: None

PARTICIPANTS & OTHER COLLABORATING ORGANIZATIONS

Individuals:

For each individual, include the following:

- Name & role in the project
- How the individual contributed to the project & with what funding support
- Whether the individual is contributing internationally

Name	Rob Kavet
Project Role	Project Manager and Principal Investigator
Nearest Person Month worked	0.815 months (150 hours over 3 month period)
Contribution to Project	R. Kavet has conducted the comparison of the modeled and empirical magnetic field data, lead the project organization, lead communications between DOE/BOEM and team members, and communicated with TransBay Cable for access to necessary data.
Funding Support	
Collaborated w/ individual in foreign country	No
Country(ies) of foreign collaborator	
Traveled to foreign country	No
If traveled to foreign country, duration of stay	

Name	A. Peter Klimley
Project Role	Co-PI at the university level for this project
Nearest Person Month worked	0.764 months (roughly 130 hours over 3 month period)
Contribution to Project	A. P. Klimley has contributed his expertise in biotelemetry to methodological discussions with other team members, provided advice on magnetic surveys based on past experience.
Funding Support	
Collaborated w/ individual in foreign country	No
Country(ies) of foreign collaborator	
Traveled to foreign country	No
If traveled to foreign country, duration of stay	

Name	Megan Wyman
Project Role	Postdoctoral Researcher
Nearest Person Month worked	3 months (100% time on the project)
Contribution to Project	M. Wyman has completed the magnetometer

	survey in the SF Bay, post-processed the survey data, created magnetic field maps of surveyed areas, summarized past fish detections in the SF bay, and co-written the progress report.
Funding Support	
Collaborated w/ individual in foreign country	No
Country(ies) of foreign collaborator	
Traveled to foreign country	No
If traveled to foreign country, duration of stay	

Name	Justin Bell
Project Role	Project Consultant
Nearest Person Month worked	0.054 months (10 hours over 3 month period)
Contribution to Project	Worked on developing models of magnetic fields in the locations of the fish detection arrays based on available data and survey results.
Funding Support	
Collaborated w/ individual in foreign country	No
Country(ies) of foreign collaborator	
Traveled to foreign country	No
If traveled to foreign country, duration of stay	

Organizations:

- Electric Power Research Institute, Palo Alto, CA
- Contribution to the Project
  - Primary contractor
  - Cost share
  - Collaborative research

- University of California: Davis, CA (subcontractor)
- Contribution to the Project
  - In-kind support
  - Facilities
  - Collaborative research

IMPACT [OPTIONAL]

Discuss the impact of this project relative to:

- The development of the principal discipline(s) of the project;
- Other disciplines;
- The development of human resources;

- Physical, institutional, and information resources that form infrastructure;
- Technology transfer (include transfer of results to entities in government or industry, adoption of new practices, or instances where research has led to the initiation of a startup company); or
- Society beyond science and technology.

CHANGES / PROBLEMS

Discuss the following if applicable:

- Changes in approach and reasons for change.
- Actual or anticipated problems or delays and actions or plans to resolve them.
- Changes that have a significant impact on expenditures.
- Significant changes in use or care of animals, human subjects, and/or biohazards.

BUDGETARY INFORMATION

Complete the following tables in the Excel template accordingly (see Attached):

- Spending Summary – TAB B
- Cost Share Contributions – TAB C
- Spend Plan Data – TAB D

Project Schedule & Milestones

DE-EE0006382.000

SOPO Task Number	Title / Task Description	Task Completion Date				Progress Notes
		Original Planned	Revised Planned	Actual	Percent Complete	
1	Development of a detailed work plan	3/31/2014	3/31/2014	4/15/2014	100%	Finished for RPPR Q1
2	Collect magnetic field measurements in SF Bay	6/30/2014	6/30/2014	9/30/2014	100%	Survey completed Aug 8, 2014
3	Download and describe fish detections within SF Bay	9/30/2014	9/30/2014	9/30/2014	100%	Fish detections are summarized
2 & 3	Summary of 1) qualitative comparison of measured and modeled magnetic field data and 2) fish detection data	12/31/2014	12/31/2014	12/31/2014	100%	Measured and modeled data and fish detection data reported in "Go/No-Go" Report submitted in December (w/follow-up webcast in Jan)
4	Acquire data on other environmental factors, such as flow, bathymetry, salinity, etc.	3/31/2015	3/31/2015		0%	
5	Data analysis: final model selection. Select the final statistical models for data analysis	6/30/2015	6/30/2015		0%	
5	Data analysis: fitting data into models. Fish behavior will be analyzed in relation to magnetic field magnitude and other environmental factors	9/30/2015	9/30/2015		0%	
5	Map of georeferenced measurements	9/30/2015	9/30/2015		0%	
6	Communication of primary results. Primary results will be submitted to peer-reviewed literature; follow-up papers may be submitted past the period of performance	12/31/2015	12/31/2015		0%	
7						
8						
9						
10						

Appendix A
Total magnetic field maps and quasi-analytic signal maps

In total, 475 survey lines were completed with data logging covering 582.4 linear km (Figure 1). Locations included (from approximately north to south: Benicia Bridge, San Pablo Bay, Richmond Bridge, and Bay Bridge). After post-processing was complete, two types of maps were constructed from the survey data: total field maps and quasi-analytic field maps of the local magnetic anomalies. The total field maps depict the measured local magnetic anomalies after the Earth's magnetic field (as measured from the Jasper Ridge station) is subtracted from the field measures. The quasi-analytic signal maps depict the rate of change in the local magnetic anomalies in nT/m. These two types of maps were created for the surface and deep tows at each survey location (Figures 2-5). Deep tows were only conducted in areas where the magnetometers were more than 10 m above the channel bottom during the surface tows.

In each map, the track of the cable is indicated by the thin red line running across the survey line paths. The measured anomalies associated with the cable can be seen as small peaks in the survey line data from the magnetometers. The bridge distortions are visible as the large purple/blue sections in the middle of the bridge location maps.

The anomaly associated with the cable is visible in both the surface and deep tows in all locations. As expected, it is detected more strongly in the deep tows which are closer in proximity to the cable. The cable anomaly was weakest in the surface tows at the Bay Bridge location due to high distortion from other magnetic sources in the area. For instance, the underground route of the Bay Area Rapid Transit (BART) system is clearly visible as the large linear anomaly running southwest to northeast through the survey area.

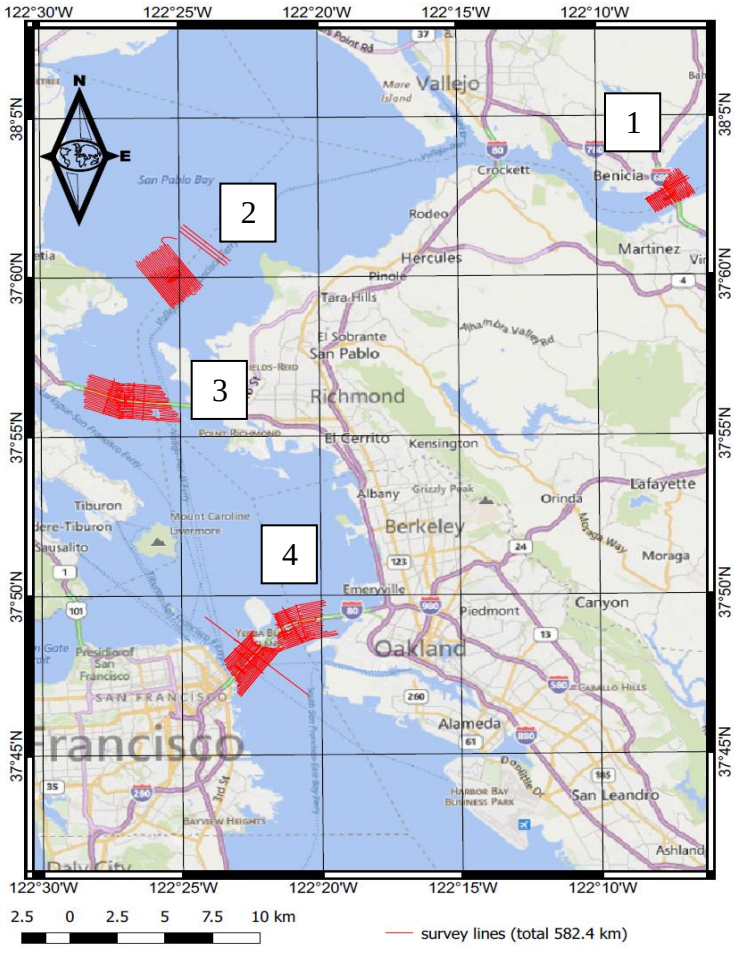

Figure 1. Survey lines (in red) completed in the San Francisco Bay: 1) Benicia Bridge, 2) San Pablo Bay, 3) Richmond Bridge, and 4) Bay Bridge.

Figure 2. Benicia Bridge: Total field maps of surface tows (upper left) and deep tows (lower left) and quasi-analytic signal maps of surface tows (upper right) and deep tows (lower right).

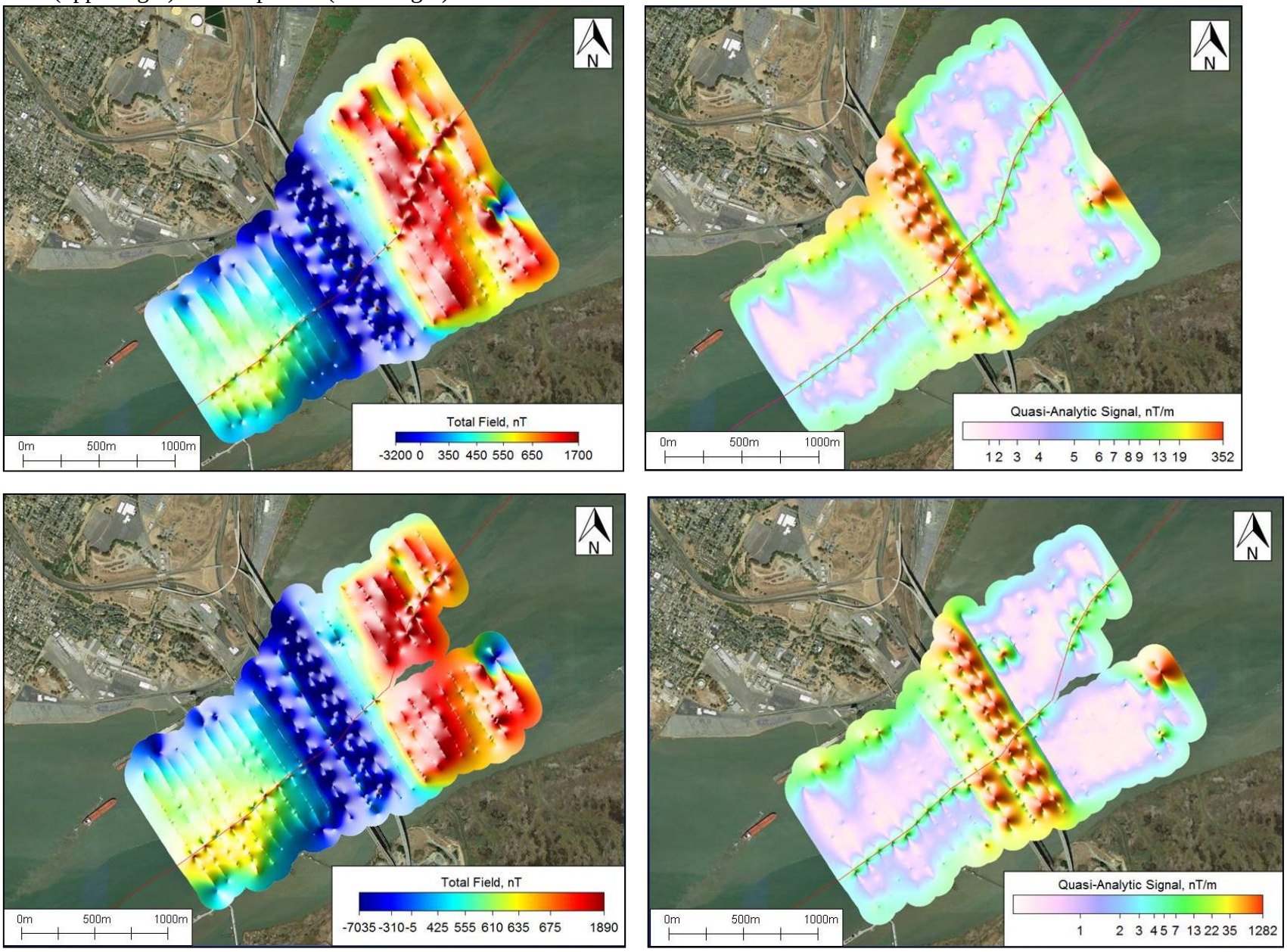

Figure 3. San Pablo Bay: Total field maps of surface tows (upper left) and deep tows (lower left) and quasi-analytic signal maps of surface tows (upper right) and deep tows (lower right).

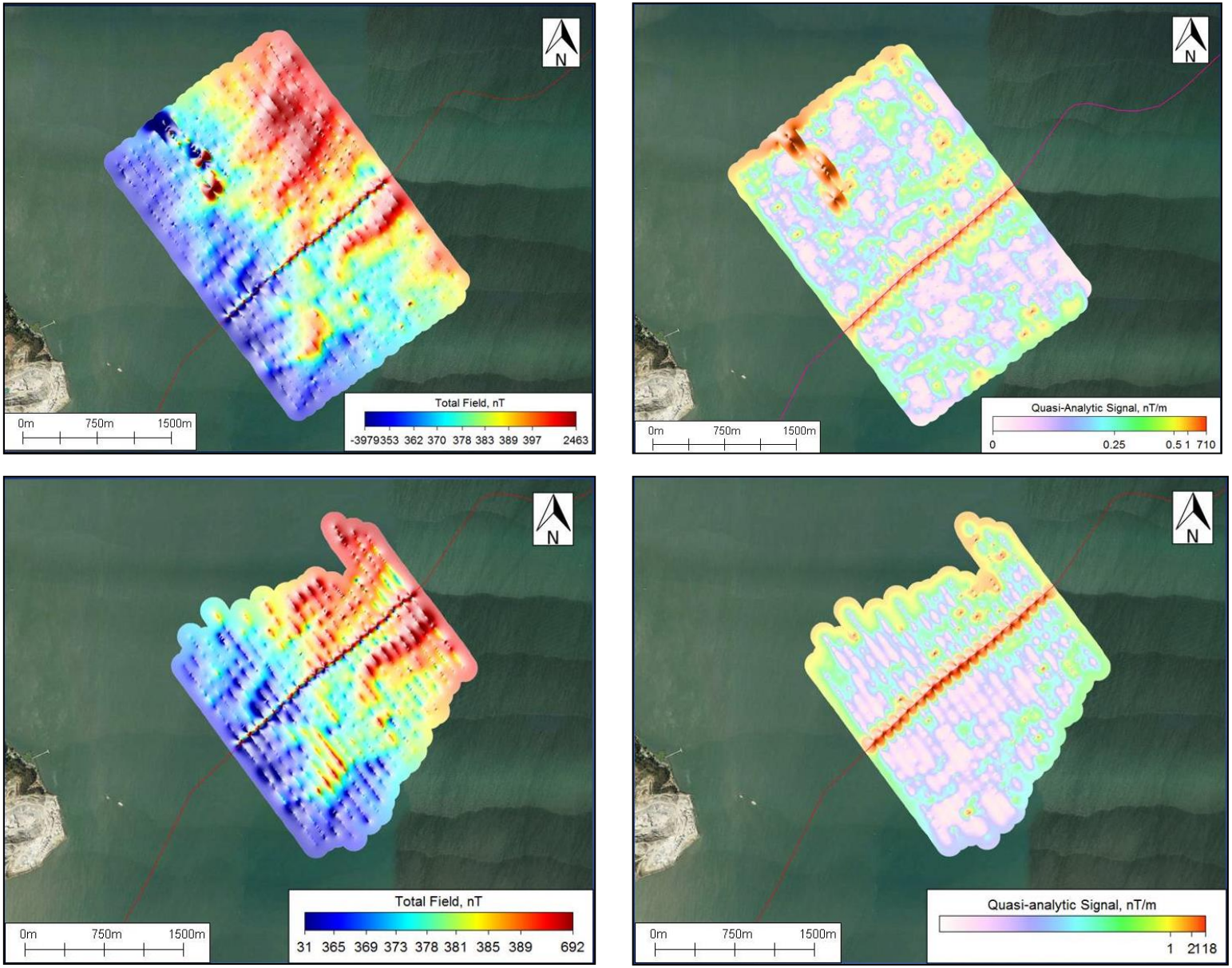

Figure 4. Richmond Bridge: Total field maps of surface tows (upper left) and deep tows (lower left) and quasi-analytic signal maps of surface tows (upper right) and deep tows (lower right).

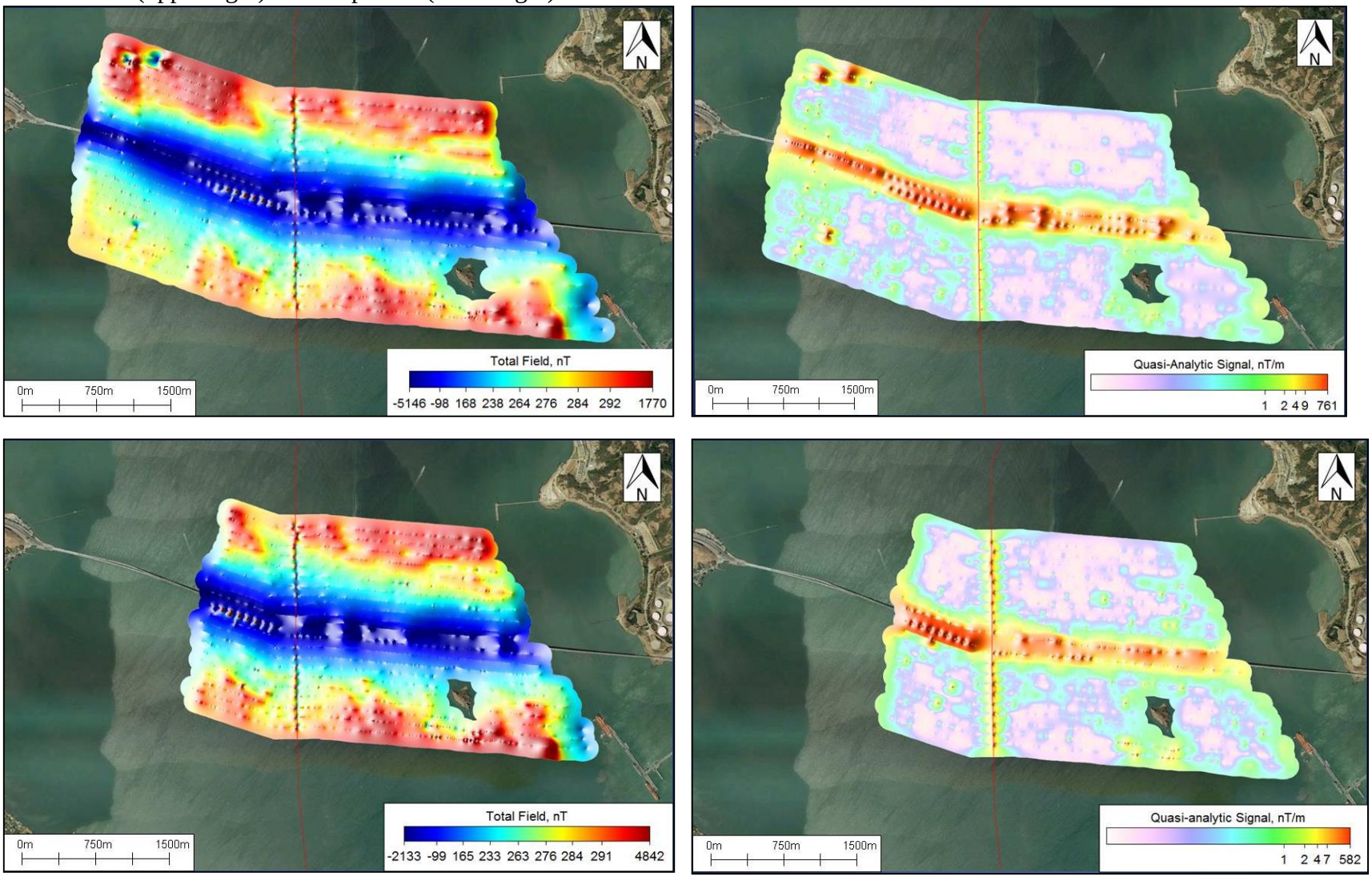

Figure 5. Bay Bridge: Total field maps of surface tows (upper left) and deep tows (lower left) and quasi-analytic signal maps of surface tows (upper right) and deep tows (lower right).

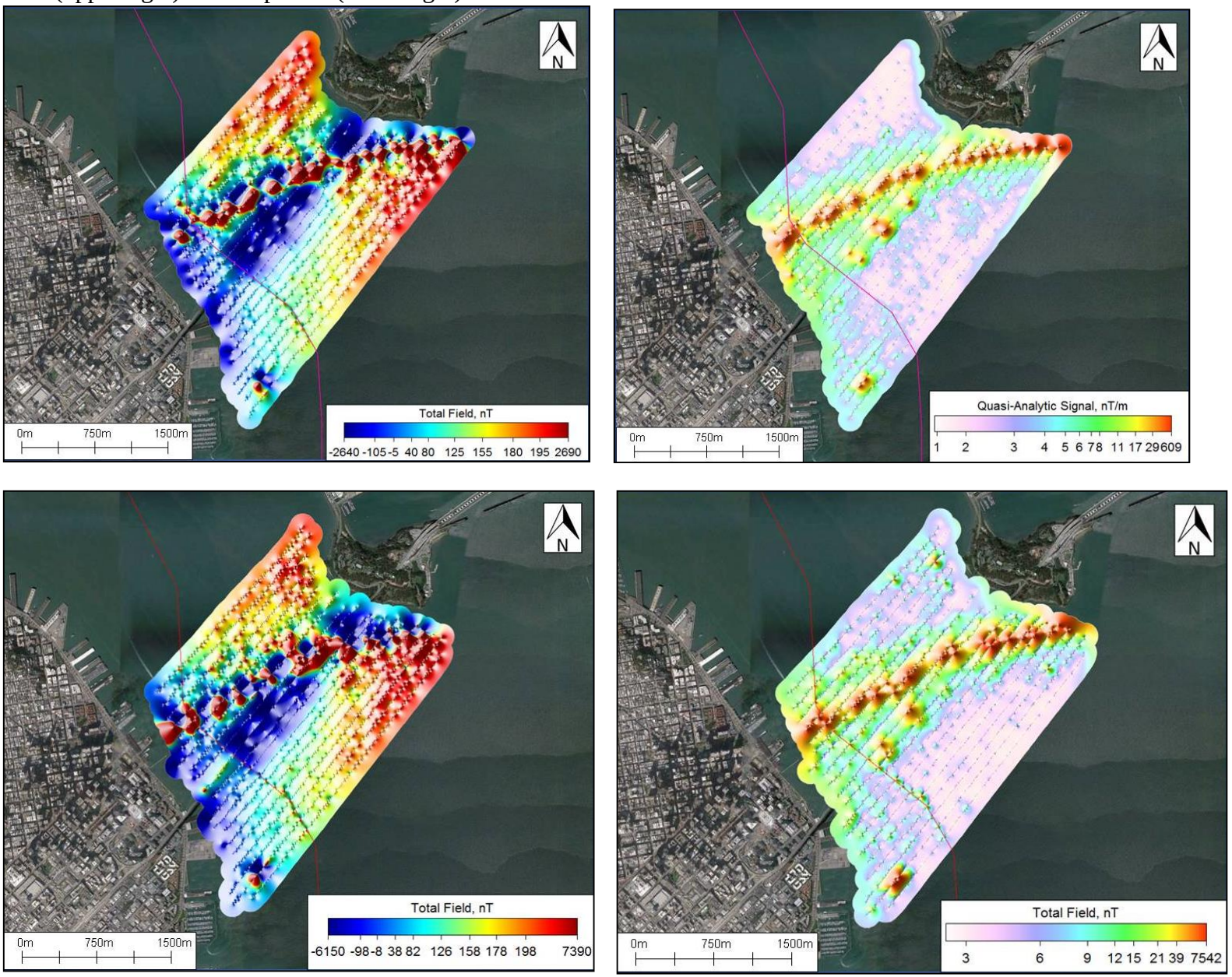

Appendix I

Modeling the Effects on the Anomaly produced by the DC Cable of (1) Twist Angle (Θ) and (2) Profile Angle (Φ) Relative to East-West

Modeling Conditions

- Cable separation = 0.1143 m (4.5 in);
- Current = 1,000 Amps in each conductor;
- Magnetic fields calculated for a distance of 5 m above the horizontal plane of the line;
- Earth field for the exercise is 22.746 μT (North), 5.595 μT (East), and 42.671 μT (Vertical, w/vector pointing down), about the magnitude of the field near, but not perturbed by, the Bay Bridge);
- Value in upper left of each profile page are: Twist Angle (Θ), Angle of Lateral Profile Relative to East-West (Φ, i.e., the cable's reference orientation is North-South) (see examples that follow);
- Red dots on profiles (blue curves in slides 3-51) are maxima and minima, with the difference between the two equal to the local ***Anomaly***;
- Horizontal broken gray line is the unperturbed earth field;
- Last chart indicates Anomaly vs Twist Angle ($0° \le \Theta \le +180°$) by Angle of Lateral Profile Relative to E-W ($-180° \le \Phi \le 0°$).

Line Twist

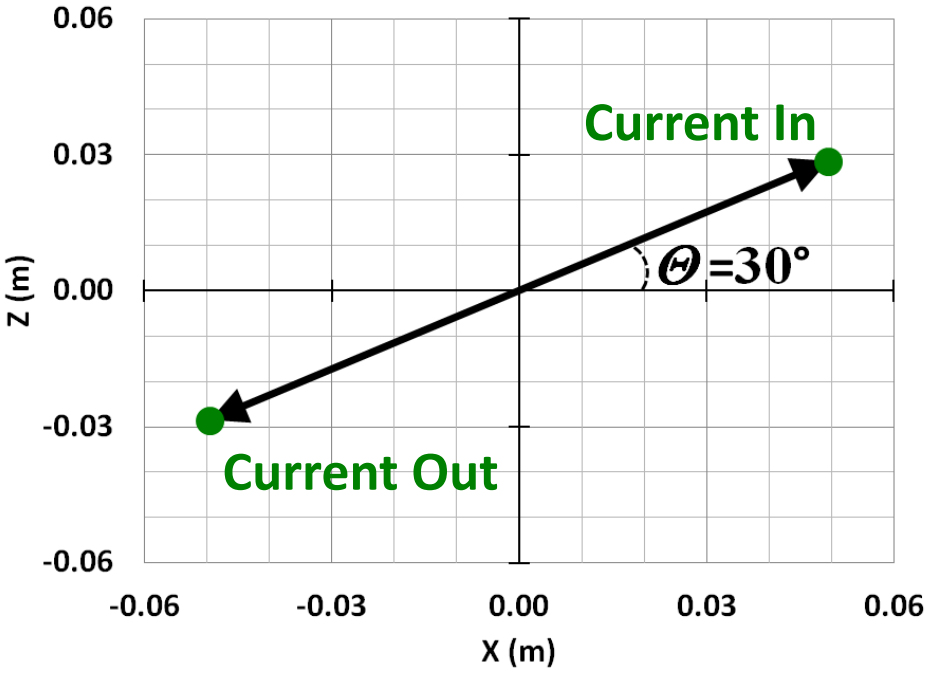

Lateral Profile Relative to E-W

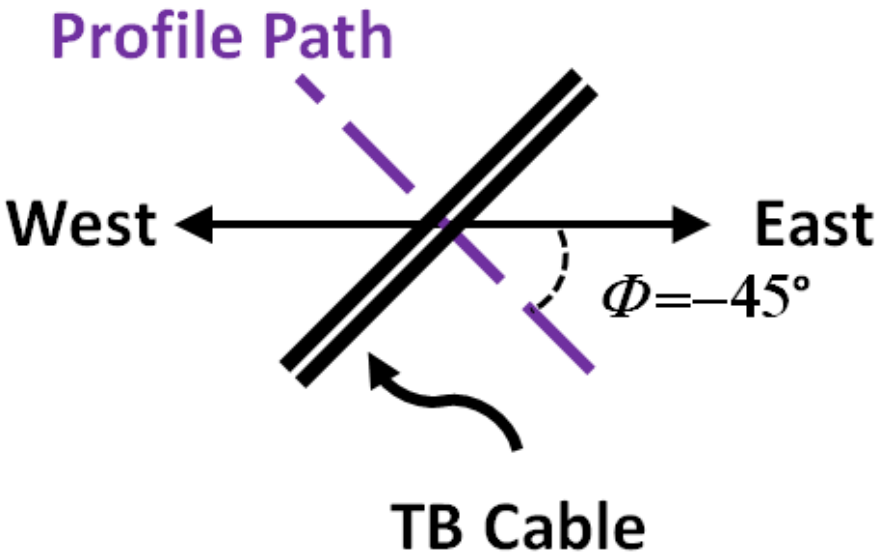

0,0

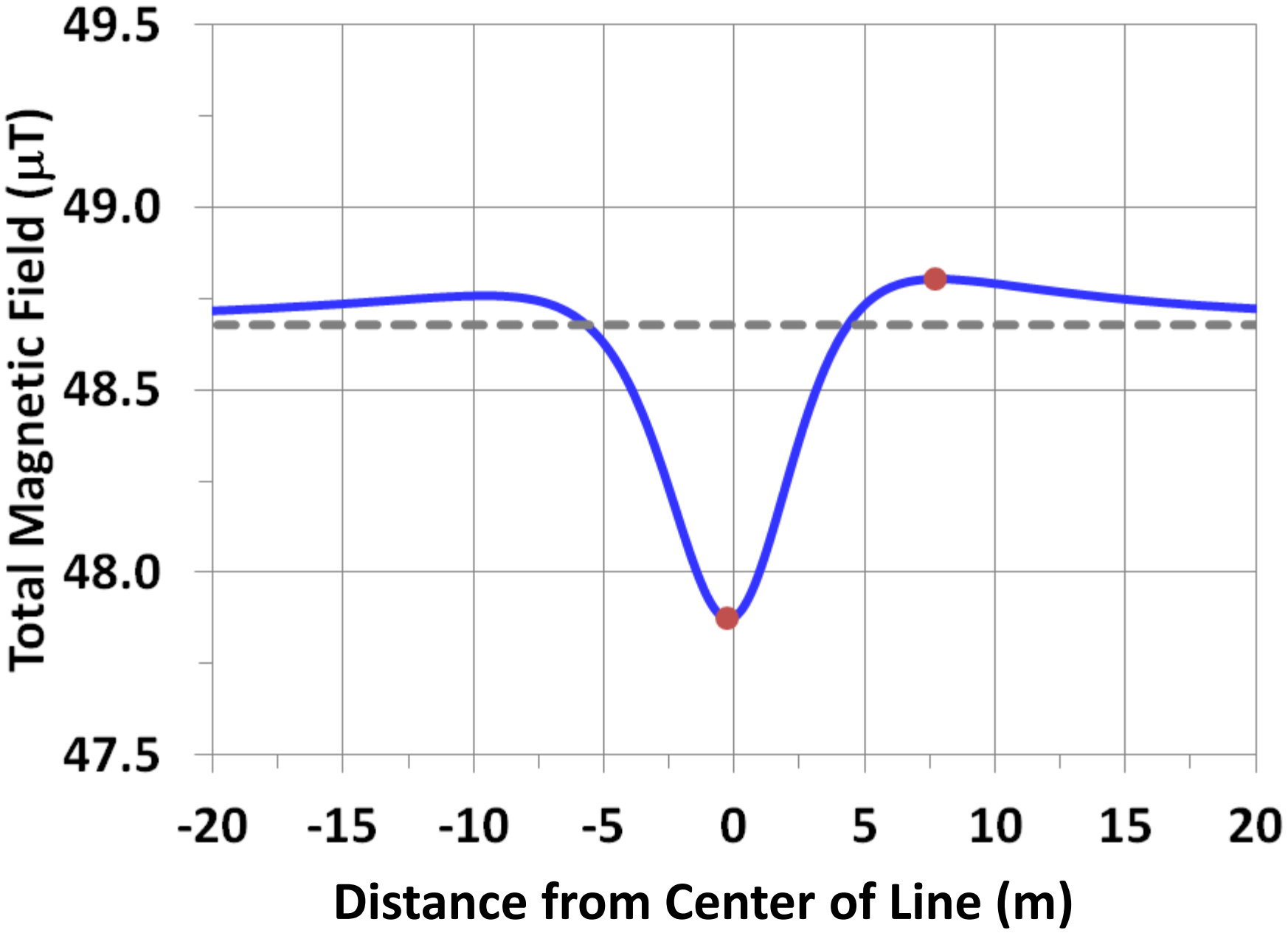
49.5
49.0
48.5
48.0
47.5
Total Magnetic Field (µT)
-20
-15
-10
-5
0
5
10
15
20
Distance from Center of Line (m)

0,-15

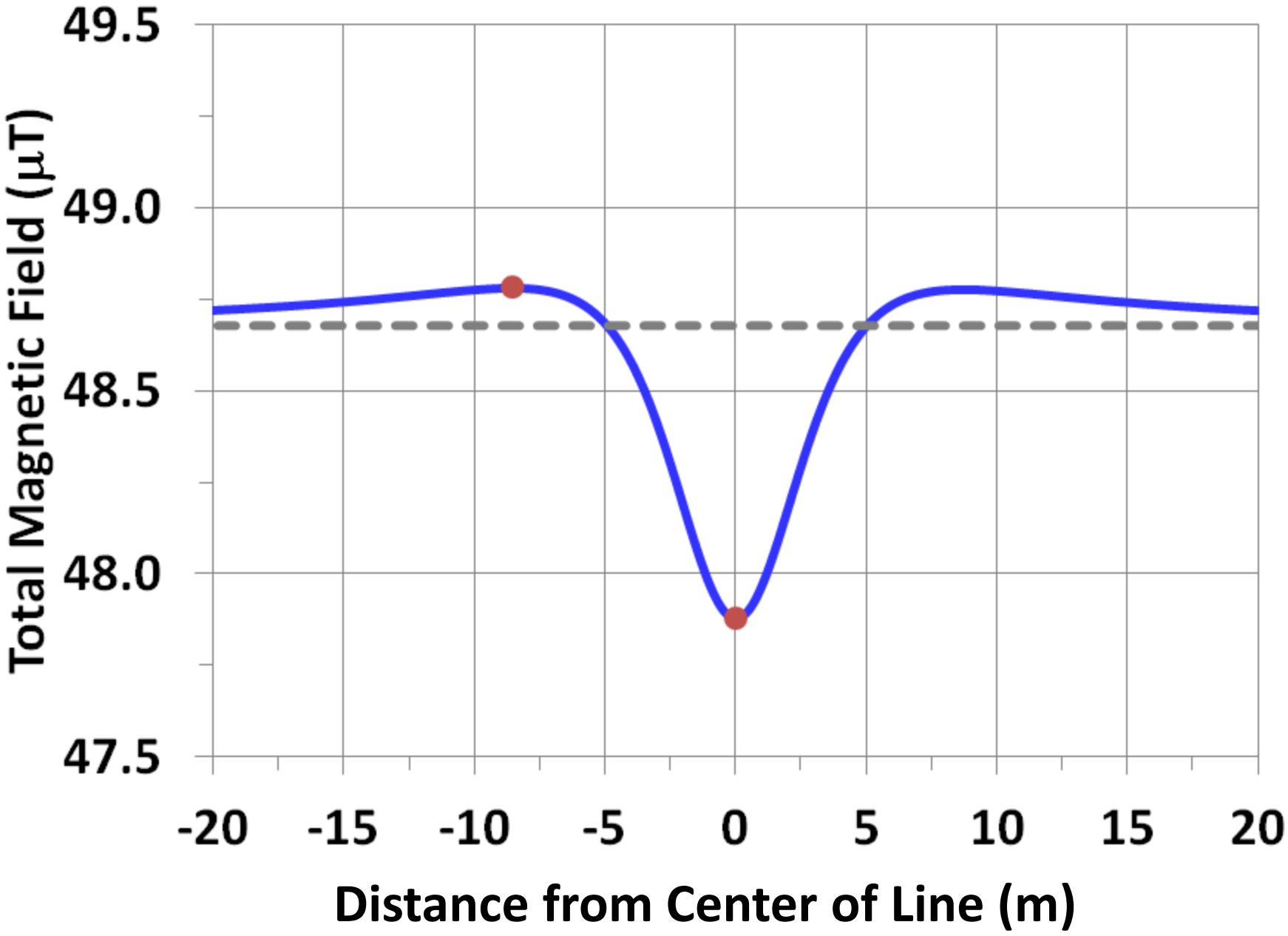
49.5
49.0
48.5
48.0
47.5
Total Magnetic Field (µT)
-20
-15
-10
-5
0
5
10
15
20
Distance from Center of Line (m)

0,-30

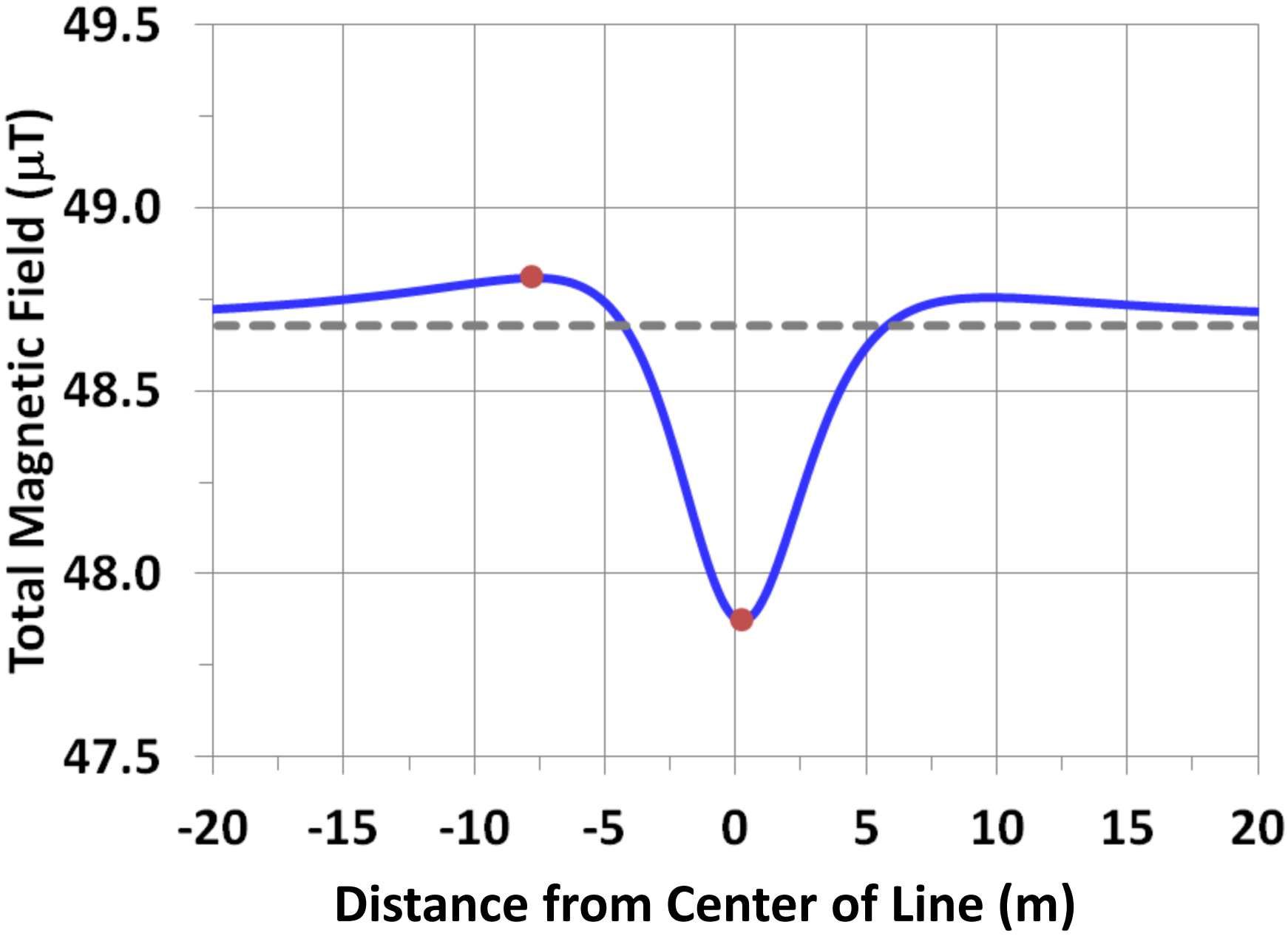
49.5
49.0
48.5
48.0
47.5
Total Magnetic Field (µT)
-20
-15
-10
-5
0
5
10
15
20
Distance from Center of Line (m)

0,-45

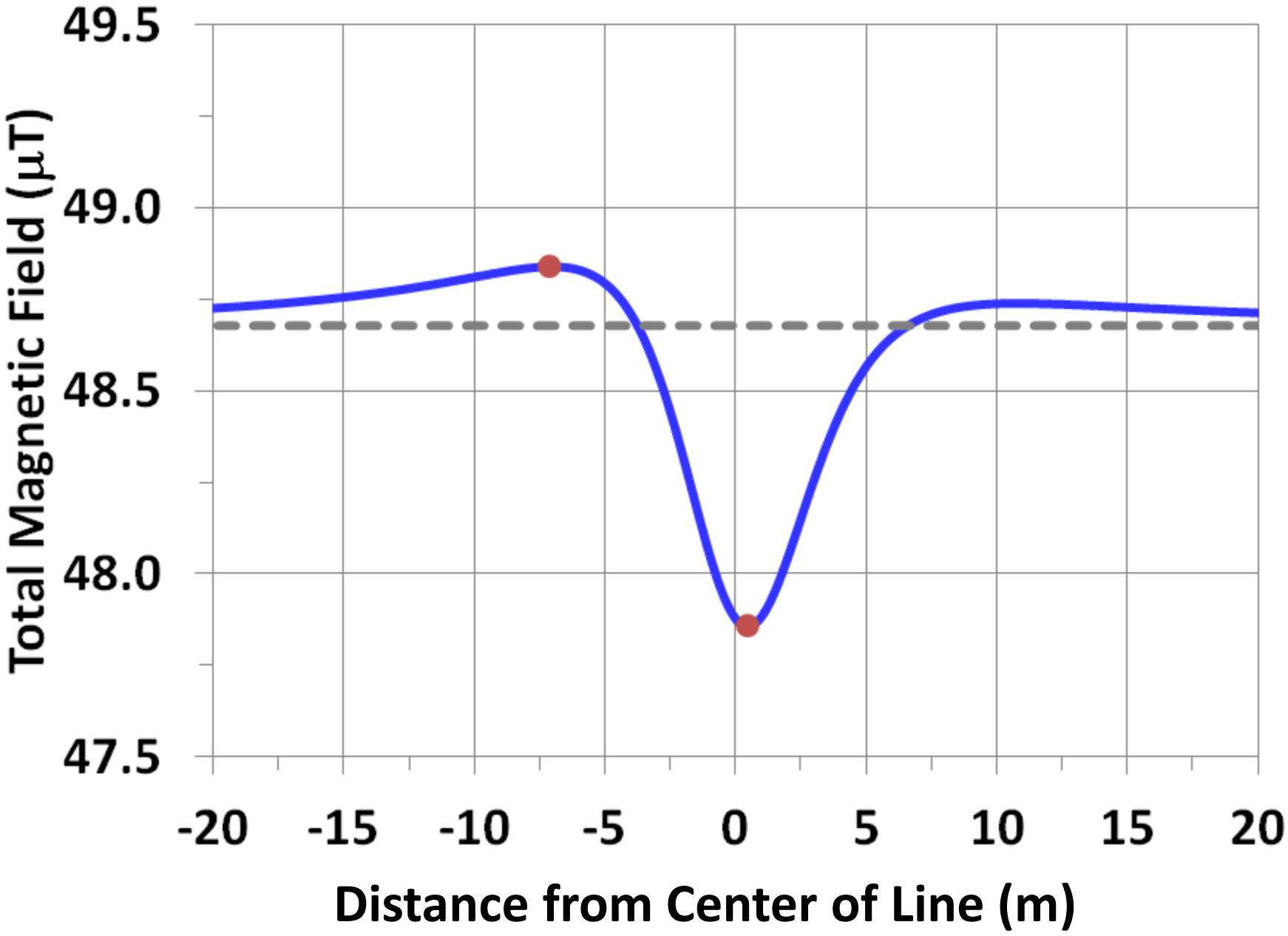
49.5
49.0
48.5
48.0
47.5
Total Magnetic Field (µT)
-20
-15
-10
-5
0
5
10
15
20
Distance from Center of Line (m)

0,-60

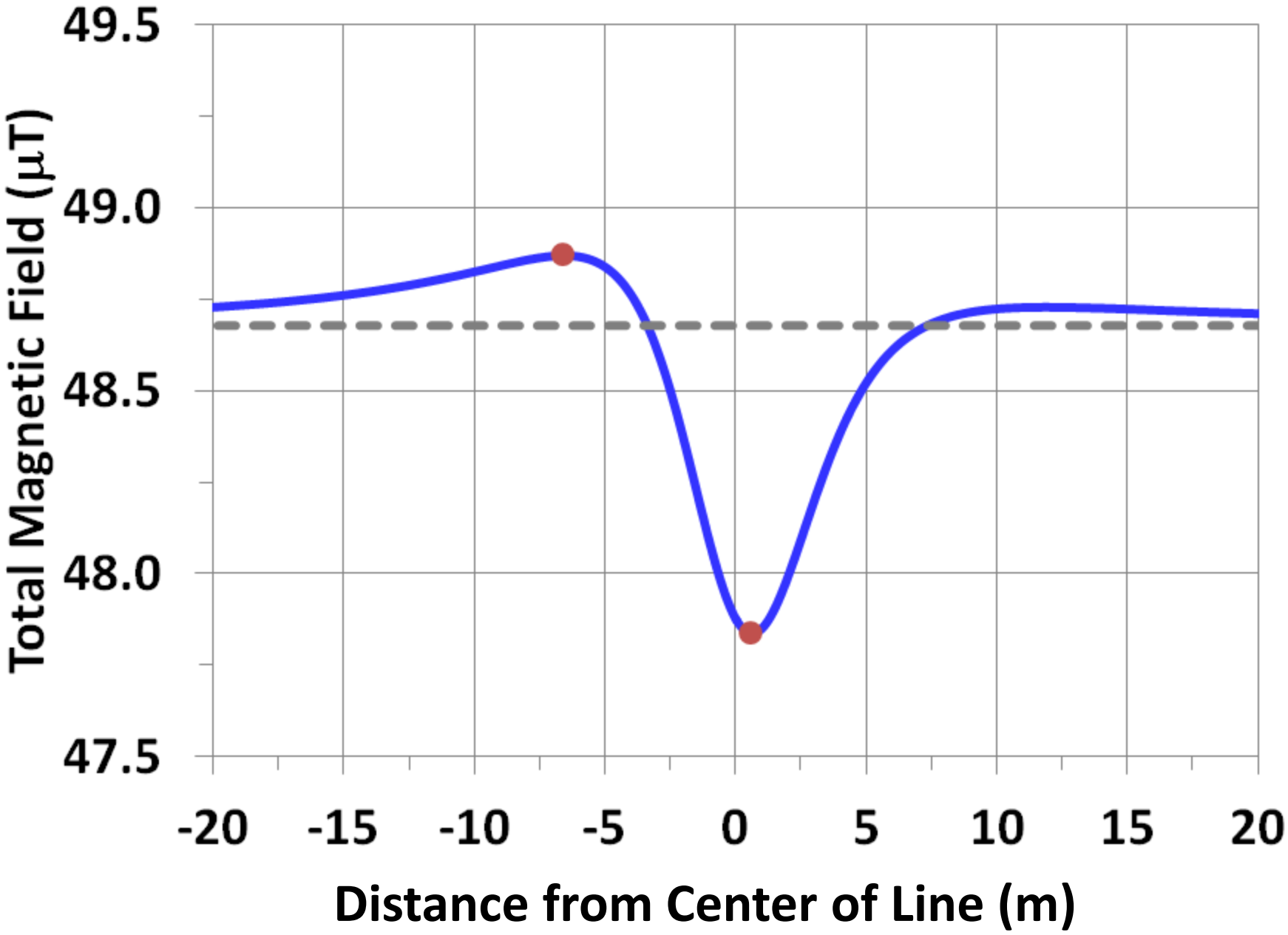
49.5
49.0
48.5
48.0
47.5
Total Magnetic Field (µT)
-20
-15
-10
-5
0
5
10
15
20
Distance from Center of Line (m)

0,-75

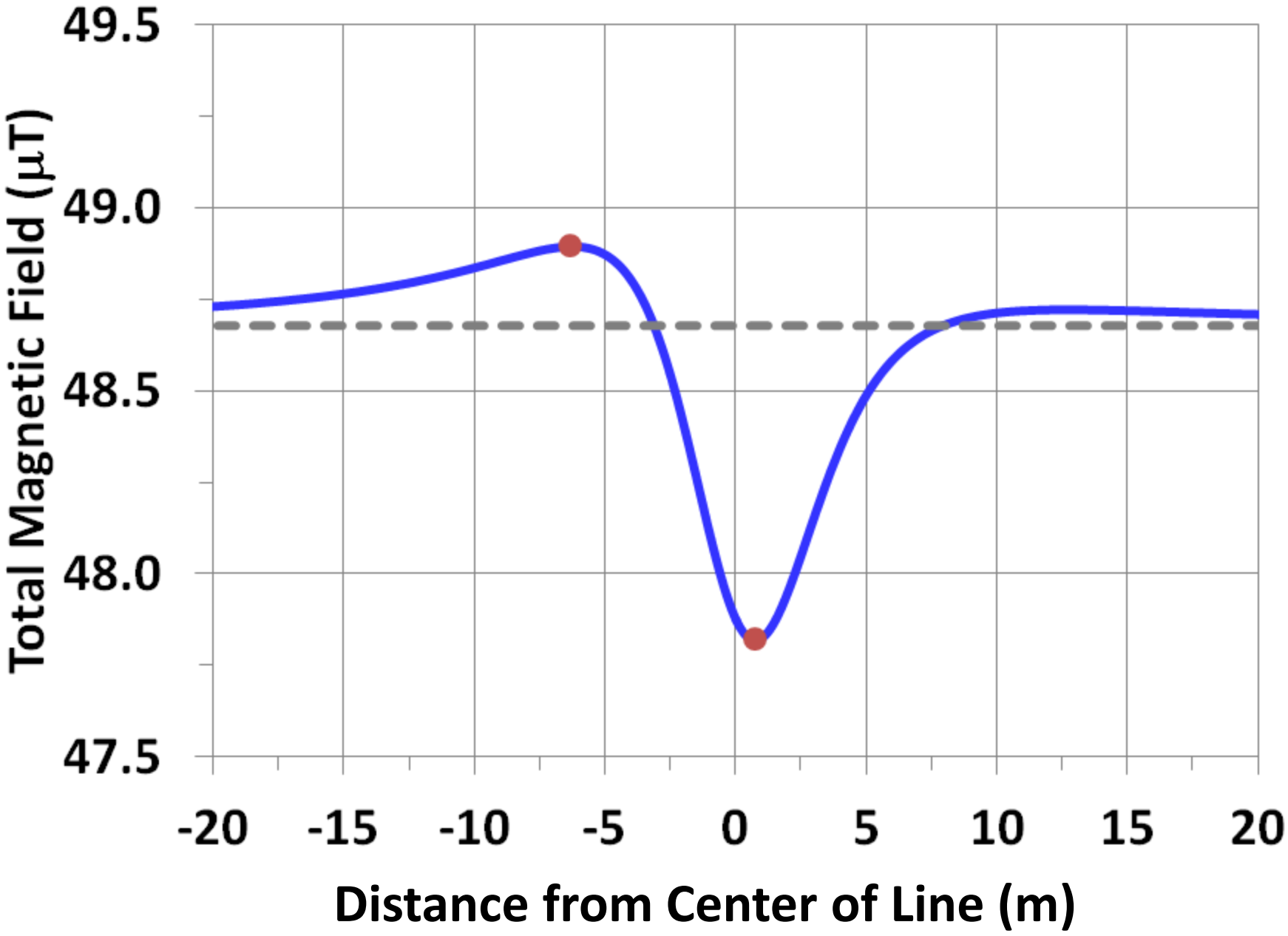
49.5
49.0
48.5
48.0
47.5
Total Magnetic Field (µT)
-20
-15
-10
-5
0
5
10
15
20
Distance from Center of Line (m)

0,-90

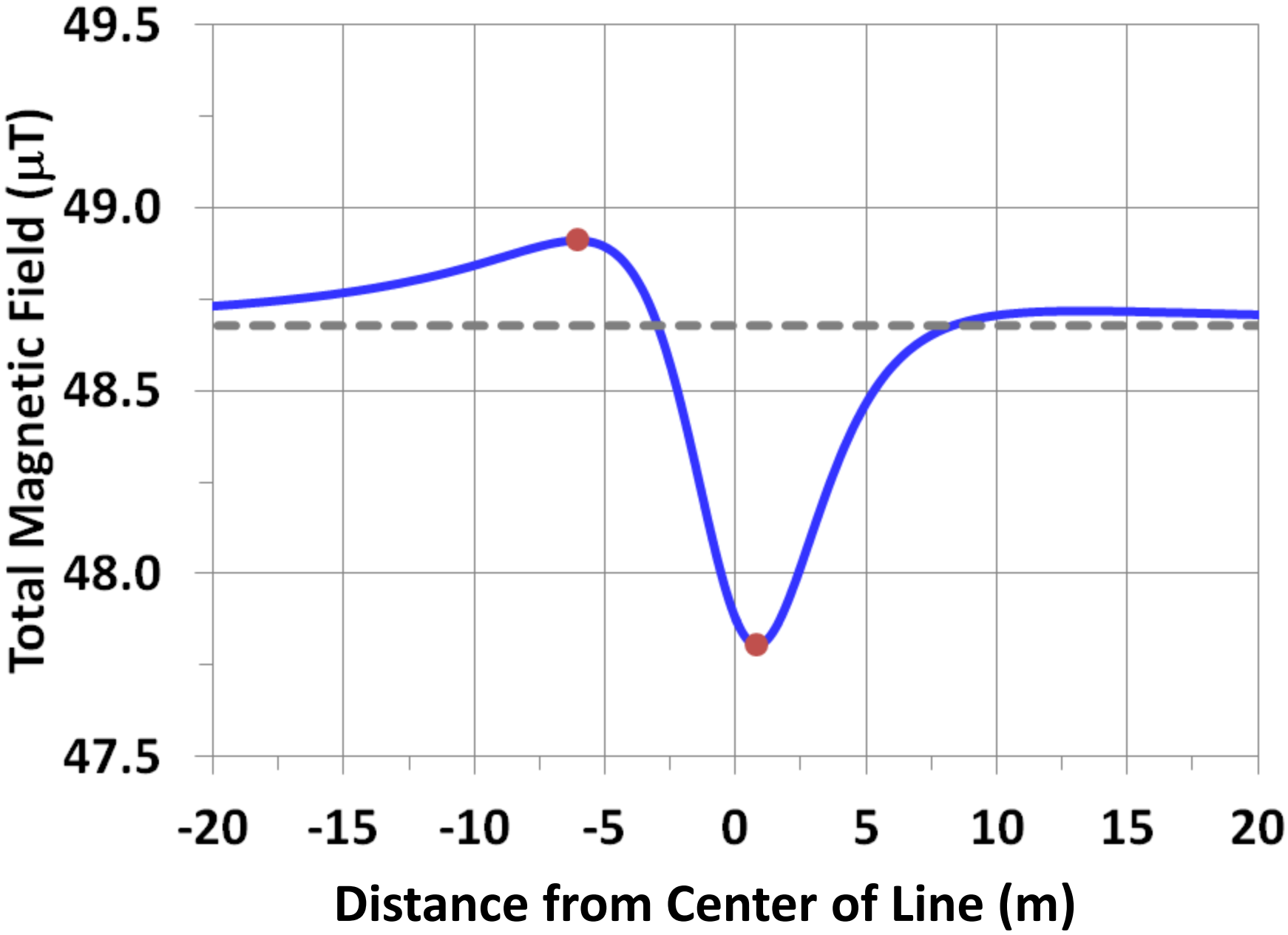
49.5
49.0
48.5
48.0
47.5
Total Magnetic Field (µT)
-20
-15
-10
-5
0
5
10
15
20
Distance from Center of Line (m)

15,0

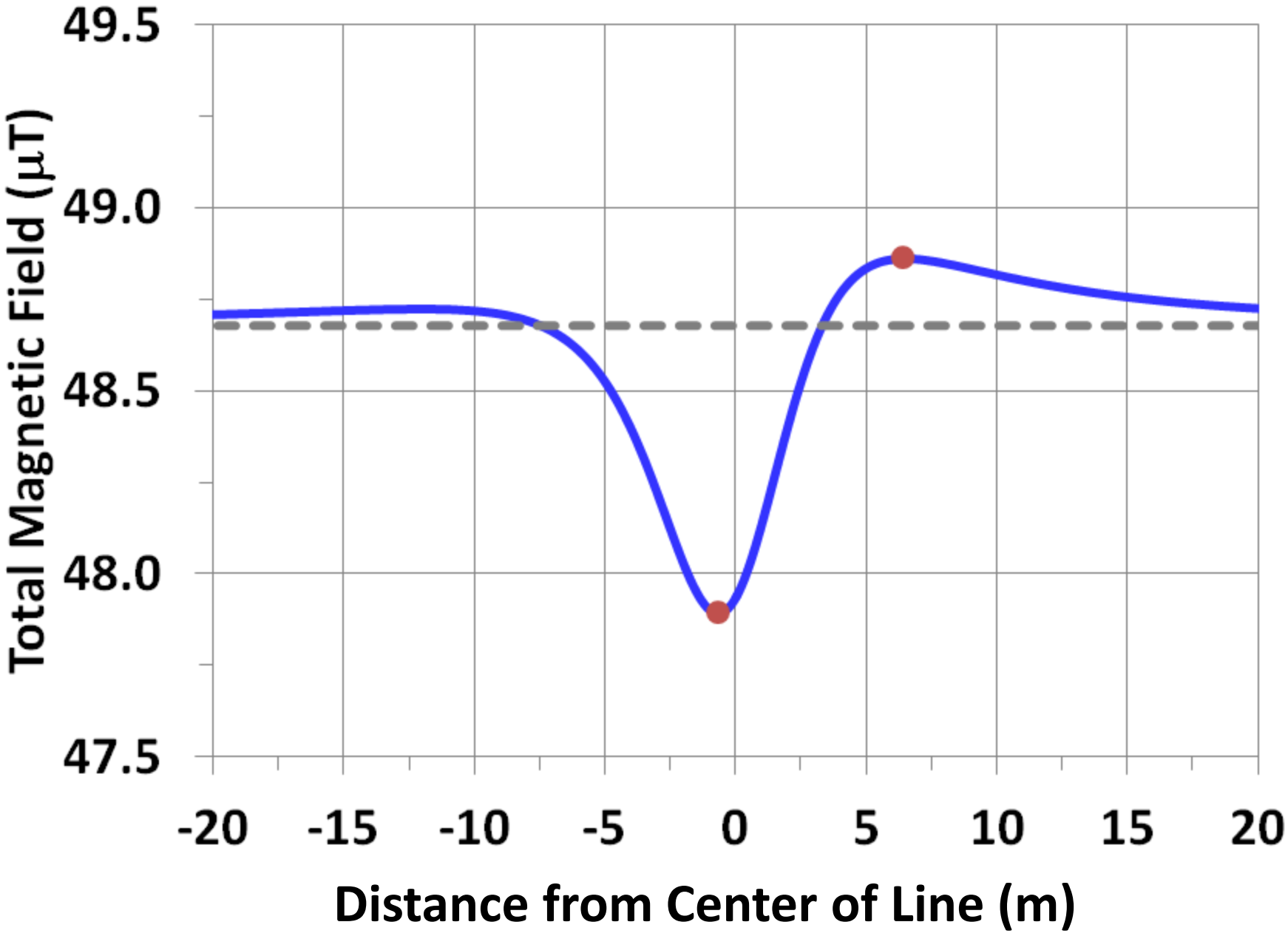
49.5
49.0
48.5
48.0
47.5
Total Magnetic Field (µT)
-20
-15
-10
-5
0
5
10
15
20
Distance from Center of Line (m)

15,-15

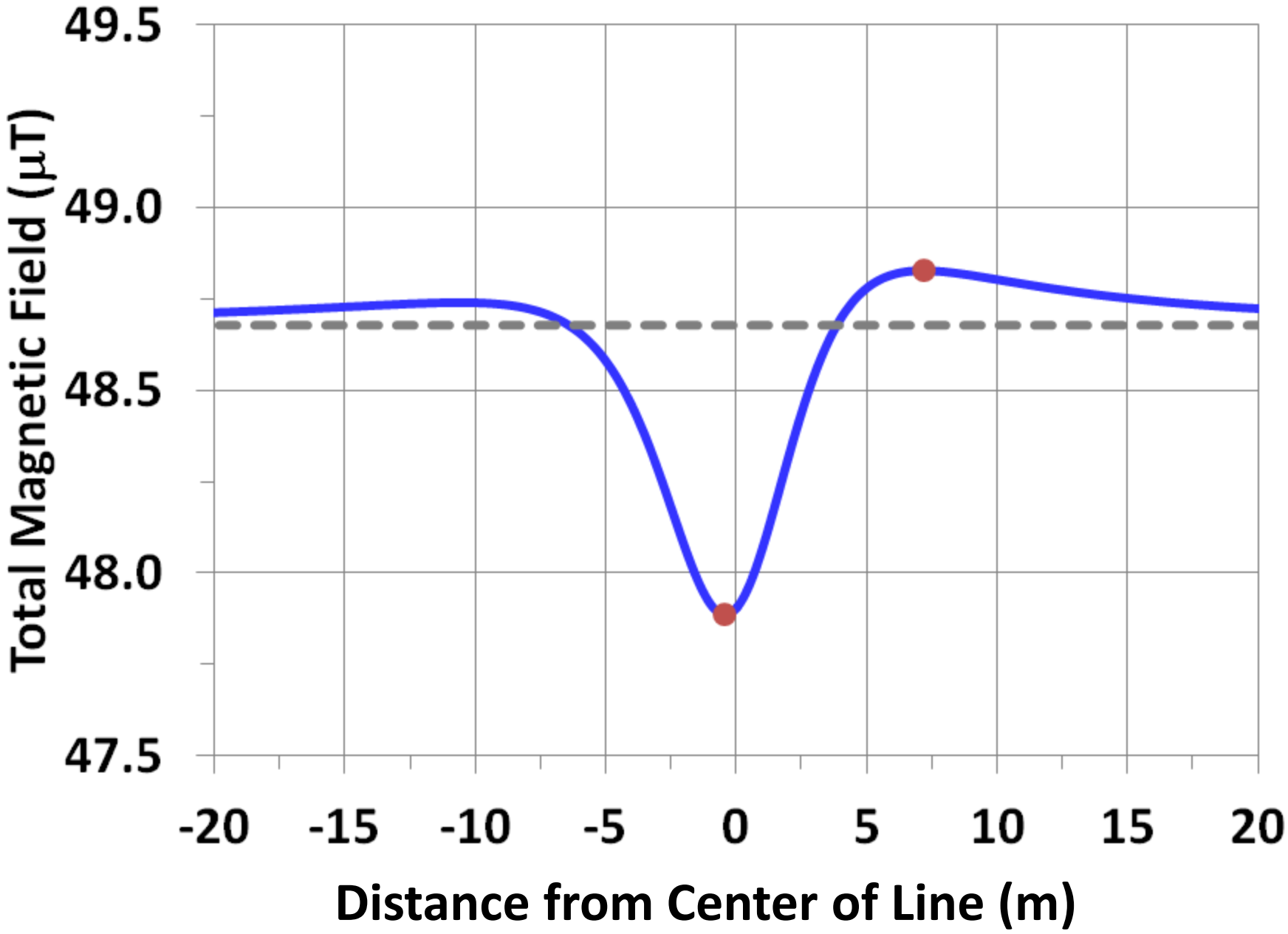
49.5
49.0
48.5
48.0
47.5
Total Magnetic Field (µT)
-20
-15
-10
-5
0
5
10
15
20
Distance from Center of Line (m)

15,-30

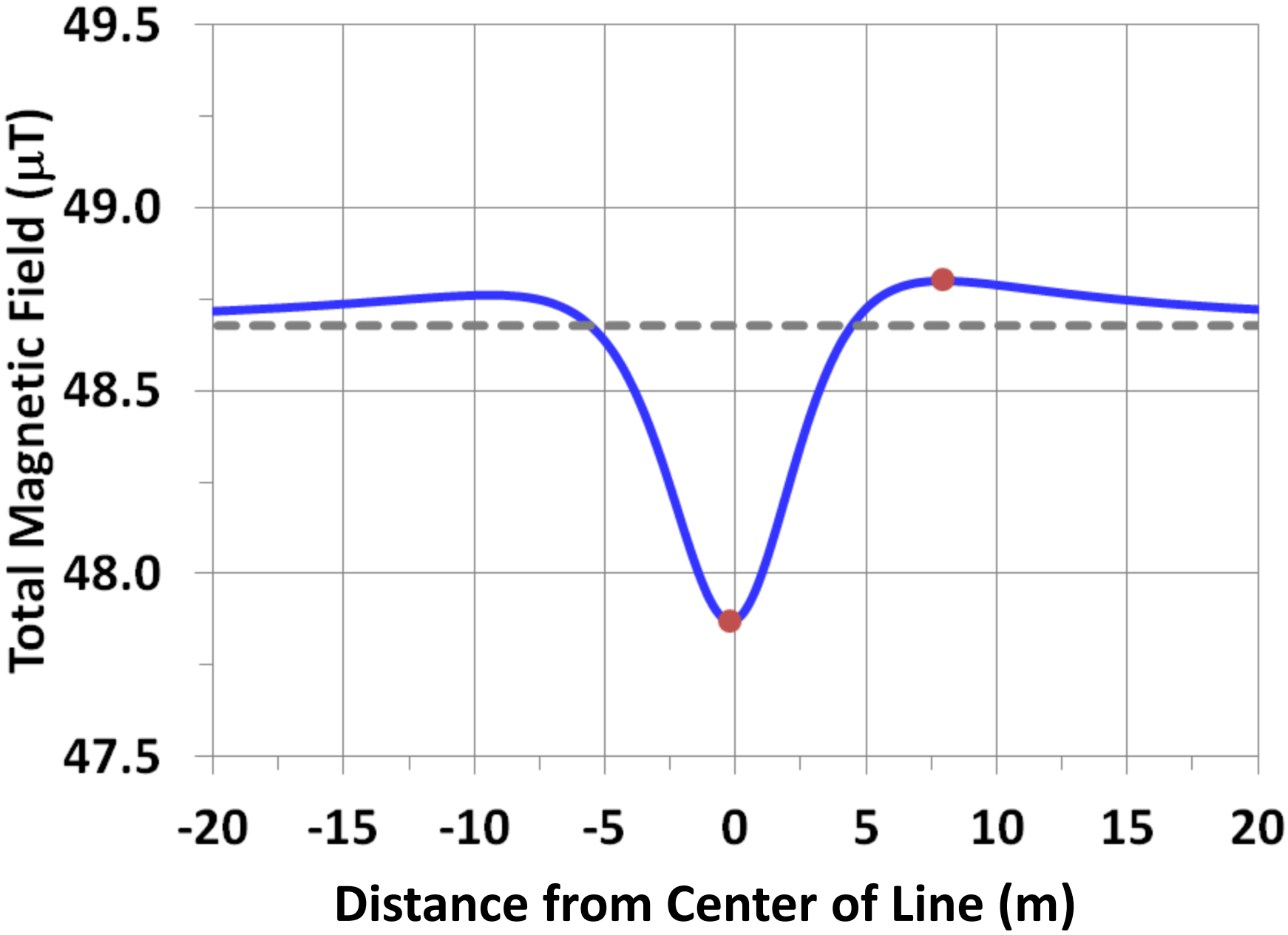
49.5
49.0
48.5
48.0
47.5
Total Magnetic Field (µT)
-20
-15
-10
-5
0
5
10
15
20
Distance from Center of Line (m)

15,-45

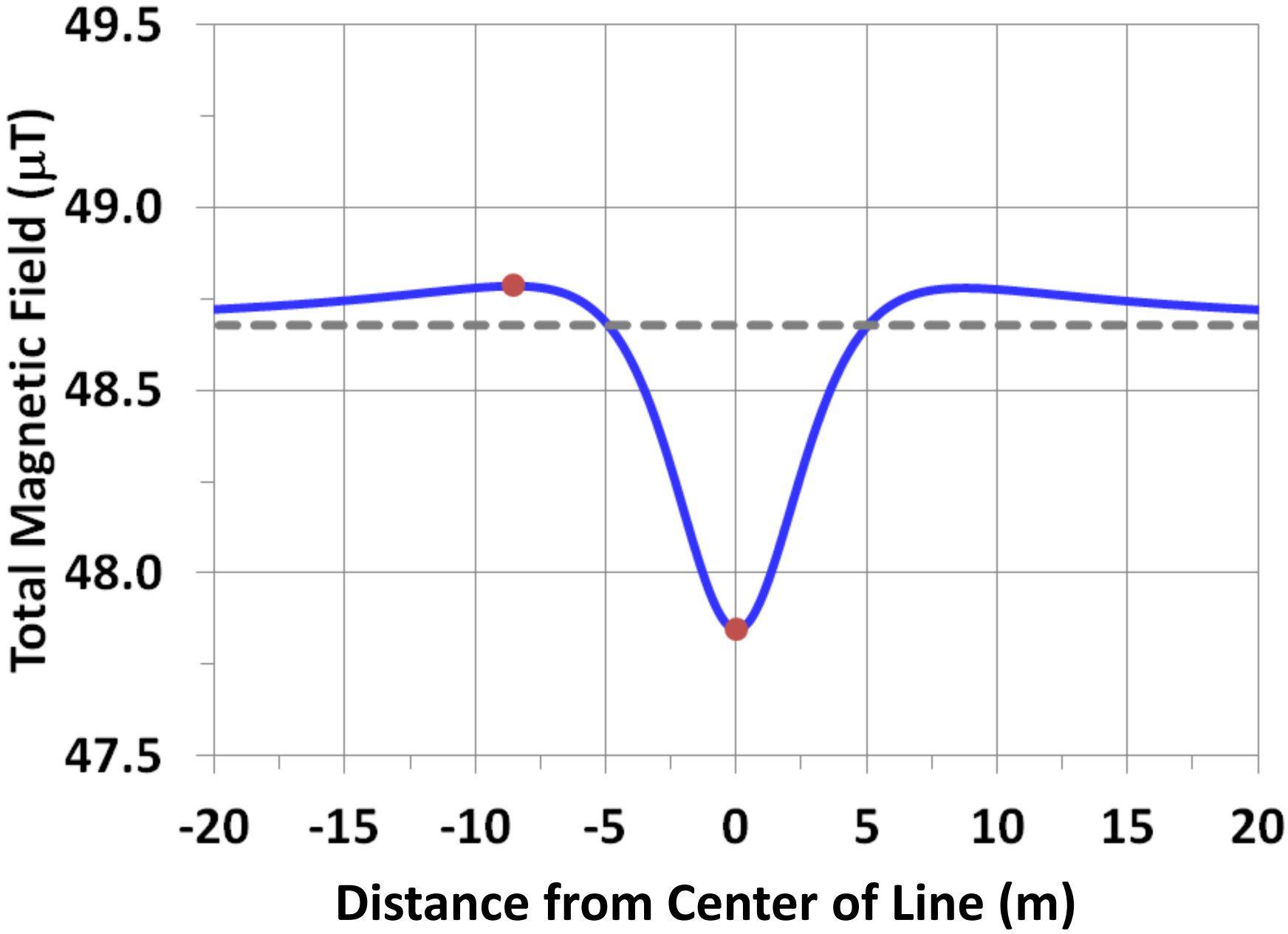
49.5
49.0
48.5
48.0
47.5
Total Magnetic Field (µT)
-20
-15
-10
-5
0
5
10
15
20
Distance from Center of Line (m)

15,-60

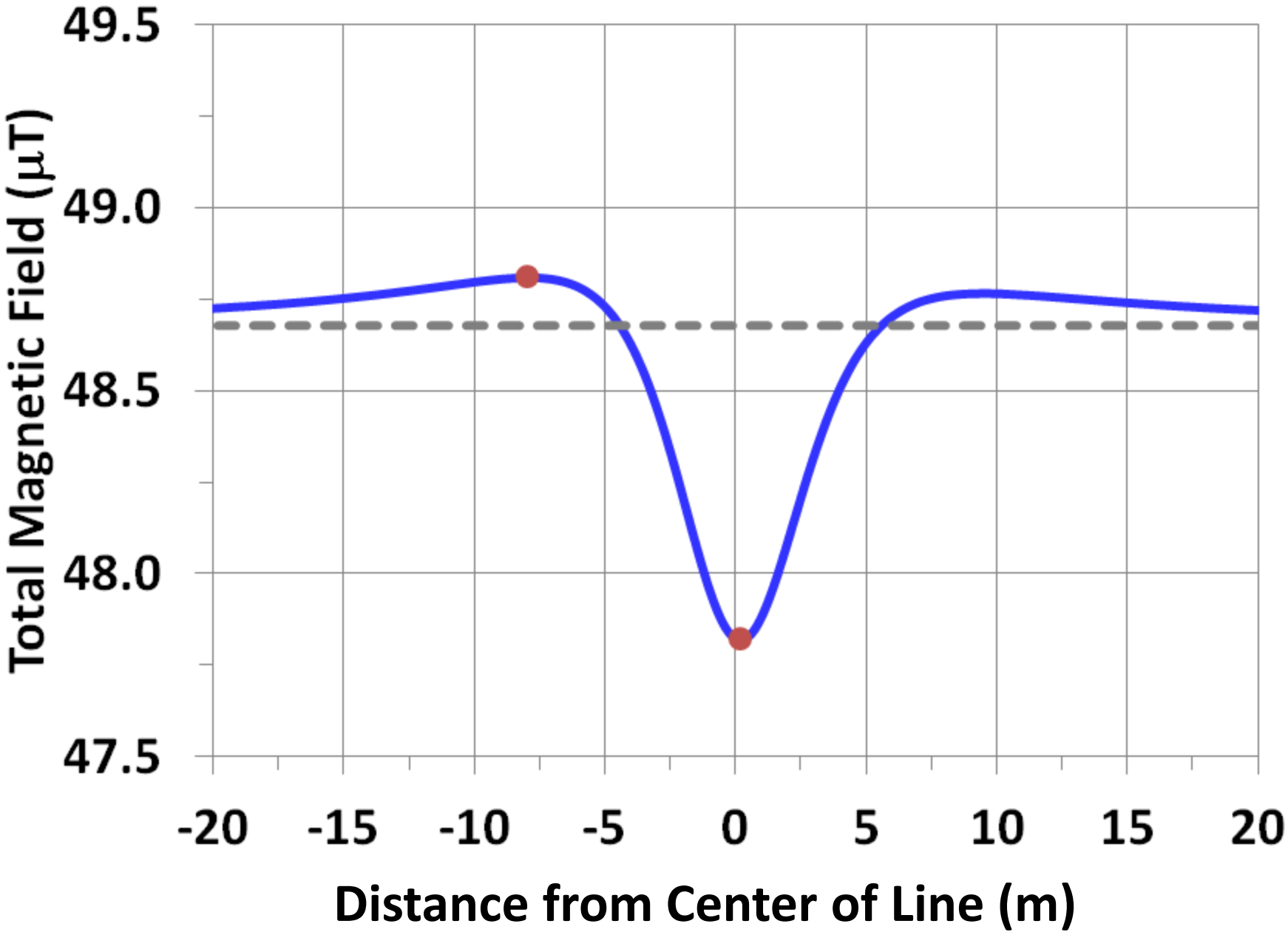
49.5
49.0
48.5
48.0
47.5
Total Magnetic Field (µT)
-20
-15
-10
-5
0
5
10
15
20
Distance from Center of Line (m)

15,-75

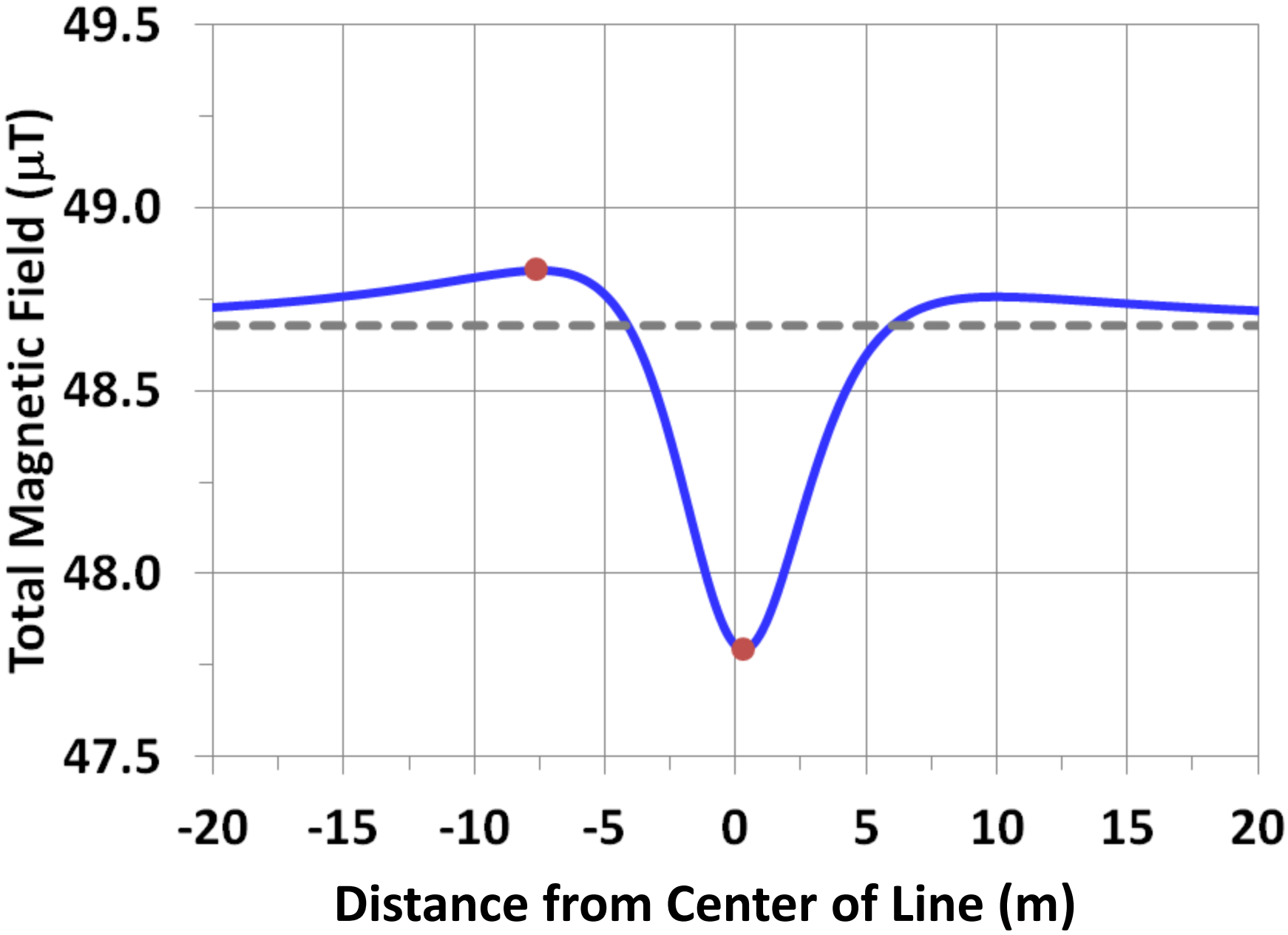
49.5
49.0
48.5
48.0
47.5
Total Magnetic Field (µT)
-20
-15
-10
-5
0
5
10
15
20
Distance from Center of Line (m)

15,-90

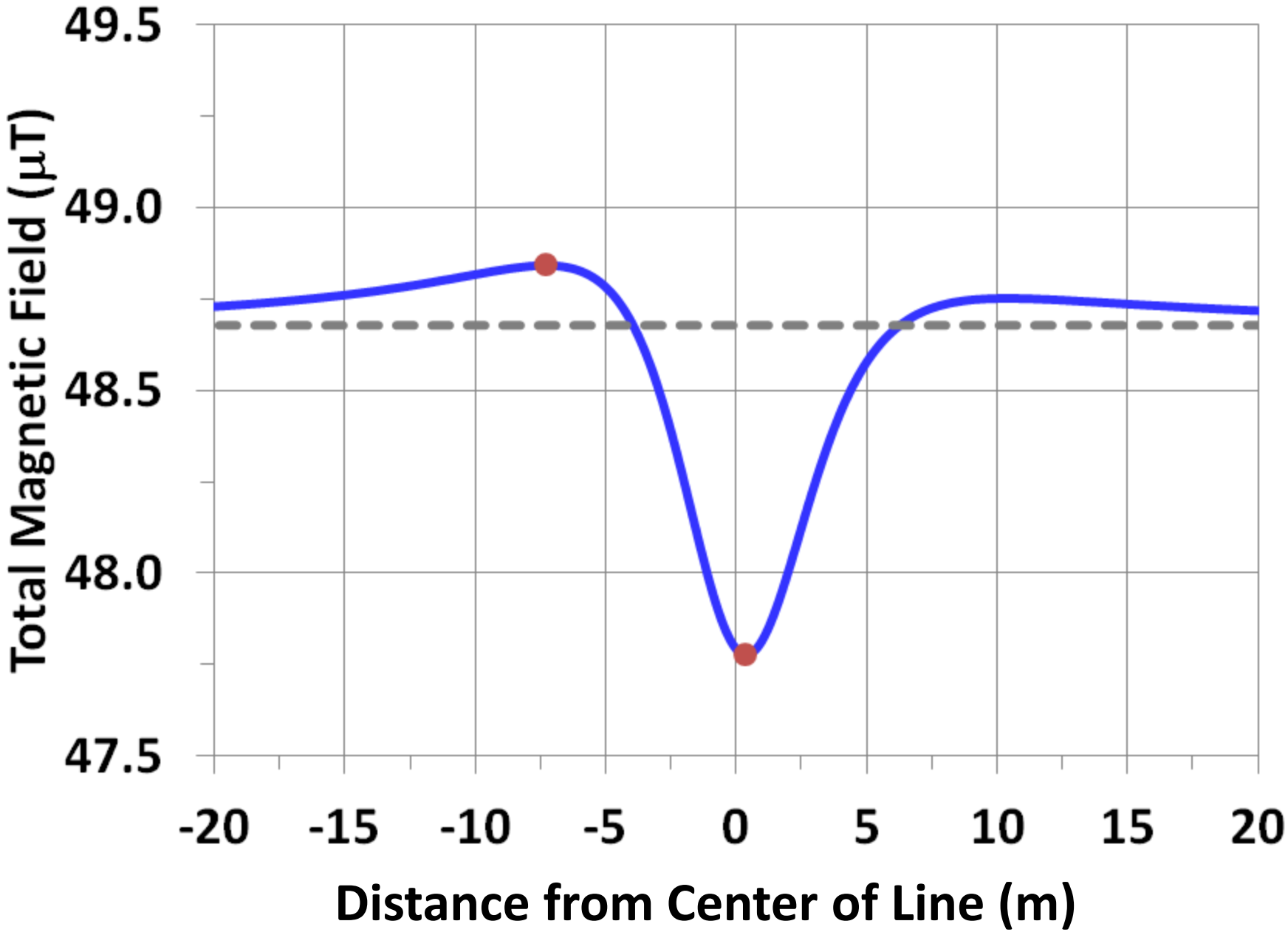
49.5
49.0
48.5
48.0
47.5
Total Magnetic Field (µT)
-20
-15
-10
-5
0
5
10
15
20
Distance from Center of Line (m)

30,0

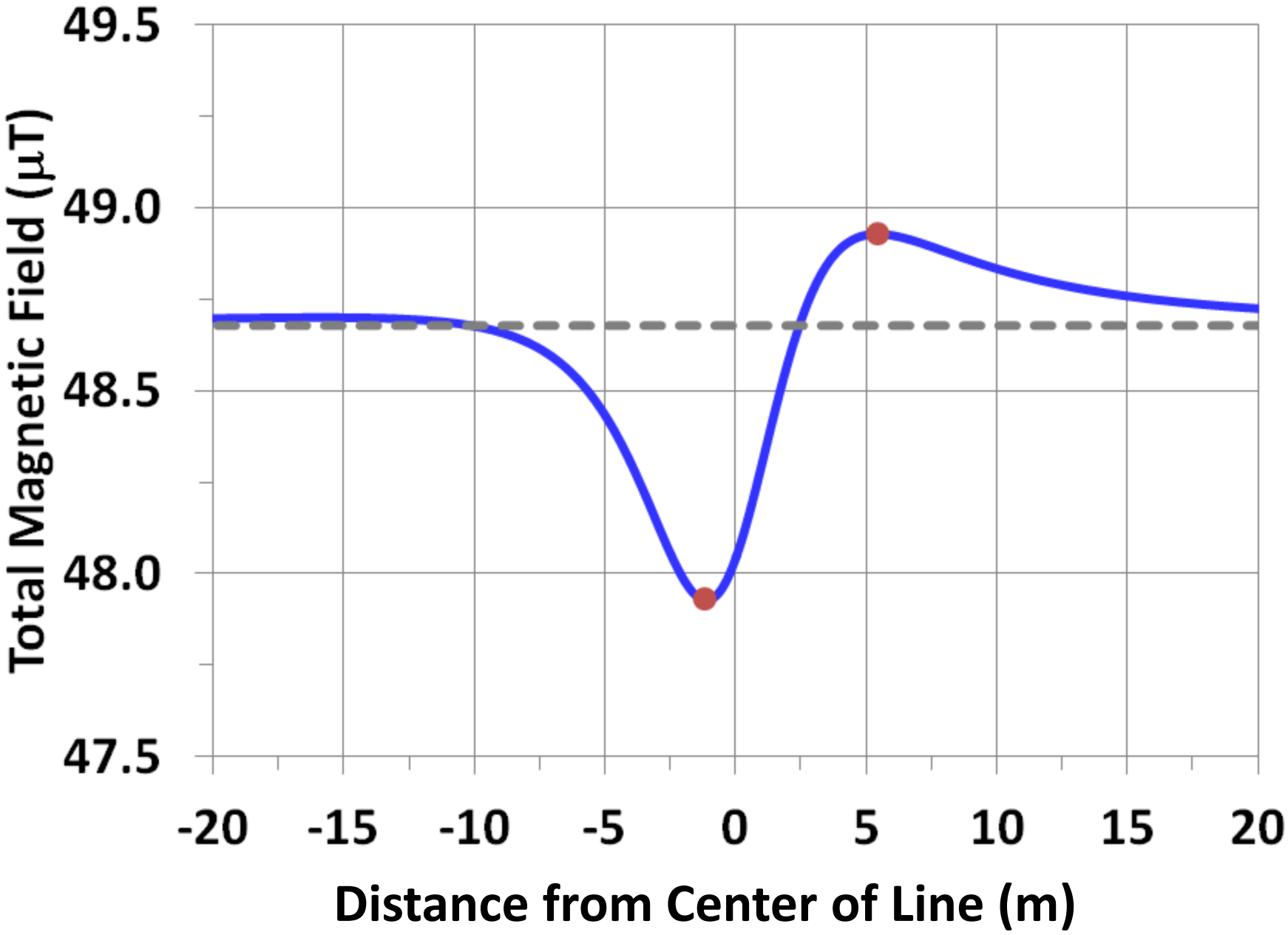
49.5
49.0
48.5
48.0
47.5
Total Magnetic Field (µT)
-20
-15
-10
-5
0
5
10
15
20
Distance from Center of Line (m)

30,-15

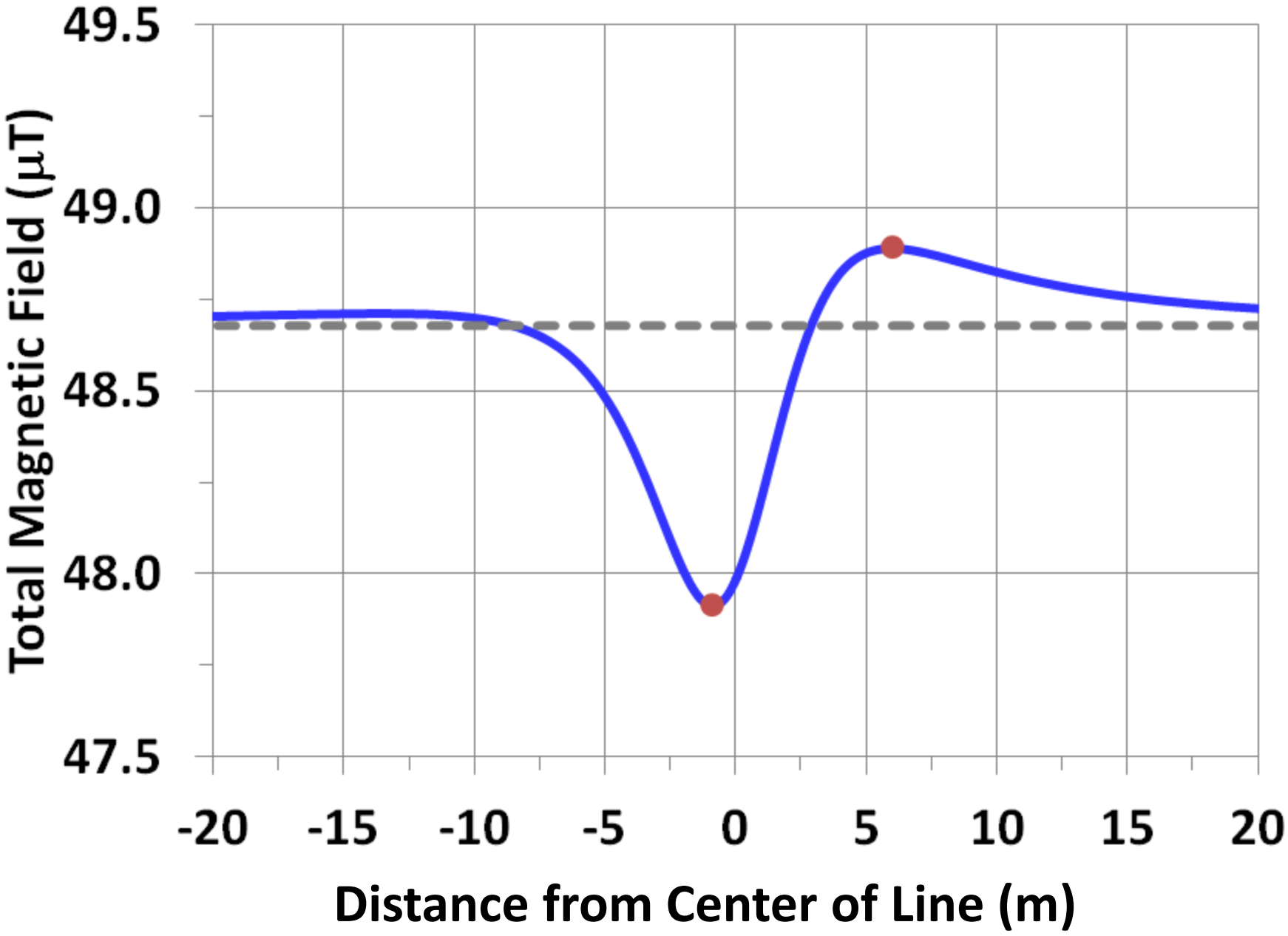
49.5
49.0
48.5
48.0
47.5
Total Magnetic Field (µT)
-20
-15
-10
-5
0
5
10
15
20
Distance from Center of Line (m)

30,-30

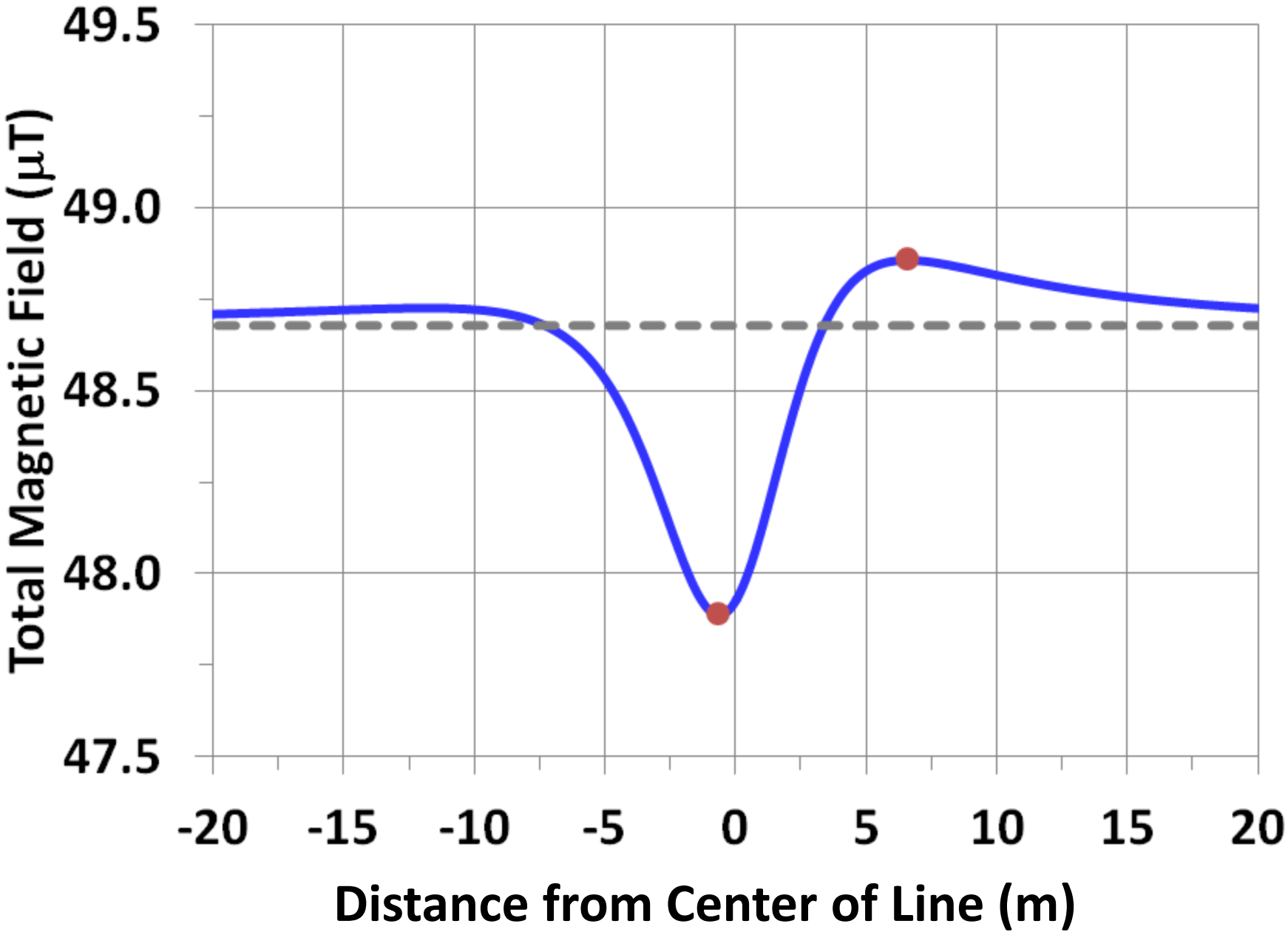
49.5
49.0
48.5
48.0
47.5
Total Magnetic Field (µT)
-20
-15
-10
-5
0
5
10
15
20
Distance from Center of Line (m)

30,-45

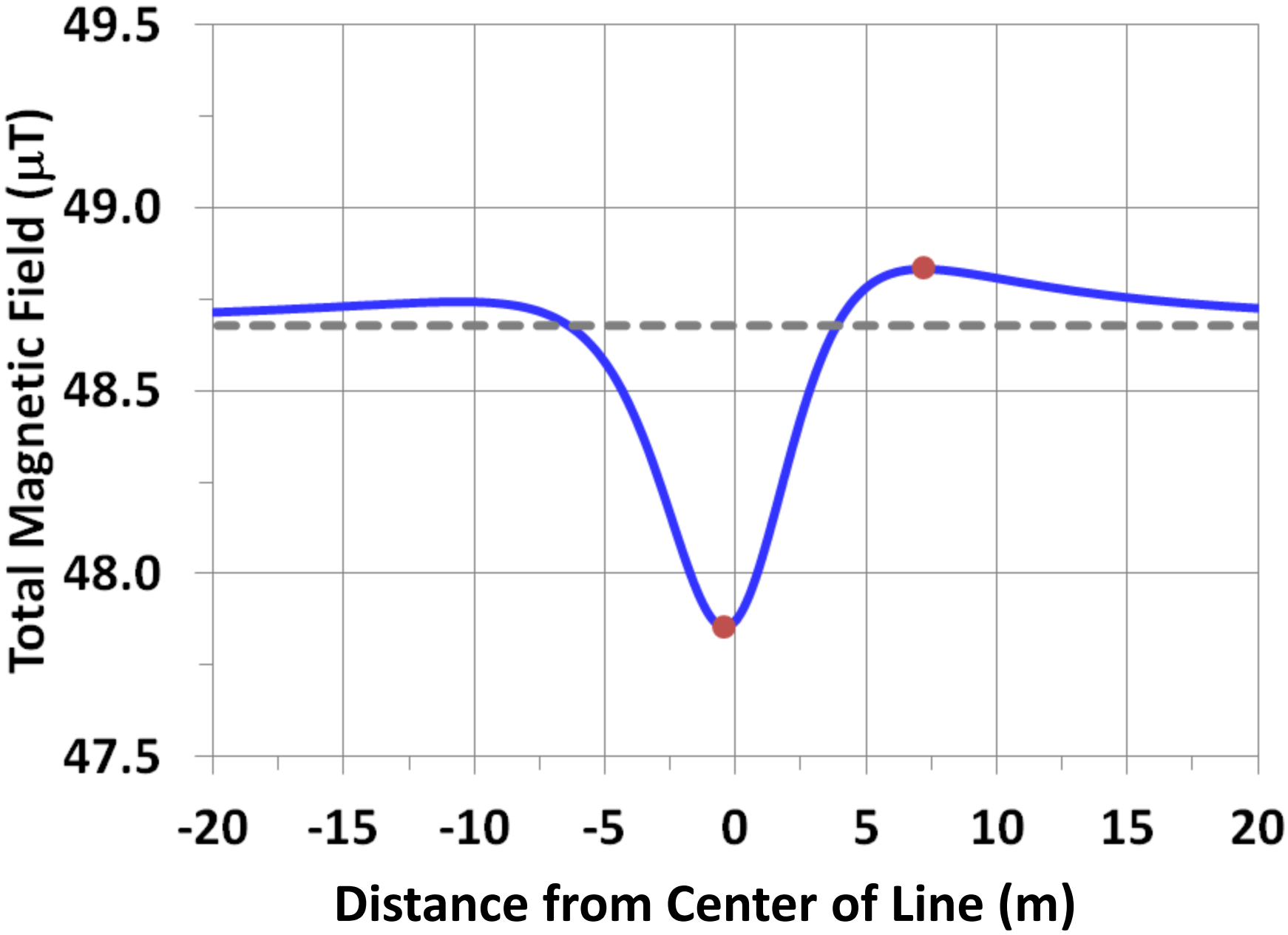
49.5
49.0
48.5
48.0
47.5
Total Magnetic Field (µT)
-20
-15
-10
-5
0
5
10
15
20
Distance from Center of Line (m)

30,-60

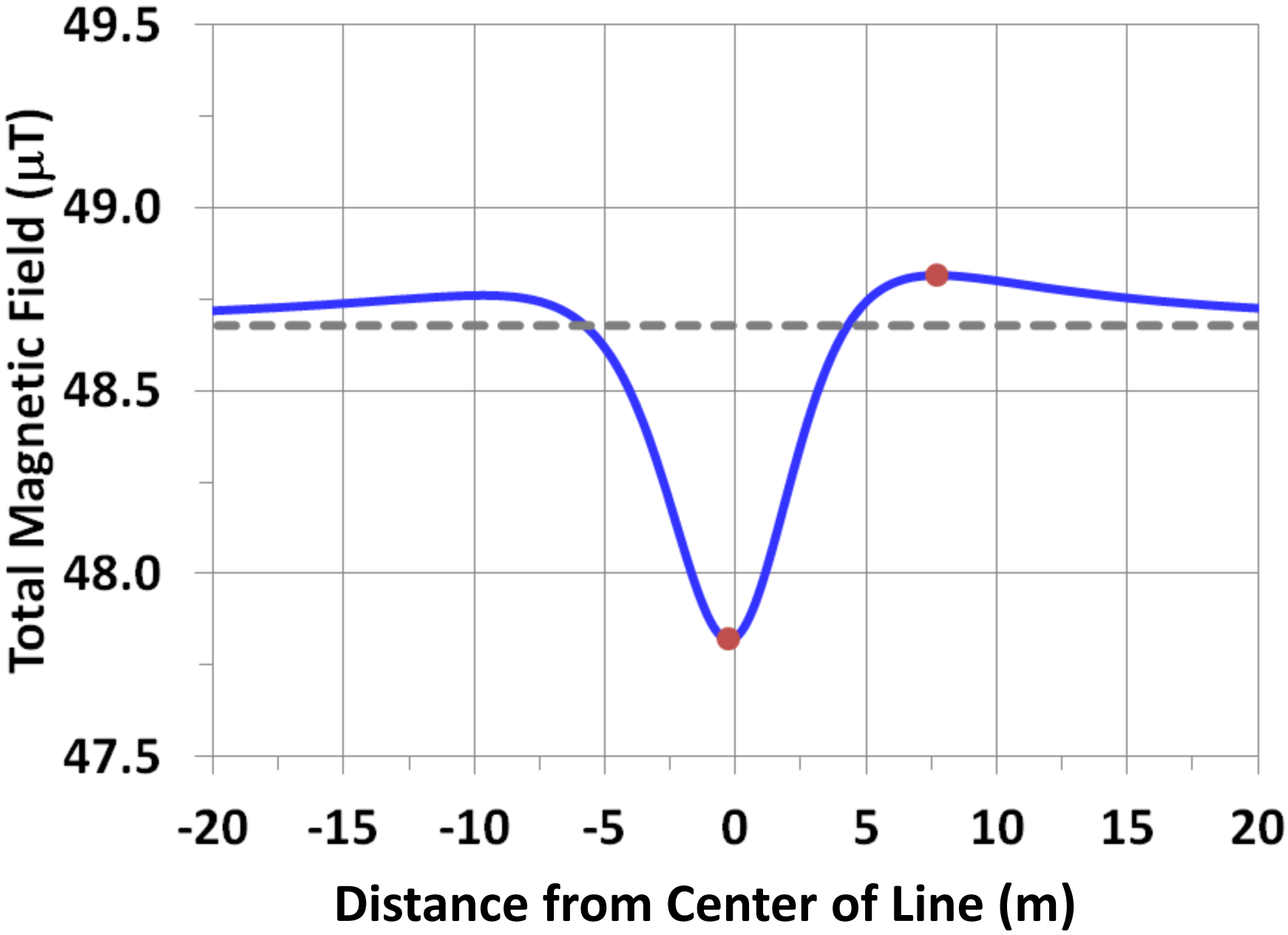
49.5
49.0
48.5
48.0
47.5
Total Magnetic Field (µT)
-20
-15
-10
-5
0
5
10
15
20
Distance from Center of Line (m)

30,-75

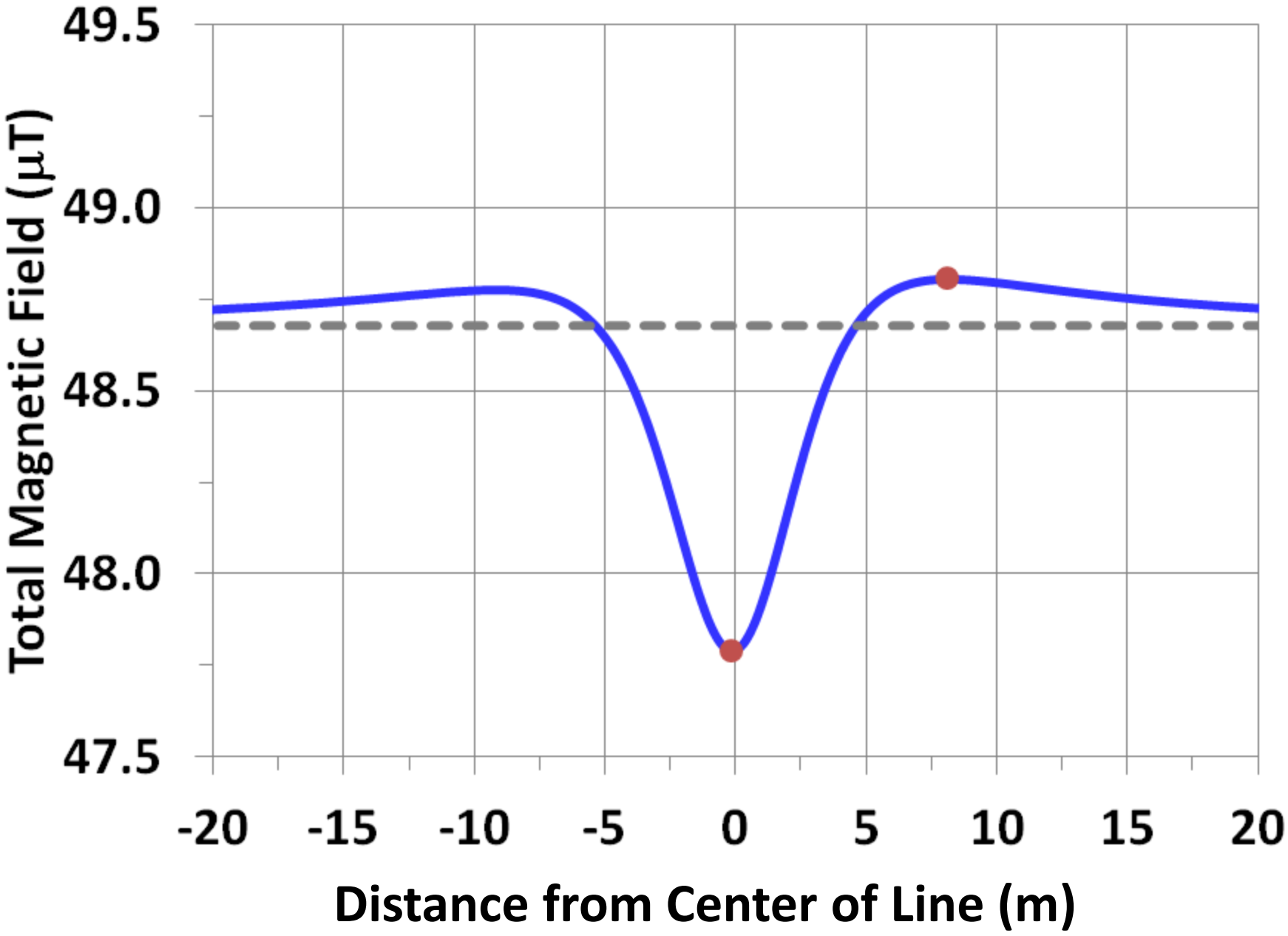
49.5
49.0
48.5
48.0
47.5
Total Magnetic Field (µT)
-20
-15
-10
-5
0
5
10
15
20
Distance from Center of Line (m)

30,-90

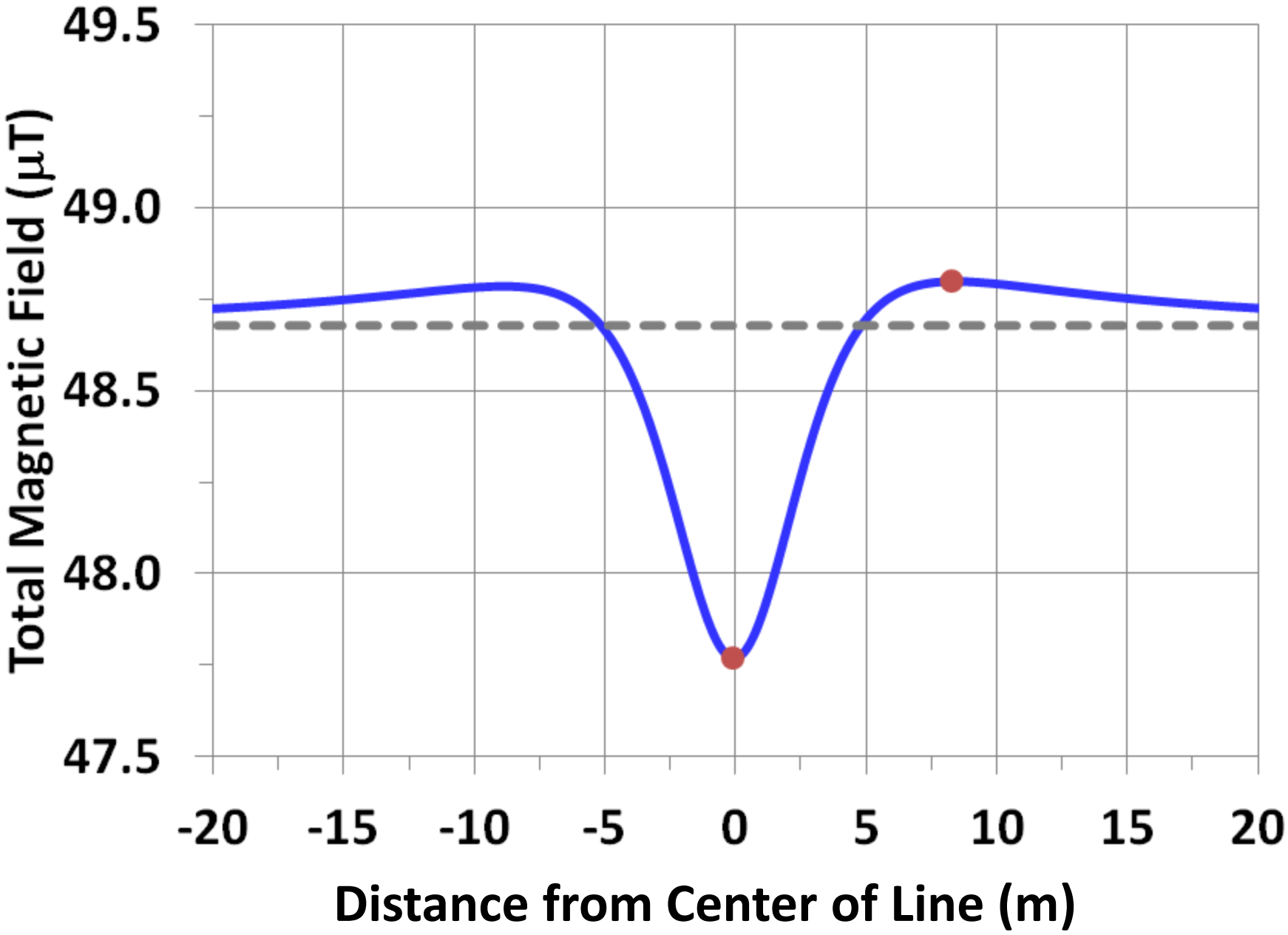
49.5
49.0
48.5
48.0
47.5
Total Magnetic Field (µT)
-20
-15
-10
-5
0
5
10
15
20
Distance from Center of Line (m)

45,0

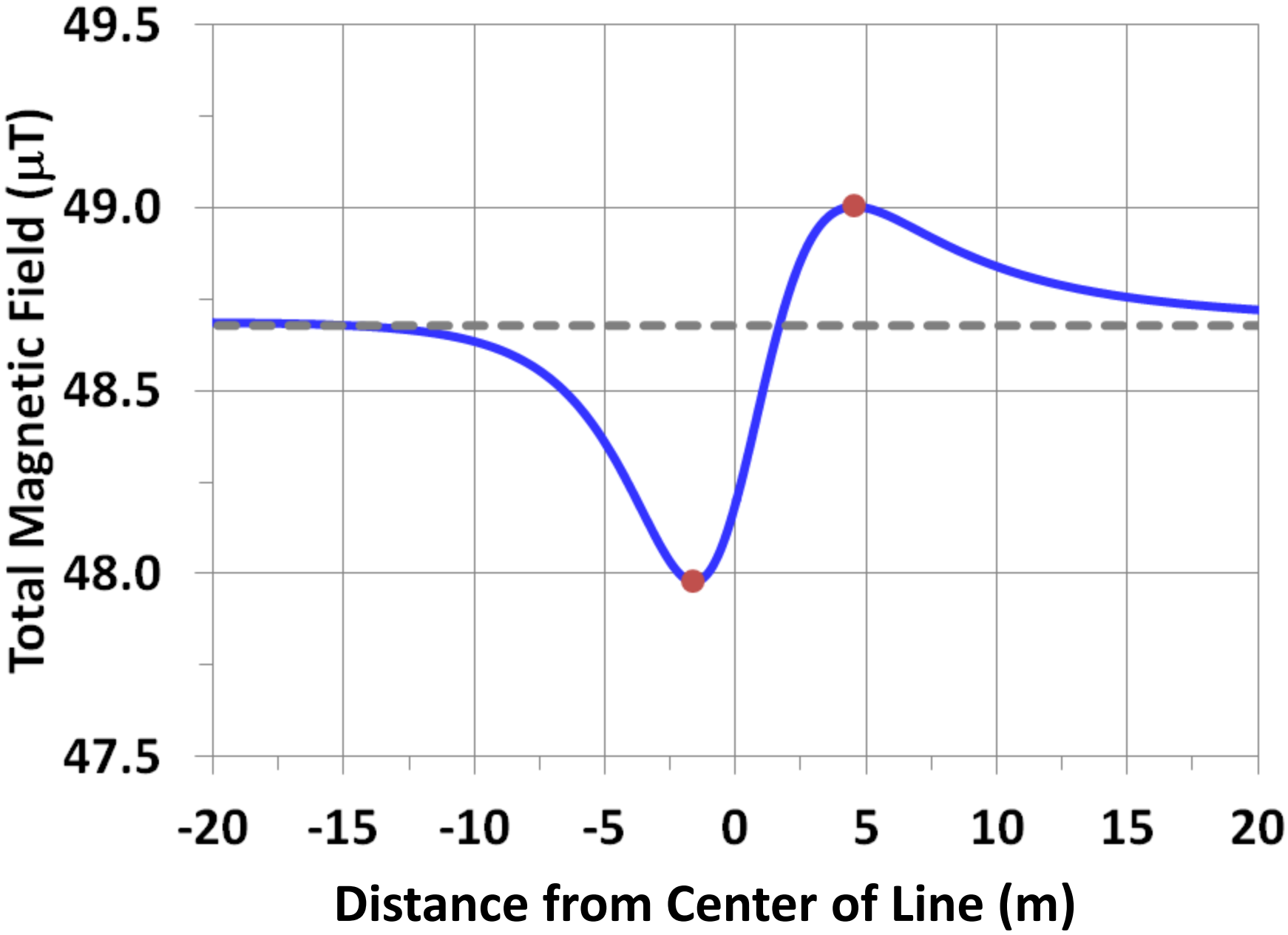
49.5
49.0
48.5
48.0
47.5
Total Magnetic Field (µT)
-20
-15
-10
-5
0
5
10
15
20
Distance from Center of Line (m)

45,-15

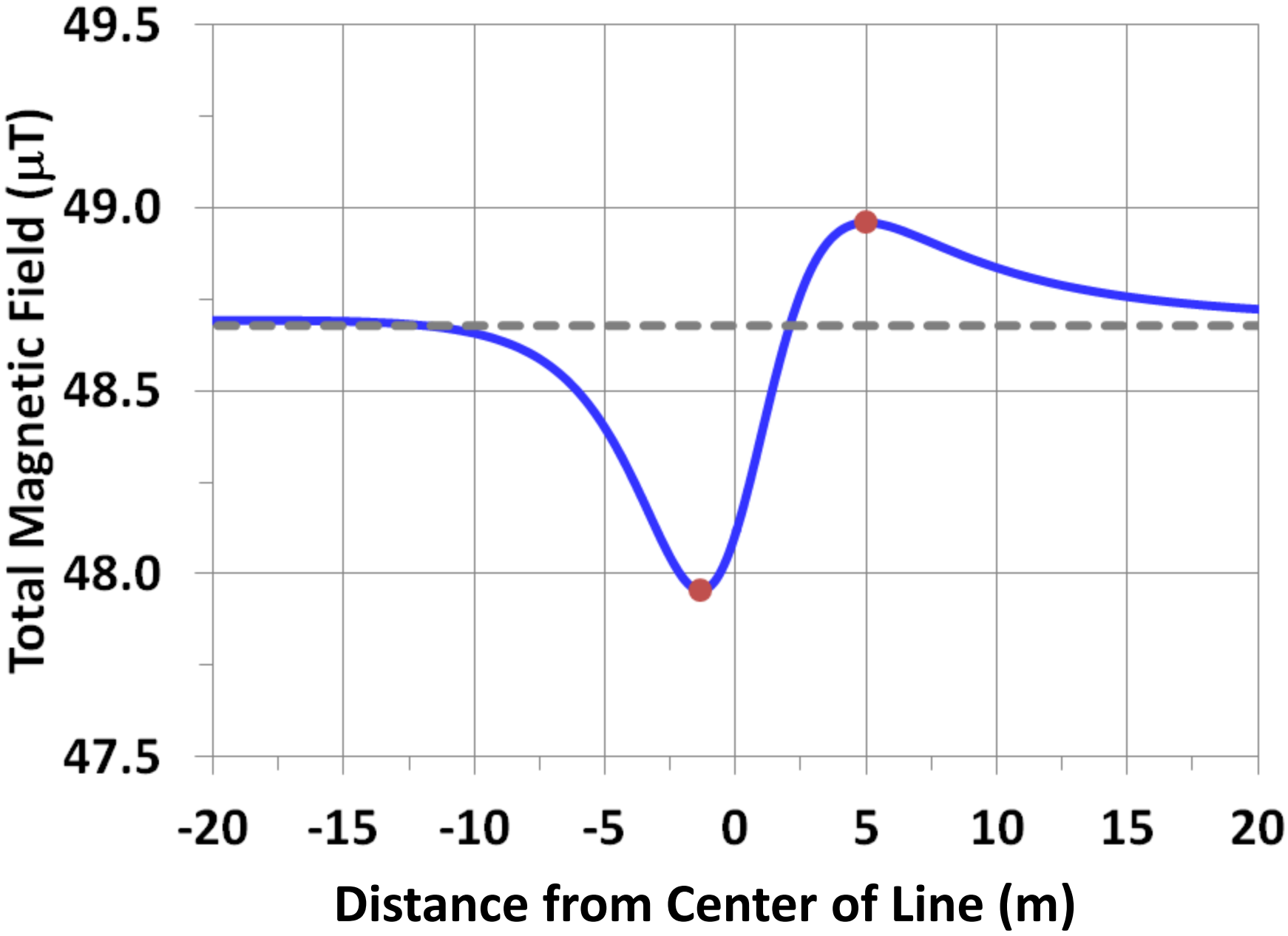
49.5
49.0
48.5
48.0
47.5
Total Magnetic Field (µT)
-20
-15
-10
-5
0
5
10
15
20
Distance from Center of Line (m)

45,-30

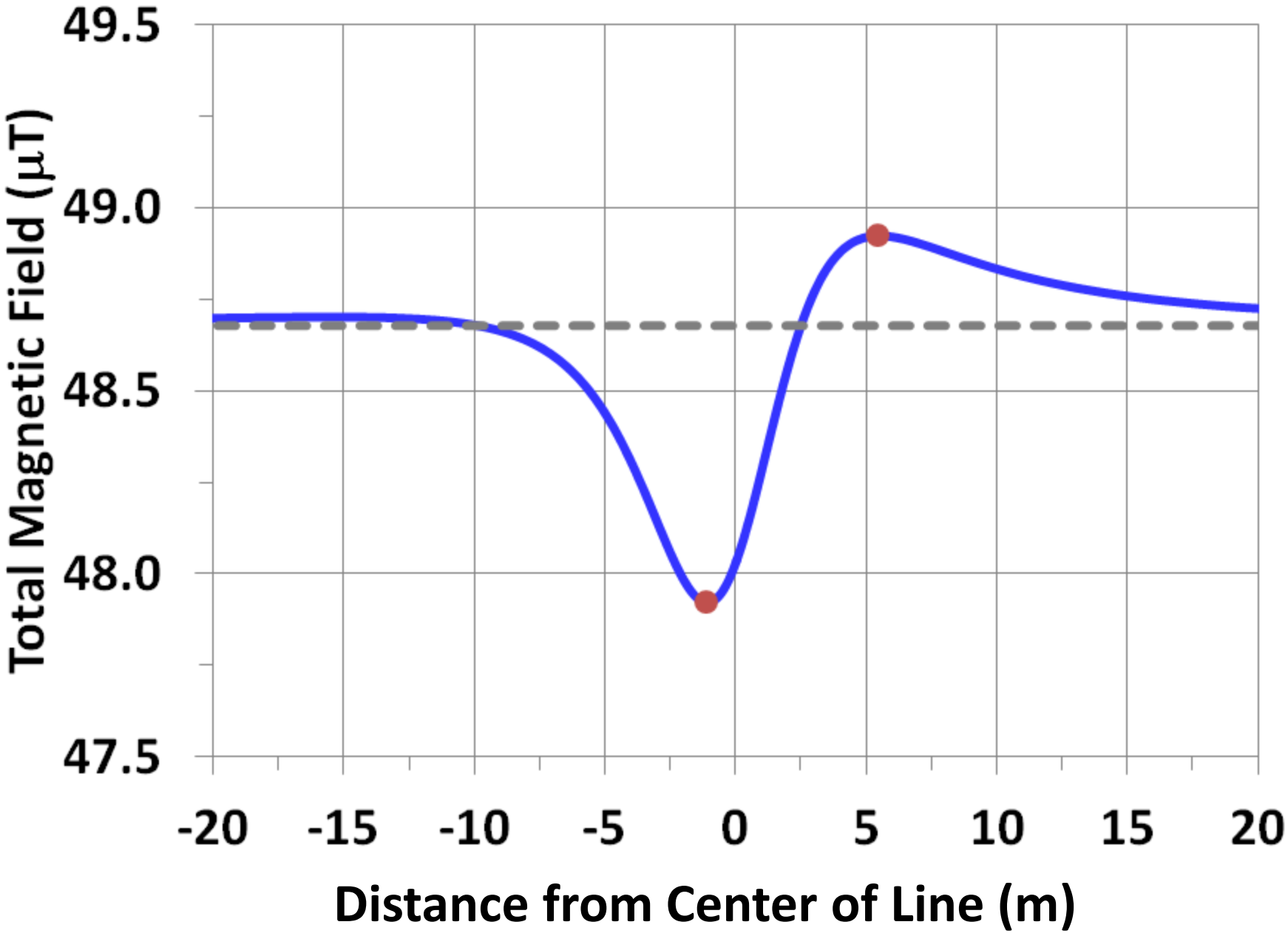
49.5
49.0
48.5
48.0
47.5
Total Magnetic Field (µT)
-20
-15
-10
-5
0
5
10
15
20
Distance from Center of Line (m)

45,-45

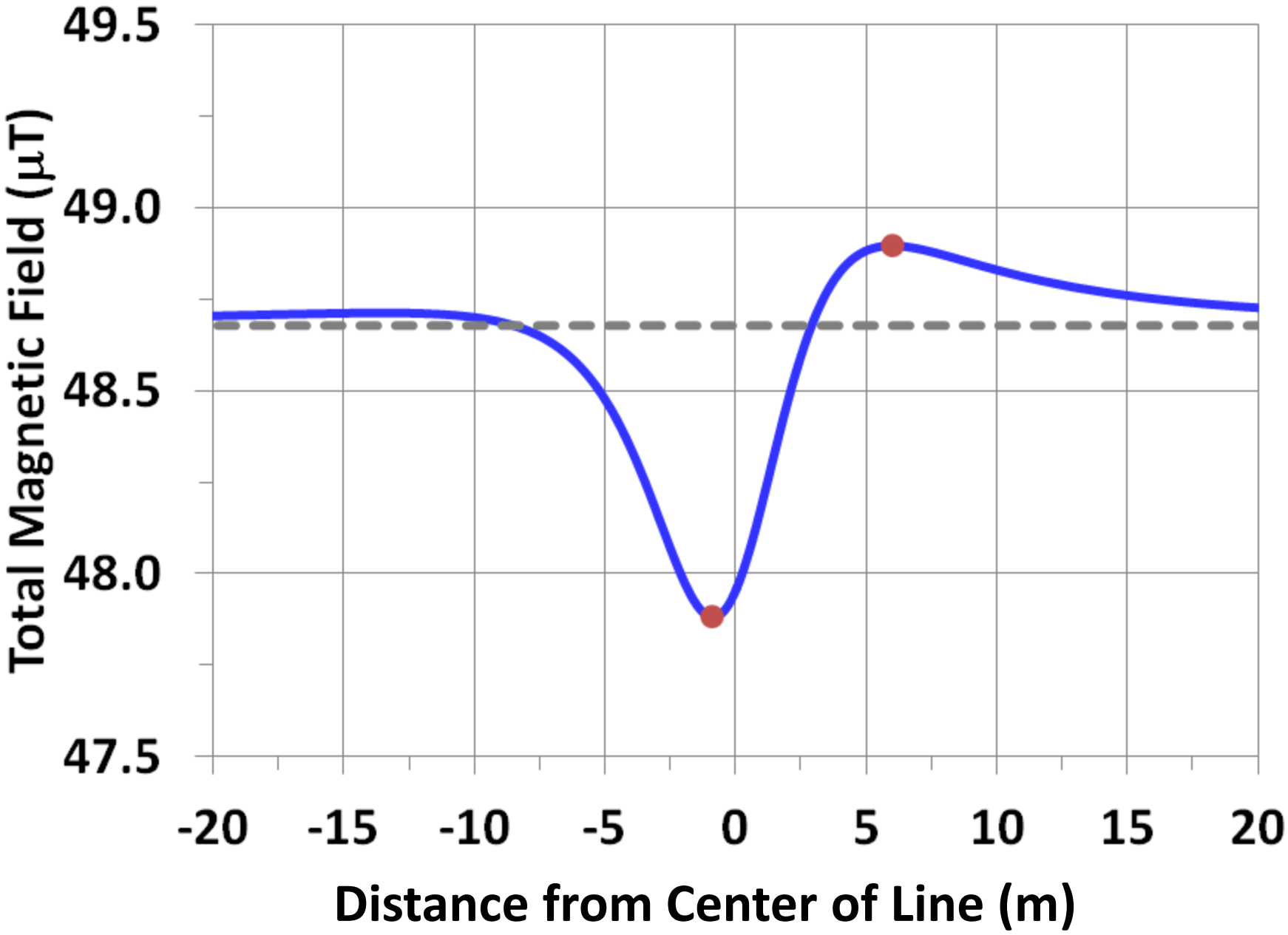
49.5
49.0
48.5
48.0
47.5
Total Magnetic Field (µT)
-20
-15
-10
-5
0
5
10
15
20
Distance from Center of Line (m)

45,-60

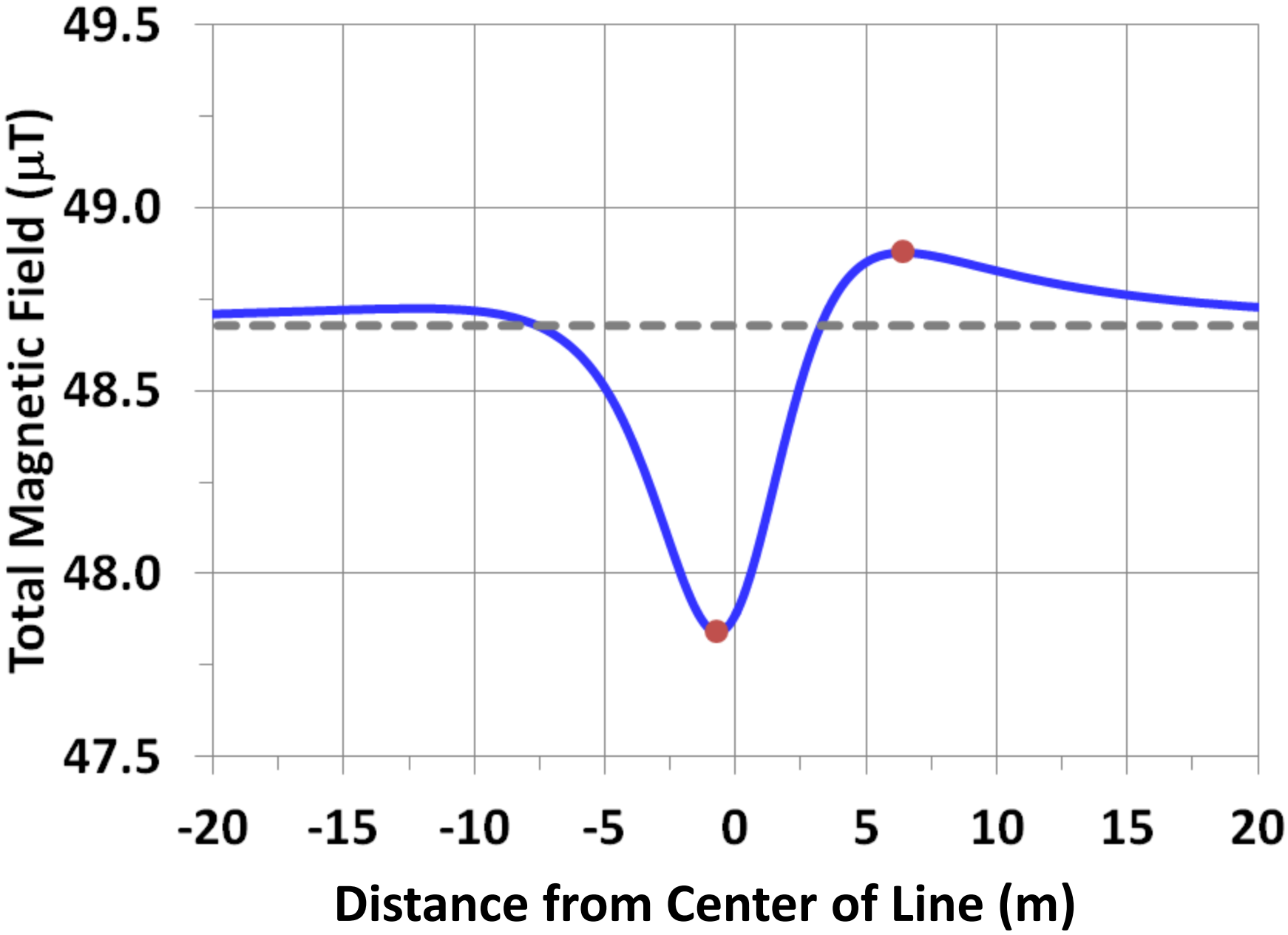
49.5
49.0
48.5
48.0
47.5
Total Magnetic Field (µT)
-20
-15
-10
-5
0
5
10
15
20
Distance from Center of Line (m)

45,-75

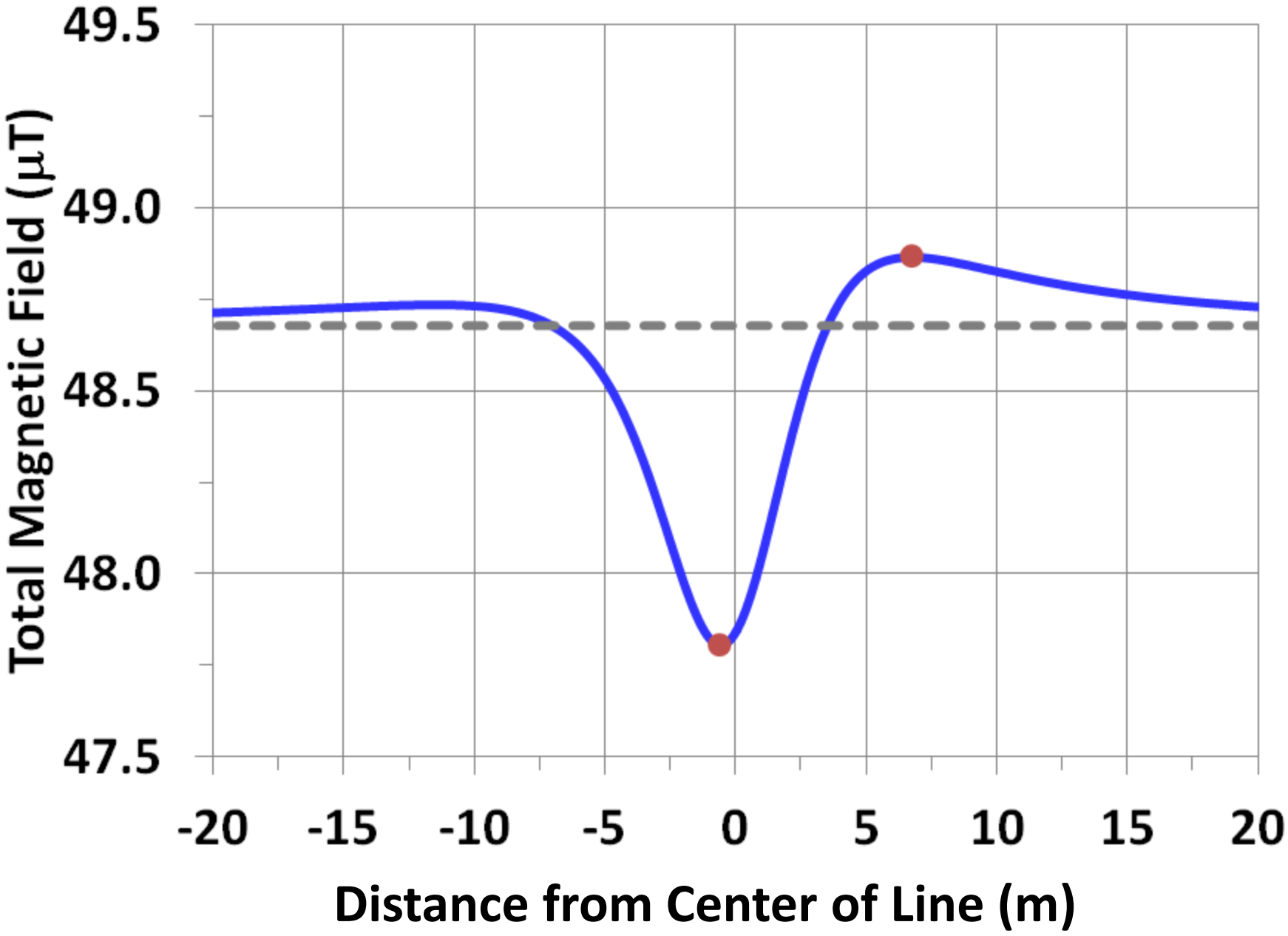
49.5
49.0
48.5
48.0
47.5
Total Magnetic Field (µT)
-20
-15
-10
-5
0
5
10
15
20
Distance from Center of Line (m)

45,-90

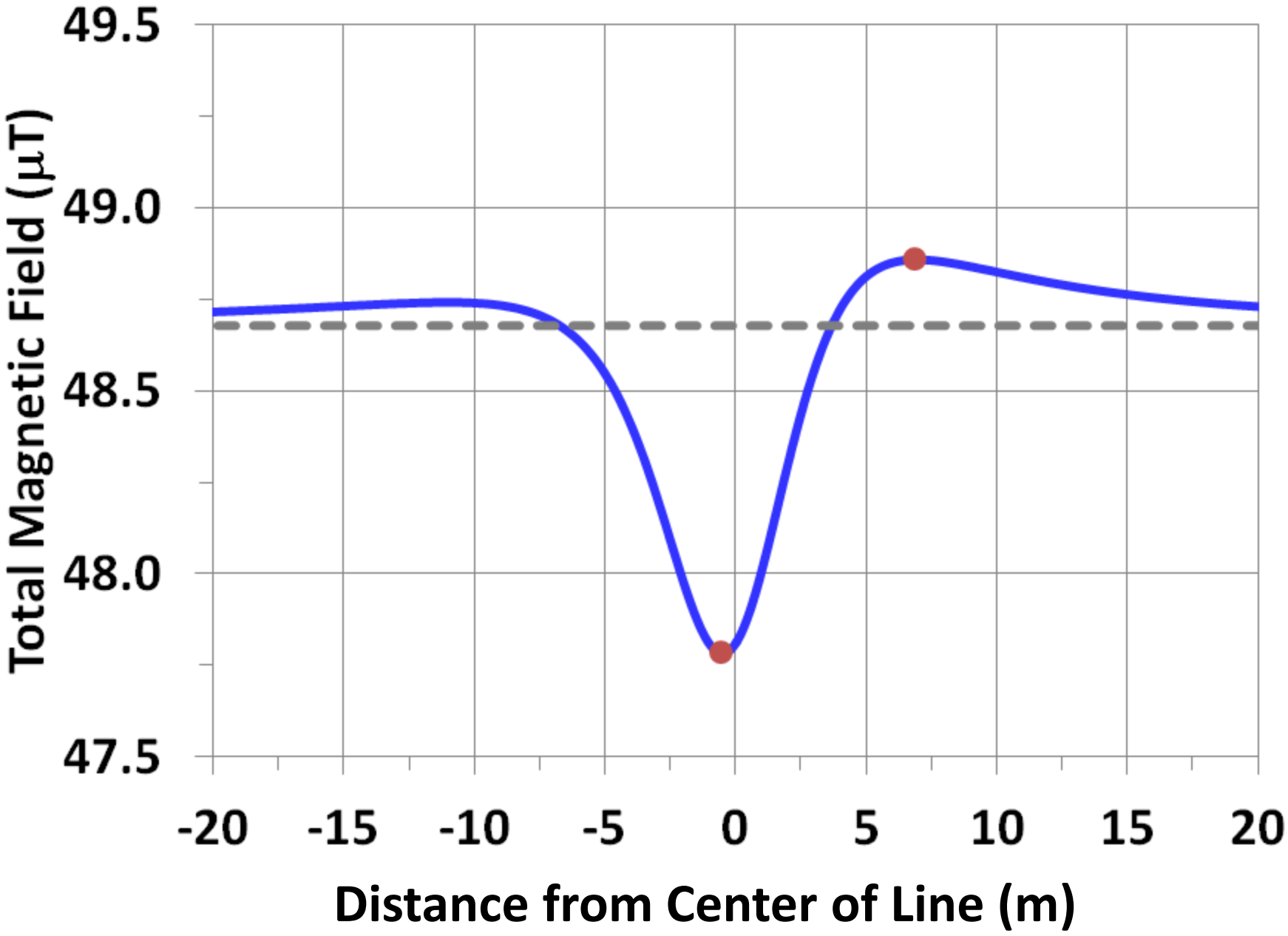
49.5
49.0
48.5
48.0
47.5
Total Magnetic Field (µT)
-20
-15
-10
-5
0
5
10
15
20
Distance from Center of Line (m)

60,0

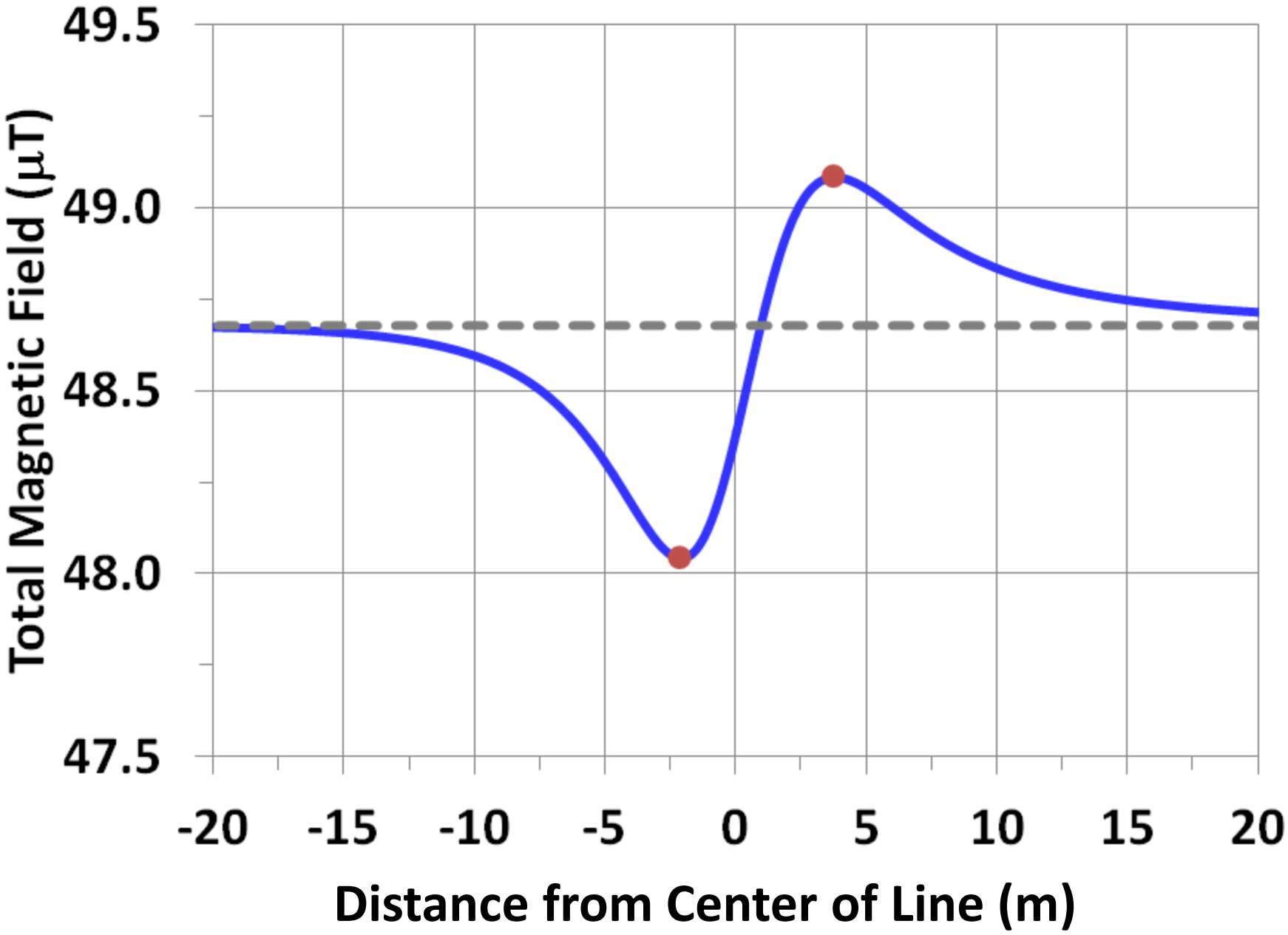
49.5
49.0
48.5
48.0
47.5
Total Magnetic Field (µT)
-20
-15
-10
-5
0
5
10
15
20
Distance from Center of Line (m)

60,-15

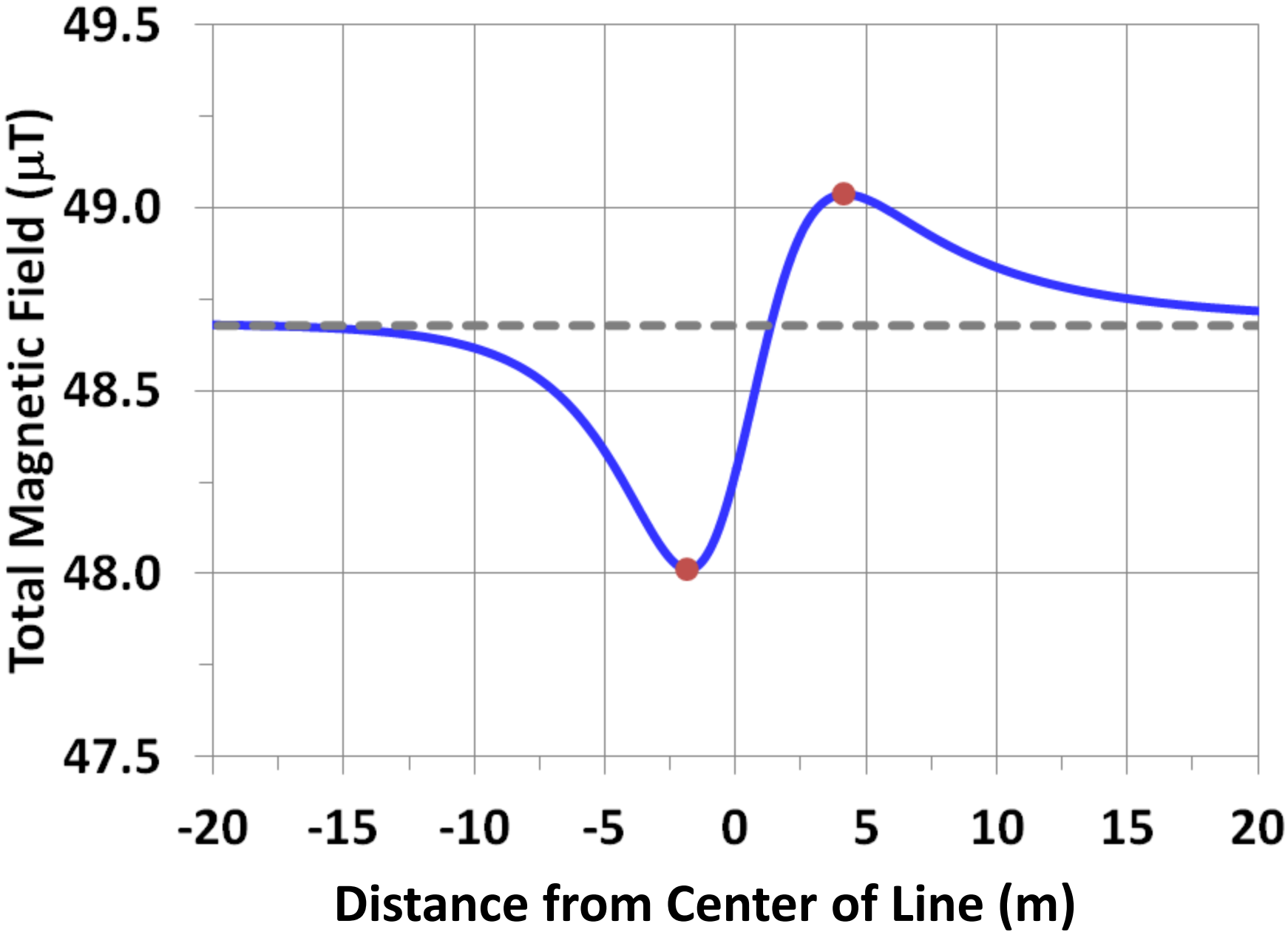
49.5
49.0
48.5
48.0
47.5
Total Magnetic Field (µT)
-20
-15
-10
-5
0
5
10
15
20
Distance from Center of Line (m)

60,-30

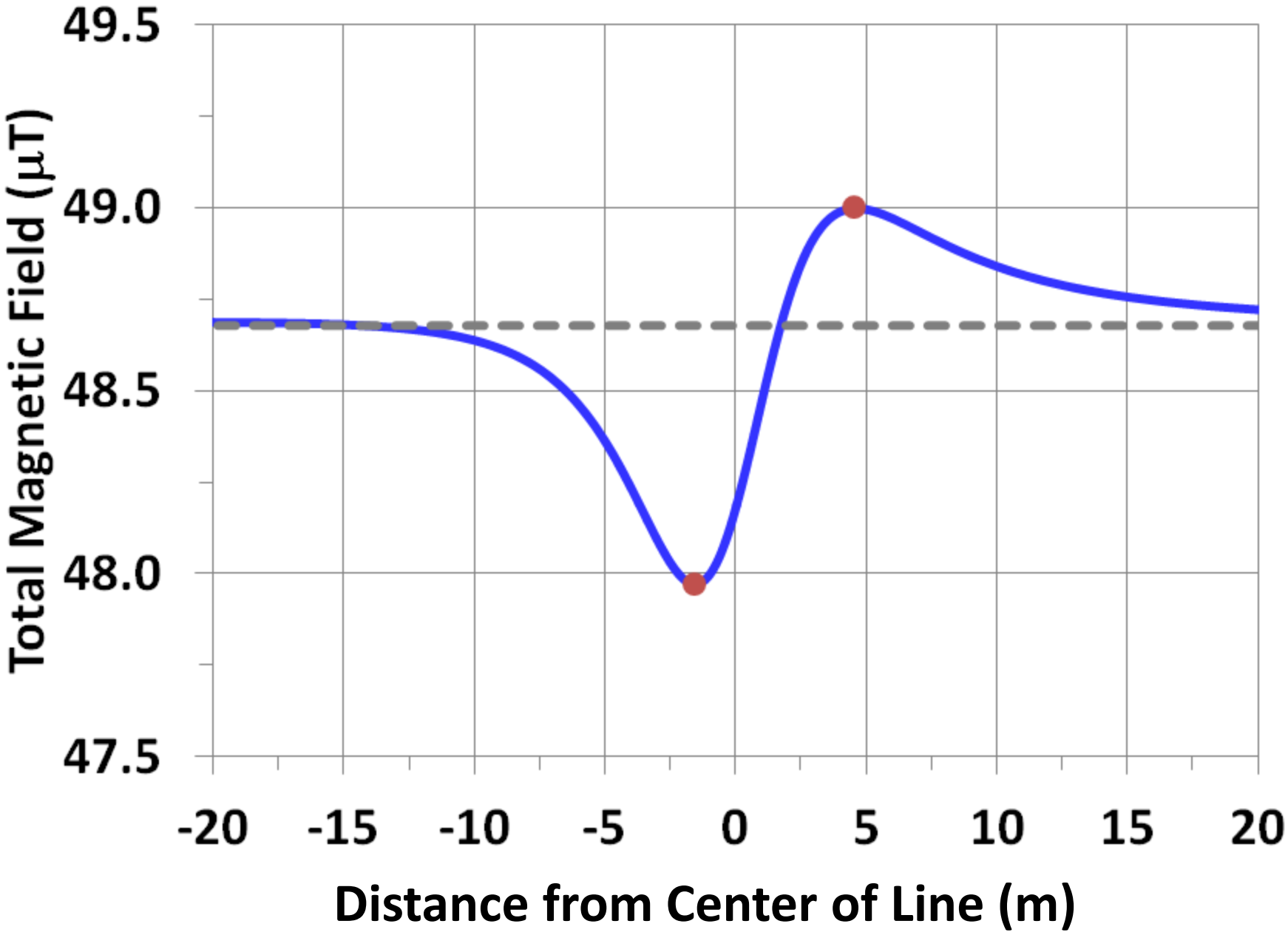
49.5
49.0
48.5
48.0
47.5
Total Magnetic Field (µT)
-20
-15
-10
-5
0
5
10
15
20
Distance from Center of Line (m)

60,-45

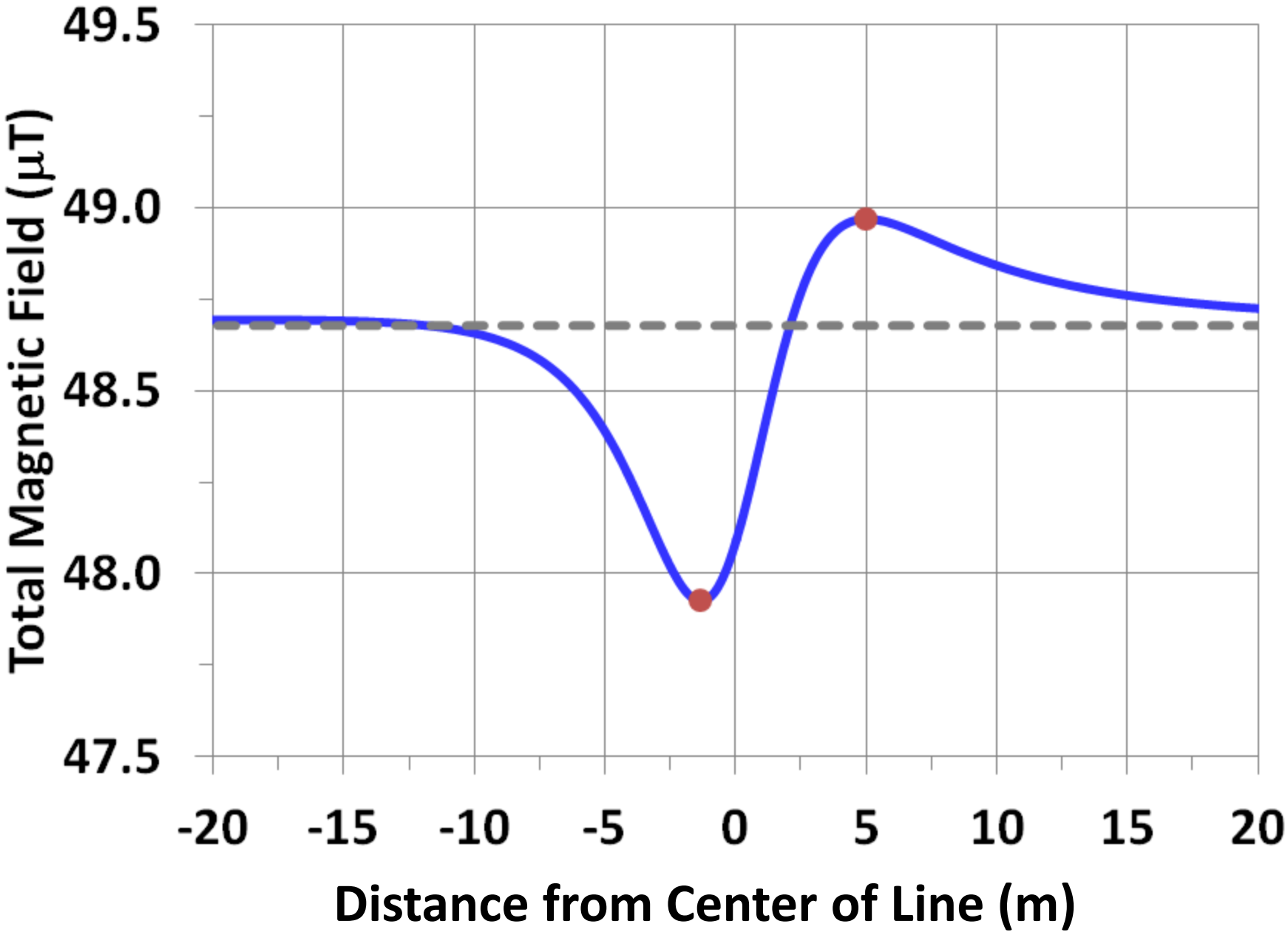
49.5
49.0
48.5
48.0
47.5
Total Magnetic Field (µT)
-20
-15
-10
-5
0
5
10
15
20
Distance from Center of Line (m)

60,-60

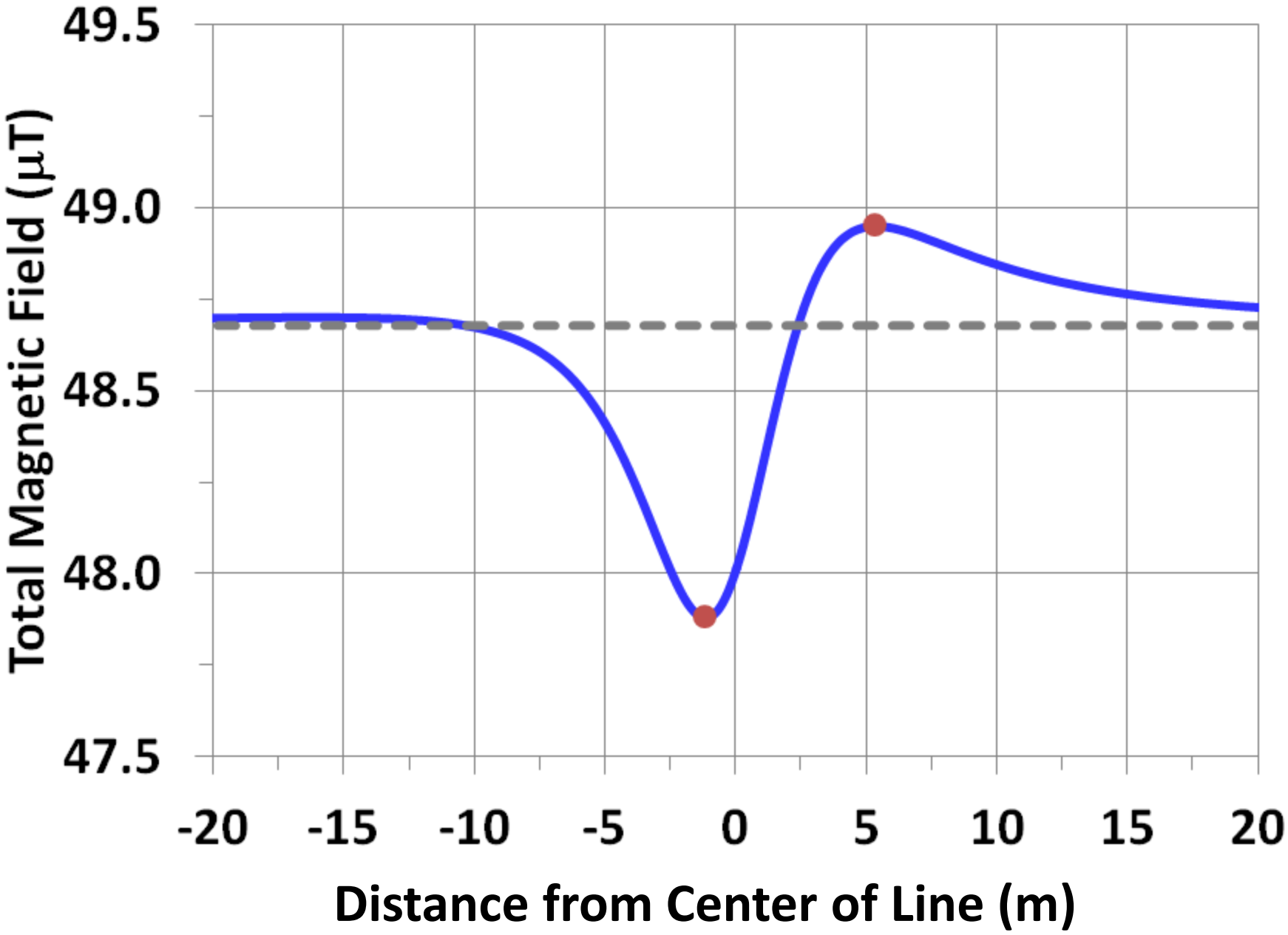
49.5
49.0
48.5
48.0
47.5
Total Magnetic Field (µT)
-20
-15
-10
-5
0
5
10
15
20
Distance from Center of Line (m)

60,-75

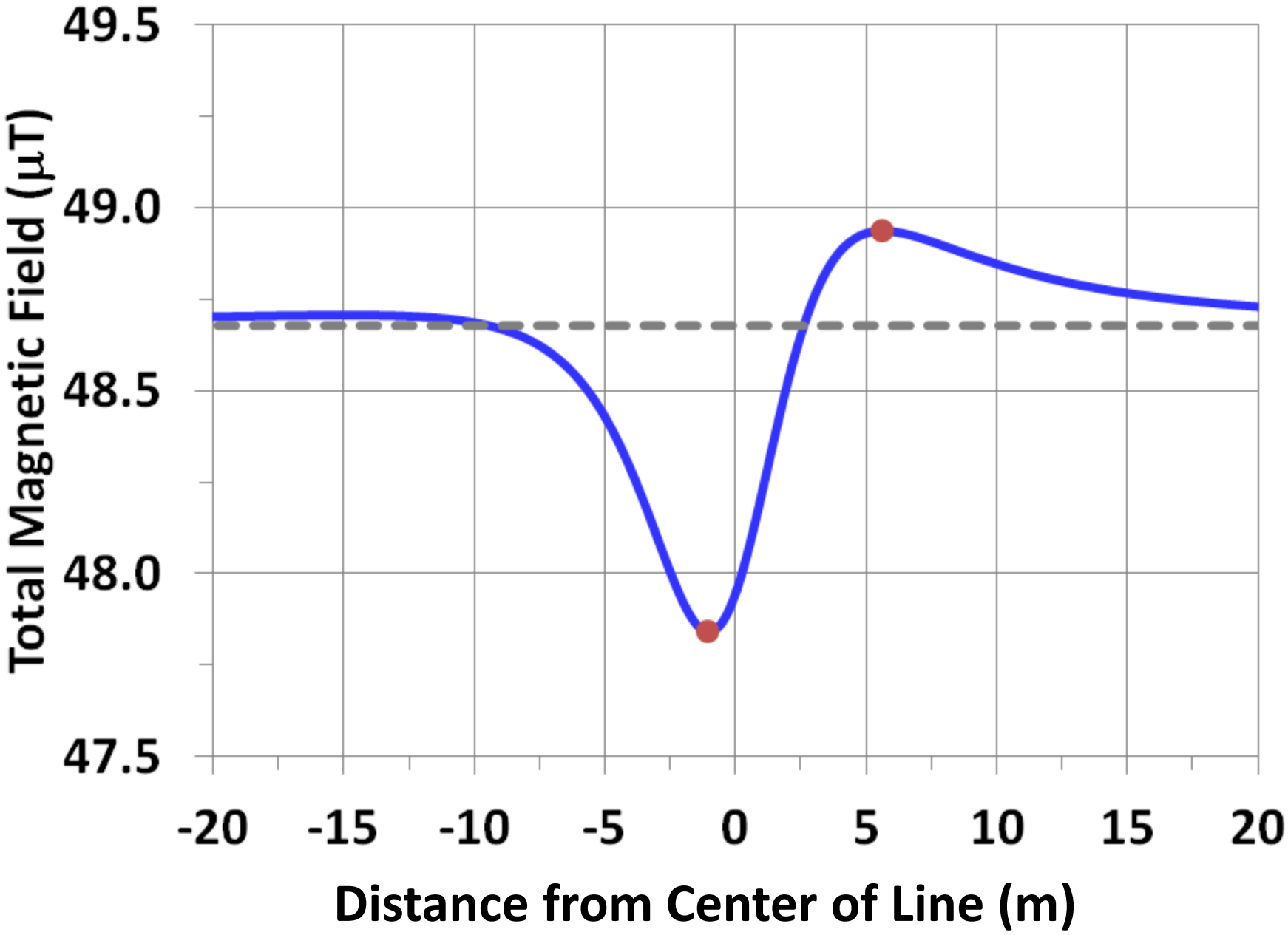
49.5
49.0
48.5
48.0
47.5
Total Magnetic Field (µT)
-20
-15
-10
-5
0
5
10
15
20
Distance from Center of Line (m)

60,-90

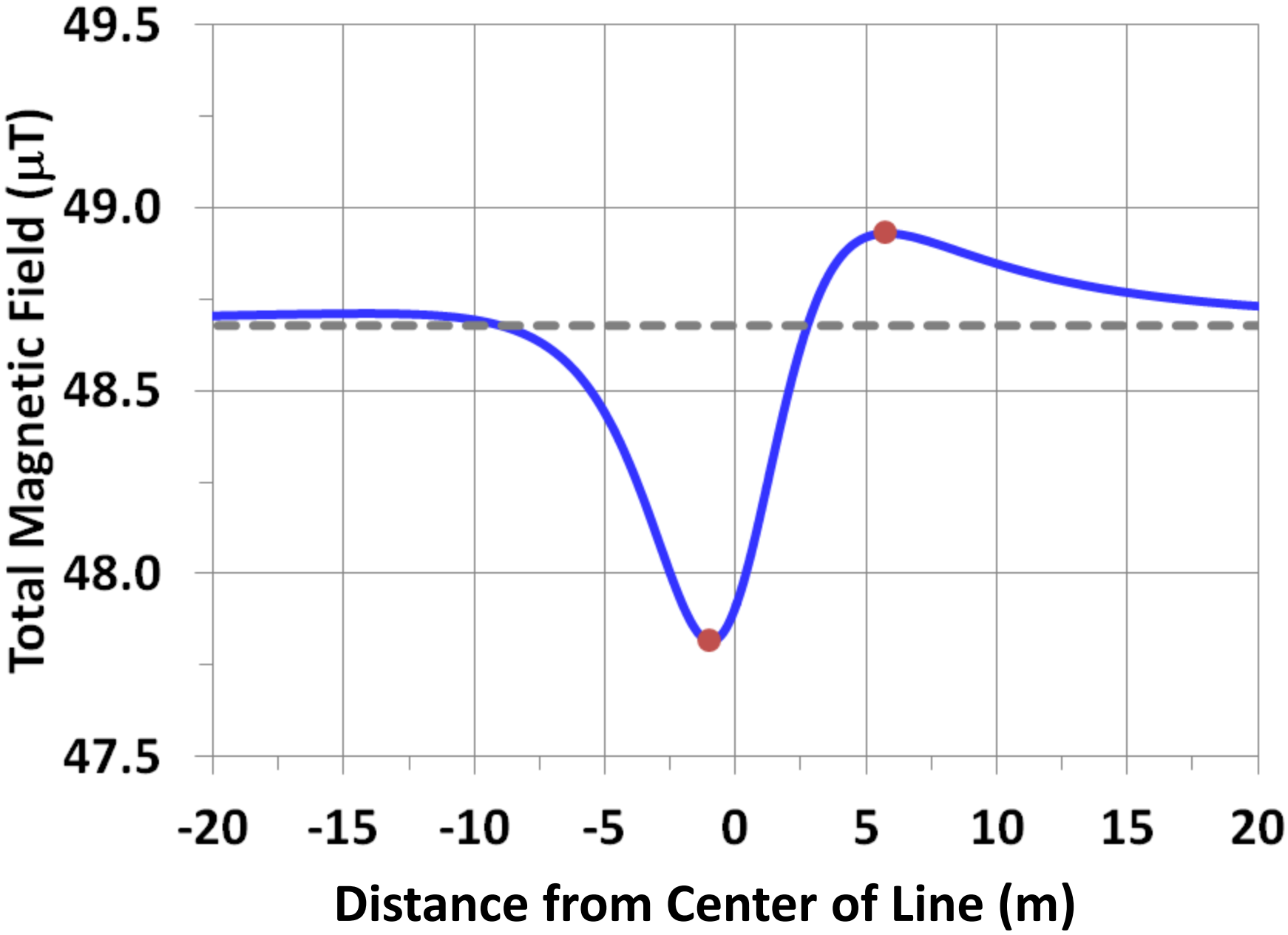
49.5
49.0
48.5
48.0
47.5
Total Magnetic Field (µT)
-20
-15
-10
-5
0
5
10
15
20
Distance from Center of Line (m)

75,0

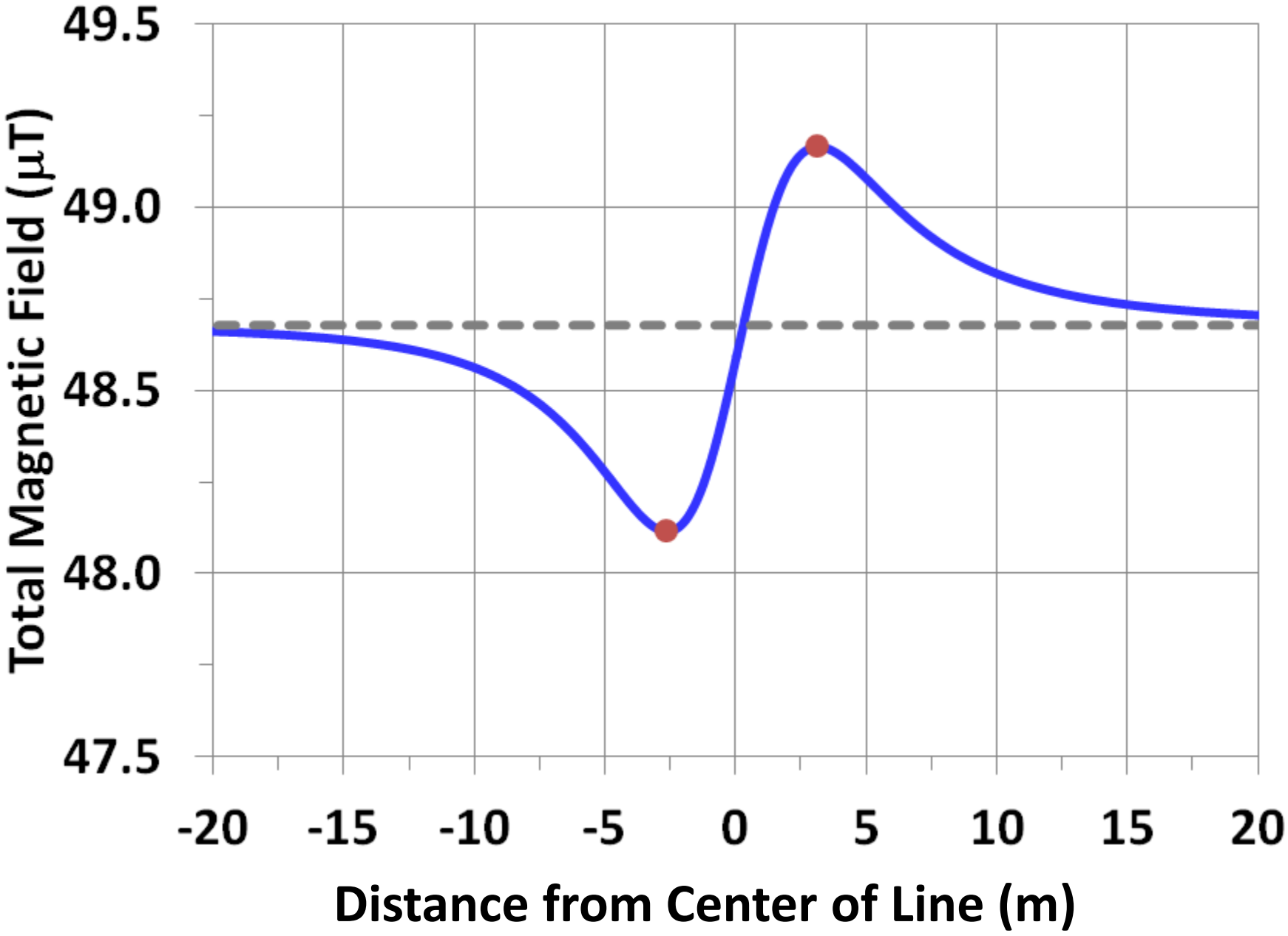
49.5
49.0
48.5
48.0
47.5
Total Magnetic Field (µT)
-20
-15
-10
-5
0
5
10
15
20
Distance from Center of Line (m)

75,-15

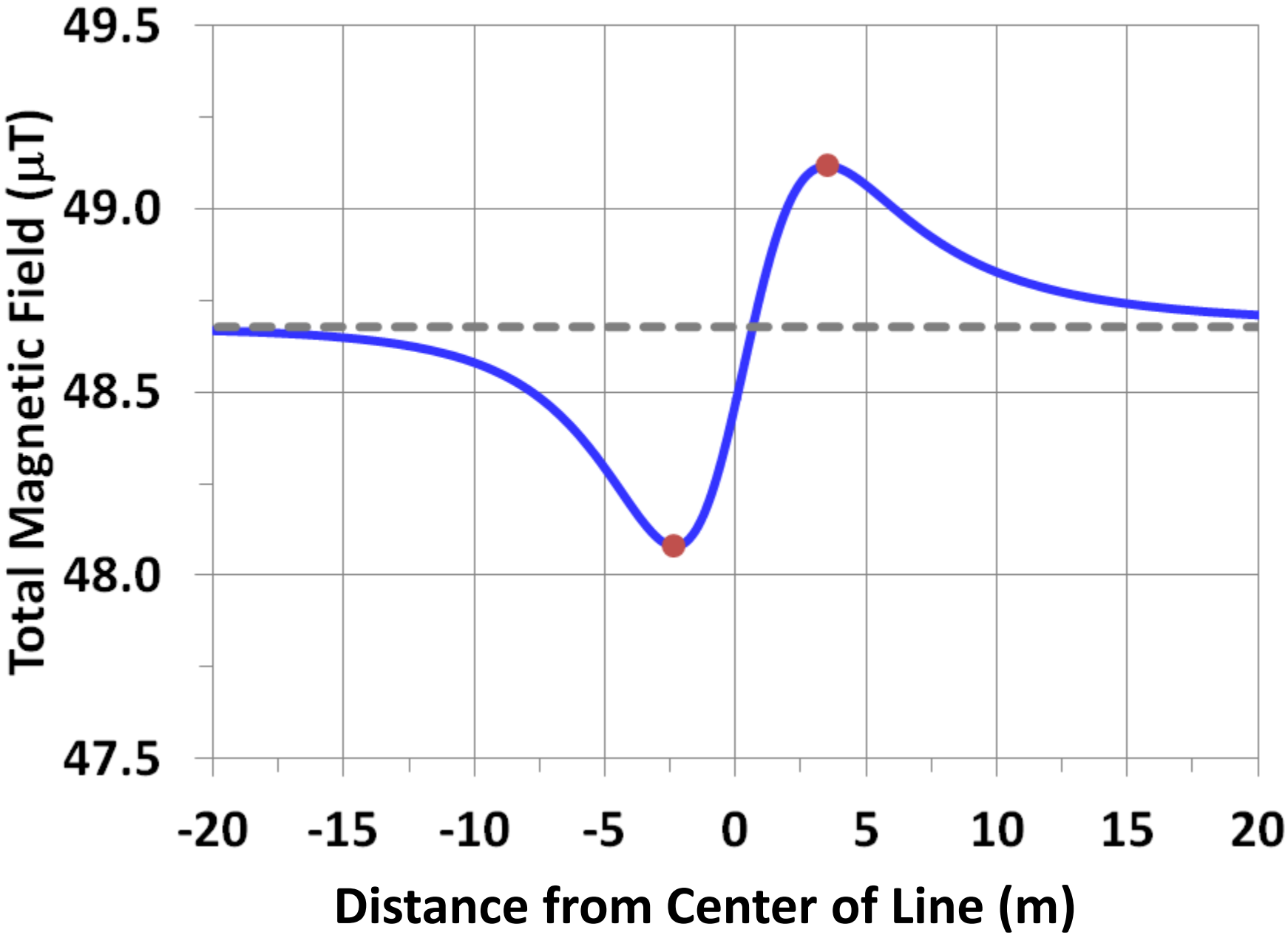
49.5
49.0
48.5
48.0
47.5
Total Magnetic Field (µT)
-20
-15
-10
-5
0
5
10
15
20
Distance from Center of Line (m)

75,-30

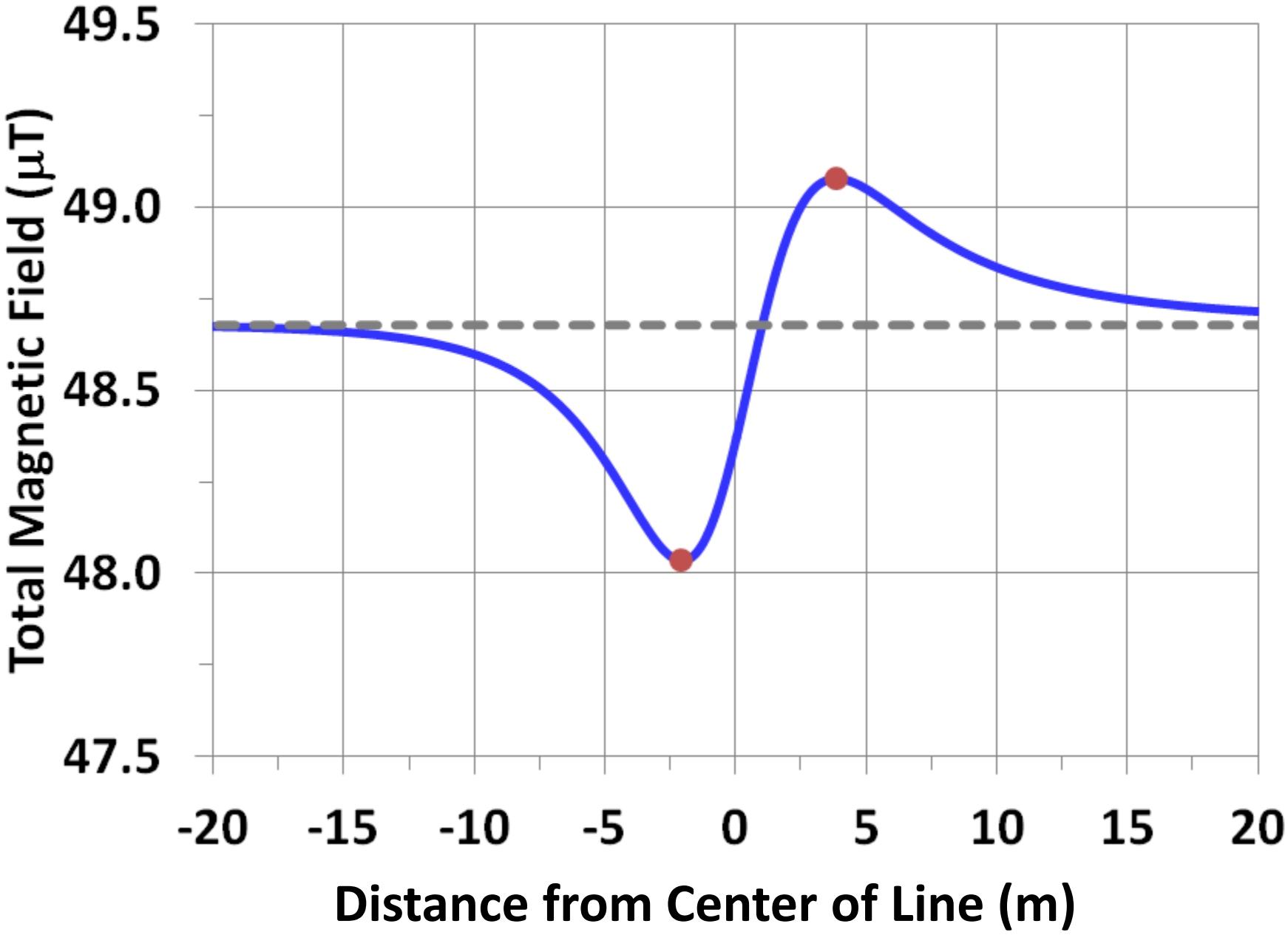
49.5
49.0
48.5
48.0
47.5
Total Magnetic Field (µT)
-20
-15
-10
-5
0
5
10
15
20
Distance from Center of Line (m)

75,-45

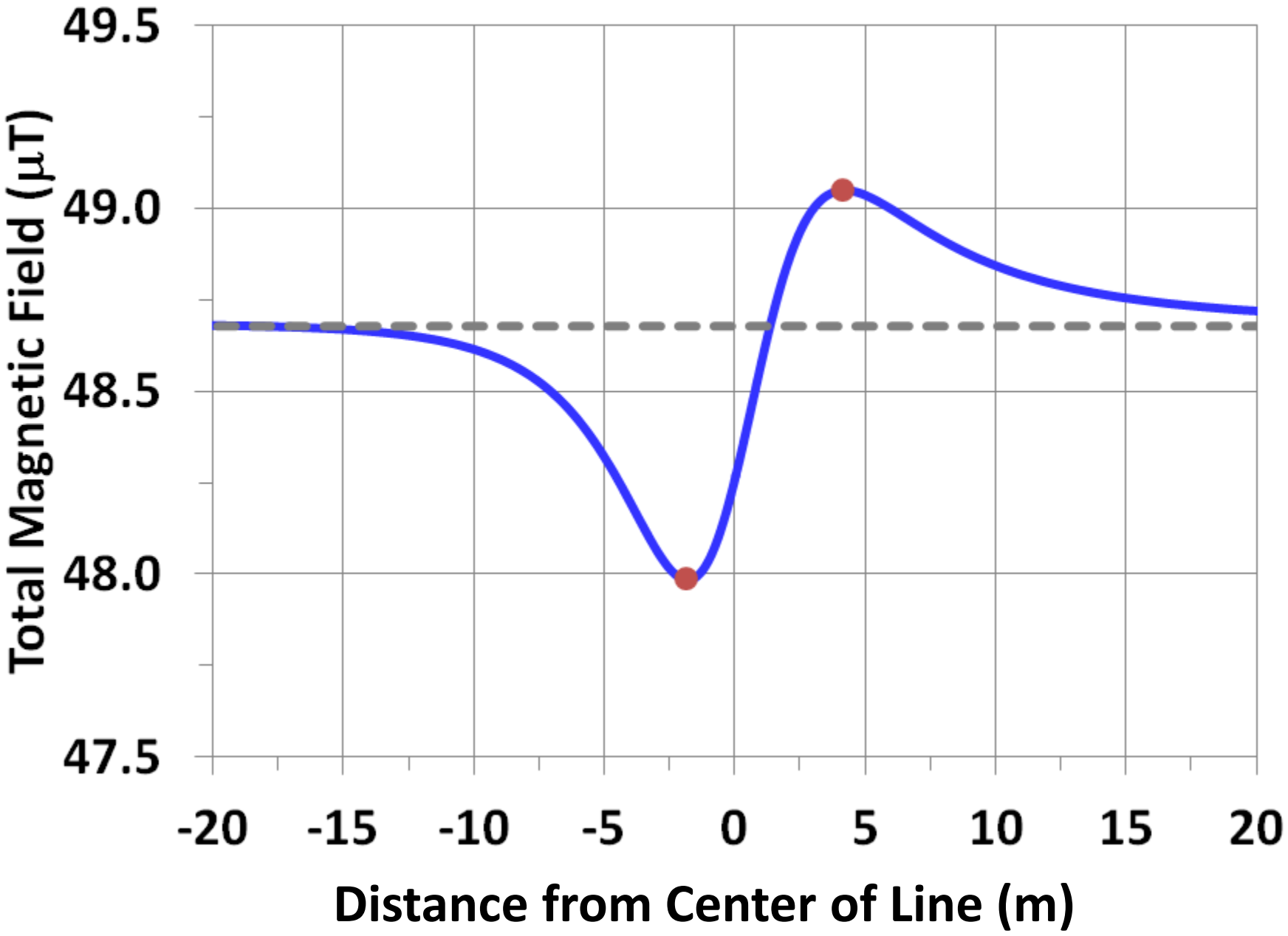
49.5
49.0
48.5
48.0
47.5
Total Magnetic Field (µT)
-20
-15
-10
-5
0
5
10
15
20
Distance from Center of Line (m)

75,-60

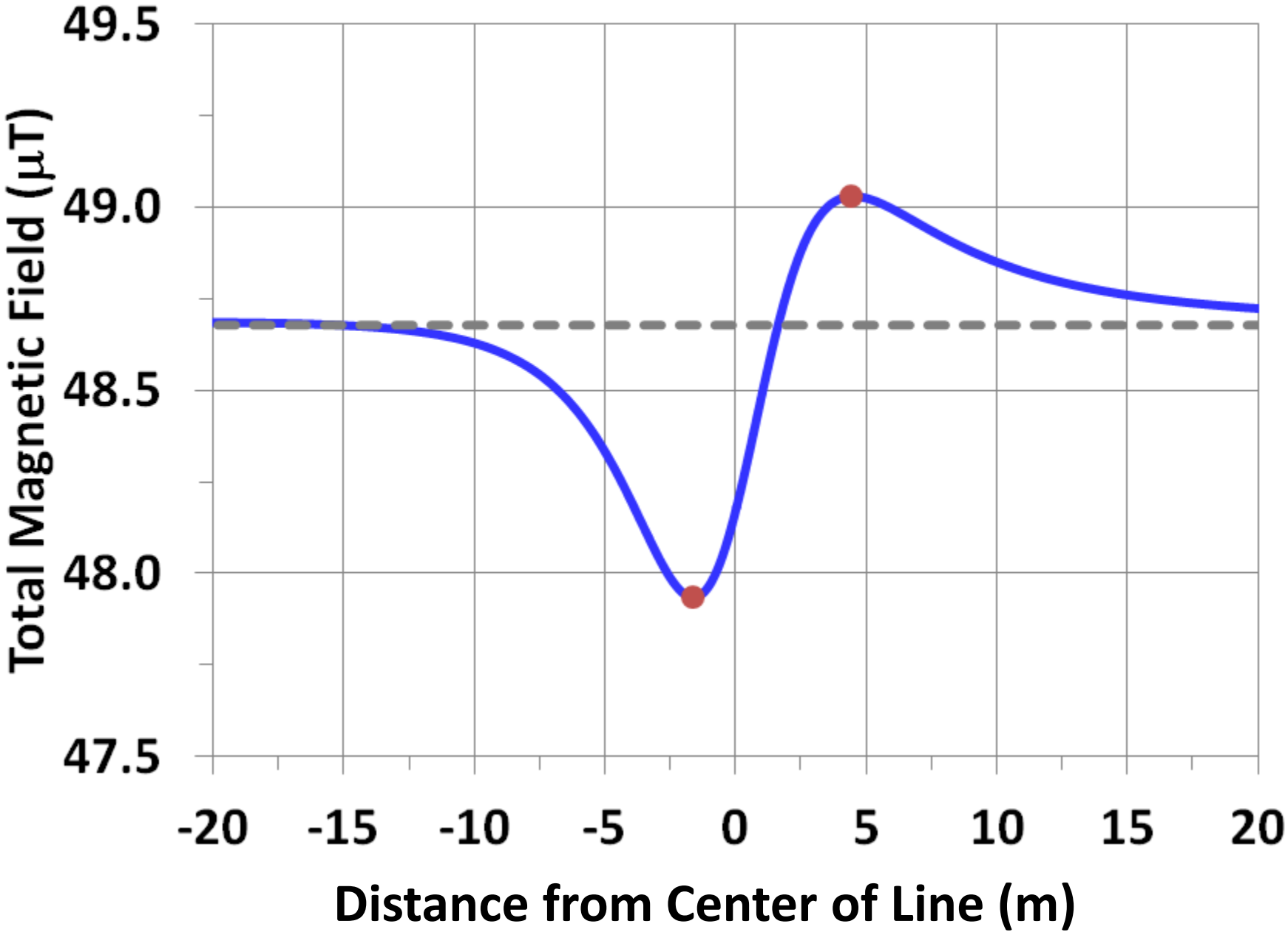
49.5
49.0
48.5
48.0
47.5
Total Magnetic Field (µT)
-20
-15
-10
-5
0
5
10
15
20
Distance from Center of Line (m)

75,-75

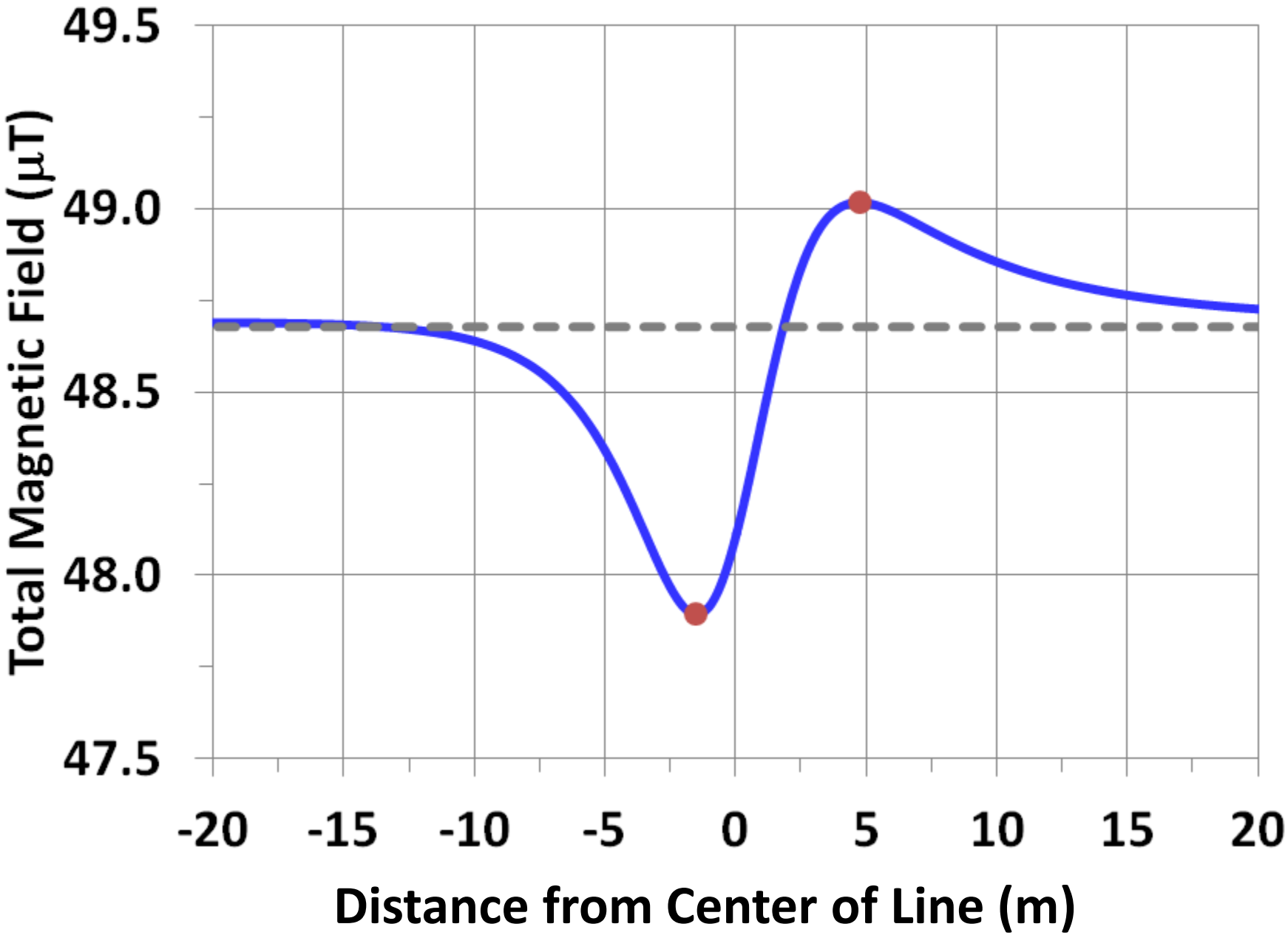
49.5
49.0
48.5
48.0
47.5
Total Magnetic Field (µT)
-20
-15
-10
-5
0
5
10
15
20
Distance from Center of Line (m)

75,-90

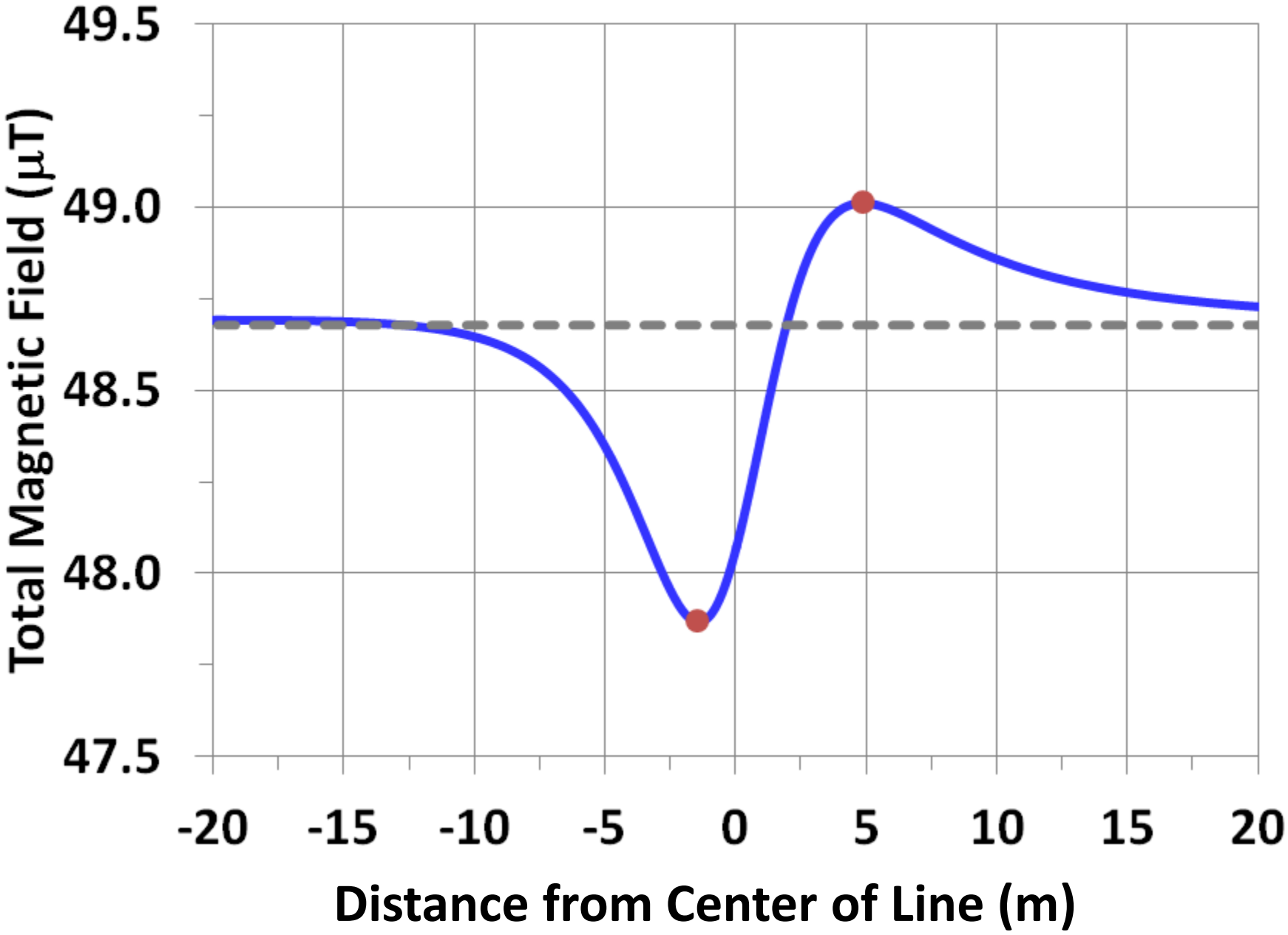
49.5
49.0
48.5
48.0
47.5
Total Magnetic Field (µT)
-20
-15
-10
-5
0
5
10
15
20
Distance from Center of Line (m)

90,0

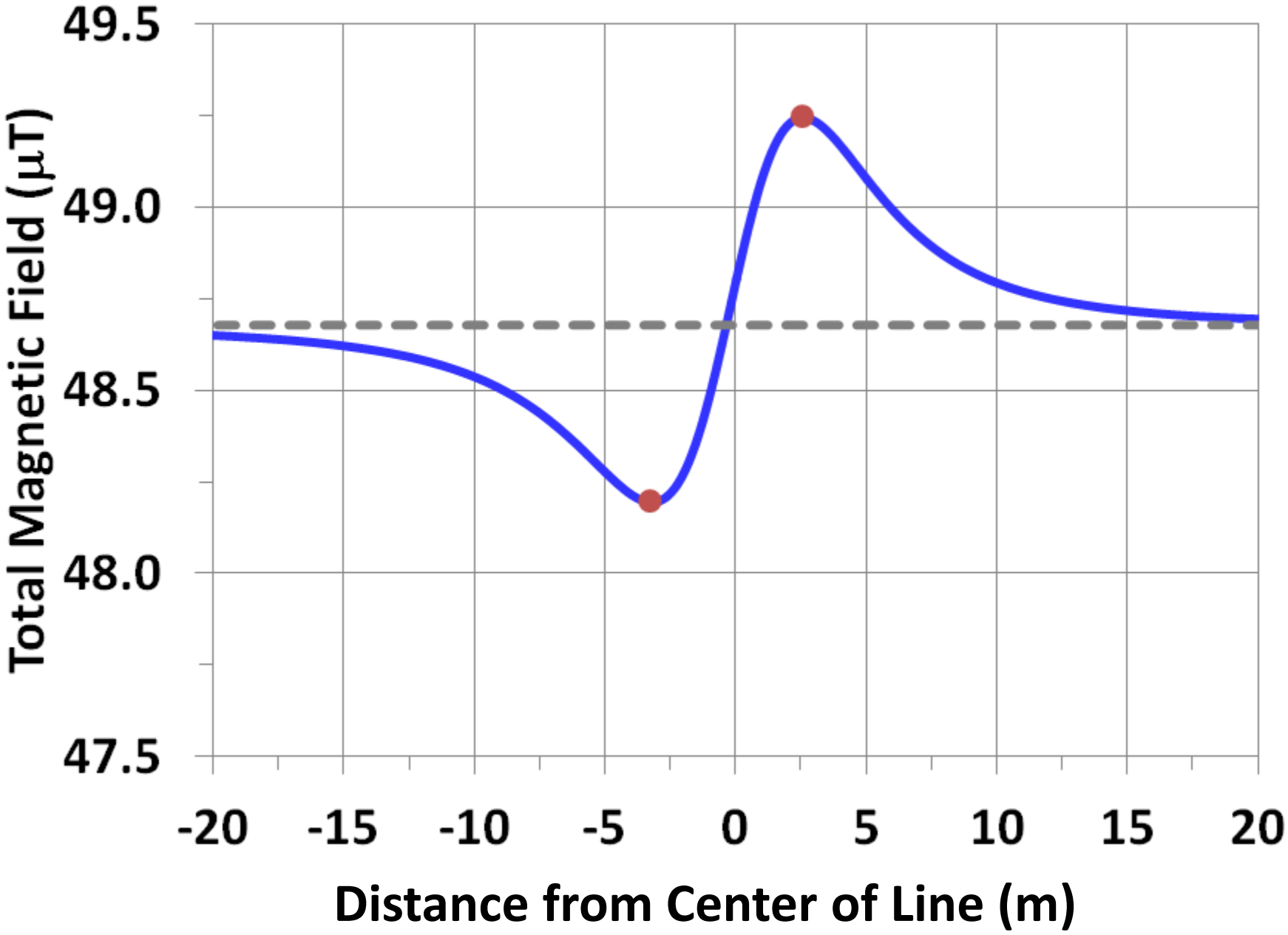
49.5
49.0
48.5
48.0
47.5
Total Magnetic Field (µT)
-20
-15
-10
-5
0
5
10
15
20
Distance from Center of Line (m)

90,-15

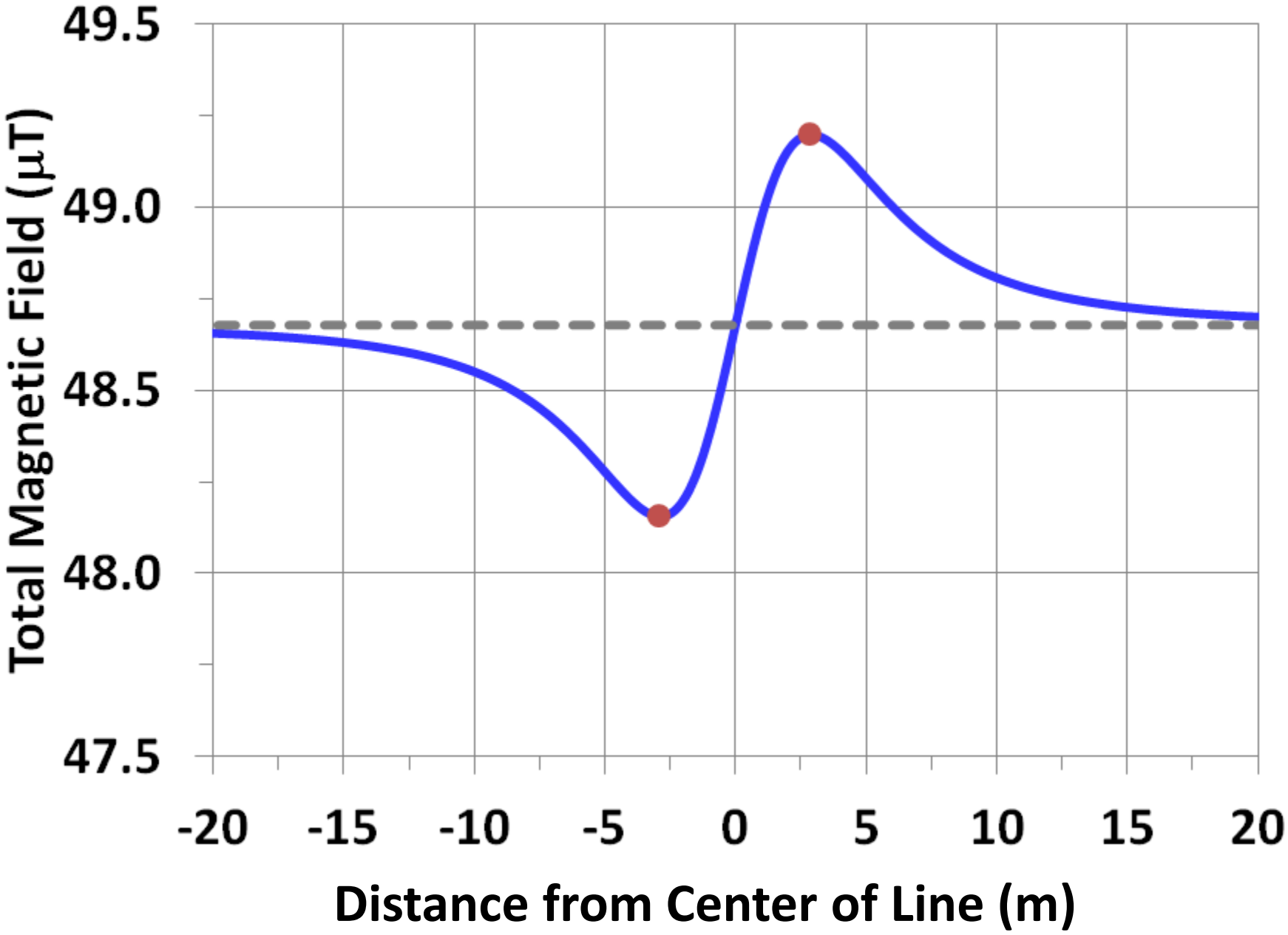
49.5
49.0
48.5
48.0
47.5
Total Magnetic Field (µT)
-20
-15
-10
-5
0
5
10
15
20
Distance from Center of Line (m)

90,-30

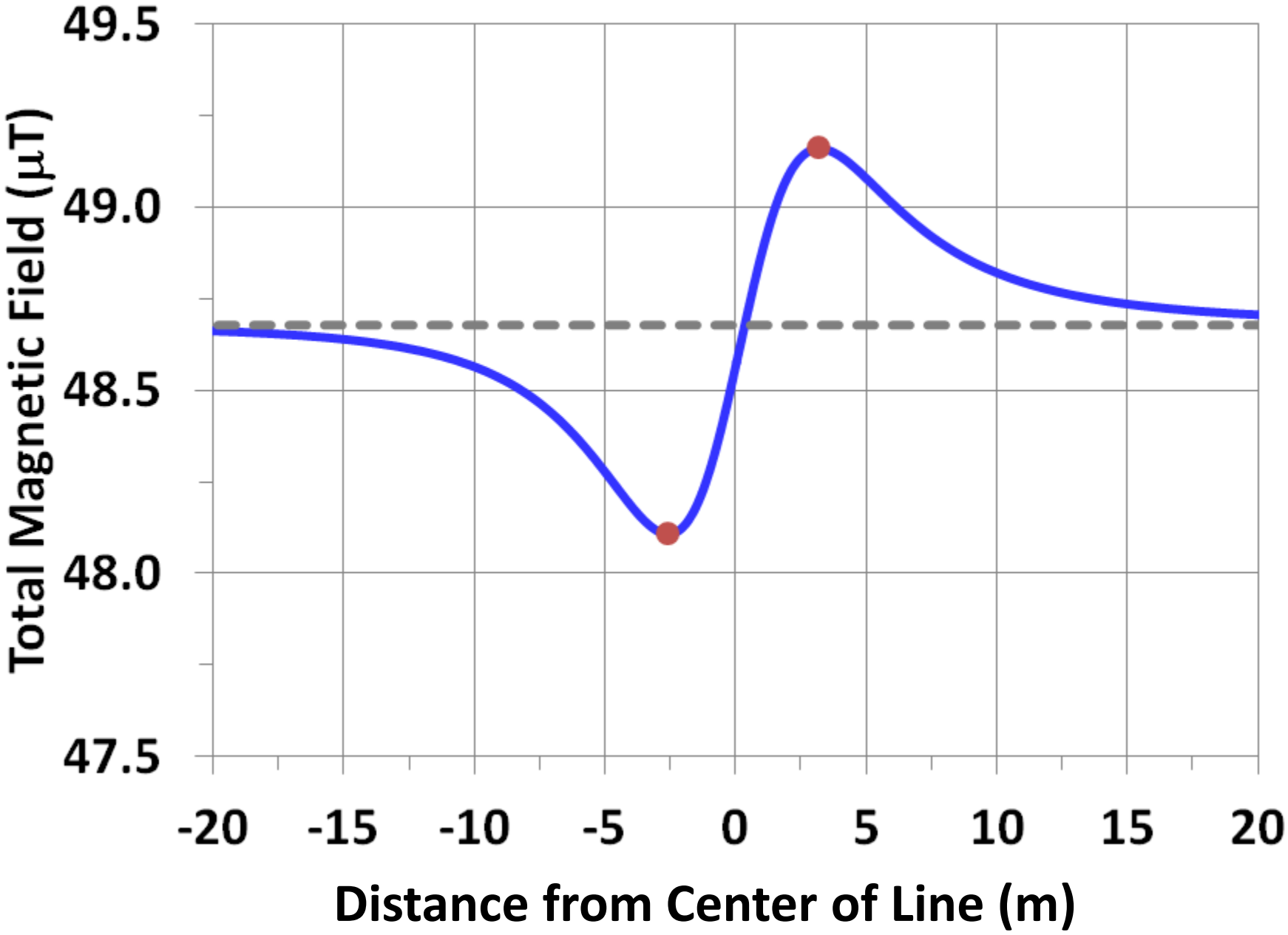
49.5
49.0
48.5
48.0
47.5
Total Magnetic Field (µT)
-20
-15
-10
-5
0
5
10
15
20
Distance from Center of Line (m)

90,-45

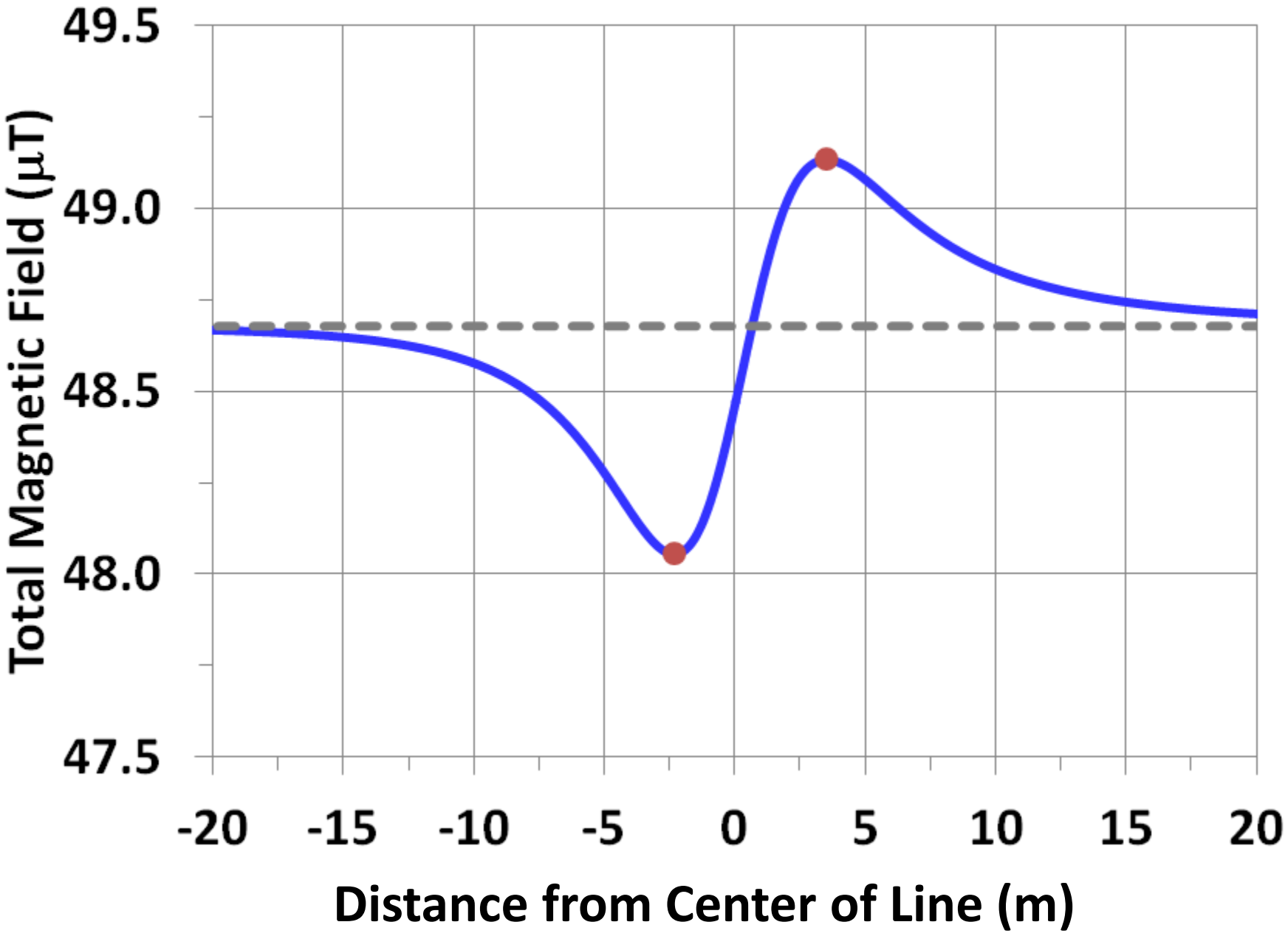
49.5
49.0
48.5
48.0
47.5
Total Magnetic Field (µT)
-20
-15
-10
-5
0
5
10
15
20
Distance from Center of Line (m)

90,-60

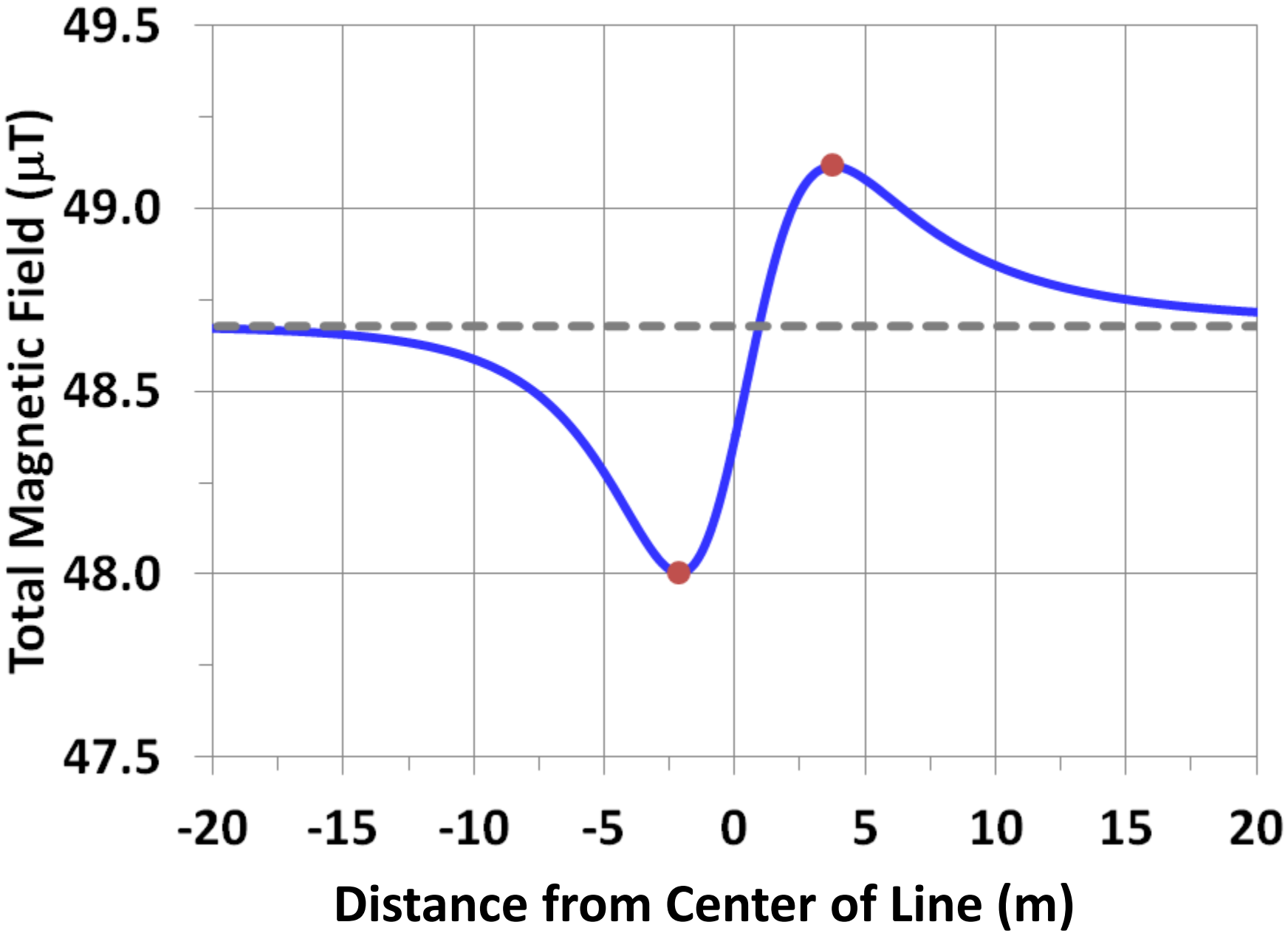
49.5
49.0
48.5
48.0
47.5
Total Magnetic Field (µT)
-20
-15
-10
-5
0
5
10
15
20
Distance from Center of Line (m)

90,-75

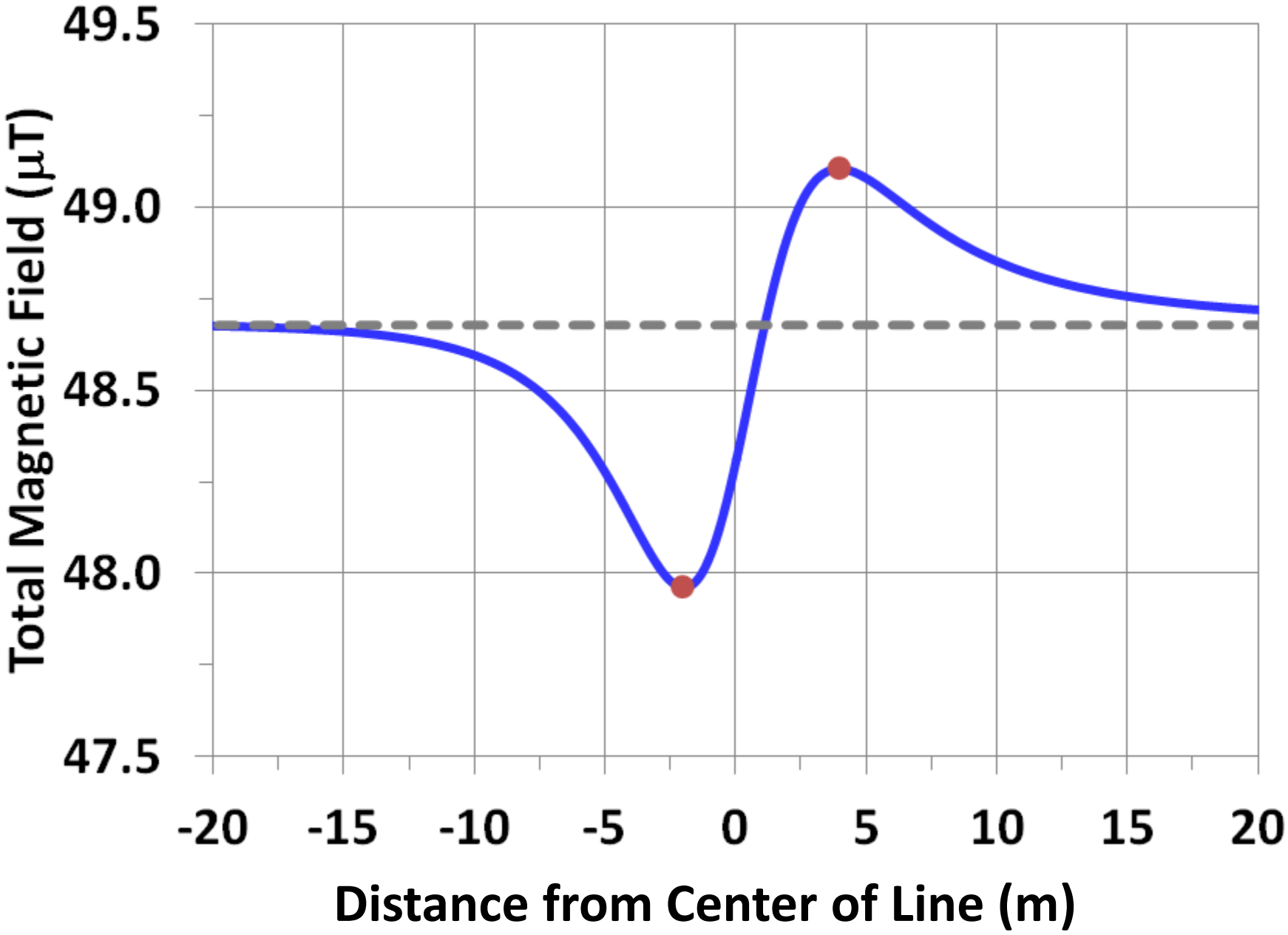
49.5
49.0
48.5
48.0
47.5
Total Magnetic Field (µT)
-20
-15
-10
-5
0
5
10
15
20
Distance from Center of Line (m)

90,-90

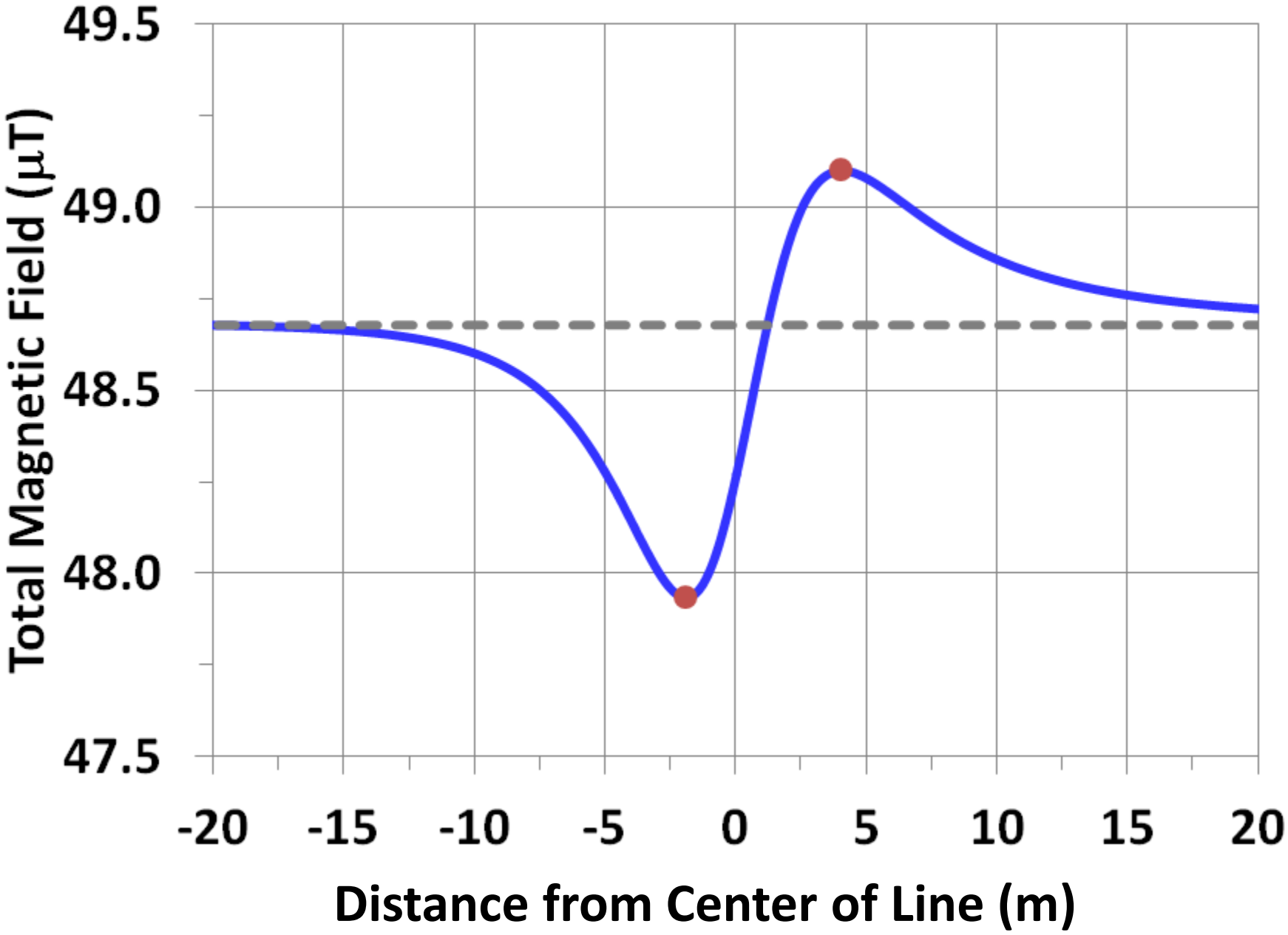
49.5
49.0
48.5
48.0
47.5
Total Magnetic Field (µT)
-20
-15
-10
-5
0
5
10
15
20
Distance from Center of Line (m)

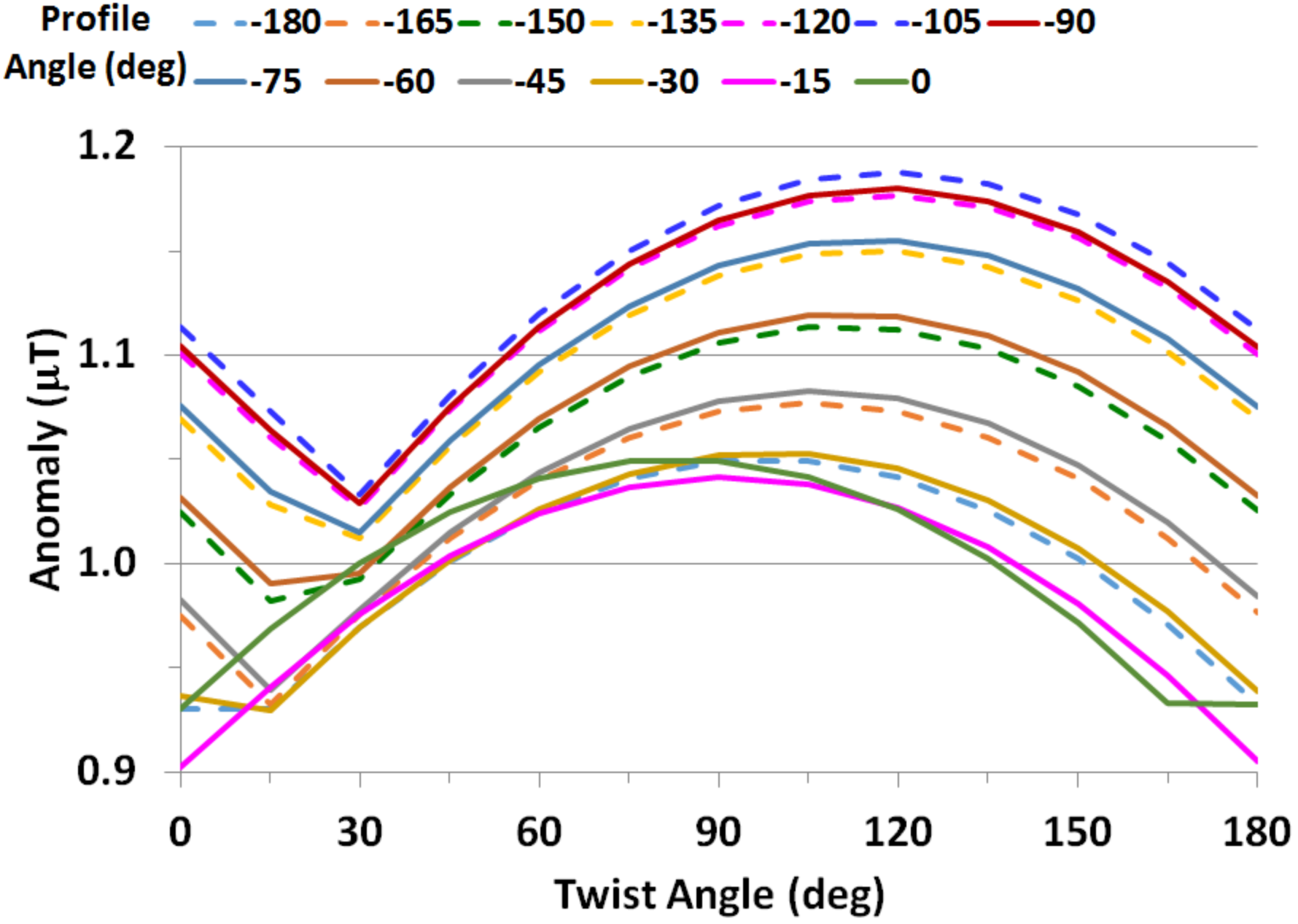
Profile Angle (deg)
-180
-165
-150
-135
-120
-105
-90
-75
-60
-45
-30
-15
0
1.2
1.1
1.0
0.9
Anomaly (μT)
0
30
60
90
120
150
180
Twist Angle (deg)

Appendix II

Regressed Net Magnetic Field Profiles from San Pablo Bay (SP) and the Richmond-San Rafael Bridge (RSR)

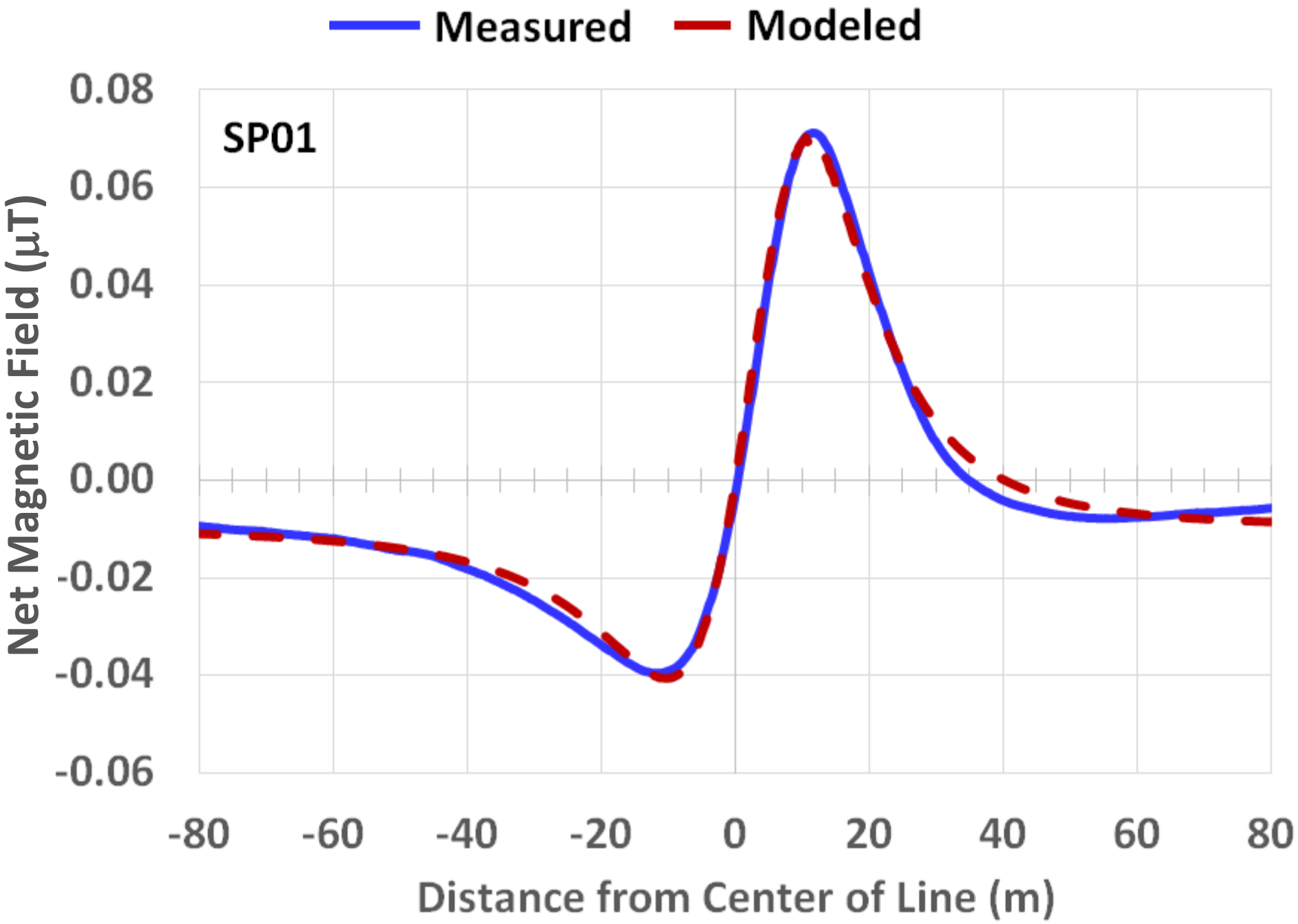
Measured
Modeled
SP01
0.08
0.06
0.04
0.02
0.00
-0.02
-0.04
-0.06
Net Magnetic Field (µT)
-80
-60
-40
-20
0
20
40
60
80
Distance from Center of Line (m)

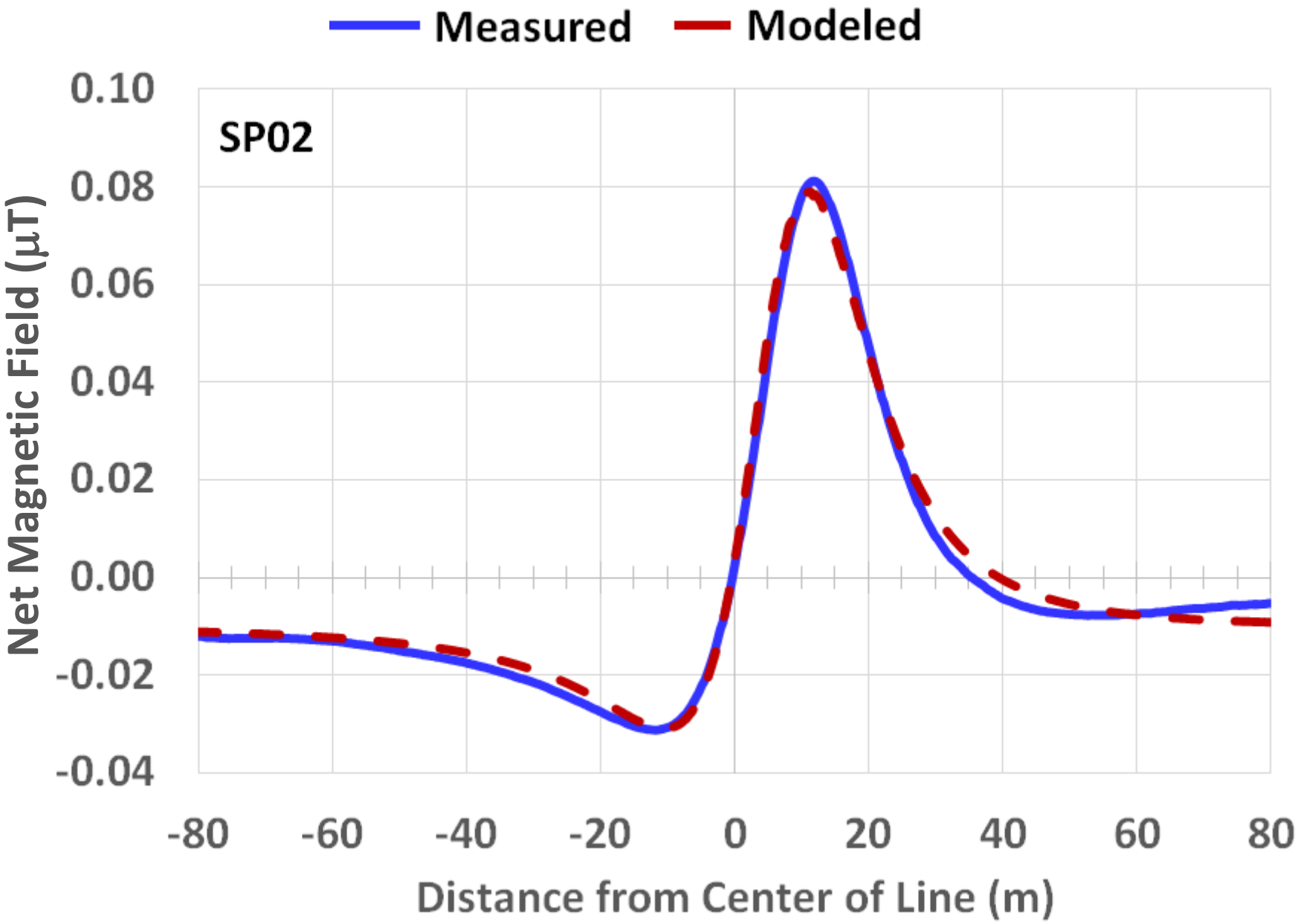
Measured
Modeled
SP02
0.10
0.08
0.06
0.04
0.02
0.00
-0.02
-0.04
Net Magnetic Field (µT)
-80
-60
-40
-20
0
20
40
60
80
Distance from Center of Line (m)

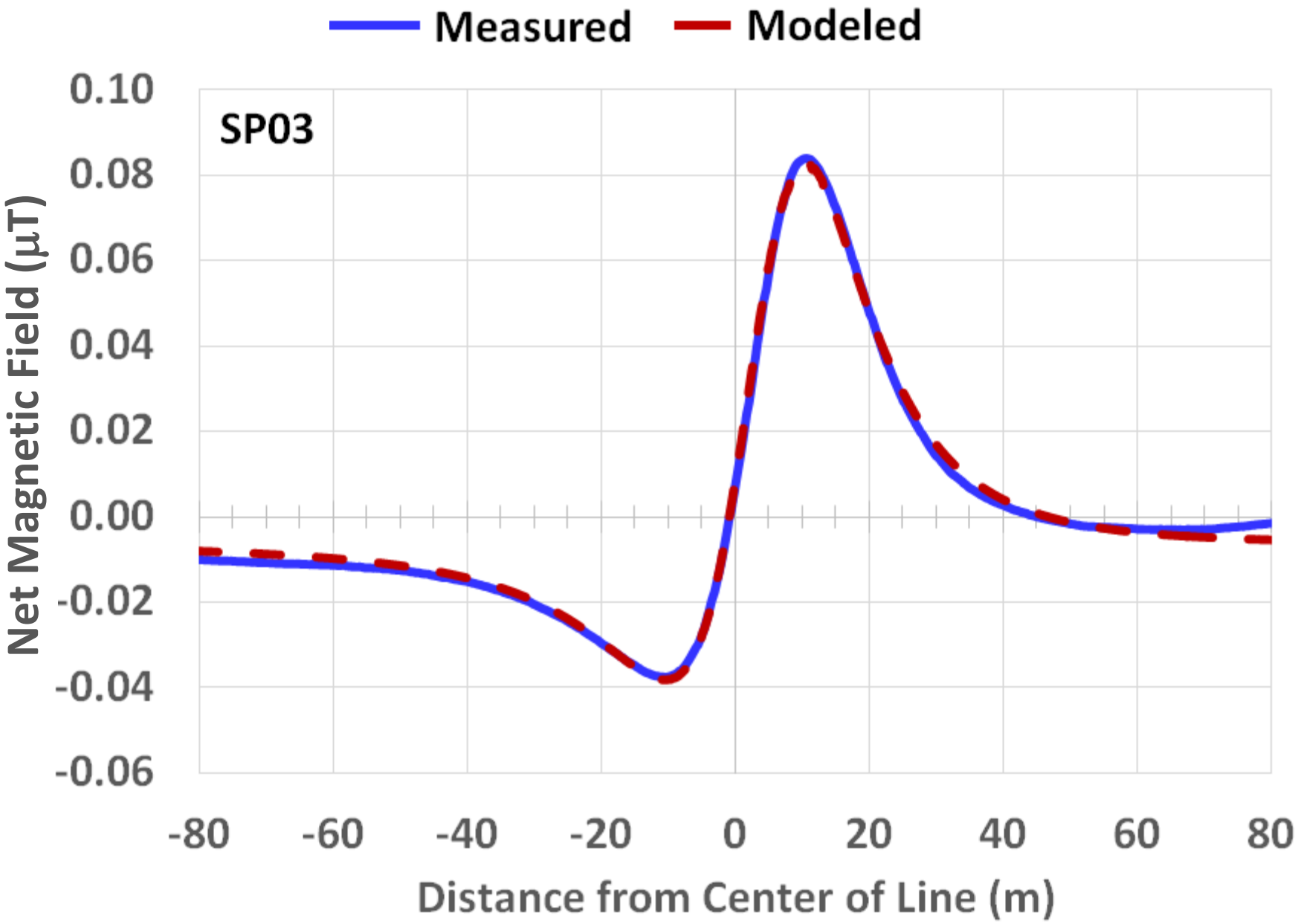
Measured
Modeled
SP03
0.10
0.08
0.06
0.04
0.02
0.00
-0.02
-0.04
-0.06
Net Magnetic Field (µT)
-80
-60
-40
-20
0
20
40
60
80
Distance from Center of Line (m)

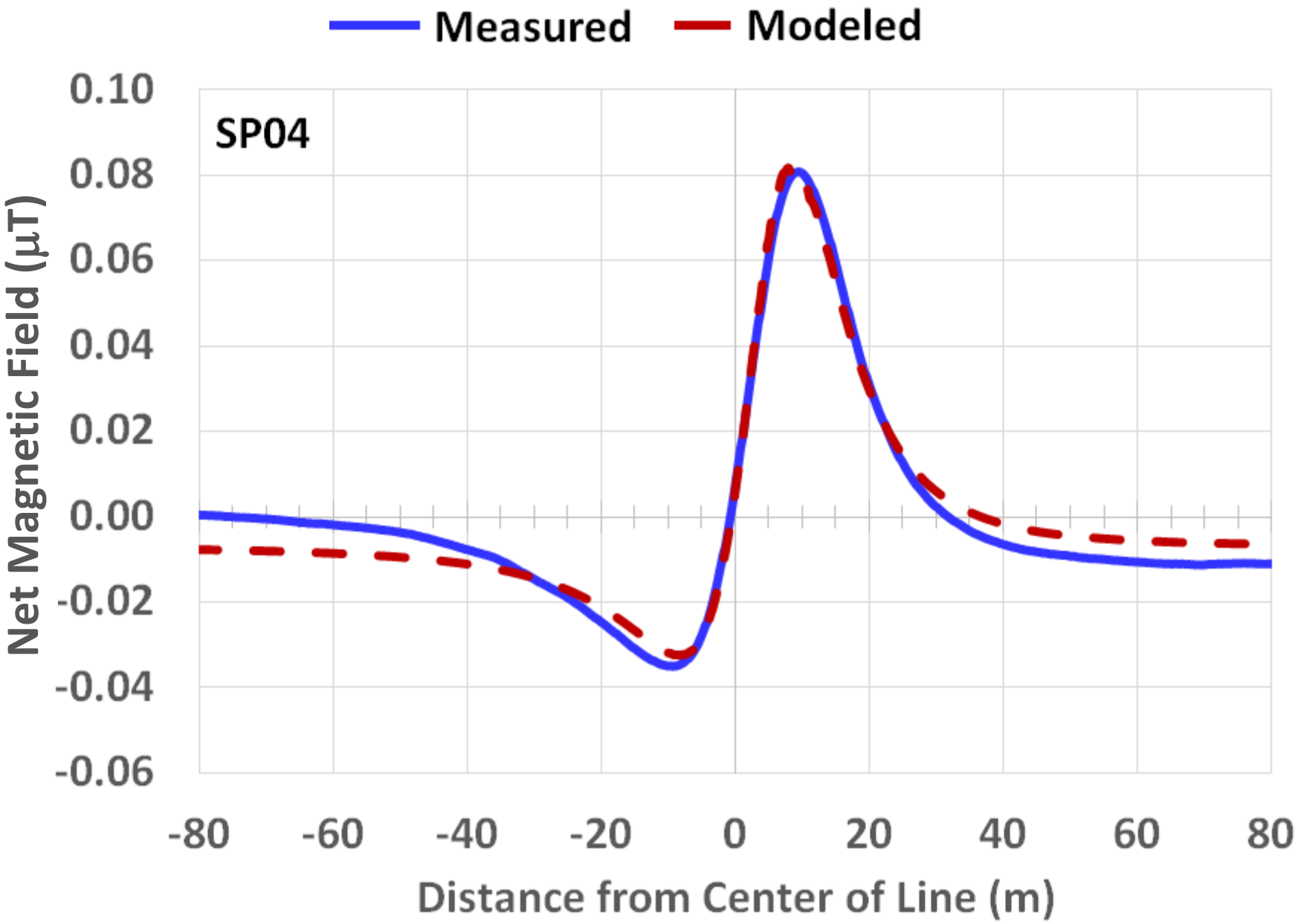
Measured
Modeled
SP04
0.10
0.08
0.06
0.04
0.02
0.00
-0.02
-0.04
-0.06
Net Magnetic Field (µT)
-80
-60
-40
-20
0
20
40
60
80
Distance from Center of Line (m)

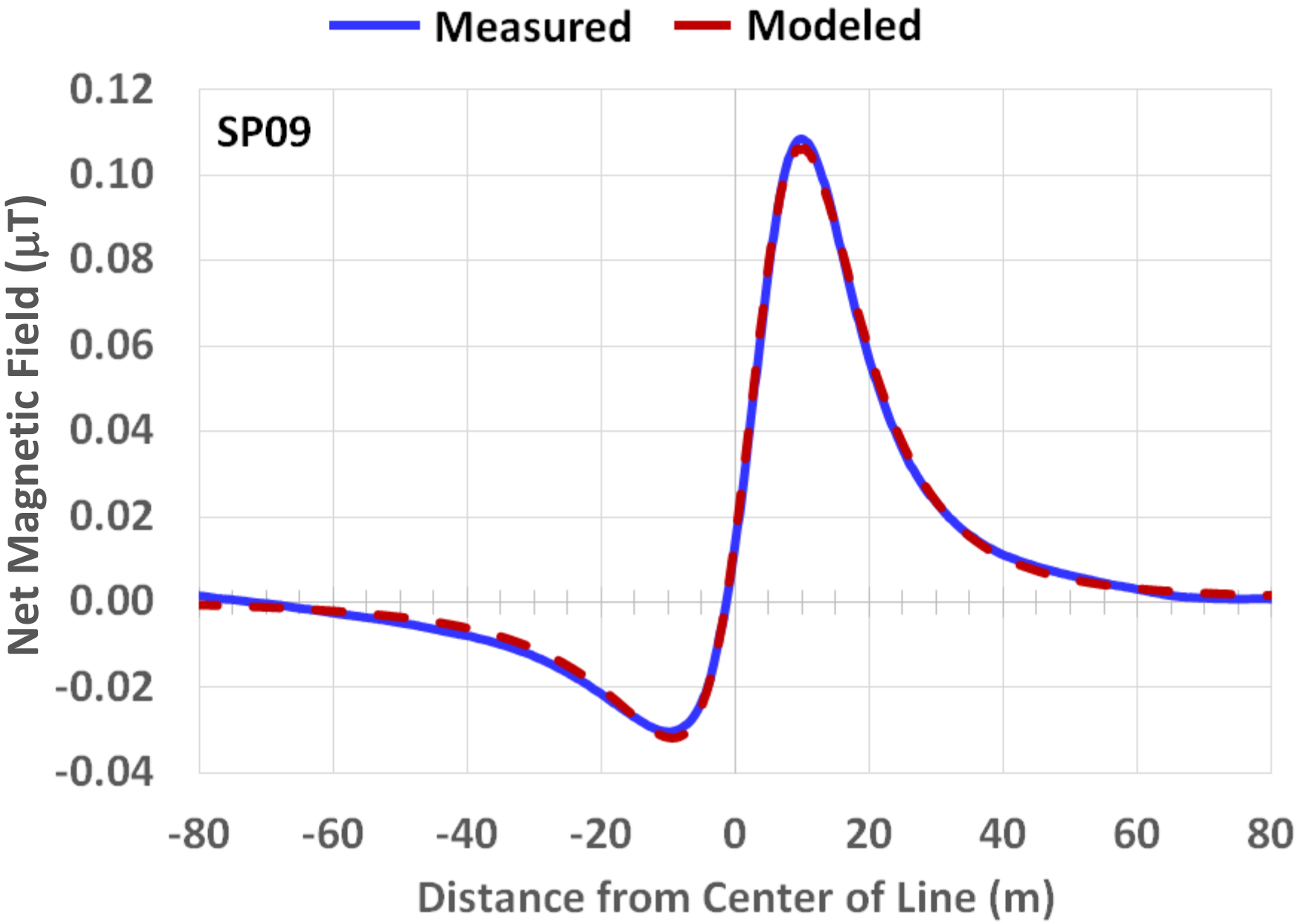
Measured
Modeled
SP09
0.12
0.10
0.08
0.06
0.04
0.02
0.00
-0.02
-0.04
Net Magnetic Field (µT)
-80
-60
-40
-20
0
20
40
60
80
Distance from Center of Line (m)

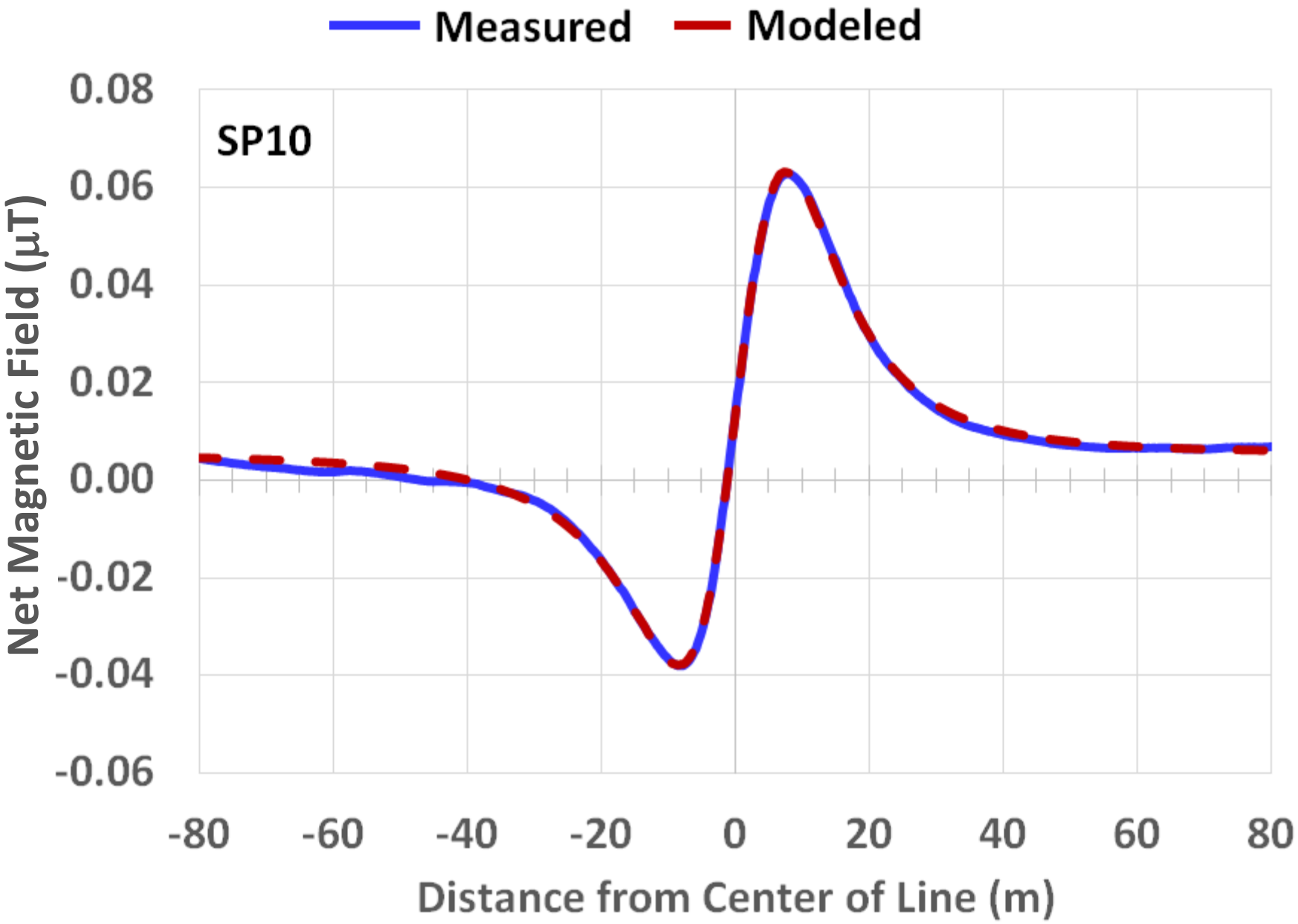
Measured
Modeled
SP10
0.08
0.06
0.04
0.02
0.00
-0.02
-0.04
-0.06
Net Magnetic Field (µT)
-80
-60
-40
-20
0
20
40
60
80
Distance from Center of Line (m)

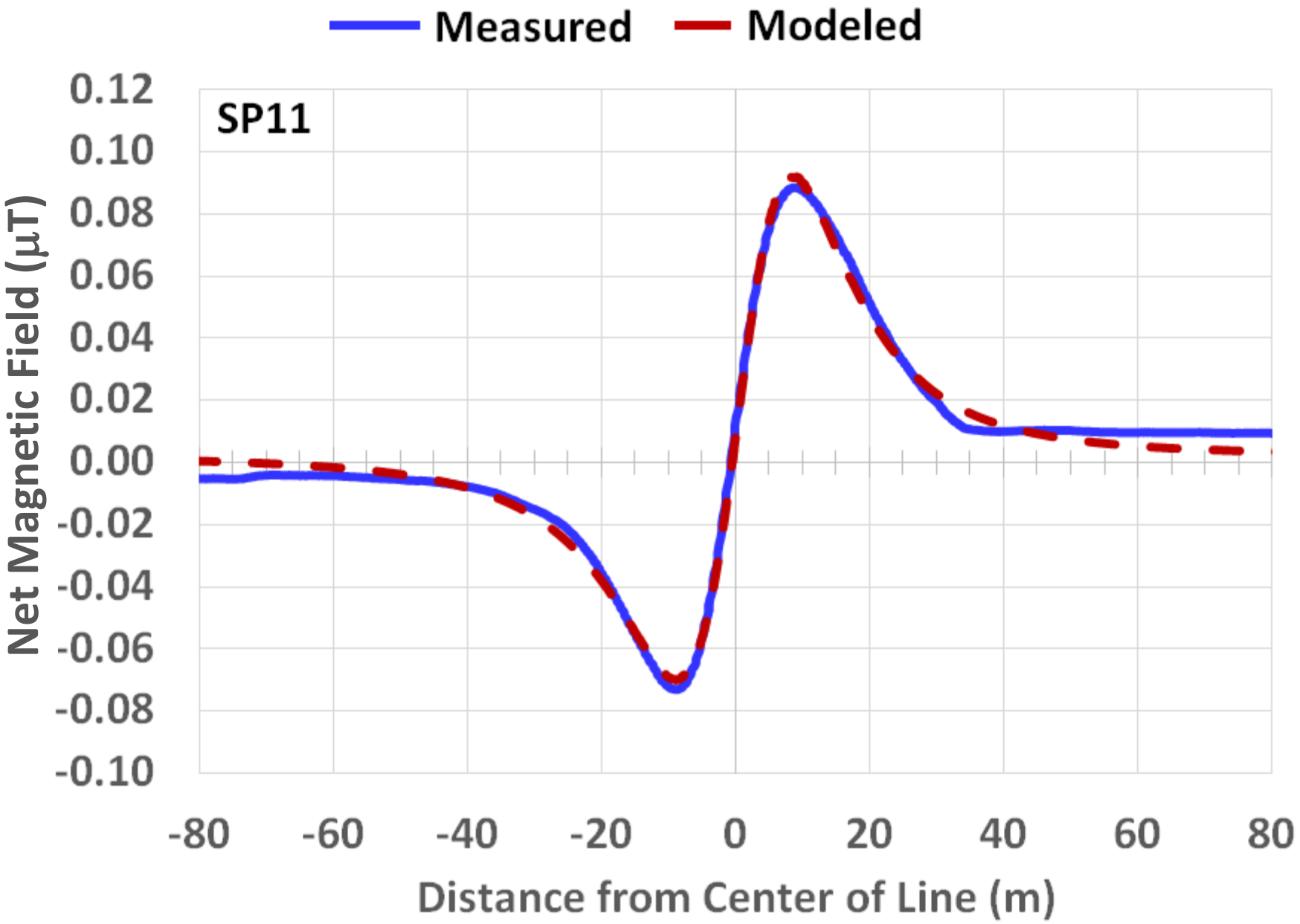
Measured
Modeled
SP11
0.12
0.10
0.08
0.06
0.04
0.02
0.00
-0.02
-0.04
-0.06
-0.08
-0.10
Net Magnetic Field (µT)
-80
-60
-40
-20
0
20
40
60
80
Distance from Center of Line (m)

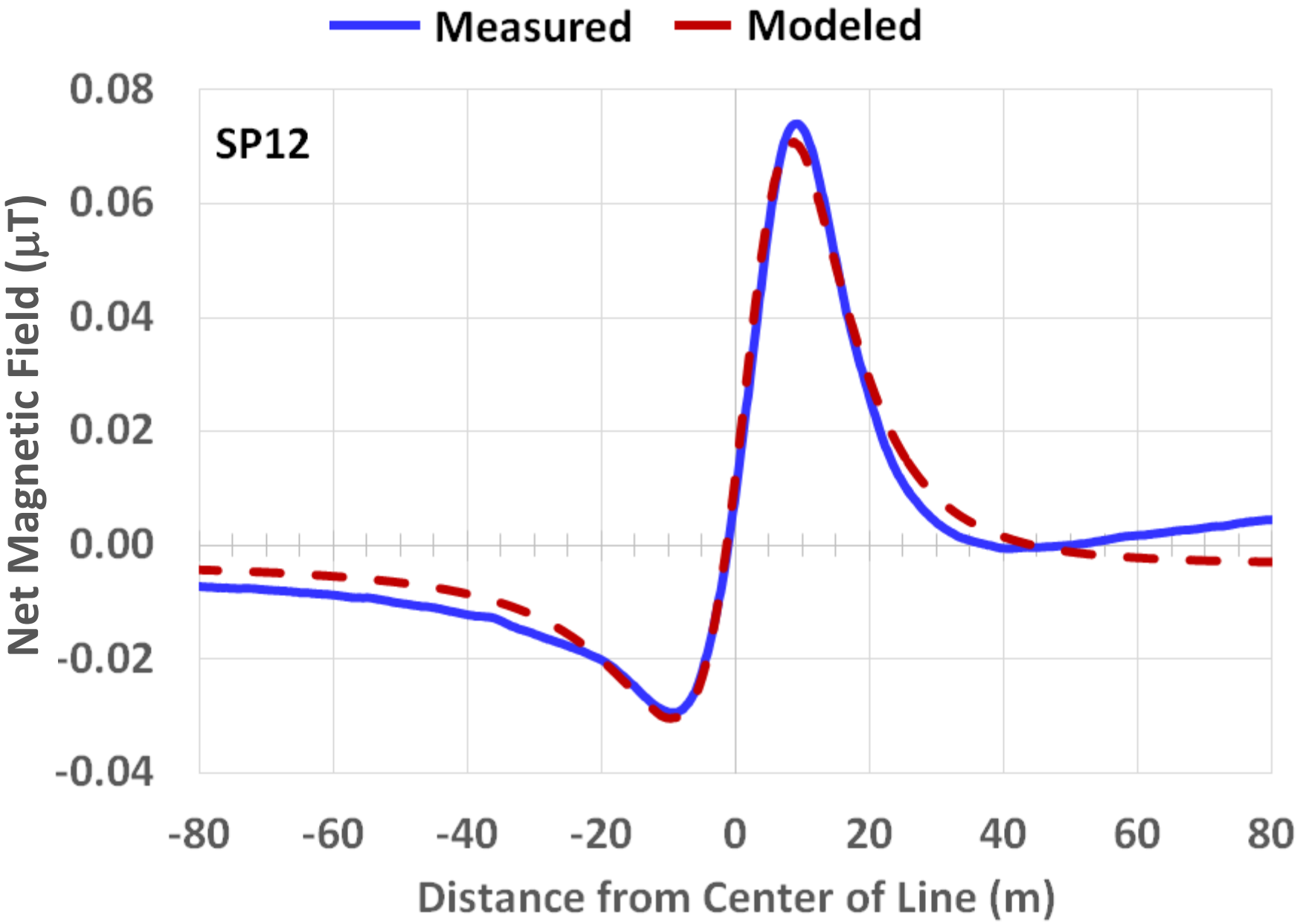
Measured
Modeled
SP12
0.08
0.06
0.04
0.02
0.00
-0.02
-0.04
Net Magnetic Field (µT)
-80
-60
-40
-20
0
20
40
60
80
Distance from Center of Line (m)

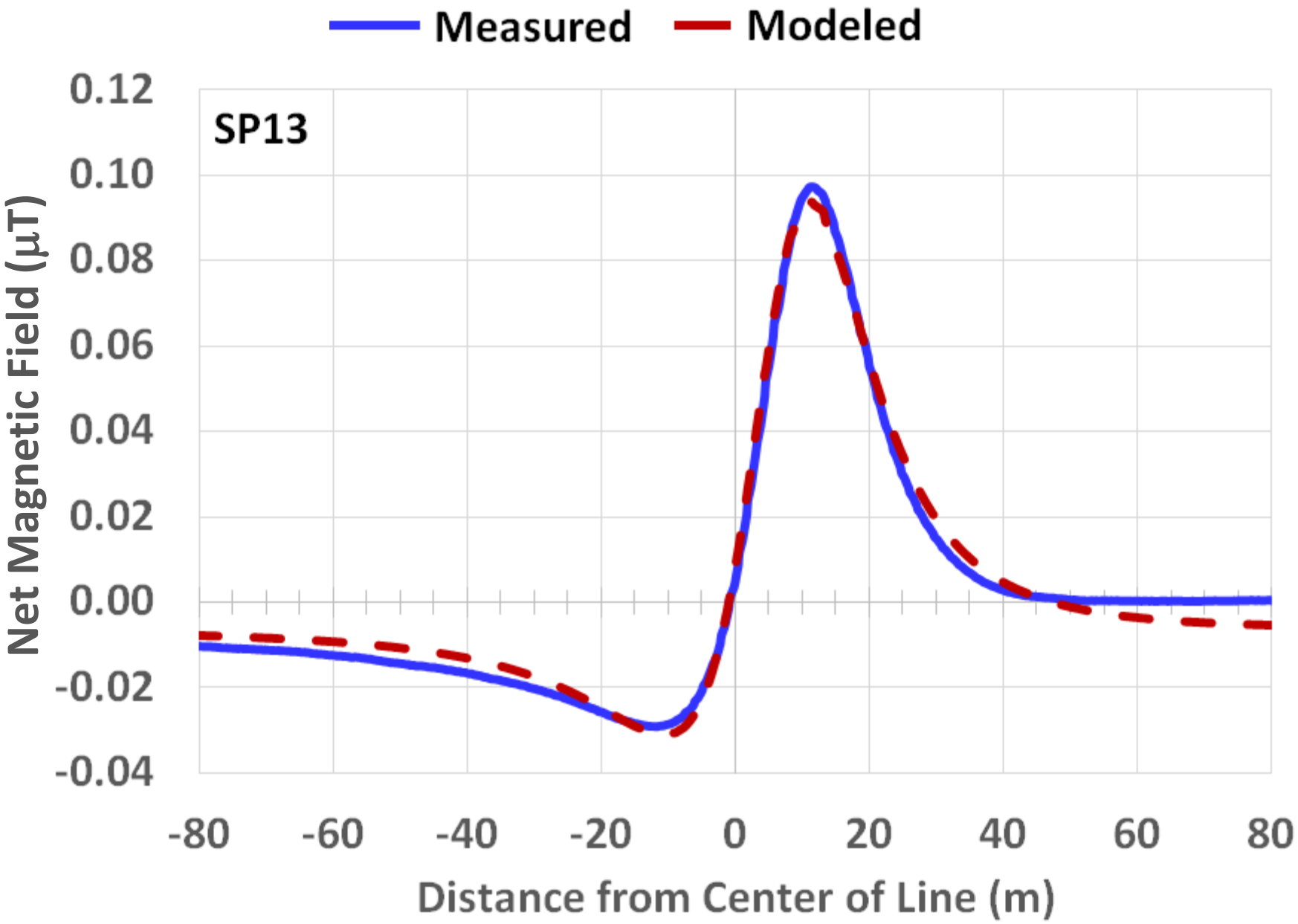
Measured
Modeled
SP13
0.12
0.10
0.08
0.06
0.04
0.02
0.00
-0.02
-0.04
Net Magnetic Field (µT)
-80
-60
-40
-20
0
20
40
60
80
Distance from Center of Line (m)

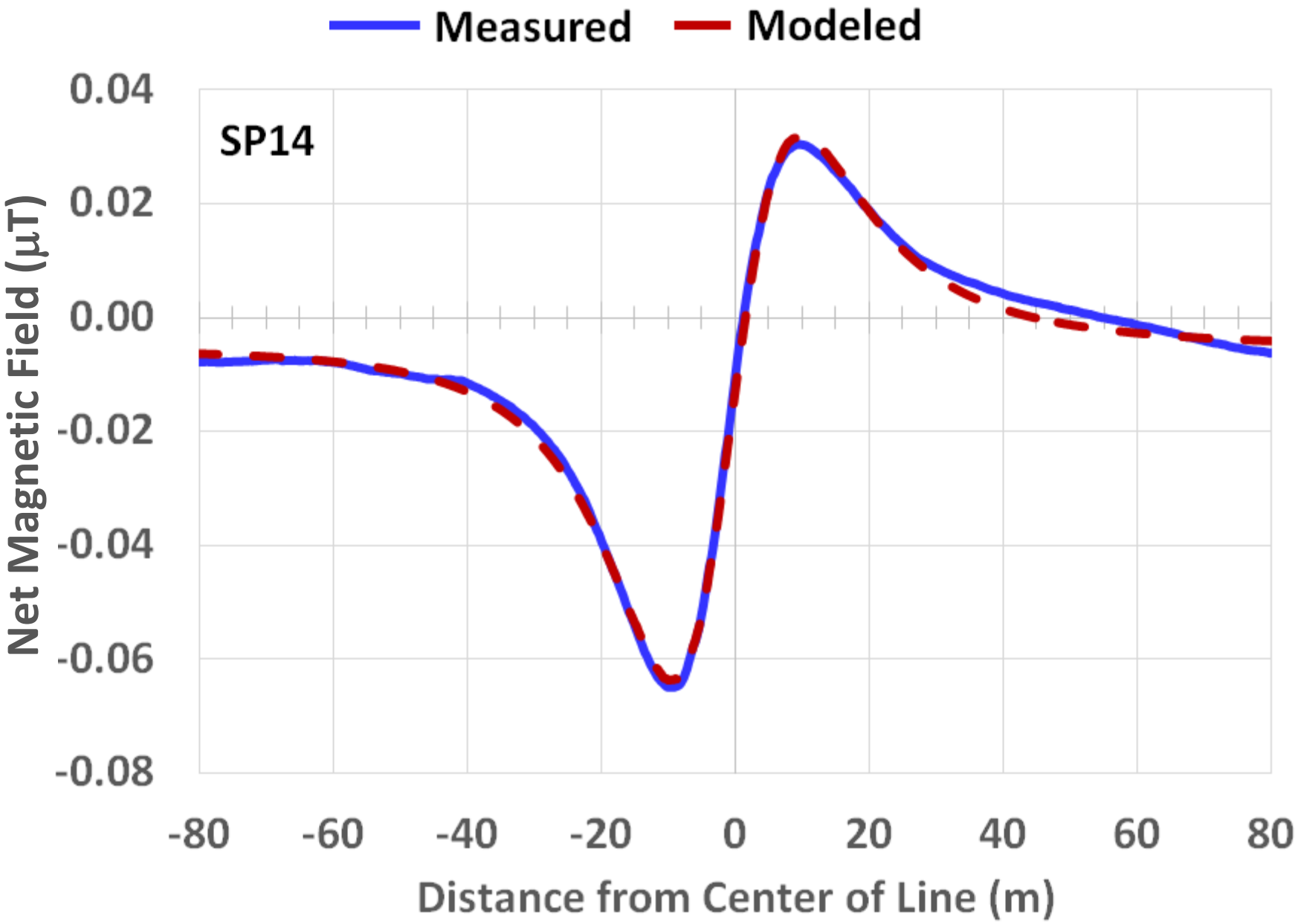
Measured
Modeled
SP14
0.04
0.02
0.00
-0.02
-0.04
-0.06
-0.08
Net Magnetic Field (µT)
-80
-60
-40
-20
0
20
40
60
80
Distance from Center of Line (m)

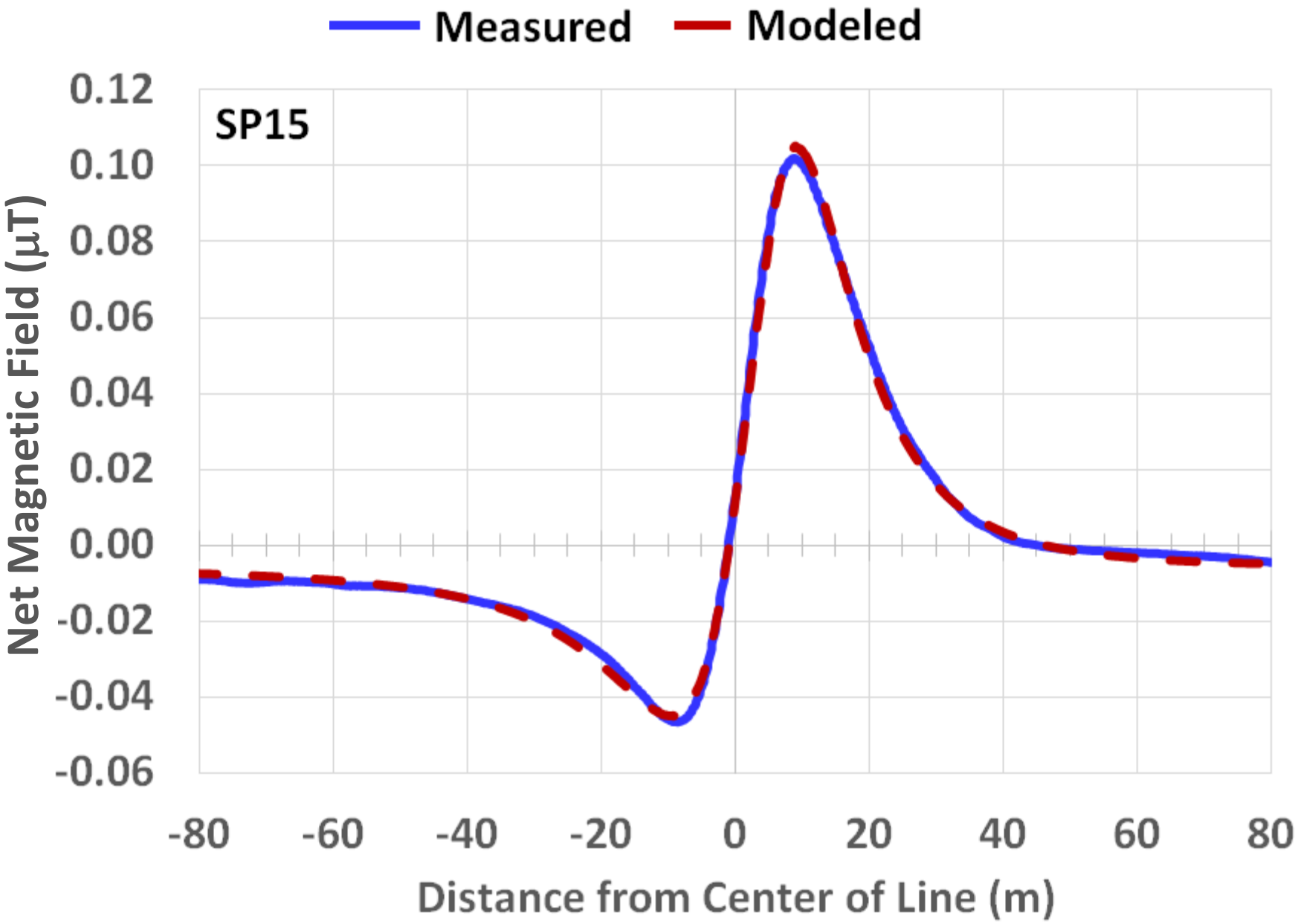
Measured
Modeled
SP15
0.12
0.10
0.08
0.06
0.04
0.02
0.00
-0.02
-0.04
-0.06
Net Magnetic Field (µT)
-80
-60
-40
-20
0
20
40
60
80
Distance from Center of Line (m)

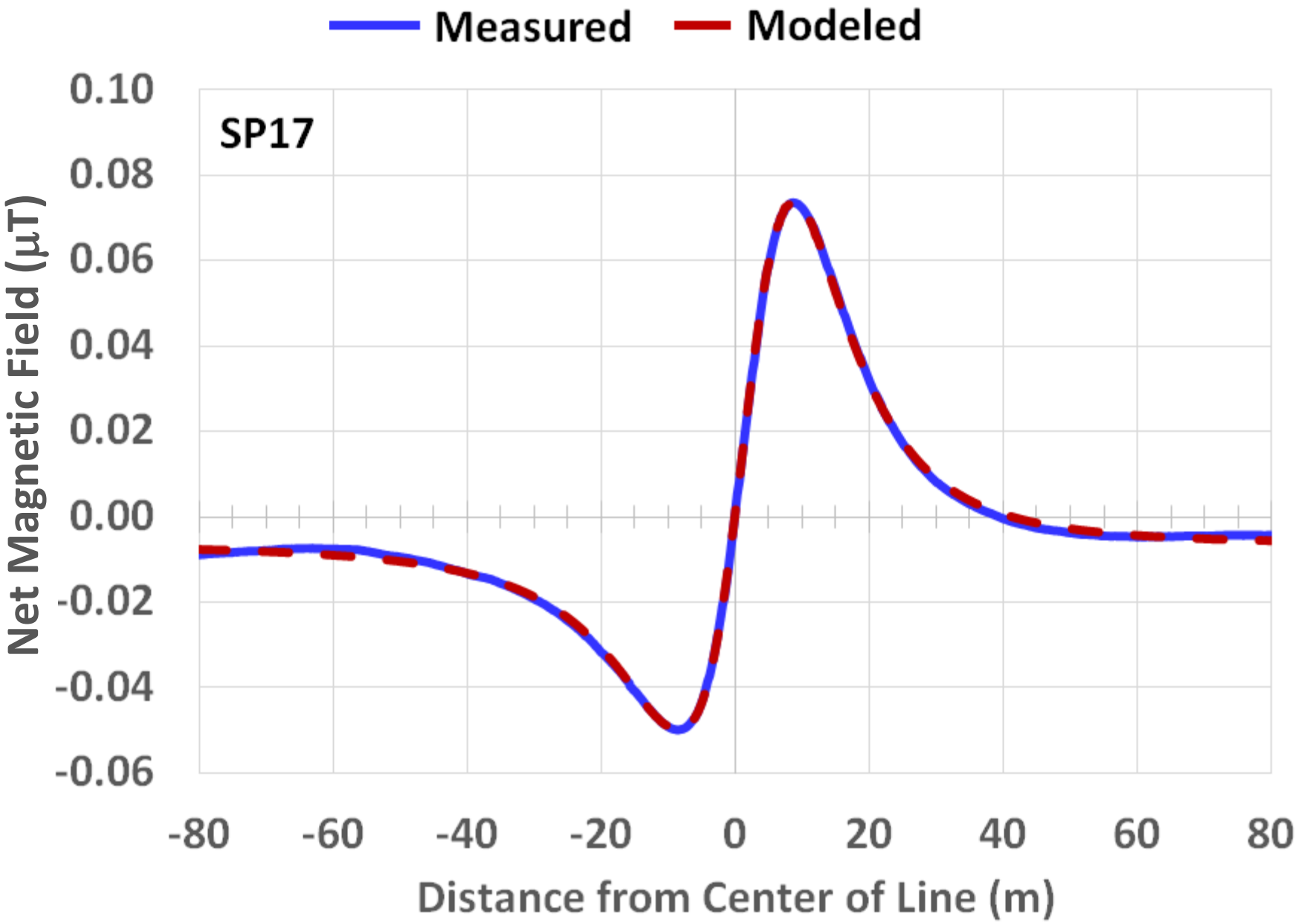
Measured
Modeled
SP17
0.10
0.08
0.06
0.04
0.02
0.00
-0.02
-0.04
-0.06
Net Magnetic Field (µT)
-80
-60
-40
-20
0
20
40
60
80
Distance from Center of Line (m)

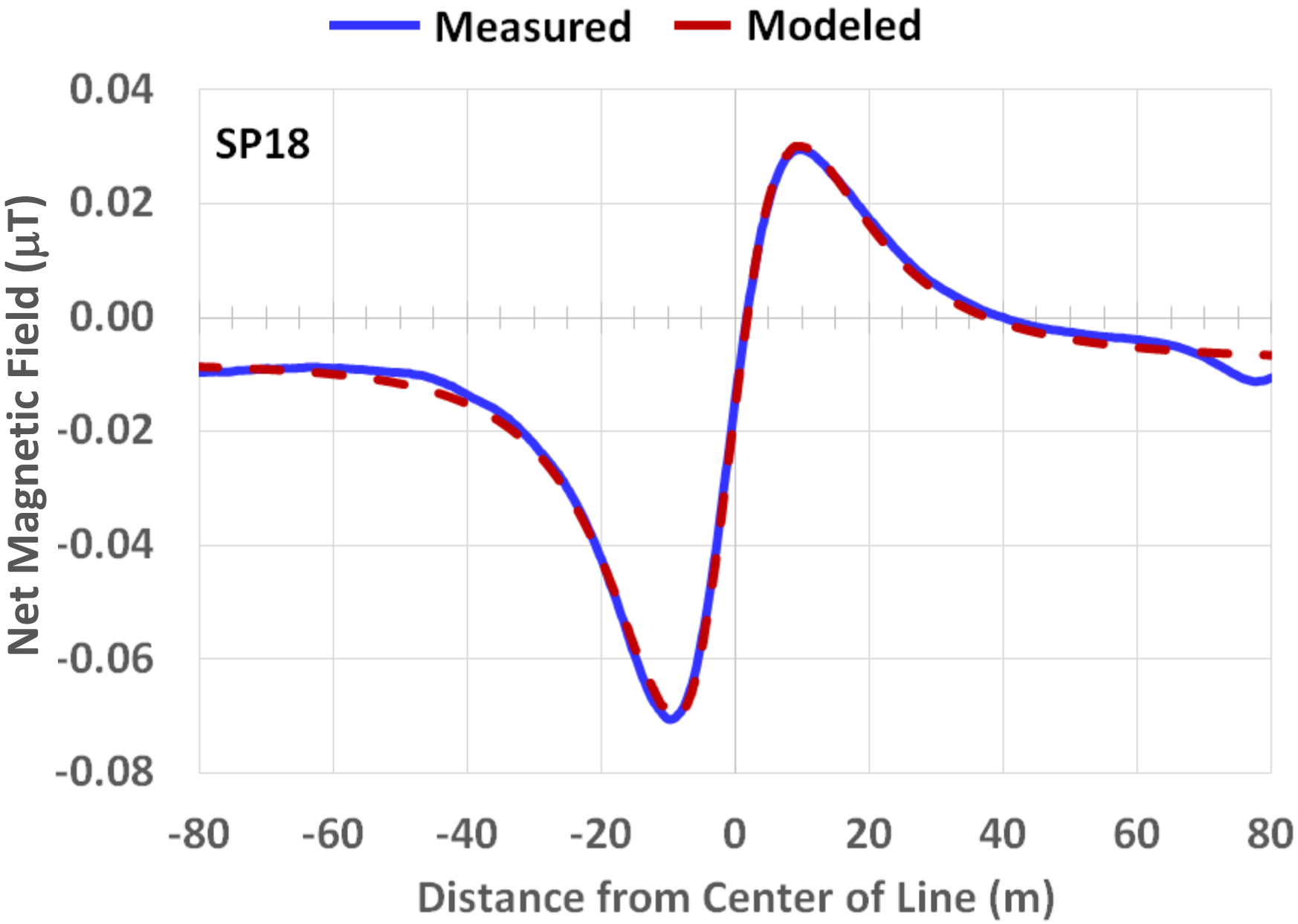
Measured
Modeled
SP18
0.04
0.02
0.00
-0.02
-0.04
-0.06
-0.08
Net Magnetic Field (µT)
-80
-60
-40
-20
0
20
40
60
80
Distance from Center of Line (m)

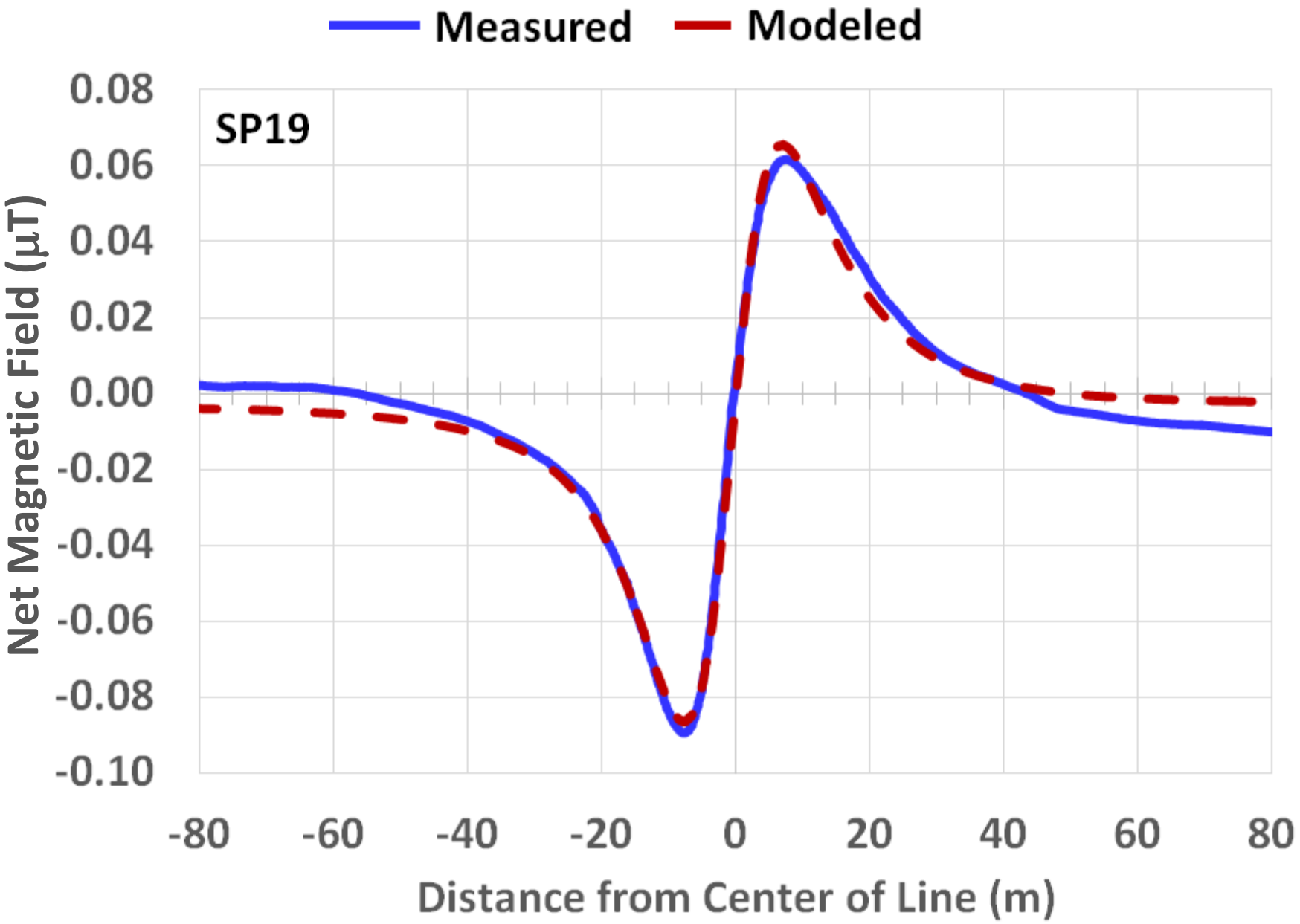
Measured
Modeled
SP19
0.08
0.06
0.04
0.02
0.00
-0.02
-0.04
-0.06
-0.08
-0.10
Net Magnetic Field (µT)
-80
-60
-40
-20
0
20
40
60
80
Distance from Center of Line (m)

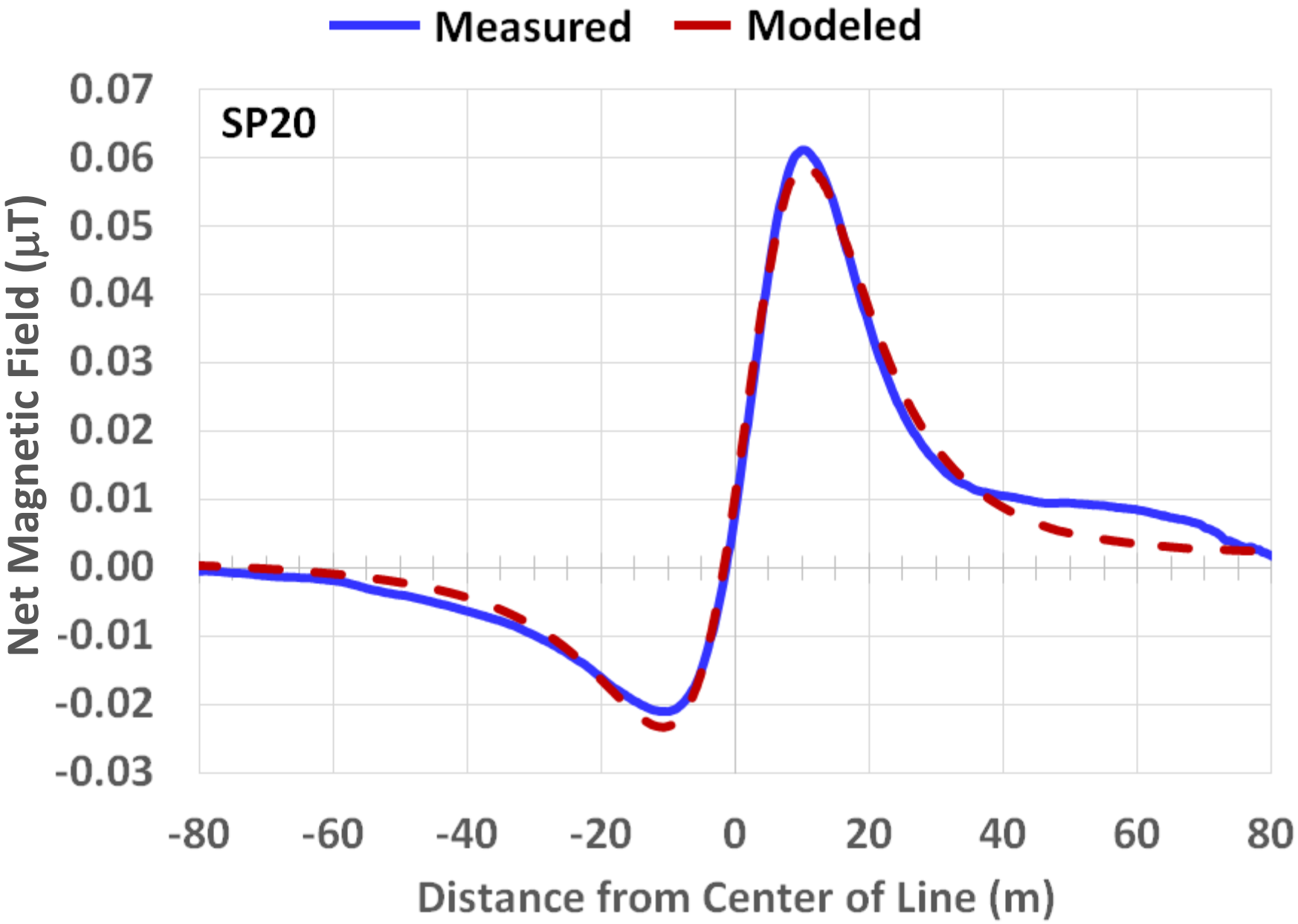
Measured
Modeled
SP20
0.07
0.06
0.05
0.04
0.03
0.02
0.01
0.00
-0.01
-0.02
-0.03
Net Magnetic Field (μT)
-80
-60
-40
-20
0
20
40
60
80
Distance from Center of Line (m)

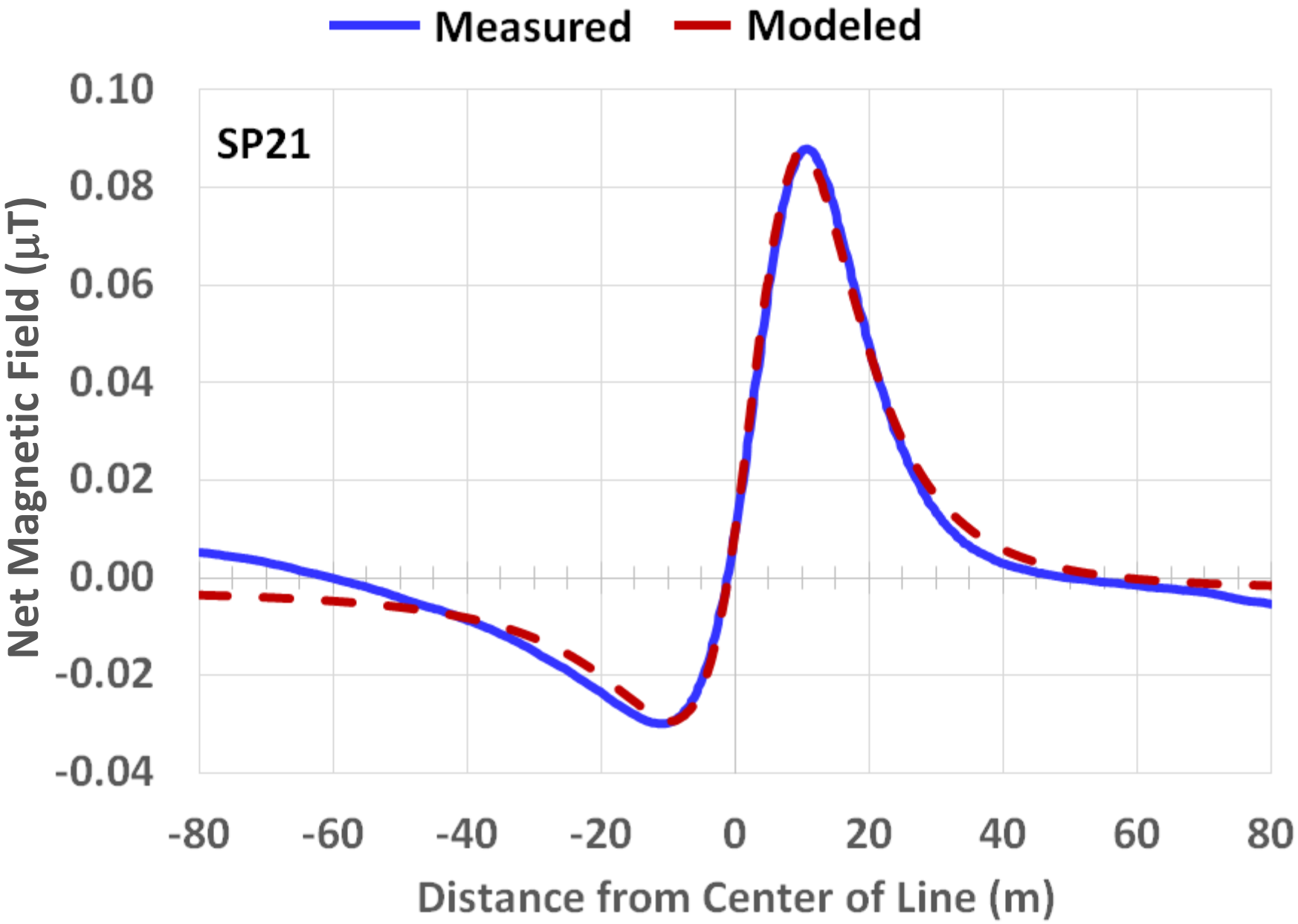
Measured
Modeled
SP21
0.10
0.08
0.06
0.04
0.02
0.00
-0.02
-0.04
Net Magnetic Field (µT)
-80
-60
-40
-20
0
20
40
60
80
Distance from Center of Line (m)

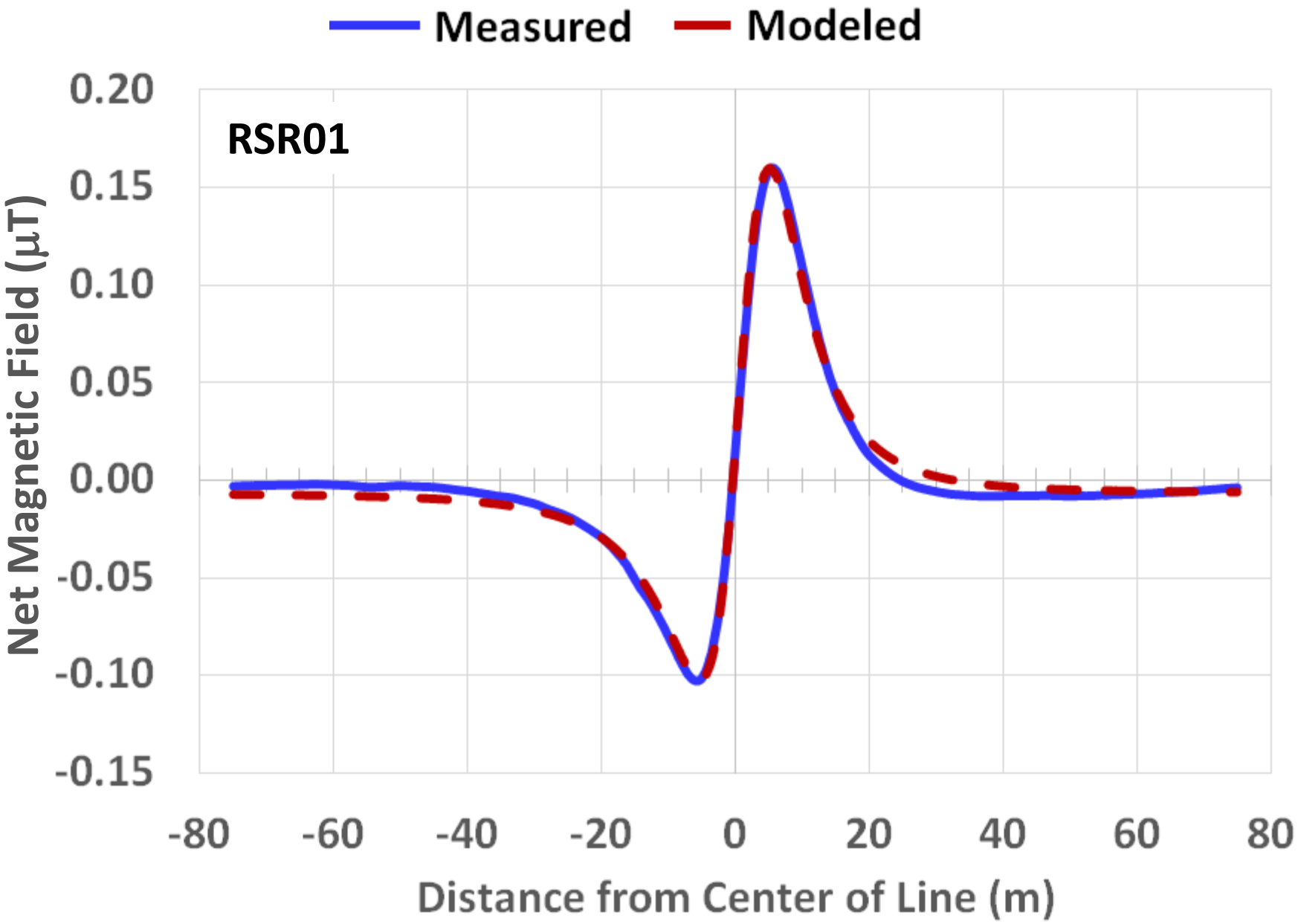
Measured
Modeled
RSR01
0.20
0.15
0.10
0.05
0.00
-0.05
-0.10
-0.15
Net Magnetic Field (µT)
-80
-60
-40
-20
0
20
40
60
80
Distance from Center of Line (m)

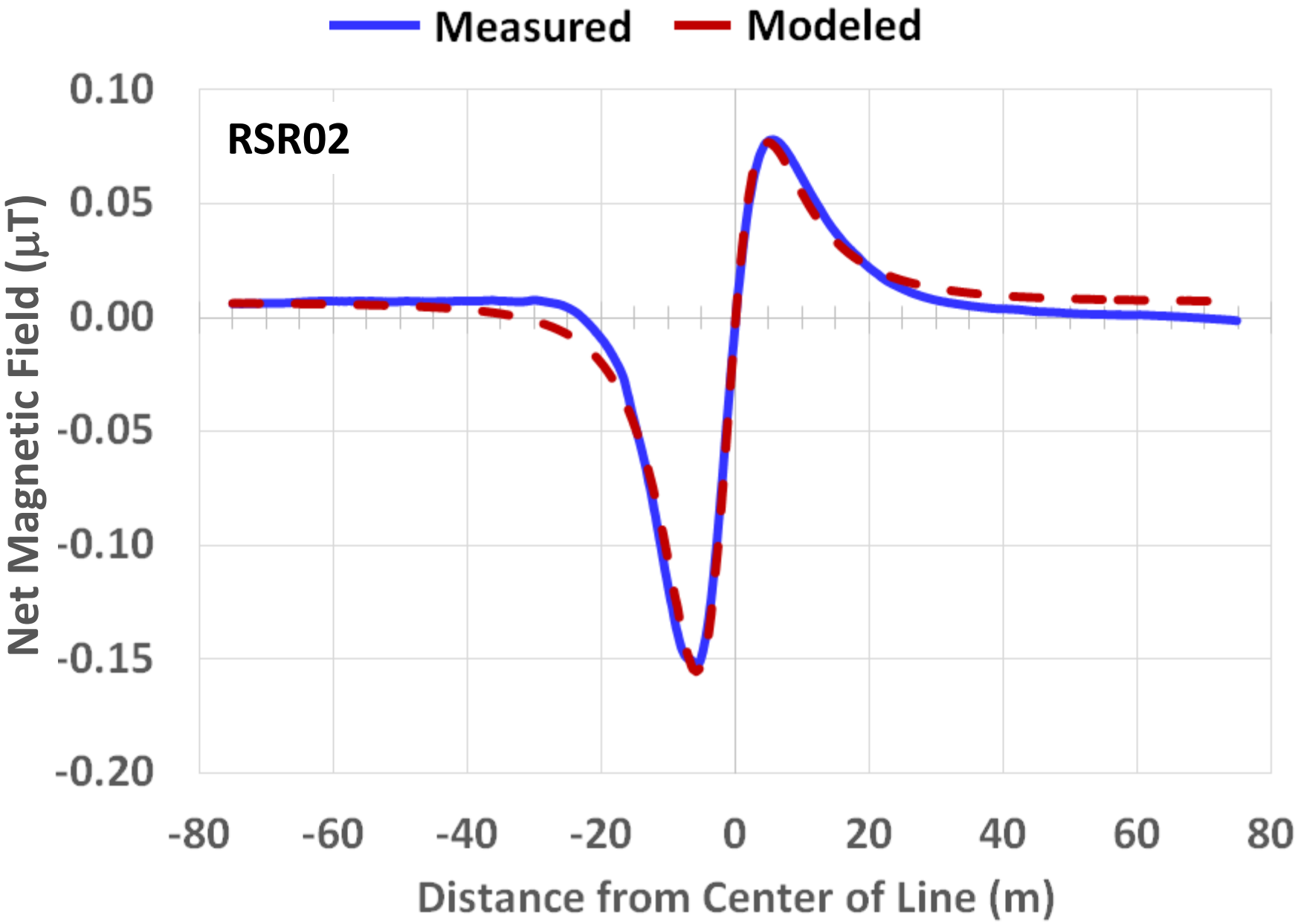
Measured
Modeled
RSR02
0.10
0.05
0.00
-0.05
-0.10
-0.15
-0.20
Net Magnetic Field (µT)
-80
-60
-40
-20
0
20
40
60
80
Distance from Center of Line (m)

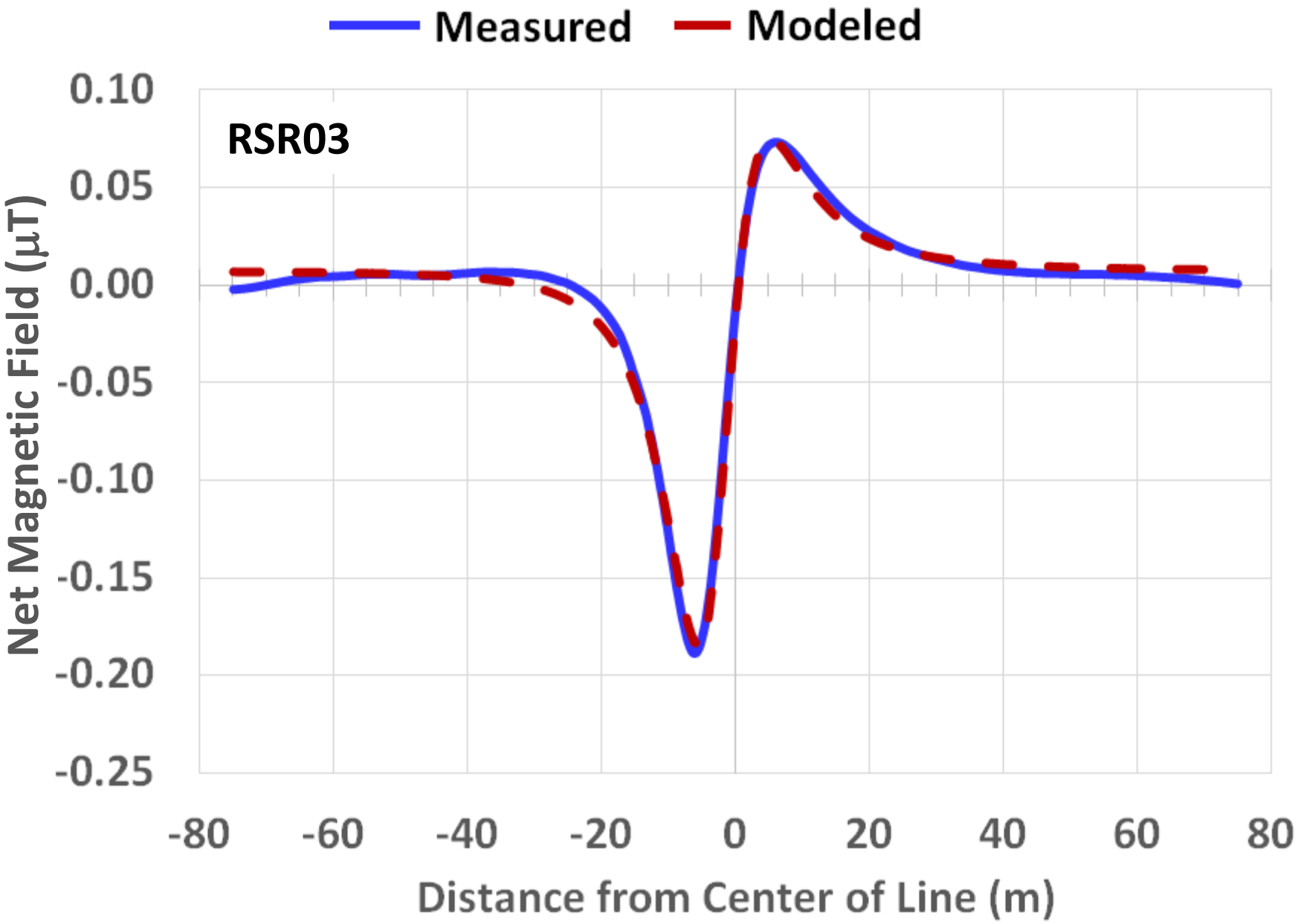
Measured
Modeled
RSR03
0.10
0.05
0.00
-0.05
-0.10
-0.15
-0.20
-0.25
Net Magnetic Field (µT)
-80
-60
-40
-20
0
20
40
60
80
Distance from Center of Line (m)

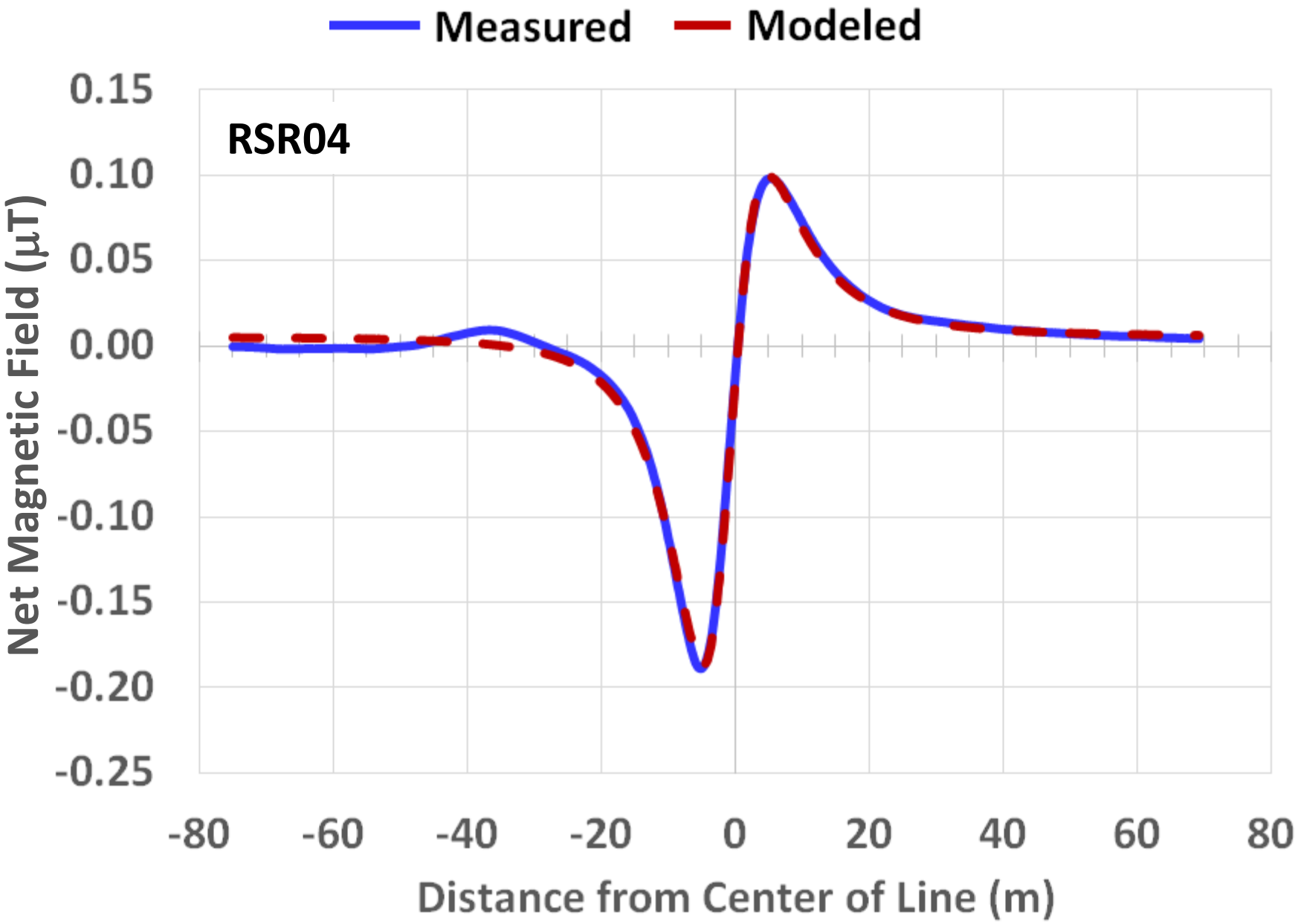
Measured
Modeled
RSR04
0.15
0.10
0.05
0.00
-0.05
-0.10
-0.15
-0.20
-0.25
Net Magnetic Field (µT)
-80
-60
-40
-20
0
20
40
60
80
Distance from Center of Line (m)

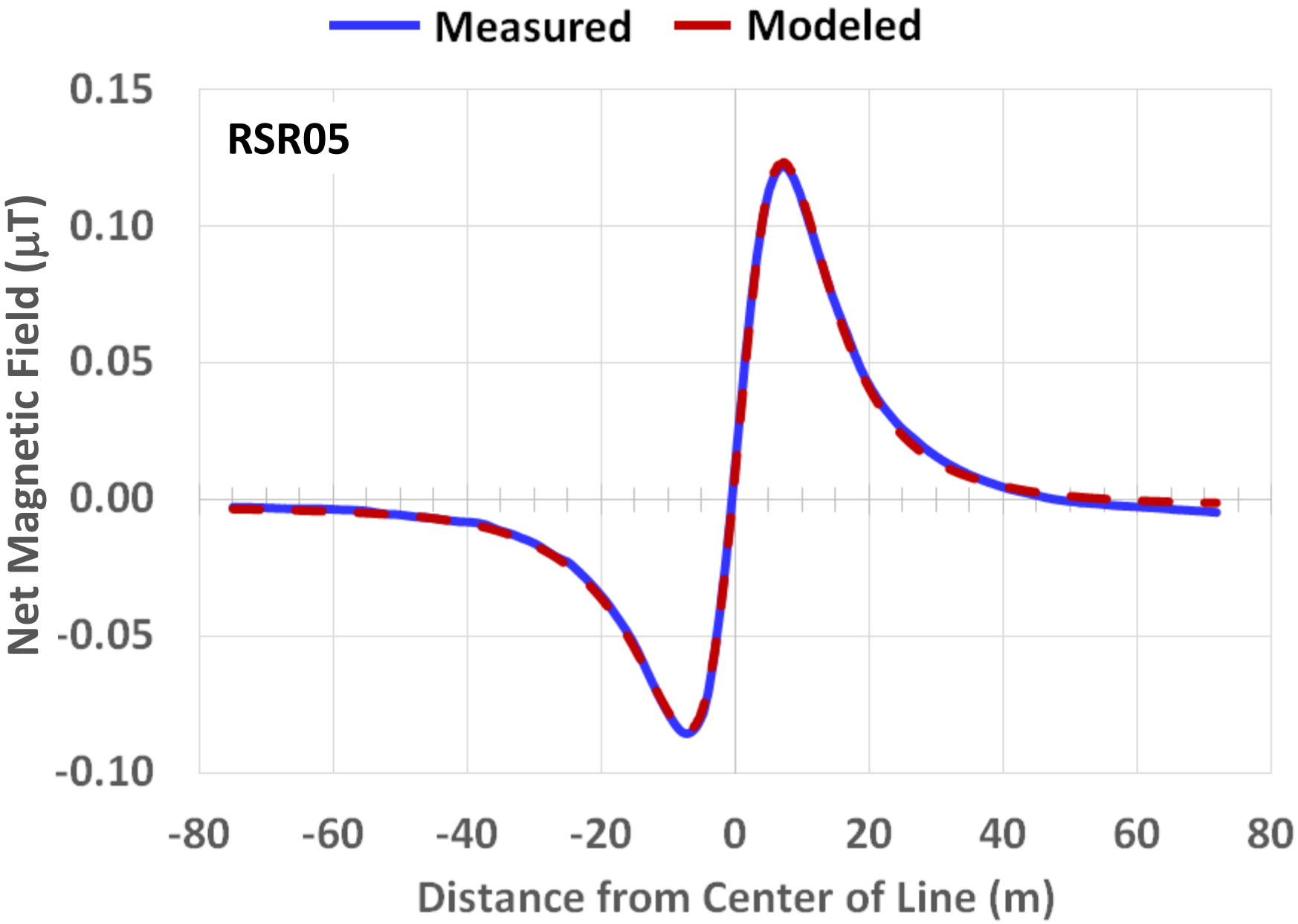
Measured
Modeled
RSR05
0.15
0.10
0.05
0.00
-0.05
-0.10
Net Magnetic Field (µT)
-80
-60
-40
-20
0
20
40
60
80
Distance from Center of Line (m)

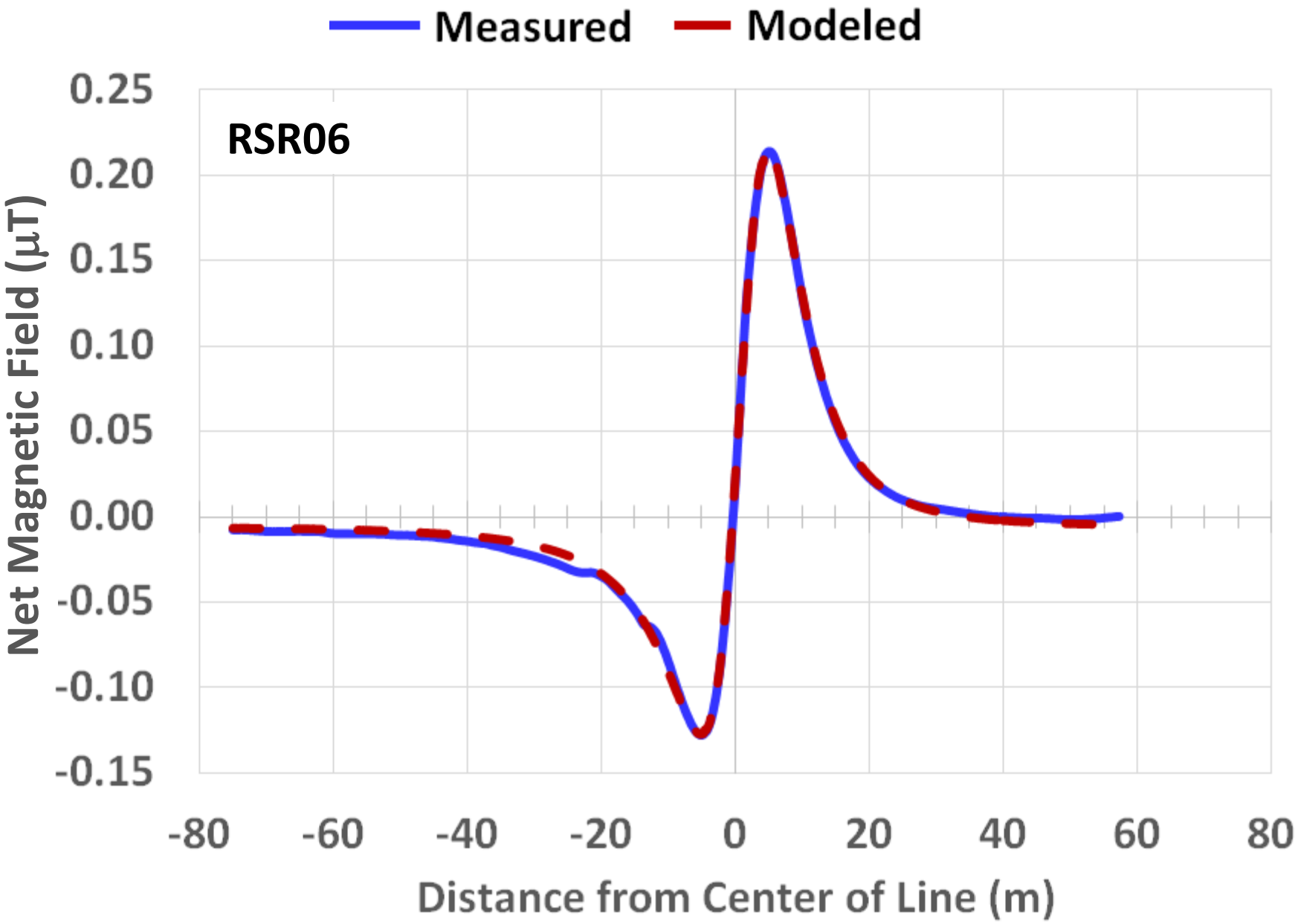
Measured
Modeled
RSR06
Net Magnetic Field (µT)
0.25
0.20
0.15
0.10
0.05
0.00
-0.05
-0.10
-0.15
-80
-60
-40
-20
0
20
40
60
80
Distance from Center of Line (m)

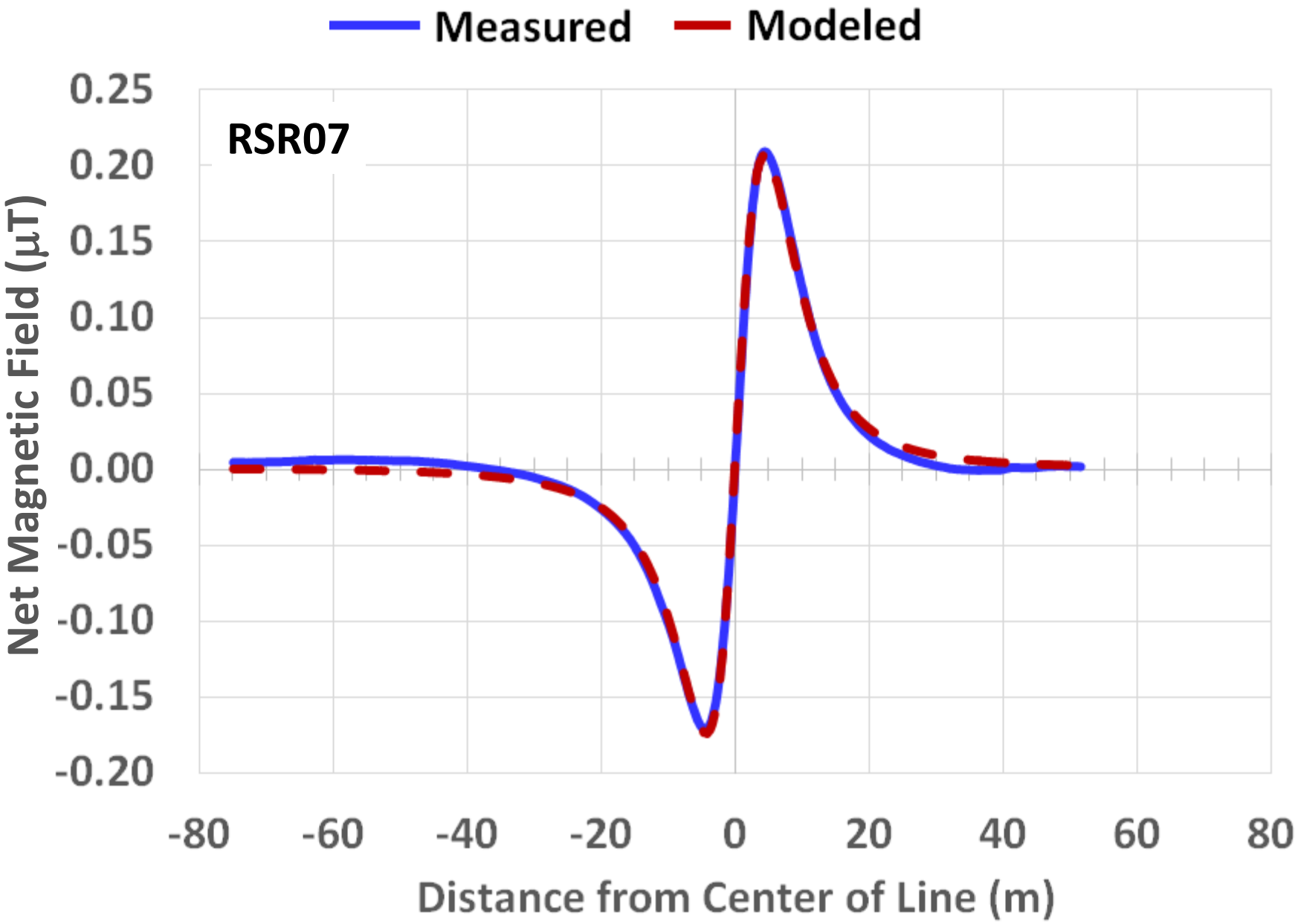
Measured
Modeled
RSR07
0.25
0.20
0.15
0.10
0.05
0.00
-0.05
-0.10
-0.15
-0.20
Net Magnetic Field (µT)
-80
-60
-40
-20
0
20
40
60
80
Distance from Center of Line (m)

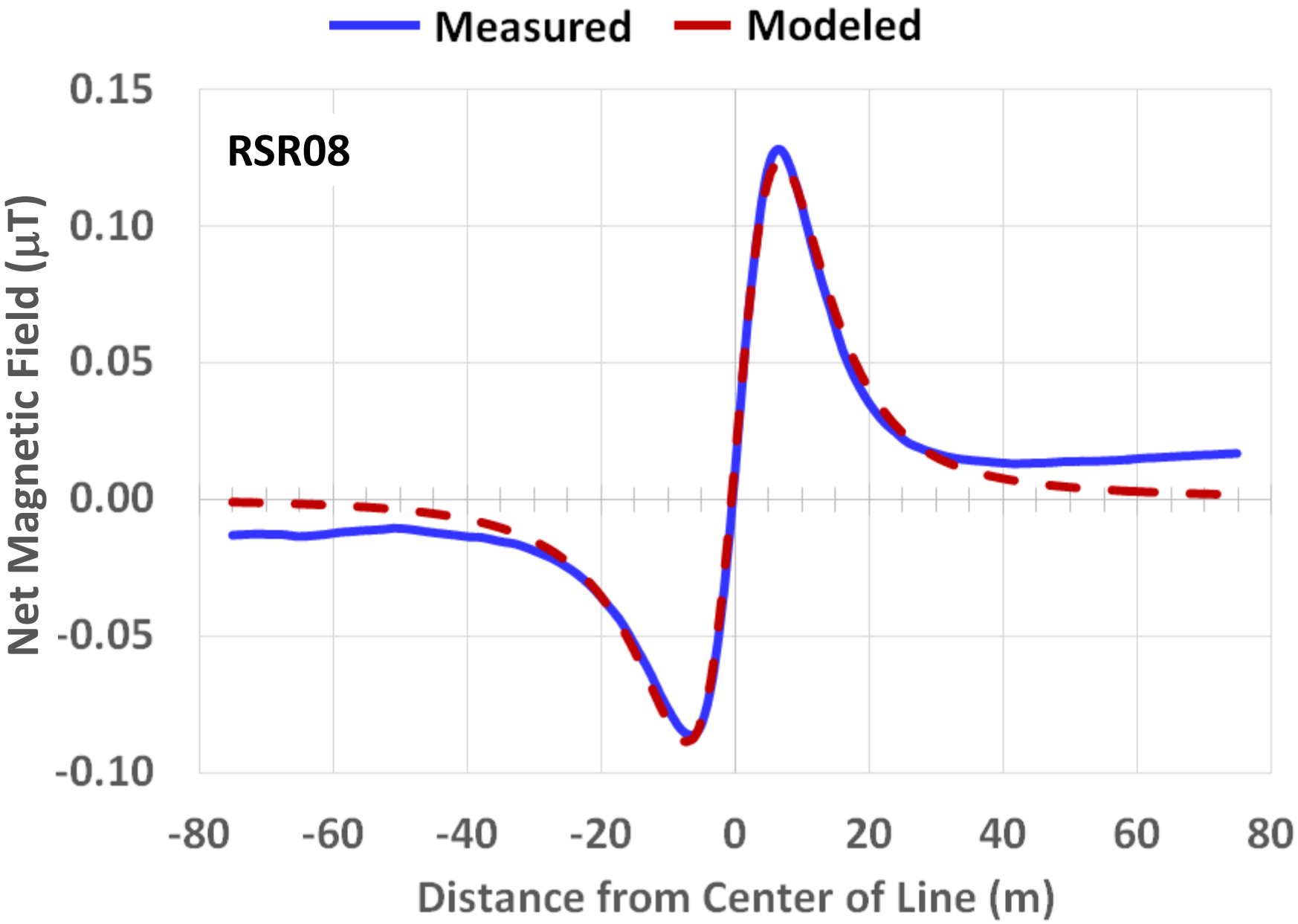
Measured
Modeled
RSR08
0.15
0.10
0.05
0.00
-0.05
-0.10
Net Magnetic Field (µT)
-80
-60
-40
-20
0
20
40
60
80
Distance from Center of Line (m)

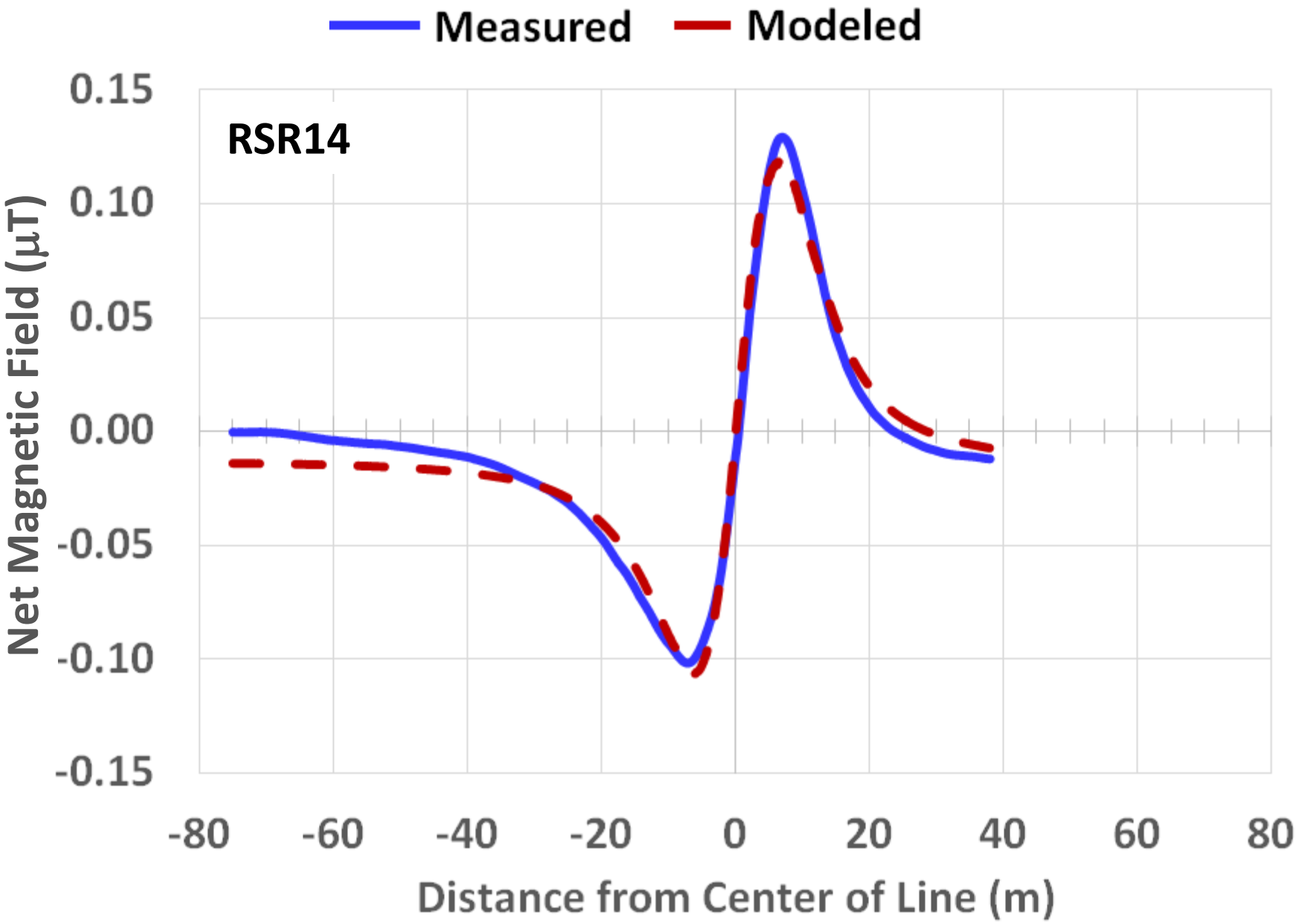
Measured
Modeled
RSR14
0.15
0.10
0.05
0.00
-0.05
-0.10
-0.15
Net Magnetic Field (µT)
-80
-60
-40
-20
0
20
40
60
80
Distance from Center of Line (m)

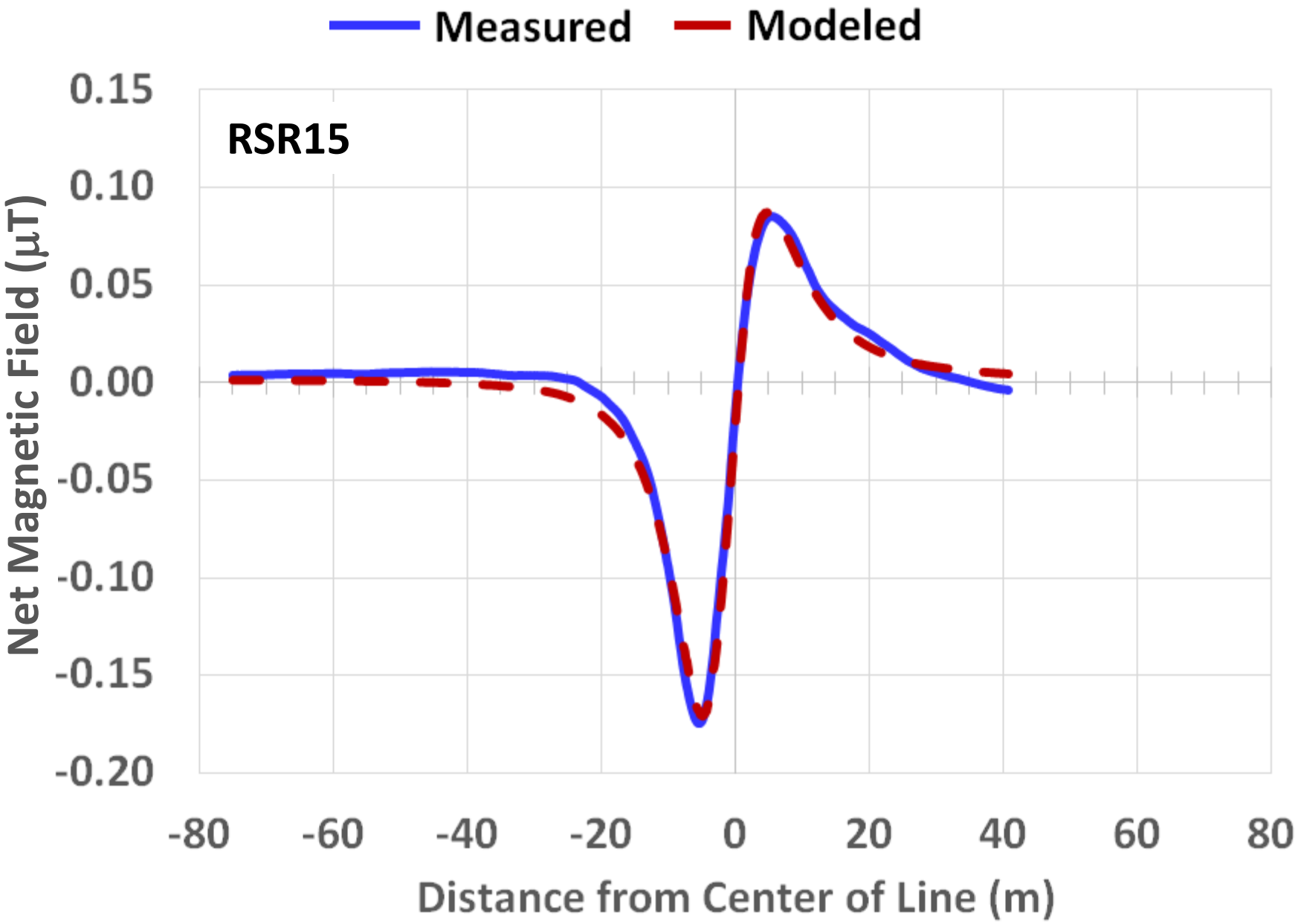
Measured
Modeled
RSR15
0.15
0.10
0.05
0.00
-0.05
-0.10
-0.15
-0.20
Net Magnetic Field (µT)
-80
-60
-40
-20
0
20
40
60
80
Distance from Center of Line (m)

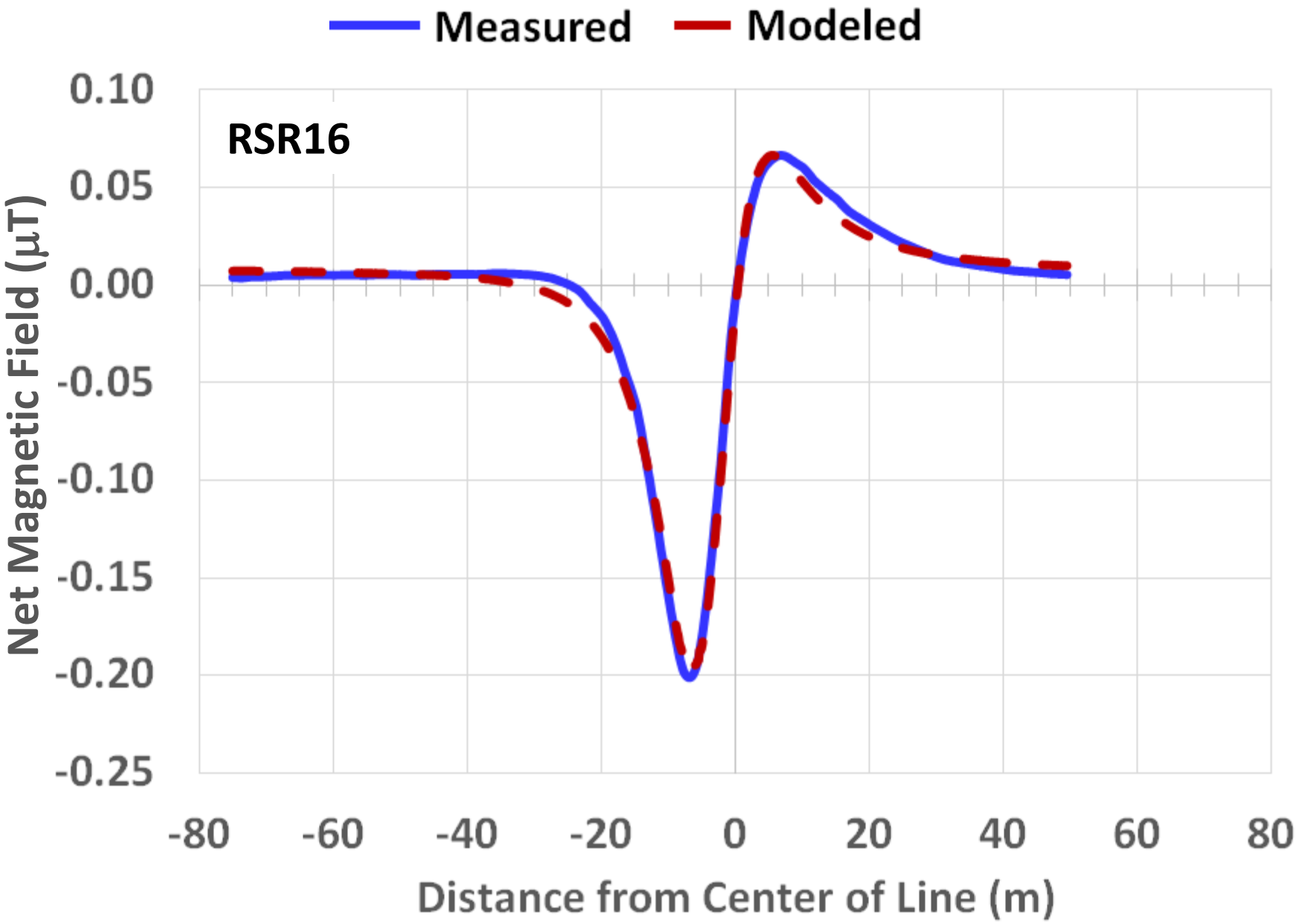
Measured
Modeled
RSR16
0.10
0.05
0.00
-0.05
-0.10
-0.15
-0.20
-0.25
Net Magnetic Field (µT)
-80
-60
-40
-20
0
20
40
60
80
Distance from Center of Line (m)

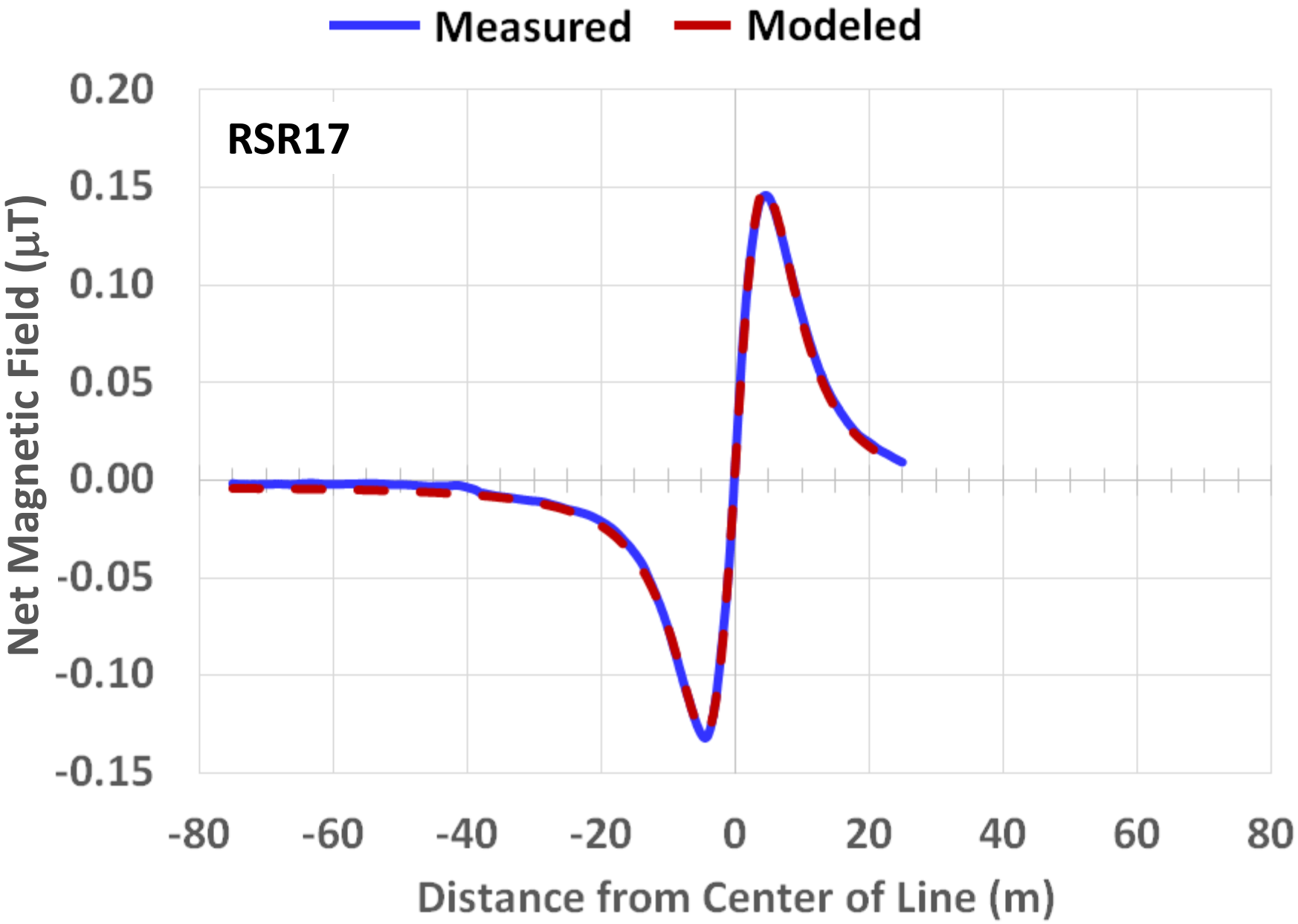
Measured
Modeled
RSR17
Net Magnetic Field (µT)
0.20
0.15
0.10
0.05
0.00
-0.05
-0.10
-0.15
-80
-60
-40
-20
0
20
40
60
80
Distance from Center of Line (m)

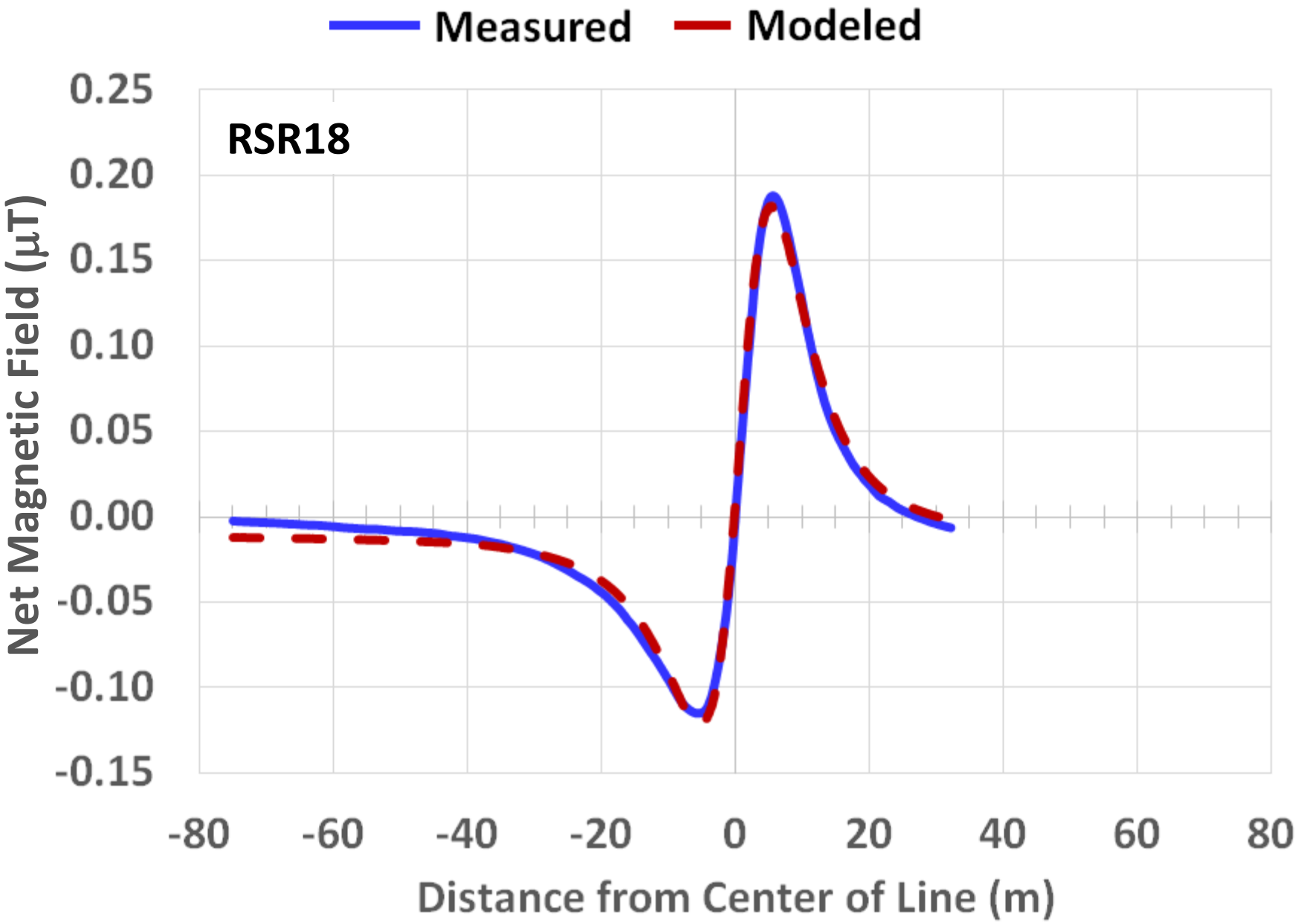
Measured
Modeled
RSR18
Net Magnetic Field (µT)
0.25
0.20
0.15
0.10
0.05
0.00
-0.05
-0.10
-0.15
-80
-60
-40
-20
0
20
40
60
80
Distance from Center of Line (m)

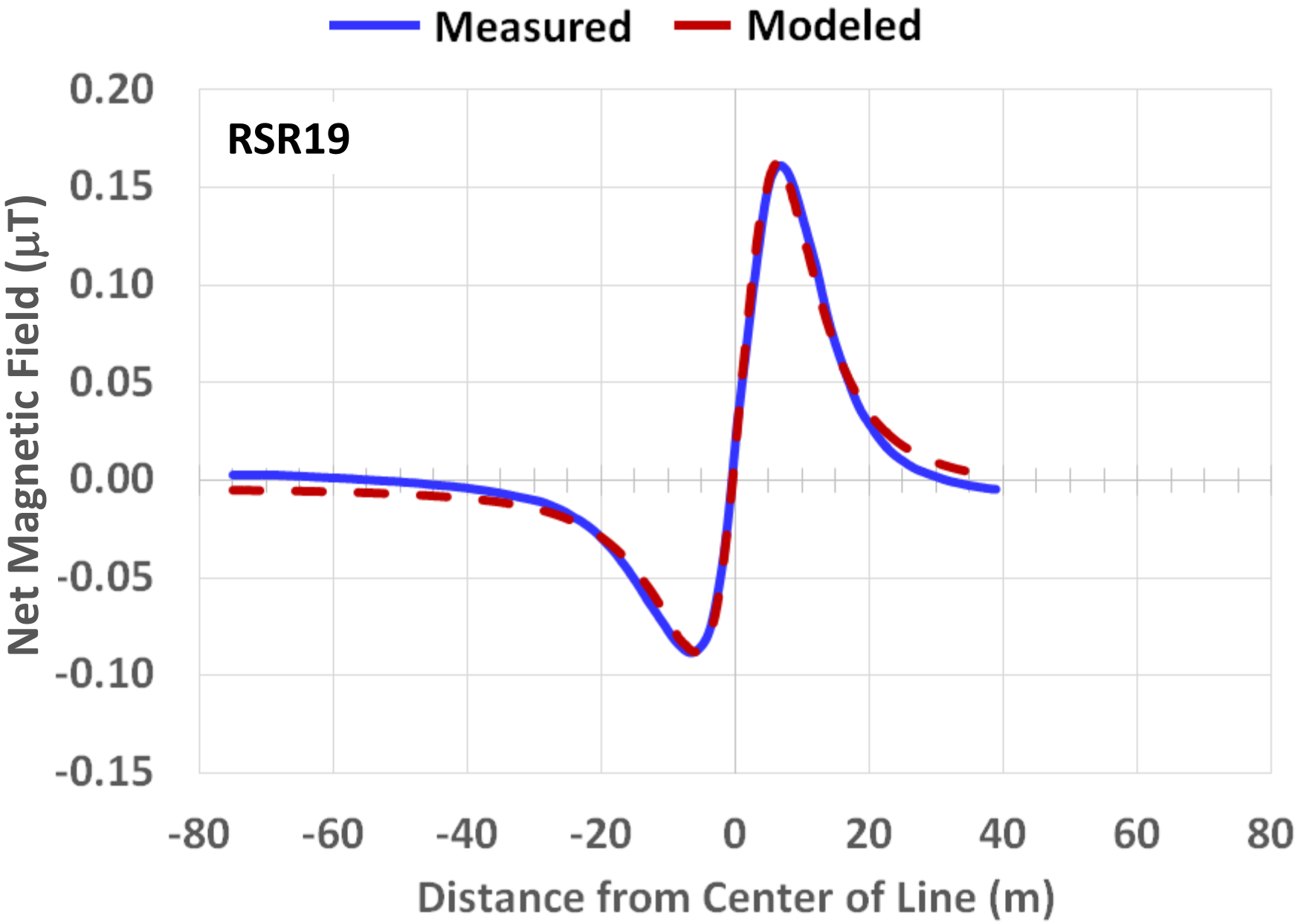
Measured
Modeled
RSR19
0.20
0.15
0.10
0.05
0.00
-0.05
-0.10
-0.15
Net Magnetic Field (µT)
-80
-60
-40
-20
0
20
40
60
80
Distance from Center of Line (m)

Appendix III

Net Magnetic Field Profiles from San Pablo Bay (SP) and the Richmond-San Rafael Bridge (RSR) Not Regressed

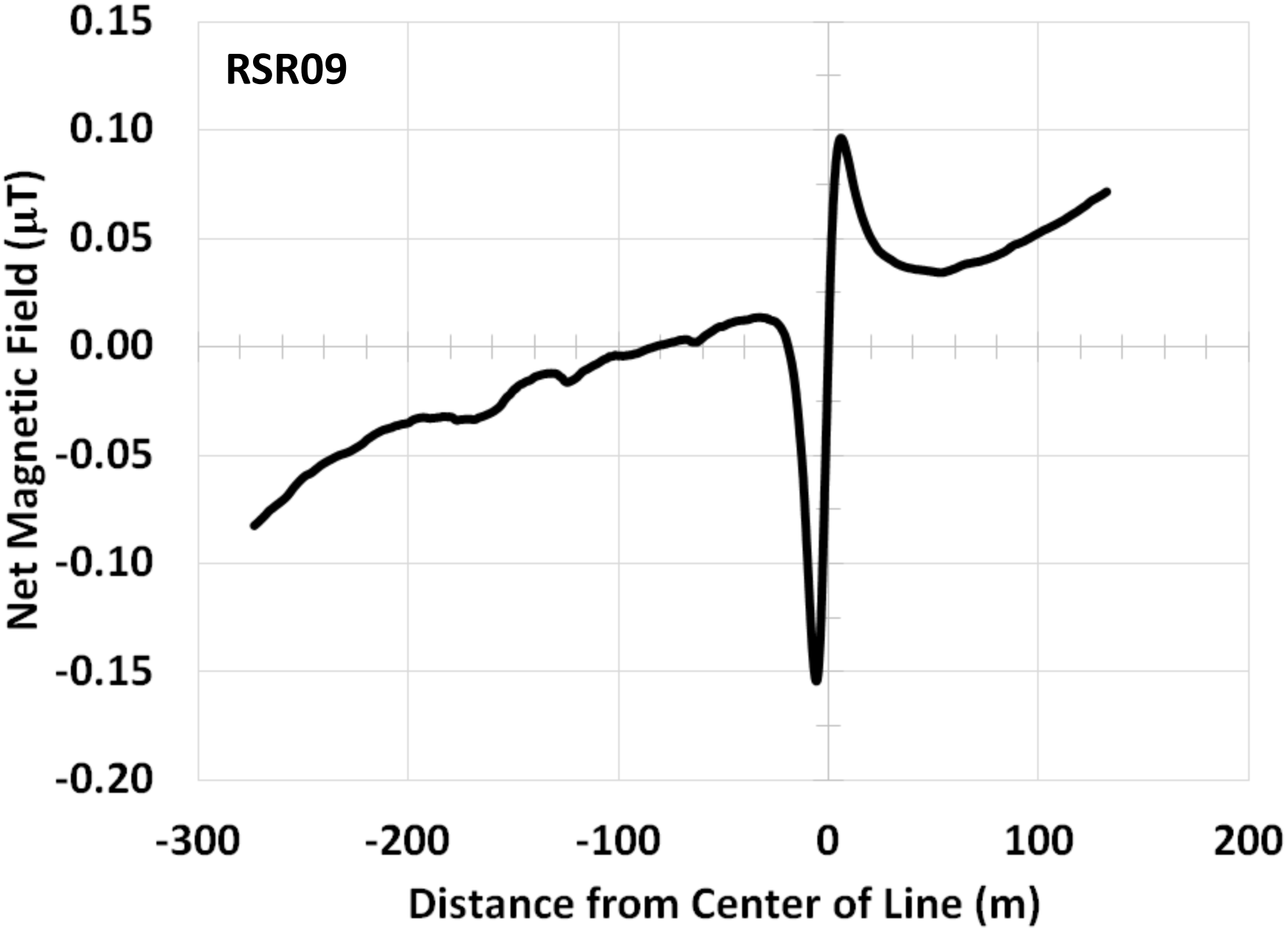
RSR09
0.15
0.10
0.05
0.00
-0.05
-0.10
-0.15
-0.20
Net Magnetic Field (µT)
-300
-200
-100
0
100
200
Distance from Center of Line (m)

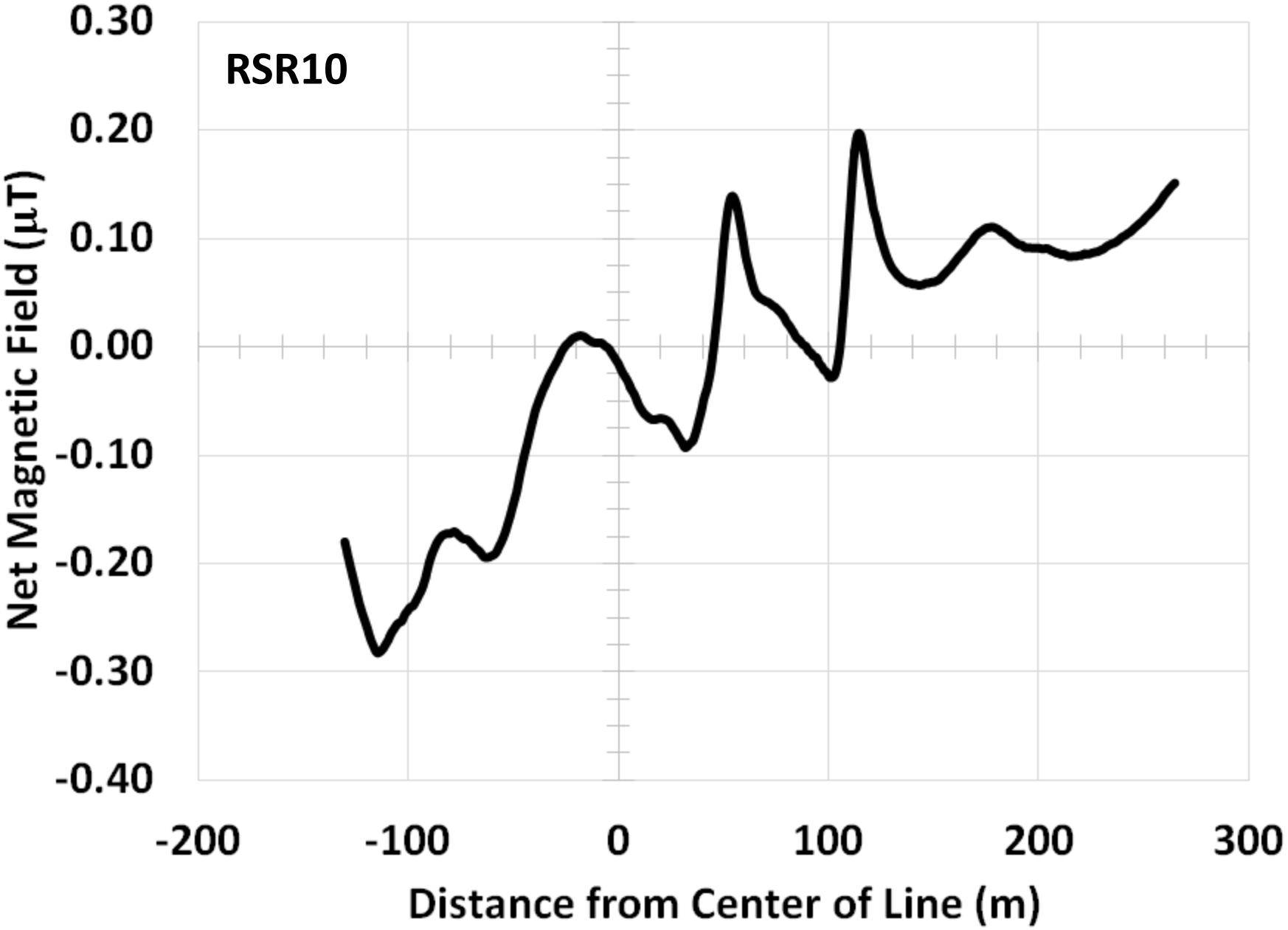
RSR10
0.30
0.20
0.10
0.00
-0.10
-0.20
-0.30
-0.40
Net Magnetic Field (µT)
-200
-100
0
100
200
300
Distance from Center of Line (m)

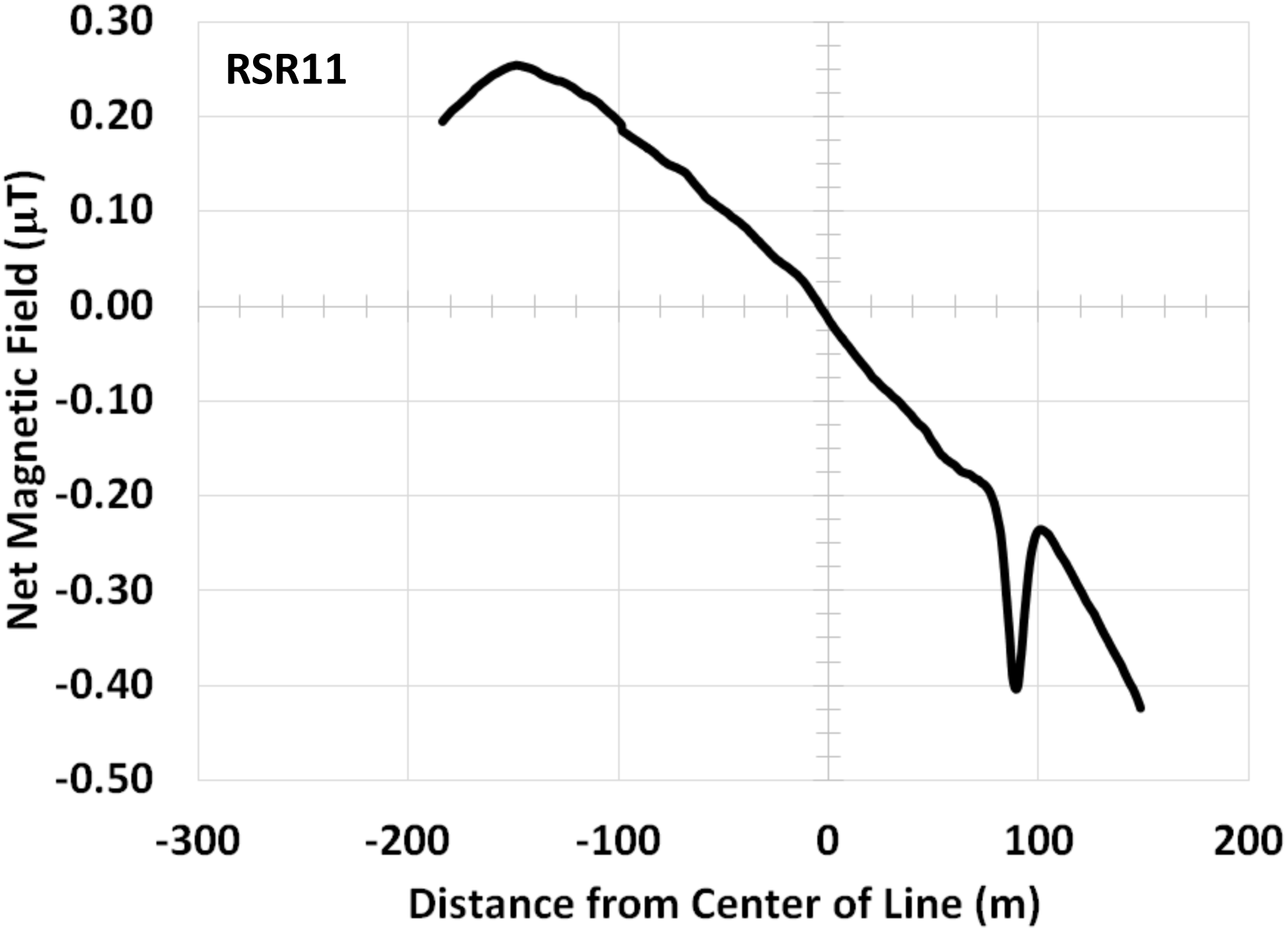
RSR11
0.30
0.20
0.10
0.00
-0.10
-0.20
-0.30
-0.40
-0.50
Net Magnetic Field (µT)
-300
-200
-100
0
100
200
Distance from Center of Line (m)

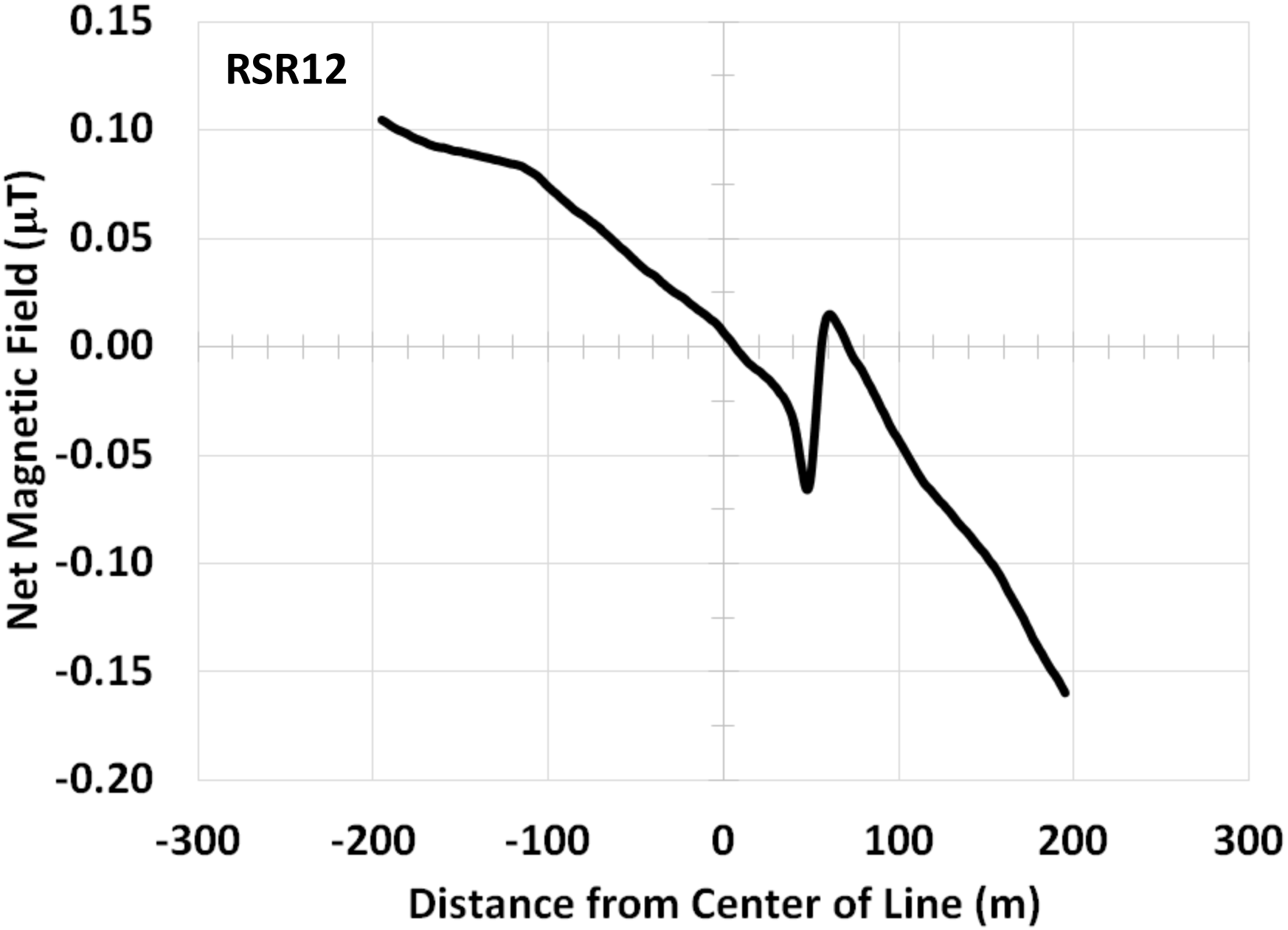
RSR12
0.15
0.10
0.05
0.00
-0.05
-0.10
-0.15
-0.20
Net Magnetic Field (µT)
-300
-200
-100
0
100
200
300
Distance from Center of Line (m)

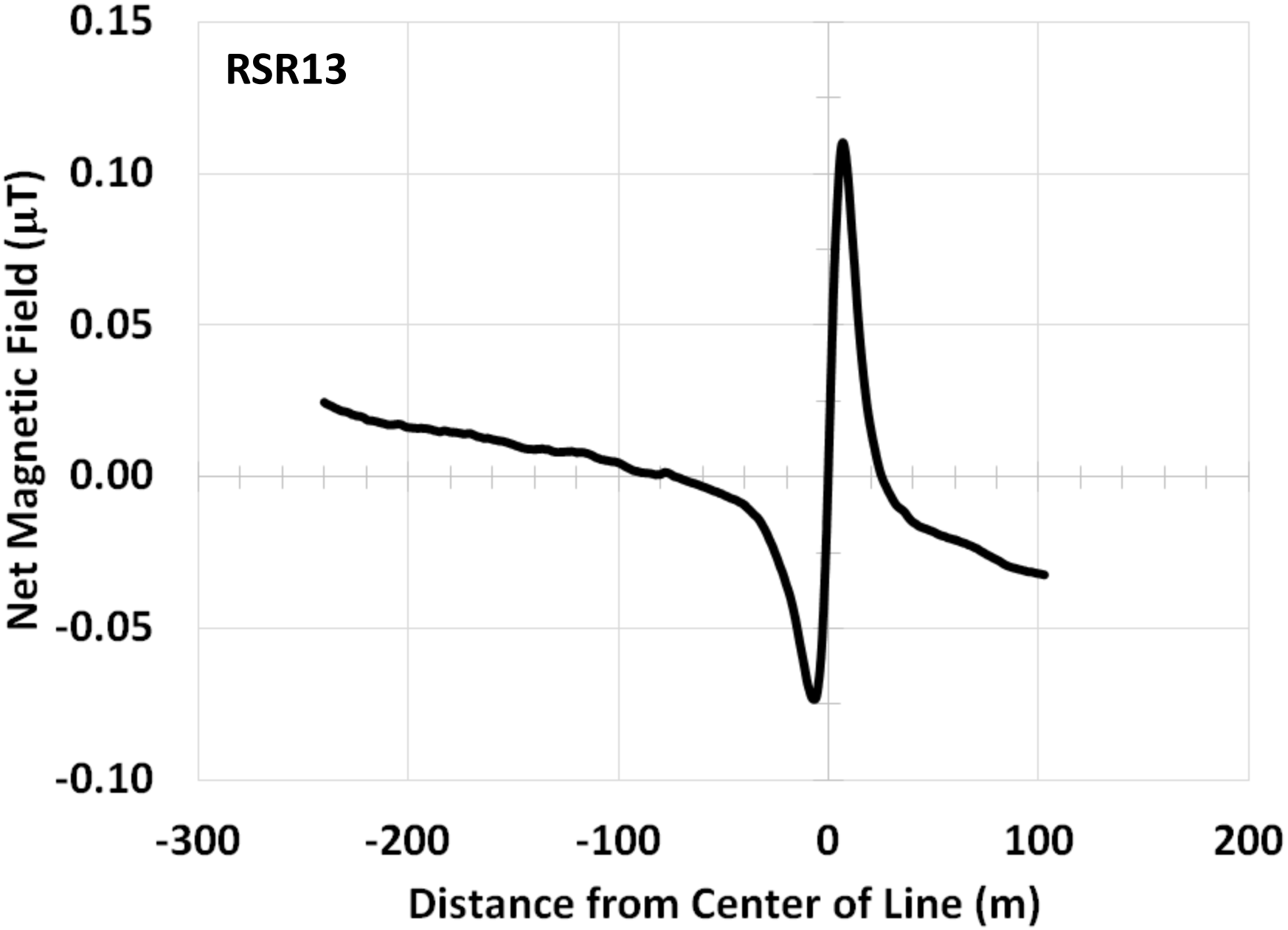
RSR13
0.15
0.10
0.05
0.00
-0.05
-0.10
Net Magnetic Field (μT)
-300
-200
-100
0
100
200
Distance from Center of Line (m)

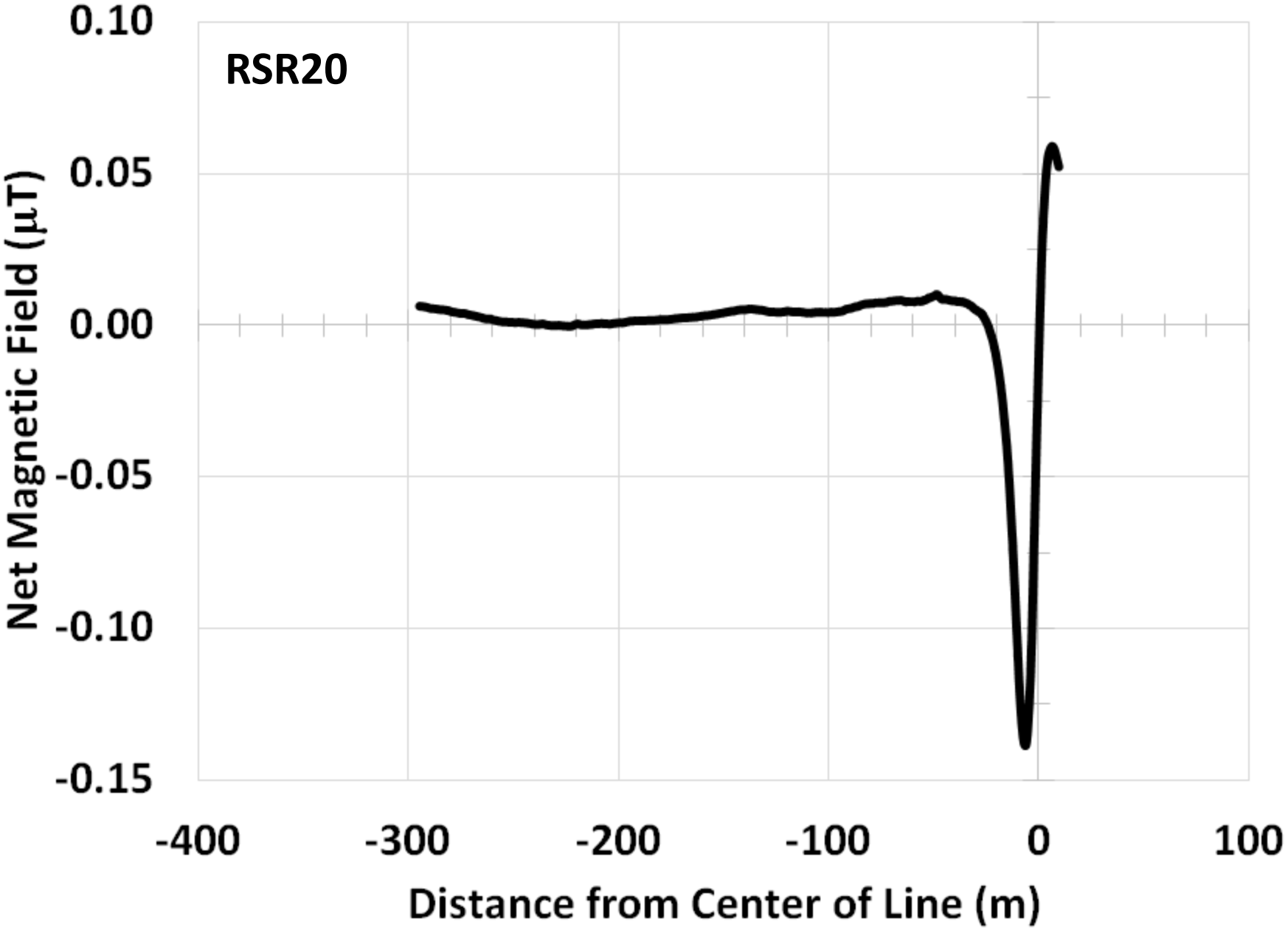
RSR20
0.10
0.05
0.00
-0.05
-0.10
-0.15
Net Magnetic Field (μT)
-400
-300
-200
-100
0
100
Distance from Center of Line (m)

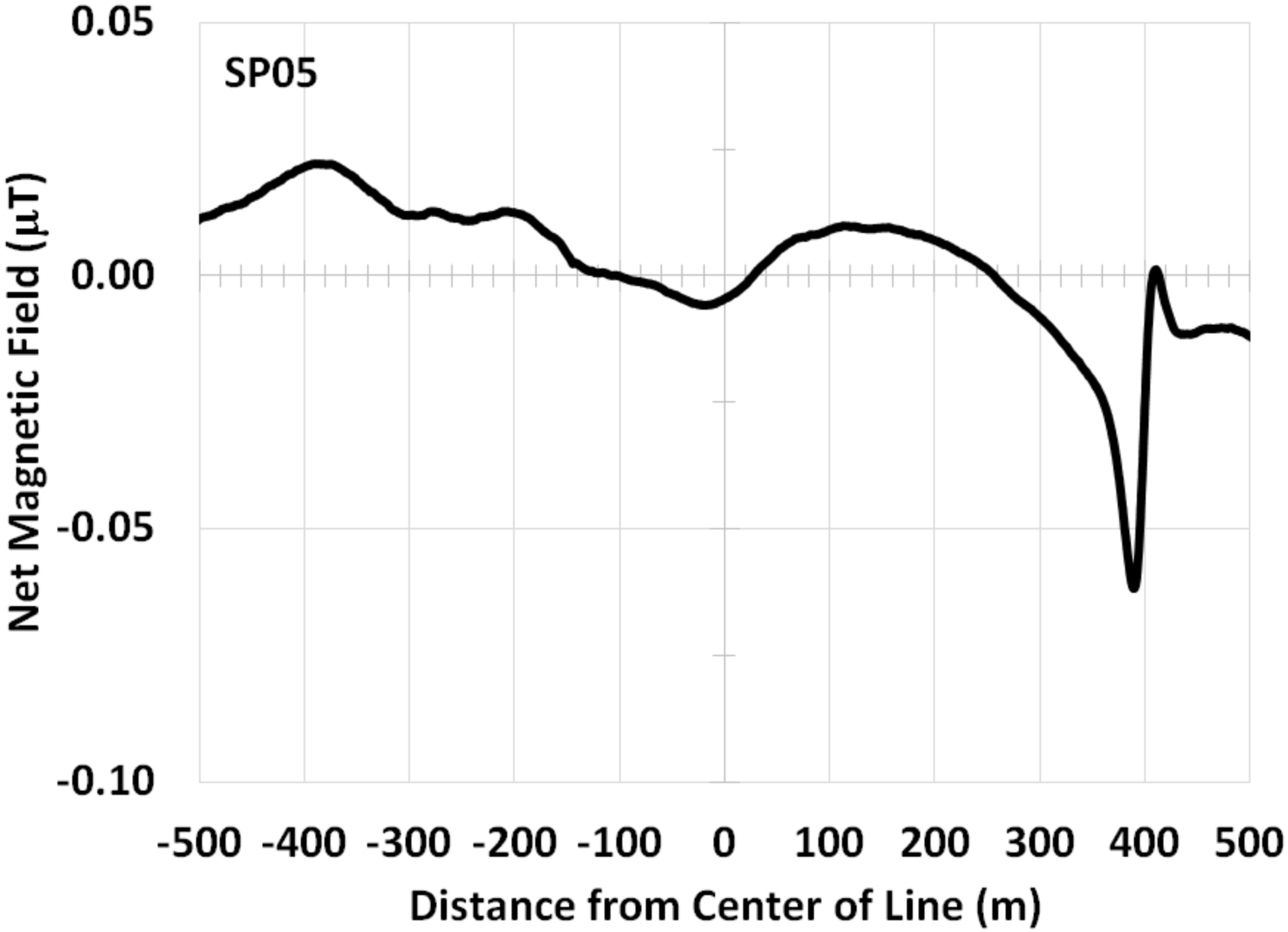
SP05
0.05
0.00
-0.05
-0.10
Net Magnetic Field (µT)
-500 -400 -300 -200 -100 0 100 200 300 400 500
Distance from Center of Line (m)

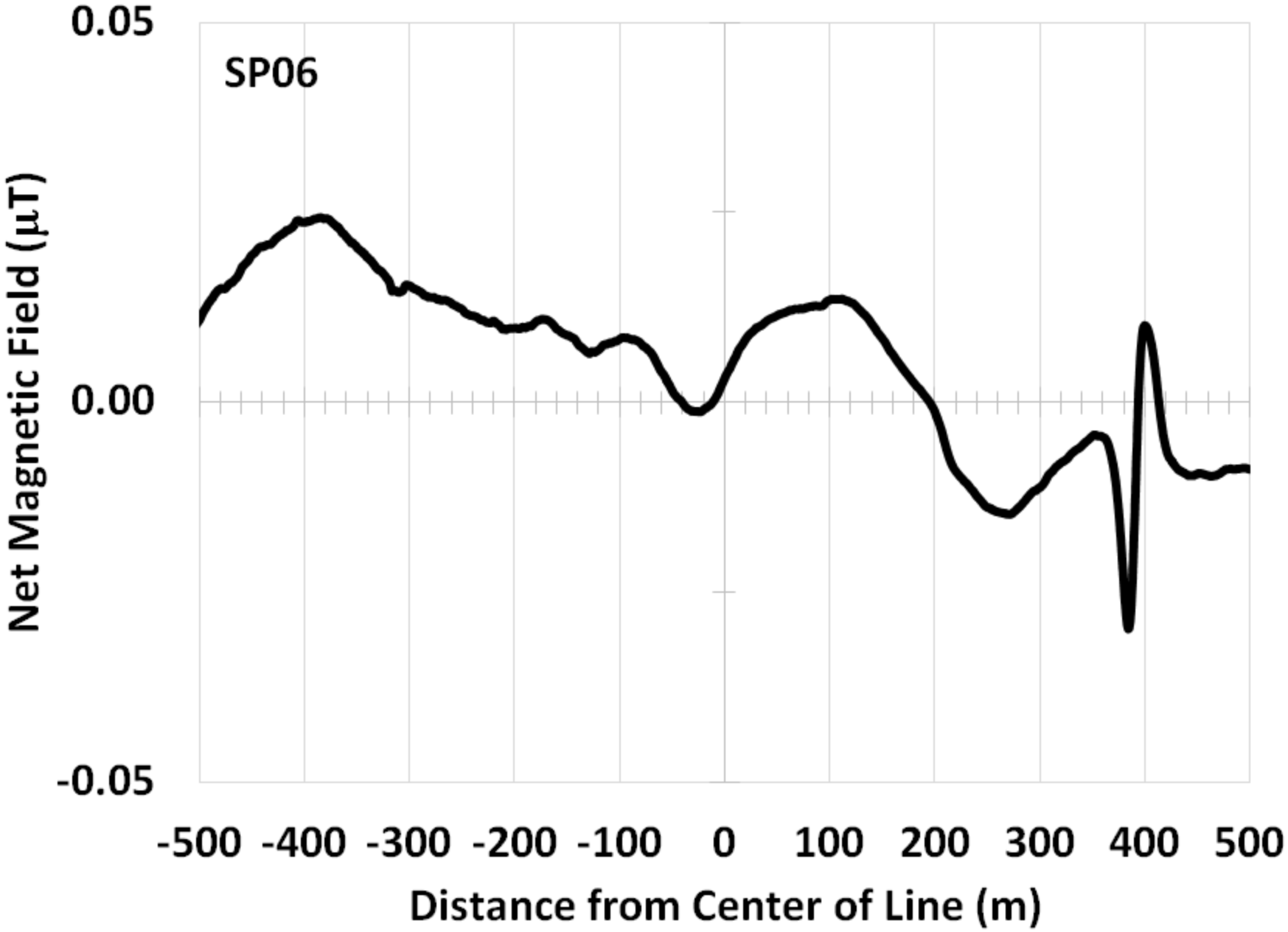
SP06
0.05
0.00
-0.05
Net Magnetic Field (μT)
-500 -400 -300 -200 -100 0 100 200 300 400 500
Distance from Center of Line (m)

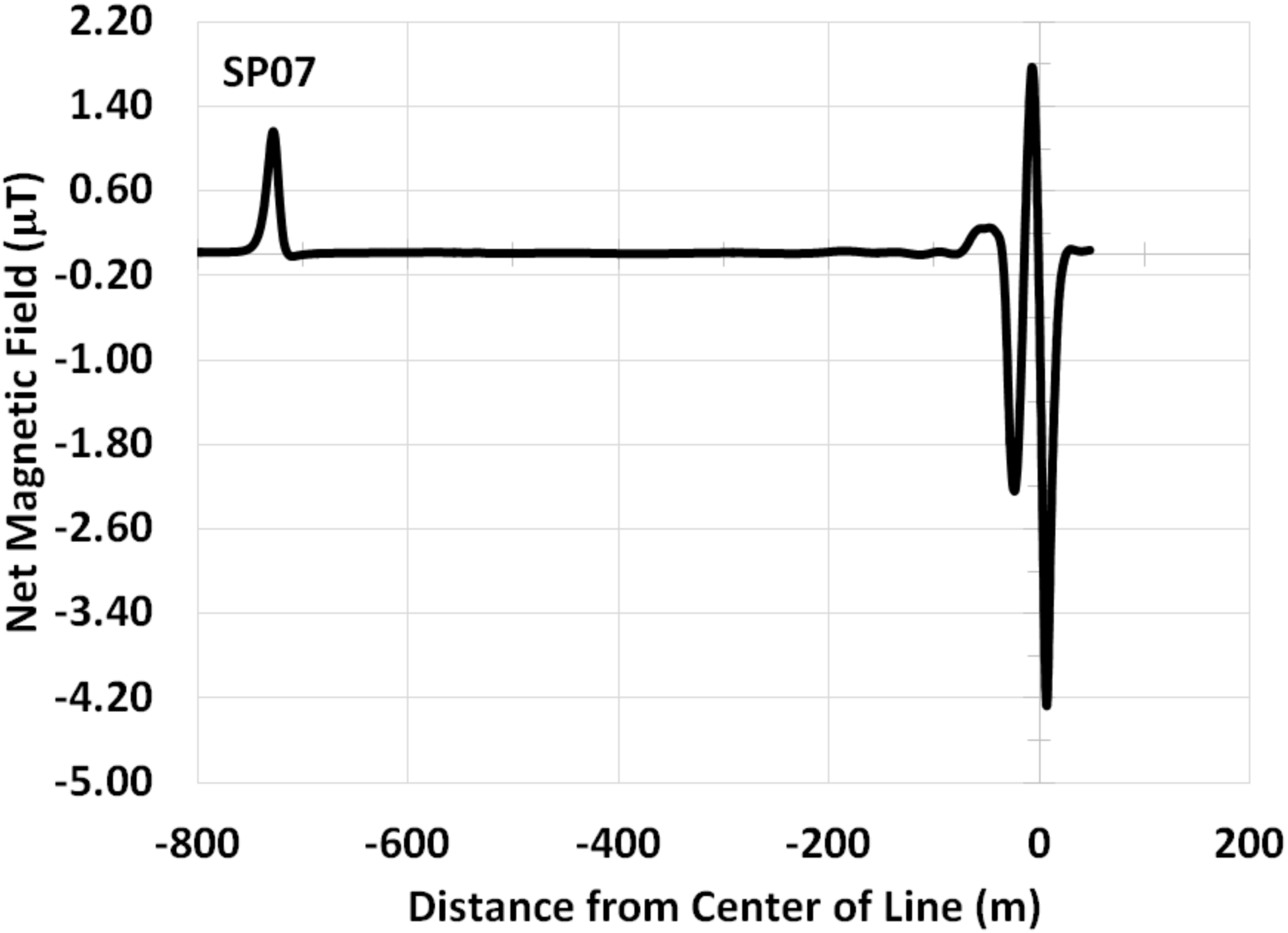
SP07
2.20
1.40
0.60
-0.20
-1.00
-1.80
-2.60
-3.40
-4.20
-5.00
Net Magnetic Field (µT)
-800
-600
-400
-200
0
200
Distance from Center of Line (m)

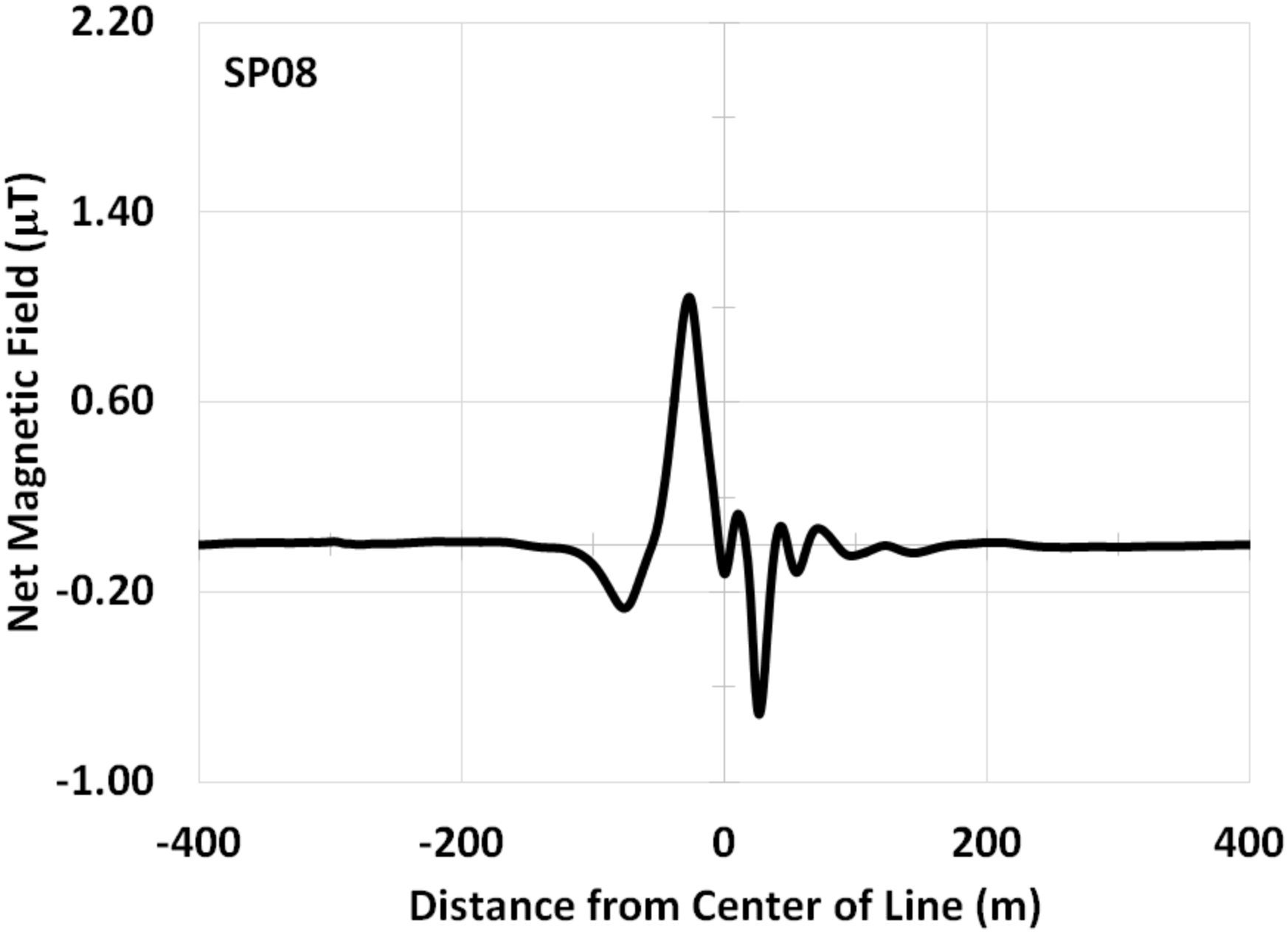
SP08
2.20
1.40
0.60
-0.20
-1.00
Net Magnetic Field (µT)
-400
-200
0
200
400
Distance from Center of Line (m)

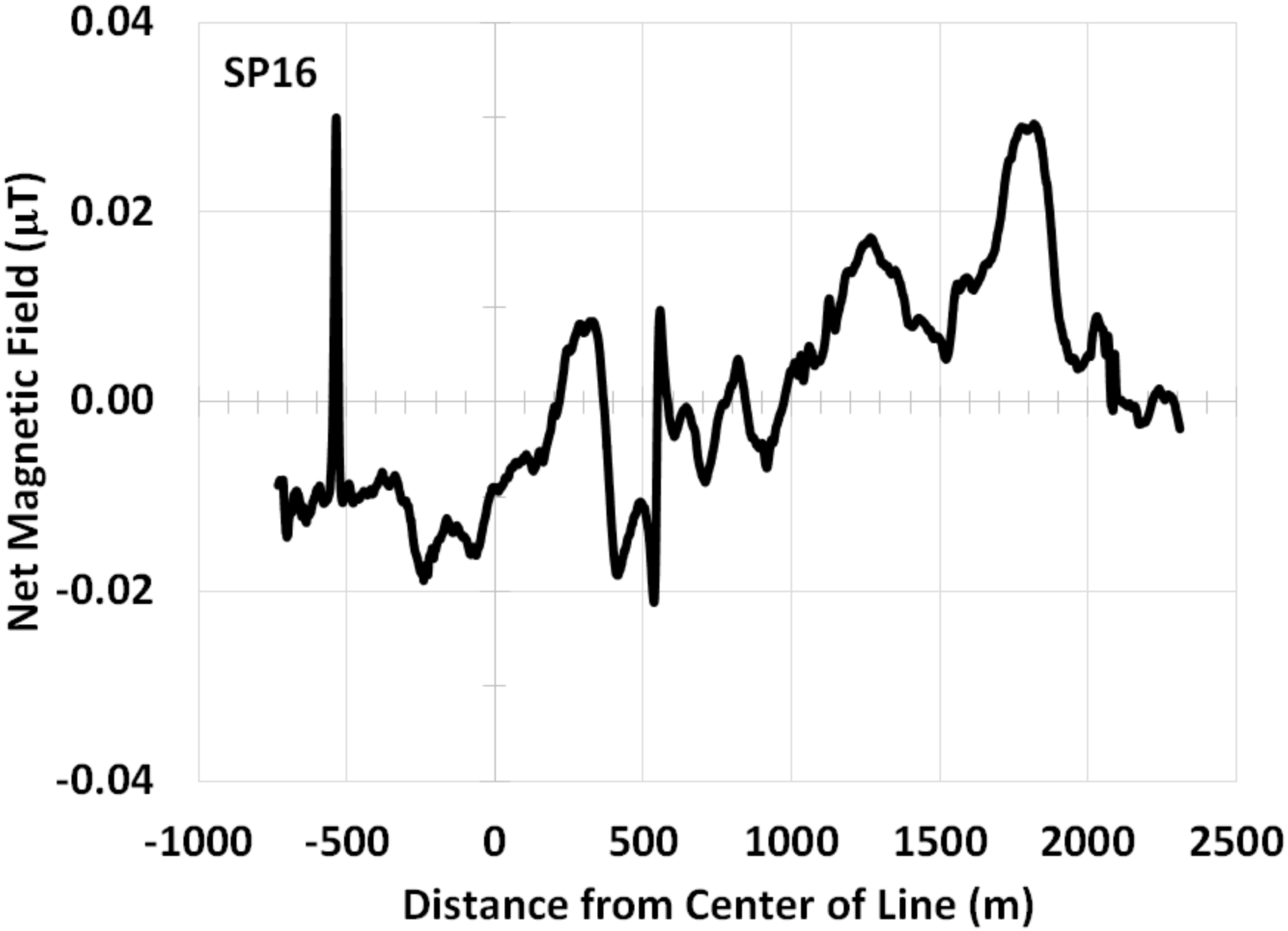
SP16
0.04
0.02
0.00
-0.02
-0.04
Net Magnetic Field (μT)
-1000
-500
0
500
1000
1500
2000
2500
Distance from Center of Line (m)

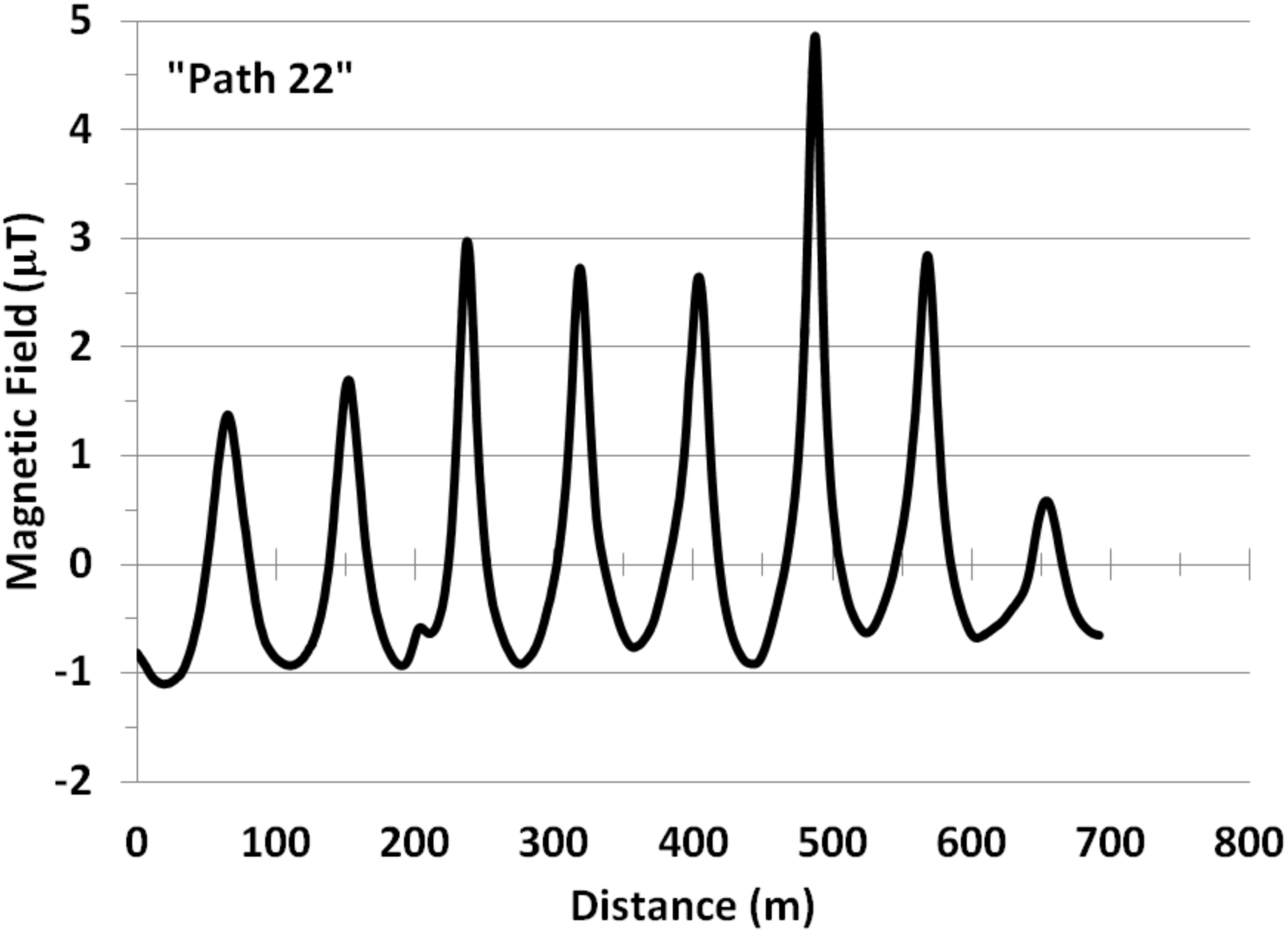
"Path 22"
Magnetic Field (μT)
5
4
3
2
1
0
-1
-2
0
100
200
300
400
500
600
700
800
Distance (m)